



University of Strathclyde

Department of Mechanical and Aerospace Engineering

University of Strathclyde,

James Weir Building, 75 Montrose St.,

Glasgow, UK, G1 1XJ

Tribo-corrosion maps for steels, titanium and titanium carbide materials

By

GHULAM RASOOL

A thesis presented in fulfilment of the requirements for the degree of

Doctor of Philosophy

2015

Tribo-corrosion maps for steels, titanium and titanium carbide materials

GHULAM RASOOL

Submitted for the degree of Doctor of Philosophy

2015

Abstract

In this project, research work was carried out on the tribo-corrosion behaviour of titanium carbide composite coatings produced by Tungsten Inert Gas (TIG) welding torch melting process on steel and titanium substrates. The integrity of TiC composite coatings were checked and analysed on the substrates. The effects of change in sliding speeds and normal loads on wear behaviours were investigated for dry sliding conditions and tribo-corrosion maps were constructed with a tribo-system approach. The work was carried out in the following phases:

In phase I, a fundamental study of the wear behaviour of two steels of different Cr contents and hardness were carried out. Pin-on-disk apparatus was used for testing 303stainless steel (303SS) disks and 8620 low alloy steel pins. For 303SS adhesive wear and tribo-oxidation were predominated at relatively low sliding speeds and adhesive wear was predominated at high sliding speeds and normal loads. In contrast, oxidative wear was more prevalent for the low alloy steel. Wear mapping approaches were undertaken to represent the transitions in wear modes and wear mechanisms as a function of sliding speeds and applied loads. The different wear maps generated for the pins and disks were discussed in the context of the wear mechanisms observed in the tribological contact.

In phase II, dry sliding wear tests were carried out on 303SS disks (uncoated and coated with TiC composite coatings) against alumina balls as a counterface on pin-on-disk configuration. The composite coatings increased the surface hardness hence the sliding

wear resistance of the 303SS substrate. Wear maps for both uncoated and coated materials were developed on the basis of tests results. These maps show that the mild wear regime for the composite coating was expanded to a higher range of sliding speeds and normal loads. For the composite coating, an additional wear mode transition i.e. from the mild to very mild regime occurred at low sliding speeds and normal loads.

In phase III, experimental work was carried out on a pin-on-disk sliding wear testing rig on hardened steel (A.I.S.I. 0-1-Ground Flat Stock) disks and titanium (Ti) uncoated and coated pins with titanium carbide (TiC) composite coatings. For uncoated Ti and hardened steel tribo-couple, pins' material was transferred to disks and covered the wear tracks almost for each combination of sliding speed and normal load. High wear of Ti was found against hardened steel. Adhesive wear was prevalent for Ti pins along with abrasive, plastic deformation and delamination against hardened steel disks.

While for the Ti base TiC composite coatings against hardened steel different wear behaviour observed. The composite coating increased the surface hardness hence the sliding wear resistance of the Ti substrate. Dry sliding wear behaviour of hardened steel disks was characterized by abrasive-oxidative wear at lower normal load while adhesive-oxidative wear was predominated at high normal load with iron oxide transfer to the coated pins for the range of sliding speed. In contrast, micro-abrasion and oxidative wear were predominated for the TiC composite coatings pins along with very mild adhesive-abrasive wear. A tribo-system approach was adopted to investigate the wear behaviour of TiC coatings and hardened steel against each other. Wear maps for both uncoated and coated materials were constructed on the basis of tests results. The tribo-corrosion maps show that due to TiC composite coating wear resistance of the substrate was increased.

Higher tribo-corrosion resistance of the TiC composite coatings was found on Ti substrate than that of 303SS substrate. Moreover, the surfaces treated with TiC coatings by TIG welding torch as heat source, expanded the mild wear regime to a higher range of sliding speeds and normal loads with creation of a new wear regime i.e. very mild wear and elimination of severe wear regime.

Keywords: pin-on-disk, dry sliding wear, sliding speed, normal load, Cr containing steels, titanium, TIG process, TiC composite coatings, oxidative wear, tribo-corrosion maps

The objective of this study

There are different techniques included thermal spray, electron beam, laser processing, physical vapour deposition (PVD), chemical vapour deposition (CVD) and ion implantation for surface engineering to enhance the tribological properties of metals. PVD, CVD and ion implantation are limited in producing thin coatings. While laser and electron beam processing methods can produce thick coatings which are more suitable for tribological applications. All these coatings methods and techniques are expensive and require specific conditions, e.g. high vacuum. To overcome such problems, Tungsten Inert Gas (TIG) welding torch melting process can be used to produce hard coatings on different substrates. This metal coating technique has significant advantages over the methods mentioned above, such as simple instrument, ease of operation and low net cost.

The aims of this work are:

- 1- To analyse the integrity of TiC incorporated composite coatings produced by the TIG welding torch melting method on steel and titanium substrates.
- 2- To study wear behaviour of the substrate and coatings with respect to change in sliding speed and normal load.
- 3- Construction of tribo-corrosion maps for these materials to analyse the transitions in wear mode and wear mechanisms regimes in dry sliding contacts.

Structure of the thesis

The structure of this thesis is as follows:

- (a) Introduction – Chapter 1
- (b) Literature review – Chapter 2
- (c) Experimental Methodology – Chapter 3

Results and discussion

- (d) High and zero Cr contents steel in dry sliding contact – Chapter 4
- (e) Wear maps for titanium carbide composite based coatings deposited on 303stainless steel – Chapter 5
- (f) Titanium against hardened steel (A.I.S.I. 0-1-Ground Flat Stock) in dry sliding – Chapter 6
- (g) Titanium base titanium carbide composite coatings in tribological contact – Chapter 7
- (h) Tribo-corrosion maps for titanium uncoated and coated with titanium carbide composite coatings – Chapter 8
- (i) Conclusions and future work – Chapter 9

Declaration

This thesis is comprised the experimental work which was carried out in the Department of Mechanical and Aerospace Engineering, University of Strathclyde Glasgow, United Kingdom under the supervision of Professor Margaret Stack during the period October 2011 to September 2014. No part of this thesis has been submitted elsewhere for any other degree or qualification and it is all my own work unless referenced to the contrary in the text. A part of this thesis has been published in journals as listed below:

Journal publications

1 - G. Rasool and M.M. Stack, Mapping the role of Cr content in dry sliding of steels: comparison between maps for material and counterface, Tribology International, Volume 80, December 2014, pages 49-57 (Published), **based on chapter 4.**

2 - G. Rasool and M.M. Stack, Wear maps for TiC composite based coatings deposited on 303stainless steel, Tribology International, Volume 74, June 2014, Pages 93-102 (Published), **based on chapter 5.**

3 - G. Rasool and M.M. Stack, Tribo-Oxidation maps for Ti against steel, in press in the Journal of Tribology International, **based on chapter 6.**

4 - G. Rasool, S. Mridha and M.M. Stack, Mapping wear mechanisms for TiC/Ti composite coatings, Wear 328-329 (2015), Pages 498-508 (Published) **based on chapter 7.**

Acknowledgements

I take this opportunity to express my sincere gratitude to Professor Margaret Stack for her supervision, guidance and support throughout this period of study.

I gratefully acknowledge the University of Strathclyde, Glasgow, UK, for giving me the chance of research work and awarding me, Fee Only Scholarship, to carry out this study that led to the degree of Doctor of Philosophy (PhD).

I am also thankful to the International Islamic University Malaysia (IIUM) for collaboration and providing the all test specimens and facilities to perform a part of the experimental work. I am particularly thankful to Professor Shahjahan Mridha, Leverhulme Trust Visiting Professor – grant RL7583- to the University of Strathclyde, 2012-2013, and Professor Neville Baker, PI of grant, for collaboration on this project.

Moreover, I am thankful to Dr Shayan Sharifi (Postdoctoral Researcher), and all staff of the Department of Mechanical and Aerospace Engineering, University of Strathclyde for providing me help to perform experimental and testing work of this project.

Dedication

I would like to dedicate this work to my late parents, my wife and my sons.

Copyright @ 2014 by Ghulam Rasool

“The copyright of this thesis belong to the author under the terms of the United Kingdom Copyright Acts as qualified by the University of Strathclyde Regulation 3.49. No quotations from this should be published without the author’s prior written consent. Due acknowledgement must always be made of the use of any material contained in or derived from this thesis”.

LIST OF TABLES

Table 1 Variation in multimeter reading with increase in loads	58
Table 2 Tests frequency and tests duration for 303SS disks against 8620 low alloy steel pins (chapter 4).	61
Table 3 Tests frequency and tests duration for Ti and Ti base TiC composite coatings pins against hardened steel disks (chapter 6-8).....	61
Table 4 The chemical composition of the 303 stainless steel disk and 8620 low alloy steel pin materials	65
Table 5 Tests frequency and tests duration for 303SS disks (uncoated and coated with TiC composite coatings) against alumina ball (chapter 5)	66
Table 6 The composition of the 303 stainless steel disk	66
Table 7 The composition of the 303 stainless steel base TiC coating disk surface	66
Table 8 The chemical composition of the steel (A.I.S.I. 0-1-Ground Flat Stock) disk.....	68
Table 9 Mass loss of 303SS disks and 8620 low alloy steel pins at 0.38m s^{-1} sliding speed. ...	76
Table 10 Mass loss of 303SS disks and 8620 low alloy steel pins at 0.5m s^{-1} sliding speed. ...	76
Table 11 Mass loss of 303SS disk and 8620 low alloy steel pin at 0.86m s^{-1} sliding speed. ...	77
Table 12 Mass loss of 303SS disks and 8620 low alloy steel pins at 1.2 m s^{-1} sliding speed. .	78
Table 13 Mass loss of 303SS disk and 8620 low alloy steel pin against each other at 1.5 m s^{-1} sliding speed.	79
Table 14 Mass loss of 303 stainless steel disks against 8620 low alloy steel pins.	80
Table 15 Mass loss of 303 stainless steel disks against 8620 low alloy steel pins.	81
Table 16 Mass loss of 8620 low alloy steel pins against 303 stainless steel disks.	81
Table 17 Mass loss of 8620 low alloy steel pins against 303 stainless steel disks.	82
Table 18 The total mass loss of 303 stainless steel disks and 8620 low alloy steel pins.....	83
Table 19 Wear rate of 303SS disks against alumina ball at 3 cm s^{-1} and various normal loads.	96
Table 20 Wear rate of 303SS disks against alumina ball at 7 cm s^{-1} and various normal loads.	98
Table 21 Wear rate of 303SS disks against alumina ball at 11cm s^{-1} and various normal loads.....	99
Table 22 Wear rate of 303SS disks against alumina ball at 15cm s^{-1} and various normal loads.....	101
Table 23 Wear rate of 303stainless steel against alumina at constant sliding speeds and various normal loads.....	102
Table 24 Wear rate of 303stainless steel against alumina at constant normal loads and various sliding speeds.	103
Table 25 Wear rate of 303SS disks against alumina ball at 3cm s^{-1} and various normal loads.	107
Table 26 Wear rate of 303SS base TiC coatings disks against alumina ball at sliding speed 7cm. s^{-1} and various normal loads.....	108

Table 27 Wear rate of 303SS base TiC coatings disks against alumina ball at 11cm. s ⁻¹ and various normal loads.....	110
Table 28 Wear rate of 303SS base TiC coatings disks against alumina balls at 15cm s ⁻¹ and various normal loads.....	111
Table 29 Wear rate of TiC coatings against alumina at constant sliding speeds and various normal loads.	112
Table 30 Wear rate of TiC coating against alumina at constant normal loads and various sliding speeds.....	113
Table 31 Wear rate of 303SS and 303SS base TiC coatings disks against alumina balls.	117
Table 32 Wear rate of 303SS and 303SS base TiC coatings disks against alumina balls.	118
Table 33 Wear rate of 303SS and 303SS base TiC coatings disks against alumina balls.	118
Table 34 Wear rate of 303SS and 303SS base TiC coatings disks against alumina balls.	119
Table 35 The total mass loss of 303SS and 303SS base TiC coatings against alumina.	120
Table 36 wear rate of Ti pins and hardened steel disks against each other.	130
Table 37 Wear rate of Ti pin and hardened steel disk against each other.	130
Table 38 Wear rate of Ti pin and hardened steel disk against each other.	131
Table 39 Wear rate of Ti pin and hardened steel disk against each other.	131
Table 40 Wear rate of Ti pin and hardened steel disk against each other.	132
Table 41 Wear rate of Ti pins against hardened steel disks.	133
Table 42 Wear rate of Ti pins against hardened steel disks.	133
Table 43 Wear rate of hardened steel disks against Ti pins.	134
Table 44 Wear rate of hardened steel disks against Ti pins.	135
Table 45 The total mass loss of Ti pins and hardened steel disks against each other.	135
Table 46 Coefficient of friction of Ti pins against hardened steel disks.	137
Table 47 Coefficient of friction of Ti pins against hardened steel disks.	137
Table 48 Wear rate of Ti base TiC coatings pins and hardened steel disks.	154
Table 49 Wear rate of Ti base TiC coatings pins and hardened steel disks.	154
Table 50 Wear rate of Ti base TiC coatings pins and hardened steel disks.	155
Table 51 Wear rate of Ti base TiC coatings pins and hardened steel disks.	155
Table 52 Wear rate of Ti base TiC coatings pins and hardened steel disks.	156
Table 53 Wear rate of Ti base TiC coatings pins against hardened steel disks.	157
Table 54 Wear rate of Ti base TiC coatings pins against hardened steel disks.	158
Table 55 Wear rate of hardened steel disks against Ti base TiC coating pins.	159
Table 56 Wear rate of hardened steel disks against Ti base TiC coating pins.	159
Table 57 The Total mass loss of Ti base TiC composite coatings pins and hardened steel disks.	161
Table 58 Coefficient of friction of Ti base TiC coatings pins against hardened steel disks.	161
Table 59 Coefficient of friction of Ti base TiC coatings pins against hardened steel disks.	162
Table 60 Mass loss of Ti base TiC composite coatings pins against hardened steel disks for repeat tests at and experimental error.	169
Table 61 Wear rate of Ti and Ti base TiC coatings pins.	179
Table 62 Wear rate of Ti and Ti base TiC coatings pins.	179
Table 63 Wear rate of Ti and Ti base TiC coatings pins.	180

Table 64 Wear rate of Ti and Ti base TiC coatings pins.	180
Table 65 Wear rate of Ti and Ti base TiC coatings pins.....	181
Table 66 Wear rate of Ti pins against hardened steel disks.	182
Table 67 Wear rate of Ti pins against hardened steel disks.	182
Table 68 Wear rate of Ti base TiC coatings pins against hardened steel disks.	183
Table 69 Wear rate of Ti base TiC coatings pins against hardened steel disks.	184
Table 70 The total mass loss of Ti and Ti base TiC composite coatings against hardened steel.	185
Table 71 Coefficient of friction of Ti against hardened steel.	186
Table 72 Coefficient of friction of Ti against hardened steel.	186
Table 73 Coefficient of friction of Ti base TiC coatings pins against hardened steel disks. .	187
Table 74 Coefficient of friction of Ti base TiC coatings pins against hardened steel disks	188

LIST OF FIGURES

Figure 1 Expanded representation of tribo-technical system (TTS) [Springer Handbook of Mechanical Engineering].....	12
Figure 2 Geometries employed in sliding wear tests [44].	14
Figure 3 The combined influences of load and sliding speed on the sliding process in metals [62].....	15
Figure 4 Schematic shows two possibilities of break (1 and 2) during shearing of an interface [89].....	18
Figure 5 Schematic shows detachment of fragment of a material from plastic shearing of successive layers of an asperity contact [89].	18
Figure 6 Schematic of a hypothetical model of generation of a hemispherical wear particle during sliding contact [89].	20
Figure 7 The variation of wear rate with load for 0.5% plain carbon steel pin sliding at 1 m s^{-1} in air against tool steel in a pin-on-ring test [13]	22
Figure 8 The variation of wear rate with sliding speed for α/β brass sliding against steel at various temperatures in air and in pure oxygen [12]	22
Figure 9 Illustration of the differences between (a) two-body abrasion; and (b) three-body abrasion [62]	23
Figure 10 Schematics of abrasive wear processes as a result of plastic deformation by three deformation modes [89].	25
Figure 11 Schematics of ploughed groove and formation of wear particle due to ploughing as a result of fracture of flattened ridge and propagation of surface and subsurface cracks [89].....	25
Figure 12 Schematics of, (a) an abrasive surface before and after wear, showing blunting, and (b) an abrasive surface clogged by wear [89].	27
Figure 13 Spalling of a 52100 ball bearing race by subsurface fatigue [89].....	28
Figure 14 Schematic of a jet of abrasive particles hitting a surface at a high velocity [89]. ..	29
Figure 15 Rate of erosive wear as a function of angle of attack (with respect to the material plane) of impinging particles [89].	30
Figure 16 Wear tracks on steel disk [33]	37
Figure 17 The wear-rate surface for steel proposed by Okoshi and Sakai [142]	38
Figure 18 Wear regimes mapped on a base of load and sliding speed for soft steels sliding on soft steels [144].....	39
Figure 19 Wear mode-mode map for unlubricated sliding of steel on steel in the pin-on-disc configuration [135].	39
Figure 20 Wear rate maps (a) for A356 Al worn against SAE 52100 steel counterface, (b) for A356 Al-20% SiC composite worn against SAE 52100 steel counterface [73].	41
Figure 21 Wear mechanism map (a) for 7010 alloy, (b) for 7010 -25% SiCp [148].	42
Figure 22 Map showing the expansion of safety zone and least-wear regimes as a result of the application of TiN coatings on the crater wear of HSS tools during dry turning operations [63].....	43

Figure 23 Wear map for TiN sliding on steel [74].	44
Figure 24 Wear volume as a function of time for different coatings and uncoated substrate [62].	46
Figure 25 The variation of the coefficient of friction with normal load for the unlubricated sliding of steel on aluminium in air [62].	47
Figure 26 The variation of the coefficient of friction with apparent area of contact for wooden sliders on an unlubricated steel surface [62].	47
Figure 27 The coefficient of friction as a function of sliding velocity [96].	48
Figure 28 The variation of the coefficient of friction with sliding speed for pure bismuth and copper sliding against themselves [62].	50
Figure 29 The effect of normal load on the coefficient of friction for (a) steel on aluminium in air, (b) a copper on copper in air, and (c) AISI 440C stainless steel on Ni3Al alloy in air [89].	51
Figure 30 The variation of coefficient of friction with normal load for steels sliding against themselves in air, showing the results for two different plain carbon steels, with carbon contents of 0.4% (full curve) and 0.3% (broken curve) [62].	52
Figure 31 The variation of coefficient of friction with normal load for a 60° diamond cone sliding over the (0001) face of a silicon carbide single crystal. The increase for loads above ~ 4N is associated with fracture along the sliding path [62].	53
Figure 32 The variation of coefficient of friction with sliding speed reaction-bonded silicon carbide and hot-pressed silicon nitride sliding in self-mated couples in air [62].	54
Figure 33 Schematic of Pin-on-Disk wears test apparatus.	55
Figure 34 Pin-On-Disk dry sliding wear testing rig.	57
Figure 35 Schematic diagram of the load cell function.	58
Figure 36 Schematic diagram of the sliding speed control and revolution counter.	59
Figure 37 Schematic of the timer control and motor connections.	59
Figure 38 EDX analysis of titanium.	67
Figure 39 (a) Microstructure of 303 stainless steel 200X and (b) EDX analysis of 303stainless steel.	69
Figure 40 (a) Microstructure of 303stainless steel base TiC coating surface magnification X500, (b) the EDX analysis of the coated surface and (c) thickness of the 303SS base titanium carbide composite coatings after grinding the surface.	70
Figure 41 (a) The micrograph of the CP titanium base TiC coating surface, (b) the EDX analysis of the CP titanium matrix (substrate), (c) the EDX analysis of the Titanium carbide (TiC), (d) the EDX analysis of the titanium carbide composite coatings and (e) thickness of the coatings after grinding the surface.	71
Figure 42 Experimental errors (20%) for the 8620 low alloy steel pins against 303SS disks.	73
Figure 43 Experimental errors (11%) for 303SS base TiC coatings disks against alumina balls.	74
Figure 44 Mass loss of 303SS disk and 8620 low alloy steel pin at 0.38m s ⁻¹ sliding speed.	76
Figure 45 Mass loss of 303SS disks and 8620 low alloy steel pins at 0.5m s ⁻¹ sliding speed.	77
Figure 46 Mass loss of 303SS disks and 8620 low alloy steel pins against at 0.86m s ⁻¹ sliding speed.	78

Figure 47 Mass loss of 303SS disks and 8620 low alloy steel pins at 1.2 m s ⁻¹ sliding speed.	79
Figure 48 Mass loss of 303SS disks and 8620 low alloy steel pins against each other at 1.5 m s ⁻¹ sliding speed.	79
Figure 49 Mass loss vs normal load of 303 stainless steel disks against 8620 low alloy steel pins.	80
Figure 50 Mass loss vs sliding speed of 303 stainless steel disks against 8620 low alloy steel pins.	81
Figure 51 Mass loss vs. normal load 8620 low alloy steel pins against 303 stainless steel disks.	82
Figure 52 Mass loss vs normal load of 8620 low alloy steel pins against 303 stainless steel disks.	82
Figure 53 The total mass loss comparison of 303 stainless steel disks and 8620 low alloy steel pins.	83
Figure 54 SEM micrograph of 303SS disk (a) at sliding speed 0.38 m s ⁻¹ and normal load 50 N and (b) at 0.5 m s ⁻¹ and 50 N.	83
Figure 55 EDX analysis of 303SS disk (a) at sliding speed 0.38 m s ⁻¹ and normal load 50 N and (b) at 0.5 m s ⁻¹ and 50 N.	84
Figure 56 (a) Mass loss of 303SS disk and 8620 low alloy steel pin against each other at sliding speed 1.2 m s ⁻¹ and normal load 10 to 50 N, from the present work, and (b) wear rate plotted against load for the 0.52 % C steel at sliding speed 100cm s ⁻¹ (1 m s ⁻¹) and 50 g to 25 Kg (0.5 N to 250 N) load, x, for pin.; o, for ring, from [23].	87
Figure 57 (a) The comparison of change of wear trend of 303 stainless steel disk against 8620 low alloy steel pin at constant normal load 10 and 50 N in the range of sliding speed i.e. 0.38 to 1.5 m s ⁻¹ taken from Fig. 4.7 above, and (b) the trend of change of wear rate with sliding speed for the 0.52 % C steel. Loads: x, 1Kg (10 N equivalent) and ●, 5 Kg (50 N equivalent), from [23].	88
Figure 58 Variation in wear rate of brass with increase in sliding speeds against steel at 20°C in air [162].	88
Figure 59 Wear mode maps (a) 303 stainless steel disk against 8620 low alloy steel pin and (b) 8620 low alloy steel pin against 303 stainless steel disk.	90
Figure 60 Wear mechanism maps (a) 303 stainless steel disk against 8620 low alloy steel pin and (b) 8620 low alloy steel pin against 303 stainless steel disk.	90
Figure 61 Wear-mechanism map for a steel sliding pair using the pin-on-disk configuration [69].	91
Figure 62 Sliding wear and coefficient of friction trends of 303SS against alumina ball at sliding speed 3 cm s ⁻¹ and (a) normal load 2 N, (b) at 4 N, (c) at 6 N, (d) at 8 N and (e) at 10 N.	96
Figure 63 Wear rate of 303SS disks against alumina ball at 3 cm s ⁻¹ and various normal loads.	97
Figure 64 Sliding wear and coefficient of friction trends of 303SS against alumina ball at sliding speed 7 cm s ⁻¹ , and (a) at normal load 2 N, (b) at 4 N, (c) at 6 N, (d) at 8 N, and (e) at 10 N.	98

Figure 65 Wear rate of 303SS disks against alumina ball at 7 cm s ⁻¹ and various normal loads.....	98
Figure 66 Sliding wear and coefficient of friction trends of 303SS against alumina ball at 11cm s ⁻¹ and (a) at normal load 2N, (b) at 4N, (c) at 6N, (d) at 8N, and (e) at 10N.....	99
Figure 67 Wear rate of 303SS disks against alumina ball at 11cm s ⁻¹ and various normal loads.....	100
Figure 68 Sliding wear and coefficient of friction trends of 303SS against alumina ball at sliding speed 15cm s ⁻¹ and (a) at normal load 2N, (b) at 4N, (c) at 6N, (d) at 8N, and (e) at 10N.....	101
Figure 69 Wear rate of 303SS disks against alumina ball at sliding speed 15cm s ⁻¹ and various normal loads.....	101
Figure 70 Wear rate vs normal load of 303stainless steel against alumina.....	102
Figure 71 Wear rate vs sliding speed of 303stainless steel against alumina.	103
Figure 72 303SS against alumina, (a) SEM micrograph of the worn surface and (b) EDX analysis of the worn surface; at sliding speed 3cm s ⁻¹ and normal load 2N.	103
Figure 73 303SS against alumina, (a) SEM micrograph of the worn surface and b) EDX analysis of the worn surface; at sliding speed 7cm s ⁻¹ and normal load 4N.	104
Figure 74 303SS against alumina, (a) SEM micrograph of the worn surface and (b) EDX analysis of the worn surface; at sliding speed 11cm s ⁻¹ and normal load 4N.	104
Figure 75 303SS against alumina, (a) SEM micrograph of the worn surface and (b) EDX analysis of the worn surface; at sliding speed 15cm s ⁻¹ and normal load 8N.	104
Figure 76 Sliding wear and coefficient of friction trends of 303SS base TiC coatings disks against alumina balls at sliding speed 3cm s ⁻¹ and (a) at normal load 2N, (b) at 4N, (c) at 6N, (d) at 8N and (e) at 10N.	106
Figure 77 Wear rate of 303SS disks against alumina ball at sliding speed 3cm s ⁻¹ and various normal loads	107
Figure 78 Sliding wear and coefficient of friction trends of 303SS base TiC coatings disks against alumina balls at sliding speed 7cm s ⁻¹ and (a) at normal load 2N, (b) at 4N, (c) at 6N, (d) at 8N and (e) at 10N.	108
Figure 79 Wear rate of 303SS disks against alumina ball at sliding speed 7cm s ⁻¹ and various normal loads.	109
Figure 80 Sliding wear and coefficient of friction trends of 303SS base TiC coatings disks against alumina balls at 11cm. s ⁻¹ and (a) at normal load 2N, (b) at 4N, (c) at 6N, (d) at 8N, and (e) at 10N.	110
Figure 81 Wear rate of 303SS base TiC coatings disks against alumina ball at sliding speed 11cm s ⁻¹ and various normal loads.....	110
Figure 82 Sliding wear and coefficient of friction trends of 303SS against alumina ball at sliding speed 15cm s ⁻¹ and (a) at normal load 2N, (b) at 4N, (c) at 6N, (d) at 8N, and (e) at 10N.....	111
Figure 83 Wear rate of 303SS base TiC coatings disks against alumina ball at sliding speed 15cm s ⁻¹ and various normal loads.....	112
Figure 84 Wear rate vs normal load of 303SS base TiC coatings against alumina	112
Figure 85 Wear rate vs sliding speed of 303SS base TiC coatings against alumina.....	113

Figure 86 303SS base TiC coatings against alumina, (a) SEM micrograph of the worn surface and (b) EDX analysis of the worn surface; at 3 cm s ⁻¹ and 2 N.....	113
Figure 87 303SS base TiC coatings against alumina, (a) SEM micrograph of the worn surface and (b) EDX analysis of the worn surface; at 3 cm s ⁻¹ and 8 N.....	114
Figure 88 303SS base TiC coatings against alumina, (a) SEM micrograph of the worn surface and (b) EDX analysis of the worn surface; at 7 cm s ⁻¹ and 10 N.....	114
Figure 89 303SS base TiC coatings against alumina, (a) SEM micrograph of the worn surface and (b) EDX analysis of the worn surface; at 15cm s ⁻¹ and 6N.	114
Figure 90 303SS base TiC coatings against alumina, (a) SEM micrograph of the worn surface and (b) EDX analysis of the worn surface; at 11cm s ⁻¹ and 8N.	115
Figure 91 303SS base TiC coatings against alumina, (a) SEM micrograph of the worn surface and (b) EDX analysis of the worn surface; at 7cm s ⁻¹ and 8N.	115
Figure 92 Wear trends and coefficient of friction comparison of 303 stainless steel and TiC coatings against alumina, (a) wear trend of 303SS against alumina, (b) coefficient of friction of 303SS against alumina, (c) wear trend of TiC coatings against alumina, (d) coefficient of friction of TiC coatings against alumina, (e) coefficient of friction of 303SS against alumina for the range of normal loads and sliding speeds and (f) coefficient of friction of TiC coatings against alumina for the range of normal loads and sliding speeds	117
Figure 93 Wear rate of 303SS and 303SS base TiC coatings disks against alumina balls.	117
Figure 94 Wear rate of 303SS and 303SS base TiC coatings disks against alumina balls.	118
Figure 95 Wear rate of 303SS and 303SS base TiC coatings disks against alumina balls.	119
Figure 96 Wear rate of 303SS and 303SS base TiC coatings disks against alumina balls.	119
Figure 97 Total mass loss comparison of 303SS and 303SS base TiC coatings against alumina.	120
Figure 98 The optical micrograph of the cross-section of the wear tracks of TiC coating against alumina, (a) sliding speed 7 cm s ⁻¹ and normal load 10 N, (b) 11 cm s ⁻¹ and 10 N and (c) 15 cm s ⁻¹ and 10 N.....	121
Figure 99 Wear mode map, (a) 303SS against alumina and (b) 303SS base TiC coating against alumina	125
Figure 100 The wear mechanism map, (a) 303SS against alumina and (b) 303SS base TiC coating against alumina.	126
Figure 101 Wear mechanism map for 303stainless steel disk against 8620 low alloy steel (taken from chapter 4).	127
Figure 102 Wear rate of Ti pins and hardened steel disks against each other.	130
Figure 103 Wear rate of Ti pins and hardened steel disks against each other.	130
Figure 104 Wear rate of Ti pins and hardened steel disks against each other.	131
Figure 105 Wear rate of Ti pins and hardened steel disks against each other.	132
Figure 106 Wear rate of Ti pins and hardened steel disks against each other.	132
Figure 107 Wear rate of Ti pins against hardened steel disks.	133
Figure 108 Wear rate of Ti pins against hardened steel disks.	134
Figure 109 Wear rate of hardened steel disks against Ti pins.	134
Figure 110 Wear rate of hardened steel disks against Ti pins.	135
Figure 111 The total mass loss comparison of hardened steel disks and Ti pins.....	136

Figure 112 Coefficient of friction of Ti pins against hardened steel disks.	137
Figure 113 Coefficient of friction of Ti pins against hardened steel disks.	137
Figure 114 SEM micrographs of the worn surfaces of pins and wear tracks on the disks, (a) at normal load 20N and sliding speed 0.38m s^{-1} , (b) at 40N and 0.38m s^{-1} , (c) at 30N and 0.5m s^{-1} , (d) at 40N and 0.86m s^{-1} , (e) at 50N and 0.86m s^{-1} , (f) at 10N and 1.2m s^{-1} and (g) at 50N and 1.2m s^{-1}	139
Figure 115 EDX analysis of the worn surfaces of pins and wear tracks of the disks, (a) at normal load 20N and sliding speed 0.38m s^{-1} , (b) at 40N and 0.38m s^{-1} , (c) at 30N and 0.5m s^{-1} , (d) at 40N and 0.86m s^{-1} , (e) at 50N and 0.86m s^{-1} , (f) at 10N and 1.2m s^{-1} and (g) at 50N and 1.2m s^{-1}	140
Figure 116 SEM micrograph of wear debris of Ti against hardened steel, (a) at sliding speed 0.38m s^{-1} and normal load 20N, (b) at 0.38m s^{-1} and 50N, (c) at 0.5m s^{-1} and 50N, (d) at 0.86m s^{-1} and 30N, and (e) at 1.2m s^{-1} and 50N, and (f) at 1.5m s^{-1} and 30N.	142
Figure 117 EDX analysis of wear debris of Ti against hardened gauge (a) at sliding speed 0.38m s^{-1} and normal load 20N, (b) at 0.38m s^{-1} and 50N, (c) at 0.5m s^{-1} and 50N, (d) at 0.86m s^{-1} and 30N, and (e) at 1.2m s^{-1} and 50N, and (f) at 1.5m s^{-1} and 30N.	143
Figure 118 Wear mode maps (a) Ti pins against hardened steel disks and (b) hardened steel disks against Ti pins.	148
Figure 119 Wear mechanism maps, (a) Ti pins against hardened steel disks and (b) hardened steel disks against Ti pins.	149
Figure 120 Wear mechanistic maps for 303 SS against alumina (taken from chapter 5). ...	151
Figure 121 Wear rate of Ti base TiC composite coatings pins and hardened steel disks.	154
Figure 122 Wear rate of Ti base TiC coatings pins and hardened steel disks.	154
Figure 123 Wear rate of Ti base TiC coatings pins and hardened steel disks.	155
Figure 124 Wear rate of Ti base TiC coatings pins and hardened steel disks.	156
Figure 125 Wear rate of Ti base TiC coatings pins and hardened steel disks.	156
Figure 126 Wear rate of Ti base TiC coatings pins against hardened steel disks.	157
Figure 127 Wear rate of Ti base TiC coatings pins against hardened steel disks.	158
Figure 128 Wear rate of hardened steel disks against Ti base TiC coatings pins.	159
Figure 129 Wear rate of hardened steel disks against Ti base TiC coatings.	160
Figure 130 The total mass loss comparison of hardened steel disks and Ti base TiC coatings pins.	161
Figure 131 Coefficient of friction of Ti base TiC coatings pins against hardened steel disks.	162
Figure 132 Coefficient of friction of Ti base TiC coatings pins against hardened steel disks.	162
Figure 133 SEM micrographs of the worn surfaces of the TiC coatings pins and wear track of the hardened steel disks, (a) at normal load 30 N and sliding speed 0.38m s^{-1} , (b) at 50 N and 0.5m s^{-1} , (c) at 40 N and 0.86m s^{-1} , (d) at 50 N and 0.86m s^{-1} and (e) at 50 N and 1.5m s^{-1}	164
Figure 134 EDX analysis of the wear surfaces of the TiC coatings pins and wear track of the hardened steel disks, (a) at normal load 30 N and sliding speed 0.38m s^{-1} , (b) at 50 N and	

0.5 m s ⁻¹ , (c) at 40 N and 0.86 m s ⁻¹ , (d) at 50 N and 0.86 m s ⁻¹ and (e) at 50 N and 1.5 m s ⁻¹	165
Figure 135 SEM micrographs of wear debris of Ti base TiC coatings against hardened steel, (a) at sliding speed 0.38 m s ⁻¹ and normal load 30 N, (b) at 0.38 m s ⁻¹ and 30 N at high magnification, (c) at 0.5 m s ⁻¹ and 40 N point analysis, (d) at 0.5 m s ⁻¹ and 40 N point analysis, (e) at 0.5 m s ⁻¹ and 50 N, (f) at 0.86 m s ⁻¹ and 50 N, (g) at 1.2 m s ⁻¹ and 20 N high magnification, and (h) at 1.5 m s ⁻¹ and 50 N.....	166
Figure 136 EDX analysis of wear debris of Ti base TiC coatings against hardened steel, (a) at sliding speed 0.38 m s ⁻¹ and normal load 30 N, (b) at 0.38 m s ⁻¹ and 30 N at high magnification, (c) at 0.5 m s ⁻¹ and 40 N point analysis, (d) at 0.5 m s ⁻¹ and 40 N point analysis, (e) at 0.5 m s ⁻¹ and 50 N, (f) at 0.86 m s ⁻¹ and 50 N, (g) at 1.2 m s ⁻¹ and 20 N high magnification, and (h) at 1.5 m s ⁻¹ and 50 N.....	167
Figure 137 Optical micrographs of Ti base TiC coatings pins, (a) thickness of the coatings layer after grinding the surface of the coatings, (b) thickness of the coatings layer after test at sliding speed 1.2 m s ⁻¹ and normal load 50 N and (c) thickness of the coatings layer after test at sliding speed 1.5 m s ⁻¹ and normal load 40 N.....	169
Figure 138 Experimental errors (8%) for the Ti base TiC coatings pins against steel disks. .	169
Figure 139 Wear modes maps, (a) Ti base TiC coatings pins against hardened steel disks and (b) hardened steel disks against Ti base Tic coatings pins.....	174
Figure 140 Wear mechanisms maps, (a) Ti base TiC coatings pins against hardened steel disks and (b) hardened steel disks against Ti base Tic coatings pins.	175
Figure 141 Wear mode map for 303stainless steel base TiC composite coatings disk against alumina ball (taken from Chapter 5).	176
Figure 142 Wear rate of Ti and Ti base TiC coatings pins.	179
Figure 143 Wear rate of Ti and Ti base TiC coatings pins.	179
Figure 144 Wear rate of Ti and Ti base TiC coatings pins.	180
Figure 145 Wear rate of Ti and Ti base TiC coatings pins.	181
Figure 146 Wear rate of Ti and Ti base TiC coatings pins.	181
Figure 147 Wear rate of Ti pins against hardened steel disks	182
Figure 148 Wear rate of Ti pins against hardened steel disks.	183
Figure 149 Wear rate of Ti base TiC coatings pins against hardened steel disks.....	183
Figure 150 Wear rate of Ti base TiC coatings pins against hardened steel disks.....	184
Figure 151 The total mass loss comparison of Ti and Ti base TiC coatings against hardened steel.	185
Figure 152 Coefficient of friction of Ti pins against hardened steel disks.	186
Figure 153 Coefficient of friction of Ti pins against hardened steel disks.	187
Figure 154 Coefficient of friction of Ti base TiC coatings pins against hardened steel disks.	187
Figure 155 Coefficient of friction of Ti base TiC coatings pins against hardened steel disks.	188
Figure 156 SEM micrographs of the worn surfaces of the Ti and Ti base TiC composite coatings pins against hardened steel disk, (a) at normal load 30 N and sliding speed 0.38 m	

s ⁻¹ , (b) at 50 N and 0.5 m s ⁻¹ , (c) at 40 N and 0.86 m s ⁻¹ , (d) at 20 N and 1.2 m s ⁻¹ , (e) at 50 N and 1.5 m s ⁻¹ and (f) at 50 N and 0.86 m s ⁻¹	189
Figure 157 EDX analysis of the worn surfaces of Ti and Ti base TiC composite coatings pins against hardened steel disk, (a) at normal load 30 N and sliding speed 0.38 m s ⁻¹ , (b) at 50 N and 0.5 m s ⁻¹ , (c) at 40 N and 0.86 m s ⁻¹ , (d) at 20 N and 1.2 m s ⁻¹ , (e) at 50 N and 1.5 m s ⁻¹ and (f) at 50 N and 0.86 m s ⁻¹	191
Figure 158 SEM micrograph of the wear debris of Ti and Ti base TiC coatings against hardened steel (a) at sliding speed 0.38 m s ⁻¹ and normal load 30 N, (b) at 0.38 m s ⁻¹ and 50 N, (c) at 0.5 m s ⁻¹ and 50 N, (d) at 0.86 m s ⁻¹ and 30 N and (e) at 1.5m s ⁻¹ and 50 N.	193
Figure 159 EDX analysis of the wear debris of Ti and Ti base TiC composite coatings against hardened steel,(a) at sliding speed 0.38 m s ⁻¹ and normal load 30 N, (b) at 0.38 m s ⁻¹ and 50 N, (c) at 0.5 m s ⁻¹ and 50 N, (d) at 0.86 m s ⁻¹ and 30 N, and (e) at 1.5 m s ⁻¹ and 50 N.	194
Figure 160 Optical micrographs of Ti base TiC coatings, (a) thickness of the coatings layer prior to test, (b) thickness of the coatings layer after 1.2 m s ⁻¹ sliding speed and 50 N normal load, b) thickness of the coatings layer after 1.5 m s ⁻¹ sliding speed and 40 N.	196
Figure 161 Wear modes maps, (a) Ti pins against hardened steel disks and (b) Ti base TiC coatings pins against hardened steel.	202
Figure 162 Wear mechanism maps, (a) Ti pins against hardened steel disks and (b) Ti base TiC coatings pins against hardened steel.	203

Table of Contents

Abstract.....	i
The objective of this study	iii
Structure of the thesis.....	iv
Declaration.....	v
Journal publications	v
Acknowledgements.....	vi
Dedication	vi
Chapter 1	1
Introduction	1
Chapter 2	10
Literature Review (tribo-corrosion).....	10
2.2. Tribology	11
2.3. Wear.....	13
2.4 Testing Methods	13
2.4.1 Symmetrical arrangement.....	13
2.4.2 Asymmetrical arrangement.....	14
2.5 Unlubricated wear of metals	14
2.6 Mechanisms of Sliding Wear	16
2.6.1. Adhesive Wear	16
2.6.2. Abrasive Wear	22
2.6.3. Fatigue Wear	27
2.6.4. Impact Wear.....	29
2.7 Corrosion.....	32
2.8 Tribo- corrosion.....	32
2.8.1. Mild- oxidation	34
2.8.2. Severe-oxidation	35
2.8.3 Modes of wear	35
2.9 Wear-regime maps.....	37
2.10 wear of coatings.....	44
2.11. Friction	46

2.11.1 The Laws of Friction.....	46
2.11.2 Causes of Friction	48
2.12 Friction of Materials	49
2.12.1 Friction of Metals and Alloys	49
2.12.2 Effect of Operating Conditions	50
2.12.3 Friction of Ceramic Materials	52
2.13 Wear in relation to friction.....	54
Chapter 3	55
Experimental Methodology	55
3.1. Pin-on-Disk sliding wear testing rig (ASTM G99)	55
3.1.1. Introduction	55
3.1.2. General apparatus description	55
3.1.3. Significance and use	56
3.1.4. Testing apparatus (pin-on-disk sliding wear testing rig)	56
3.1.5. Function and calibration of load cell	57
3.1.6. Control system	59
3.2. Experimental	60
3.2.1. Calculations of frequency and experimental times	60
3.2.2. Test specimens	62
3.2.3 Test parameters	62
3.2.4. Test procedure	62
3.2.5. Calculation of wear and reporting.....	63
3.3 303stainless steel against 8620 low alloy steel	64
3.3.1 Experimental conditions.....	64
3.3.2 Materials	64
3.4 303stainless steel uncoated and coated with titanium carbide composite coating against alumina	65
3.4.1 Experimental conditions.....	65
3.4.2 Materials	66
3.5 Titanium uncoated and coated with titanium carbide composite coatings against hardened steel (A.I.S.I. 0-1-Ground Flat Stock)	66
3.5.1 Experimental conditions.....	66
3.5.2 Materials	67

3.6 Tungsten Inert Gas (TIG) Melting Coatings procedure	68
3.6.1. TiC powder pre-placement process.....	68
3.6.2. TiC powder placement	68
3.6.3 303SS base titanium carbide composite coating by TIG welding torch melting method.....	69
3.6.4 Optical Micrographs and EDX analysis of the specimens	69
3.6.5. Titanium base titanium carbide composite coatings by TIG welding torch melting method.....	70
3.6.6 Optical Micrographs and EDX analysis of the coated surface.....	70
3.6.7 Integrity of the coatings	71
3.6.8 Mapping tribo-corrosion	71
3.7. Experimental Error and Uncertainty	72
Chapter 4	75
High and zero Cr contents steel in dry sliding contact	75
4.1. Introduction	75
4.2. Tests results	75
4.2.1. Wear at 0.38m s ⁻¹ sliding speed for the range of normal loads	75
4.2.2. Wear at 0.5m s ⁻¹ sliding speed for the range of normal loads	76
4.2.3. Wear at 0.86m s ⁻¹ sliding speed for the range of normal loads	77
4.2.4. Wear at 1.2m s ⁻¹ sliding speed for the range of normal loads.....	78
4.2.5. Wear at 1.5m s ⁻¹ sliding speed for the range of normal loads	79
4.2.6. Mass loss of 303SS disks against 8620 low alloy steel pins at different constant sliding speeds and various normal loads	80
4.2.7. Mass loss of 303SS disks against 8620 low alloy steel pins at different constant normal loads and various sliding speeds	80
4.2.8. Mass loss of 8620 low alloy steel pins against 303SS disks at different constant sliding speeds and various normal loads	81
4.2.9. Mass loss of 8620 low alloy steel pins against 303SS disks at different constant normal loads and various sliding speeds	82
4.2.10. Total mass loss comparison.....	83
4.2.11. SEM micrographs of the worn surfaces.....	83
4.2.12. EDX analysis of the worn surfaces	84
4.3. Discussion.....	84
4.3.1. Wear Mechanisms.....	84

4.3.2. Wear regimes and wear maps	89
4.4. Links between Lim and Ashby [69] wear diagram and present work	91
4.5. Conclusions	92
Chapter 5	95
Wear maps for titanium carbide composite based coatings deposited on 303stainless steel	95
5.1 Introduction	95
5.2. Wear tests results of 303stainless steel (uncoated and coated with TiC composite coatings) disks against alumina balls.....	95
5.2.1. Wear rate of 303SS against alumina at 3 cm s ⁻¹ for the range of normal loads ...	96
5.2.2. Wear rate of 303SS against alumina at 7 cm s ⁻¹ for the range of normal loads ...	97
5.2.3. Wear rate of 303SS against alumina at 11cm s ⁻¹ for the range of normal loads ..	98
5.2.4. Wear rate of 303SS against alumina at 15cm s ⁻¹ for the range of normal loads	100
5.2.5. Wear rate of 303stainless steel against alumina at constant sliding speeds and various normal loads	102
5.2.6. Wear rate of 303stainless steel against alumina at constant normal loads and various sliding speeds	102
5.2.7. SEM micrographs and EDX analysis of worn surfaces of 303SS against alumina	103
5.2.8 Wear behaviour of 303SS against alumina	105
5.3. Wear tests results of 303SS base TiC composite coatings disks against alumina balls	106
5.3.1. Wear rate of 303SS base TiC coatings against alumina at 3cm s ⁻¹ for the range of normal loads	106
5.3.2. Wear rate of 303SS base TiC coatings against alumina at 7cm s ⁻¹ for the range of normal loads	107
5.3.3. Wear rate of 303SS base TiC coatings against alumina at 11cm s ⁻¹ for the range of normal loads	109
5.3.4. Wear rate of 303SS base TiC coatings against alumina at 15cm s ⁻¹ for the range of normal loads	110
5.3.5. Wear rate of 303SS base TiC against alumina at constant sliding speeds and various normal loads	112
5.3.6. Wear rate of 303SS base TiC coatings against alumina at constant normal loads and various sliding speeds.....	113
5.3.7. SEM micrographs of the worn surface of 303SS base TiC coatings against alumina	113

5.3.8 Wear behaviour of 303SS base TiC composite coatings against alumina	115
5.4. Dry sliding wear behaviour of 303SS (uncoated and coated with TiC) against alumina	116
5.4.1 Wear trend and coefficient of friction of 303SS (uncoated and coated with TiC) against alumina	116
5.4.2. Wear rate comparison of 303SS (uncoated and coated with TiC) against alumina at 3 cm s ⁻¹	117
5.4.3. Wear rate comparison of 303SS (uncoated and coated with TiC) against alumina at 7 cm s ⁻¹	118
5.4.4. Wear rate comparison of 303SS (uncoated and coated with TiC) against alumina at 11 cm s ⁻¹	118
5.4.5. Wear rate comparison of 303SS (uncoated and coated with TiC) against alumina at 15 cm s ⁻¹	119
5.4.6 Total mass loss comparison of 303SS uncoated and coated against alumina	120
5.4.7. Optical micrograph of 303SS base TiC composite coatings worn surfaces against alumina	120
5.4.8. Sliding wear comparison of 303SS (uncoated and coated with TiC composite coatings) against alumina.....	121
5.5. Discussion.....	122
5.5.1. Wear mechanisms of 303SS (uncoated and coated with TiC composite coatings) against alumina	122
5.5.2. Wear regimes and maps.....	125
5.5.3. Wear mode maps	125
5.5.4. Wear mechanism maps.....	126
5.5.5. Wear mechanisms and regimes for 303SS base TiC coatings	126
5.6. Comparison between wear mechanism maps for 303SS sliding against low alloy steel	127
5.7. Conclusions	128
Chapter 6	129
Titanium against hardened steel (A.I.S.I. 0-1-Ground Flat Stock) in dry sliding.....	129
6.1. Introduction	129
6.2. Sliding wear tests results.....	129
6.2.1. Wear rate at 0.38 m s ⁻¹ sliding speed for the range of normal loads.....	129
6.2.2. Wear rate at 0.5 m s ⁻¹ sliding speed for the range of normal loads.....	130
6.2.3. Wear rate at 0.86 m s ⁻¹ sliding speed for the range of normal loads.....	131

6.2.4. Wear rate at 1.2m s ⁻¹ sliding speed for the range of normal loads.....	131
6.2.5. Wear rate at 1.5 m s ⁻¹ sliding speed for the range of normal loads.....	132
6.2.6. Wear rate of Ti against hardened steel at constant sliding speeds and various normal loads	132
6.2.7. Wear rate of Ti against hardened steel at constant normal loads and various sliding speeds.....	133
6.2.8. Wear rate of hardened steel against Ti at constant sliding speeds and various normal loads	134
6.2.9. Wear rate of hardened steel against Ti at constant normal loads and various sliding speeds.....	135
6.2.10. Total mass loss comparison.....	135
6.2.11. Coefficient of friction of Ti pins against hardened steel disks	136
6.2.12. SEM of Ti pins and hardened steel disks against each other	138
6.2.13. EDX analysis of Ti pins and hardened steel disks against each other	139
6.2.14. SEM micrograph of the wear debris	142
6.2.15. EDX analysis of the wear debris.....	143
6.3. Discussion.....	144
6.3.1. Wear mechanisms and regimes	144
6.3.2. Wear regimes and wear maps.....	148
6.3.3. Wear mode maps	148
6.3.4. Wear mechanism maps.....	149
6.4. Wear mechanisms Comparison between Ti sliding against hardened steel counterface and 303SS sliding against alumina counterface [Chapter 5]	151
6.5. Conclusions	151
Chapter 7	153
Titanium base titanium carbide composite coatings in tribological contact	153
7.1. Introduction	153
7.2. Dry sliding wear tests results.....	153
7.2.1. Wear rate at 0.38m s ⁻¹ sliding speed for the range of normal loads.....	153
7.2.2. Wear rate at 0.5m s ⁻¹ sliding speed for the range of normal loads	154
7.2.3. Wear at 0.86m s ⁻¹ sliding speed for the range of normal loads	155
7.2.4. Wear at 1.2m s ⁻¹ sliding speed for the range of normal loads	155
7.2.5. Wear at 1.5 m s ⁻¹ sliding speed for the range of normal loads	156

7.2.6. Wear rate of Ti base TiC coatings against hardened steel at constant sliding speeds and various normal loads	157
7.2.7. Wear rate of Ti base TiC coatings against hardened steel at constant normal loads and various sliding speeds	157
7.2.8. Wear rate of hardened steel against Ti base TiC coatings at constant sliding speeds and various normal loads	158
7.2.9. Wear rate of hardened steel against Ti base TiC coatings at constant normal loads and various sliding speeds	159
7.2.10. Total mass loss comparison of Ti base TiC coatings pins and hardened steel disks	160
7.2.11. Coefficient of friction of Ti base TiC coatings pins against hardened steel disks	161
7.2.12. SEM micrographs of Ti base TiC coatings pins and hardened steel disks worn surfaces	162
7.2.13. EDX analysis of Ti base TiC coatings pins and hardened steel disks worn surfaces	164
7.2.14. SEM micrographs of wear debris of Ti base TiC coatings pins against hardened steel disks	165
7.2.15. EDX analysis of wear debris of Ti base TiC coatings pins against hardened steel disks	166
7.2.16. Optical micrographs of coatings layers on Ti pins	168
7.2.17 Experimental error	169
7.3. Discussion.....	170
7.3.1. Wear mechanisms and regimes	170
7.3.2 Wear mode regimes and maps.....	173
7.3.3 Wear mechanism regimes and maps	174
7.4. Wear modes comparison between Ti base TiC coatings sliding against hardened steel counterface and 303SS base TiC coatings sliding against alumina counterface [Chapter 5]	176
7.4. Conclusions	176
Chapter 8	178
Tribo-corrosion maps for titanium uncoated and coated with titanium carbide composite coatings.....	178
8.1. Introduction	178
8.2. Wear tests results	178
8.2.1 Wear at 0.38 m s^{-1} sliding speed for the range of normal loads	178

8.2.2. Wear at 0.5 m s ⁻¹ sliding speed for the range of normal loads	179
8.2.3. Wear at 0.86 m s ⁻¹ sliding speed for the range of normal loads	180
8.2.4. Wear at 1.2 m s ⁻¹ sliding speed for the range of normal loads	180
8.2.5. Wear at 1.5 m s ⁻¹ sliding speed for the range of normal loads	181
8.2.6. Wear rate of Ti against hardened steel at constant sliding speeds and various normal loads	182
8.2.7. Wear rate of Ti against hardened steel at constant normal loads and various sliding speeds	182
8.2.8. Wear rate of Ti base TiC coatings against hardened steel at constant sliding speeds and various normal loads	183
8.2.9. Wear rate of Ti base TiC coatings against hardened steel at constant normal loads and various sliding speeds	184
8.2.10. Total mass loss comparison.....	185
8.2.11. Coefficient of friction during sliding of Ti pins against hardened steel disks ...	186
8.2.12. Coefficient of friction of Ti base TiC coatings pins against hardened steel disks	187
8.2.13 SEM micrographs of the worn surfaces of Ti and Ti base TiC coatings pins against hardened steel disks	188
8.2.14 EDX analysis of the worn surfaces of Ti and Ti base TiC coatings pins against hardened steel disks	190
8.2.15 SEM micrographs of wear debris of Ti and Ti base TiC coatings pins against hardened steel disks	192
8.2.16 EDX analysis of wear debris of Ti and Ti base TiC coatings pins against hardened steel disks.....	193
8.2.17. Optical micrographs of coatings layers on Ti pins	195
8.3. Discussion.....	196
8.3.1 Wear mechanisms and regimes	196
8.3.2 Wear mode regimes and maps.....	200
8.3.3 Wear mechanism regimes and maps	202
8.4. Conclusion.....	204
Chapter 9	206
Conclusions and future work	206
9.1 Conclusions	206
9.2 Future work.....	207
References	209

Annexure.....220

Chapter 1

Introduction

Tribo-corrosion describes the combined action of wear and corrosion [1]. It occurs in many conditions ranging from energy conversion environments to bio-medical conditions. In the latter case, tribo-corrosion has been identified as an issue affecting wear of artificial hip joints in body fluids. Progress in the understanding of tribo-corrosion has led to the description of the wear-corrosion process in terms of regimes. These regimes enable the degradation to be classified in terms of wear or corrosion dominated behaviour. Such an analysis provides a means of generating tribo-corrosion maps of the overall regimes encountered. Tribo-corrosion resistance can be increased by development and using the different methods and techniques of surface engineering.

The name tribo corrosion expresses the underlying disciplines of tribology and corrosion. Tribology is concerned with the study of friction, lubrication and wear and corrosion is concerned with the chemical and electrochemical interactions between a material, normally a metal, and its environment. As a field of research tribo-corrosion is relatively new, but tribo-corrosion phenomena have been around ever since machines and installations are being used.

Wear is a mechanical material degradation process occurring on rubbing or impacting surfaces, while corrosion involves chemical or electrochemical reactions of the material. Corrosion may accelerate wear and wear may accelerate corrosion [2]. One then calls, corrosion accelerated wear or wear accelerated corrosion. Both these phenomena, as well as fretting-corrosion (which results from small amplitude oscillations between contacting surfaces) fall into the broader category of tribo-corrosion. Erosion-corrosion is another tribo-corrosion phenomenon involving mechanical and chemical effects: impacting particles or fluids erode a solid surface by abrasion, chipping or fatigue while simultaneously the surface corrodes [3].

Wastage as a result of the combined effects of wear and corrosion occurs in many environments, ranging from offshore to the healthcare industries. In such cases, the degradation is dependent on a wide range of parameters relating to the materials in

contact and the nature of the corrosive environments. Defining conditions in which the wastage is minimized is critically important for engineers charged with monitoring such processes. The nature of the tribological contact plays a critical role in determining the effect of corrosion on the wastage rate. In some cases, as in sliding wear, frictional heating may arise at high velocities and applied loads, leading to oxide film formation, even at room temperatures. In other cases, as in solid particles erosion, frictional heating may play a significant role only at very high fluxes of particles impact. The action of a corrosive medium, either in gaseous or in liquid form, thus may have very different effects on such diverse tribological processes [4].

Dry corrosion occurs in the absence of moisture, water and solution to aid corrosion. The metals, in such a situation, interact with gaseous environment and oxidize in this atmosphere. This process is very sensitive to temperature. Wear is a complex phenomenon it occurs whenever surfaces come into sliding contact. During dry sliding contact of metallic pairs, a tangential force i.e. frictional traction will be experienced at the interface. This force works on each of the rubbing surfaces. A portion of that work is used for plastic deformation of the sub-contact layer of the both rubbing materials. A major amount of that work (friction force) is converted to thermal energy [5]. Any accumulation of thermal energy tends to maximize the potential energy at the interface. In order to re-establish the stability (equilibrium) of the system, the mating materials respond in shape of oxidation, microstructural changes, plastic deformation, adhesion, cracks initiating, wear debris generation, transition in wear mechanisms, etc. [6].

It has been observed in the literature that during sliding wear [7], the variation of friction and wear rate depend on interfacial conditions such as normal load, geometry, relative surface motion, sliding speed, surface roughness of the rubbing surfaces, type of material, system rigidity, temperature, stick slip, relative humidity, lubrication and vibration. Among these considerations, sliding speed and normal load are the two major factors that play a significant role in the variation of friction and wear rate. The loss of material during sliding wear occurs due to formation of wear debris particles and their removal from the interface. Once generated, a wear debris particle is assumed to be removed from the rubbing surface, causing wear. However, in a real tribo-system, the debris can be trapped in the wear tracks and become involved in the sliding processes, significantly affecting the total wear loss [8-10].

Transitions in wear rates from initial severe wear to a mild wear has been widely found for sliding wear of metals [11]. Such a transition is caused by different parameters, such as reductions in sliding speed [12], normal load [13] and high rates of oxidation [14-15]. For many metals and alloys, a transition temperature is observed [15-18]; above this temperature, the wear rate in mild wear area decreases rapidly with the increase of temperature and smooth oxide layer 'glaze' is formed on the wear tracks [19]. This oxide layers also act as a solid lubricant and prevents metal-metal contact of the mating sliding surfaces. This tribo-oxidation process reduce the coefficient of friction and wear rate of the metals as compared to that of the same pair in vacuum (inert) environments [6,8-9,20].

Early considerations revolved around the notion of plasticity (hardness) at contact zones and it was realized for metals that large plastic strains have to be incurred at the contact before a particle can be fractured from the bulk. For adhesive and abrasive wear processes, it was shown that the material removed in both events is directly proportional to the sliding distance and the normal load and is inversely proportional to the hardness [21]. However, extensive experimental work, for a variety of metals [22-24] demonstrated that the wear rates, when measured over a wide range of normal loads and sliding speeds, show sharp transitions and non-linear trend with respect to the changes in normal load and sliding speed. The inverse linear relationship with respect to hardness was also found to break down at lower loads and higher speeds [25], as well as when the metals were alloyed and heat treated [26]. In the literature, not surprisingly given the above observations, although many mathematical models of sliding wear have been proposed, there is little agreement on the development of a universal wear equation which would be widely applicable [27-30].

In the unlubricated sliding wear of steels, adhesive and oxidative wear are widely occurred. These can lead to mild or severe wear depending on the lubricating mechanisms of the oxide scale [10]. Early studies on these mechanisms were conducted by Hirst and co-workers [11, 22, 31], who provided a complete characterization of wear mechanisms. In the case of adhesive wear, there is a strong interaction of asperities and plastic deformation. On the contrary, when oxidation rates are relatively high, the formation of oxide films inhibits metallic contact and, therefore, adhesion between surfaces. Thus, a decrease in the interfacial shear strength of sliding surfaces is obtained [32]. Mild wear results in dark and smooth surfaces, commonly termed "glaze layers" [8], while severe wear results in bright

and rougher surfaces. Small and fine oxide powdery wear debris particles are produced in oxidative wear while adhesive wear is characterized by larger and metallic wear debris. Differences in wear rates as much as three orders of magnitude are recorded [14, 22]. Wear regimes are highly dependent on variables, such as normal load, sliding speed, material properties and atmospheric conditions. Transitions in wear regimes can take place when there is a very slight change in one of these variables [34].

Quinn introduced the mild-oxidative wear model based on flash temperature concept [35-37]. According to his model, mild-oxidative wear occurs as long as an oxide layer could protect the contacting surfaces and severe-oxidation wear occurs only when the rate of oxide removal exceeds the rate of oxide formation. Later, Hong and Winer proposed the numerical oxidational wear model based on the linear oxidation wear kinetics [38]. They postulated that linear oxidation kinetics exist in sliding, where oxide growth on asperities is continuously disturbed by spalling and removal of these oxide layers. Hong et al. studied the frictional behaviour of titanium sliding against alumina [39]. They observed that presence of TiO₂ layer reduced the coefficient of friction for few order by avoiding the direct contact of the sliding surfaces of titanium and alumina. Garbar found that oxidation wear is the predominant mechanism when structural changes are minimal at the sliding surfaces [40]. He also explained that, as the normal load increases, tribo-oxidation is accompanied by the mechanism of plastic deformation.

During continued sliding, the initial transferred fragments are deformed, fractured and blended, leading to formation of mechanically mixed material layer on the sliding surfaces. Typical sliding wear debris particles come from this modified material [41]. M. Kerridge performed experimental work with a radioactive, annealed steel pin rubbing against a hardened steel ring to compare the amount of wear with the amount of metal transferred from one surface to the other by welding [42]. He concluded that the wear process consisted of three stages: transfer of metal due to adhesion, oxidation of the transferred layer due to frictional heating, and the subsequent removal of the oxide to form a loose wear-product (wear debris). M. Antler observed that unsymmetrical transfer often occurs when mating surfaces are not geometrically identical, and, indeed, many basic investigation of dry or boundary lubrication involve apparatus having such geometry, e.g., rider-flat or rider-ring machines [43]. It has been shown that the metals used and the experimental

Tribo-corrosion maps for steels, titanium and titanium carbide materials

conditions determine details of the rubbing process, whether it is in 'mild' or 'severe' regimes, and whether a transition occurs between them during a run [11].

More readily different metal transfer behaviour has been seen in air combination, and the various causes are being explained. Kerridge and Lancaster and De Gee and Zaat investigated the tribo-couple of dissimilar metals like soft copper alloy riders on hard steel rings. They found transfer from soft rider to hard steel ring followed by wear by loss of transferred material [45-46]. Brown and Armarego observed transfer from soft steel flats to hard steel riders followed by back transfer to the soft flats, along with reduction in friction and wear of the rider [47]. Cocks and Antler used riders and rings of the same metal, and found transfer of material from the larger to the smaller surface, following the wear of metal from the latter [48-49].

The applications of the titanium and its alloys are continuously increasing in the aircraft & aerospace industries, chemical industry, power engineering, environmental protection devices construction, osseous surgery and others due to their properties such as high strength, low density, good high temperature properties, biocompatibility and high corrosion resistance [50-158]. Titanium and its alloys, however, suffer from limitations such as poor frictional properties, relatively low hardness, wear resistance, inability to work hardening and to form oxide protective layer that have limited their use in a number of industries [158]. Moreover, metals, like 303 stainless steel, titanium etc. experience significant material transfer when slide against harder counterface. The wear resistance of these materials can be increased by development and using the different methods and techniques of surface engineering [50]. The alloyed and heat treated (coated) metals behave differently than that of the bulk materials in tribological applications.

Coatings deposited on the surfaces of different substrates susceptible to wear, increase the operating life and range of the operating conditions for which they may be used. In tribo-engineering applications, especially where components undergo sliding wear, metals with lower hardness, inability to form protective layer of oxide and with inability of strain hardening exhibit poor tribological properties such as low sliding wear resistance, unstable friction qualities, surface damage, adhesive wear, delaminated wear, ploughing wear, and plastic deformation. Studies on the wear behaviour of untreated and treated surfaces of different materials show that the tribological properties of the treated surfaces are increased and exhibit excellent wear resistance compared to that of the untreated surfaces

Tribo-corrosion maps for steels, titanium and titanium carbide materials

of the same material [51]. These techniques include thermal spray [173], electron beam [174], laser processing [137], physical vapour deposition (PVD), chemical vapour deposition (CVD) [42] and ion implantation. PVD, CVD and ion implantation are limited in producing thin coatings. While laser and electron beam processing methods can produce thick coatings which are more suitable for tribological applications. All these coatings methods and techniques are expensive and require specific conditions, e.g. high vacuum. To overcome such problems, a few researchers have used TIG process to produce hard coatings on different substrates [45-46]. This metal coating technique has significant advantages over methods mentioned above such as simple instrument, ease of operation, and low net cost. Nevertheless, this method has a number of drawbacks; powders are lost while argon gas is blown to the melting pool and preparation and application of powder paste on large specimens is a very difficult process. In addition, in some papers organic binders are utilized for protection of powders against argon flow. These binders are easily evaporated during the coating process and trapped in the melt and subsequently, produce pores in the coatings.

During dry sliding of uncoated 303 stainless steel and titanium, it was found that there was significant material transfer onto the harder counterface during sliding. The same results were found during the study of friction and wear thresholds of alumina- chromium steel pairs sliding at high speeds in dry conditions [54] and for the other materials [45-47]. It was observed that uncoated substrates showed very poor resistance to wear against their harder counter-faces. Titanium carbide coatings have found widespread application owing to its excellent hardness, at both room and elevated temperatures [5-57]. In some situations, a ceramic coating decreases the coefficient of friction during dry sliding, thereby resulting in decreased temperature rise and reduced adhesion at the interface, both of which promote the decrease in wear rate [56-58].

The sliding friction and wear behaviour of a ceramic coating depends upon the characteristics of the coating such as hardness, thickness, internal stress level, and load bearing capacity. When a coating cools from the high temperature of the deposition process, the internal stress within the coating is generally compressive. The compressive stress reduces the extent of surface fracture and thus increases sliding wear resistance of the coated surface [55, 59]. There is also shear stress induced between the coating and substrate. The shear stress promotes spalling of the coating during sliding wear [56]. The

Tribo-corrosion maps for steels, titanium and titanium carbide materials

ability of a coating-substrate system to withstand such stresses without spalling or cohesion failure of the coating is referred to as its load-bearing capacity [59-60]. A higher load-bearing capacity has been attributed to increased sliding wear resistance [59-60]. Several wear mechanisms have been proposed for different coating-substrate systems. These are ploughing, micro polishing, cohesive failure or fragmentation, spalling [59-60], flake formation [61], removal of hard particle phase and binder extrusion [57]. Kitsunai et al. [61] demonstrated that the wear mechanisms change with the severity of contact conditions. However, in many cases, the conditions and regimes where the coating retains integrity are not well understood.

Many different mechanisms have been proposed for the mild wear and severe wear of metals and coatings. It is very difficult to identify that which wear mechanisms may be operating in a particular situation. The critical examination of the worn surfaces and the wear debris can be useful tool to identify the mechanism of wear. By using the SEM, optical microscopy and the analytical techniques, such as EDX of the worn surface and wear debris, the wear mechanisms can be identified for any couple of metals of a tribo-system. Plate-like (flake) metallic debris particles come from severe sliding wear while fine particles of oxide come from mild wear during sliding wear of metals [63].

To the designers and engineers who have to make optimal decisions in situations where tribological considerations are significant, it is important for them to have a ready access to information pertaining to the fundamental understanding of the wear processes of interest. Some kind of user-friendly databases would be most helpful here. These databases should be able to provide the appropriate information for materials selection and choice of the suitable (optimal) operating conditions – such as contact geometry, speed and environment for a particular pair of materials in tribological contact.

There are many ways of presenting wear data. The more common modes of presentation include the tabulation of the wear rates and elucidation of the dominant mechanisms of wear observed under the sliding conditions of interest, the latter usually being accomplished through the presentation of micrographs showing the features on the worn surfaces. However, these presentations tend to be restrictive in the sense that they usually cover a relatively narrow (localised) range of the sliding conditions. This can be adequate and a more complete approach is perhaps through the linking of the wear rates and wear mechanisms over a much wider range of sliding conditions in the form of a wear-

Tribo-corrosion maps for steels, titanium and titanium carbide materials

mechanism map. Such a map not only provides a multi-dimensional graphical presentation of wear data, it also provides an overall framework for the wear behaviour of a particular sliding system into which individual wear mechanisms observed under various sliding (operating) conditions may be fitted [63-64].

Many names have been given to diagrams which describe the overall behaviour of wear; the more commonly used ones include wear-mechanism map, wear-mode map, wear-transition map, and wear-regime map. Generally, wear-mode, wear-transition and wear-regime maps tend to focus on the description of the mode of wear, namely mild wear, severe wear and the transition between them. In the case of wear-mechanism maps, details of the dominant wear mechanisms are given and the regions of their dominance are indicated; often, predicted rates of wear are also included in the maps [63]; the mechanistic changes on the worn surfaces of specimen and the counterface over a range of operating conditions [65] are included as well. Wear mode maps identify the mode of degradation and establish the level of wastage rate and potential "safe" and "unsafe" operation conditions for materials [66]. Wear mechanistic maps show the different wear mechanisms for various combinations of sliding speeds and normal loads for different materials sliding against each other under dry sliding conditions (in this case) on the basis of wear rate, surface damage and wear mechanism information [67]. They link the observed wear mechanisms to the actual conditions. These maps demonstrate clearly that transitions from one dominant wear mechanism to another may be related to the changes in measured wear rates [65].

A systematic approach to examine the observations of a tribo-system system over wide ranges of sliding speed and normal load was first adopted by Welsh in studies on mild steel sliding wear [68]. He observed the order of magnitude changes in the wear rate and wear mechanism with small changes in normal load or sliding speed. These effects were summarised on normal load vs sliding speed to develop empirical wear map to present a convenient way for predicting wear behaviour. Later on wear mechanism maps approaches have been adopted for a wide variety of material combinations including steel-on-steel [69], steel against nitride steel [70], ceramic wear [71], aluminium alloys [72], aluminium metal matrix composites [73], and TiN-coated high speed steel [67,74]. The effect of frictional heating on sliding wear mechanisms such as oxidation and seizure has also received much attention in the literature [67, 72, 75-76].

In the present study, experimental research work was carried out on the tribo-corrosion behaviour of uncoated and titanium carbide composite coatings produced by Tungsten Inert Gas (TIG) welding torch melting process on 303 stainless steel and titanium (Ti) substrates. Different metals, such as 303 stainless steel against 8620 low alloy steel against each other, 303 stainless steel uncoated and coated with titanium carbide composite coatings against alumina, and titanium uncoated and coated with titanium carbide composite against hardened steel (A.I.S.I. 0-1-Ground Flat Stock), were tested for dry sliding wear on a pin-on-disk sliding wear testing rig in air under ambient conditions at room temperature. The effects of change in sliding speeds and normal loads on wear behaviour of uncoated and coated materials' were investigated and tribo-corrosion maps were constructed with a tribo-system approach. The integrity of TiC composite coatings produced by TIG process was compared with respect to substrates and other coatings produced by different methods, found in the literature. Despite such studies above, there have been few investigations carried out of the wear mechanism map for both components of the tribological contact, i.e. the pins and disks. The Present work addresses this issue as well, by investigating the sliding wear modes and wear mechanisms of both specimen and counterface by wear maps techniques.

The TiC composite coatings, produced by TIG welding torch melting process, proved to be very effective to increase the wear resistance of the base materials. The increase in wear resistance occurred by several order of the magnitude compared with that of the substrates. The higher hardness of TiC particles and low adhesion of the composite coated surfaces to the counterface are attributed to the high wear resistance of the coatings. Due to the presence of the coatings, the mild wear regime expanded to a higher range of sliding speeds and normal loads with an additional wear mode i.e. very mild wear and with an elimination of the severe wear mode. The higher wear resistance of the Ti base TiC composite coatings than that of 303SS base TiC composite coating is attributed to the dense structure with low porosity of the coatings and the absence of cracking as the substrate and coating system have closer/favourable coefficient of thermal expansion.

Chapter 2

Literature Review (tribo-corrosion)

Tribo-corrosion is the term which describes the interaction between tribological actions with corrosion. Tribology is concerned with the study of friction, lubrication and wear, while corrosion is concerned with the chemical and electrochemical interactions between a material, normally a metal, and its environment. Wear by this process may include adhesive wear, abrasive wear, erosion by solid particles or liquid impact, or cavitation, fretting or fatigue along with corrosion. In the case, where corrosion occurs on metal at high temperature is called dry corrosion. In aqueous conditions, corrosion is an electrochemical process occurs at room temperature whereby any reaction will contain two partial reactions: oxidation or anodic partial reaction and reduction or cathodic partial reaction [67].

Tribo-corrosion started to be researched in the late 1980s and has now emerged as an active research area, as advanced experimental techniques have been developed to yield substantial insight into the complex processes present in this area. The development of in situ electrochemical techniques and post-test analysis techniques for surface film examination for example are powerful tools that can be deployed in tribo-corrosion experimental programmes.

Tribo-corrosion degradation affects the components in many industries, included mining, automotive, food, nuclear, offshore, marine and biomedical. These industries expend millions of pounds every year to repair damages that has been caused by tribo-corrosion processes. For example material removal of pumps, impellers, propellers, valves, heat exchanger tubes and other fluid handling equipment; other machines, and damage to human joints can compromise safe operation. In case of bio-tribo-corrosion of prosthesis and restorative dentistry, tribo-corrosion has implications for human health and quality of life. Tribo-corrosion is often linked to the synergy resulting from the coupling of mechanical and environmental effects. The synergism results in material losses that is often much larger or smaller than would be expected from a simple summing of the mechanical and environmental effects [149].

Tribo-corrosion maps for steels, titanium and titanium carbide materials

Bio-tribo-corrosion covers the science of surface transformations resulting from the interactions of mechanical loading and chemical or electrochemical reactions that occur between elements of a tribological system exposed to biological environments [77]. Important work has been done in tribo-corrosion of bio-materials, particularly for dental and hip joint applications [4]. It is important to understand material degradation processes for joint implants to achieve longer service life and better safety issues for such devices.

On the other hand, tribo-corrosion phenomena can also be applied to good use, for example in the chemical-mechanical polishing of silicon wafers in the electronics industry [78] or in metal grinding and cutting in presence of aqueous emulsions. At high temperatures, the more rapid generation of oxide due to a combination of temperature and tribological action during sliding wear can generate potentially wear resistant oxide layers known as 'glazes'. Under such circumstances, tribo-corrosion can be used potentially in a beneficial way.

2.2. Tribology

Tribology is the science and technology of interacting surfaces in relative motion and of related subjects and practices. It is concerned with the study of wear, friction and lubrication. Fig. 1 shows the expanded representation of tribo-technical system. Historically, the name tribology that is relatively new, but its components are in service older than recorded history [79]. It is known that drills made during the Palaeolithic period for drilling holes or producing fire were fitted with bearings made from antlers or bones and potters' wheels or stones for grinding cereals, etc., clearly had a requirement for some form of bearings [80]. A ball thrust bearing dated about AD 40 was found in Lake Nemi near Rome. Records show the use of wheels from 3500 BC, which illustrates our ancestors' concern with reducing friction in translational motion. A tomb in Egypt that was dated several thousand years BC provides the evidence of use of lubricants. A chariot in this tomb still contained some of the original animal-fat lubricant in its wheel bearings.

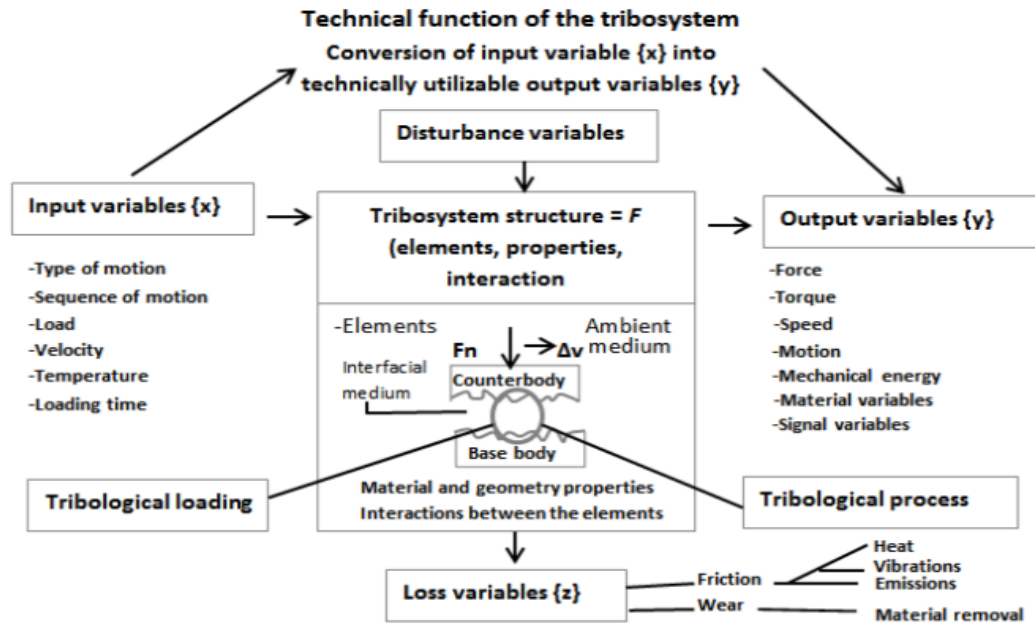


Figure 1 Expanded representation of tribo-technical system (TTS) [Springer Handbook of Mechanical Engineering].

Da Vinci deduced the rules governing the motion of a rectangular block sliding over a flat surface. He introduced, for the first time, the concept of coefficient of friction as the ratio of the friction force to the normal load. His work has no historical influence, however, because his note books remained unpublished for hundreds of years. In 1699, the French physicist Guillaume Amontons rediscovered the rules of friction after he studied dry sliding between two flat surfaces [81]. First, the friction force that resists sliding at an interface is directly proportional to the normal load. Second, the amount of friction force does not depend on the apparent area of contact. These observations were verified by French physicist Charles Augustin Coulomb [82]. He added a third rule that the friction force is independent of velocity once motion starts. He also made a clear distinction between static friction and kinetic friction.

Many other developments occurred during the 1500s, particularly in the use of improved bearing materials. In 1684, Robert Hooke suggested the combination of steel shafts and bell-metal bushes as preferable to wood shod with iron for wheel bearings. Further developments came with the growth of industrialization in the latter part of the eighteenth century and into the nineteenth century; for example, early developments in the petroleum industry in Scotland, Canada, and the United States in the 1850s [83-84].

Wear was initiated on a largely empirical basis. Scientific studies of wear developed little until the mid-twentieth century. Ragnar Holm made one of the earliest substantial contributions to the study of wear [85]. Since the beginning of the twentieth century, from huge industrial growth leading to demand for better tribology, knowledge in all areas of tribology has expanded tremendously [85-88].

2.3. Wear

Wear is the surface damage or removal of material from one or both of two solid surfaces in sliding, rolling, or impact motion relative to one another. In most cases, wear occurs through surface interactions at asperities. During relative motion, initially, material on the contacting surface may be displaced results in change of properties of the contact surface with no material loss. After that, material may be removed from the contact surface, transfer to the mating surface or break loose as a wear particle. Wear damage occurs before actual wastage of material. Definition of wear is generally based on loss of material, but it should be emphasized that damage due to material displacement or plastic deformation on a given body, without any change in weight or volume, is also called wear [89].

Removal of material due to mechanical process under sliding, rolling, and repeated impact conditions are included sliding wear, abrasive wear and fatigue wear. If sliding surfaces are lubricated then the wear that occurs is termed as lubricated sliding wear. In some engineering applications, surfaces slide in air without a lubricant, the resulting wear is then called dry sliding wear, although it usually takes place in ambient air of appreciable humidity. The distinction between abrasive wear and sliding wear is rather artificial, since under some conditions sliding wear can generate debris that can be trapped in the wear tracks and become involved in the sliding processes which may be causes further wear by abrasion. Therefore it has been concluded that the boundary between different types of wear is not rigid one [62].

2.4 Testing Methods

Different experimental arrangements are being used for the study of sliding wear.

2.4.1 Symmetrical arrangement

In these arrangements, sliding surfaces are symmetrically disposed and the wear rates of two surfaces of same material should be same. These are not often used to study wear. The

Tribo-corrosion maps for steels, titanium and titanium carbide materials

surfaces contact types in these arrangements are either along line or face to face. Both components rotate in these types of arrangements Fig. 2 (A, B).

2.4.2 Asymmetrical arrangement

In these arrangements sliding surfaces, even of same material, are asymmetrically disposed and wear rates will almost certainly experience different for each body. The most common asymmetric test rigs employ a pin pressed against a disc, either on a flat face Fig. 2 (C) or on the rim Fig. 2 (D), a block loaded against a ring Fig. 2 (E) or a pin on a flat Fig. 2 (F).

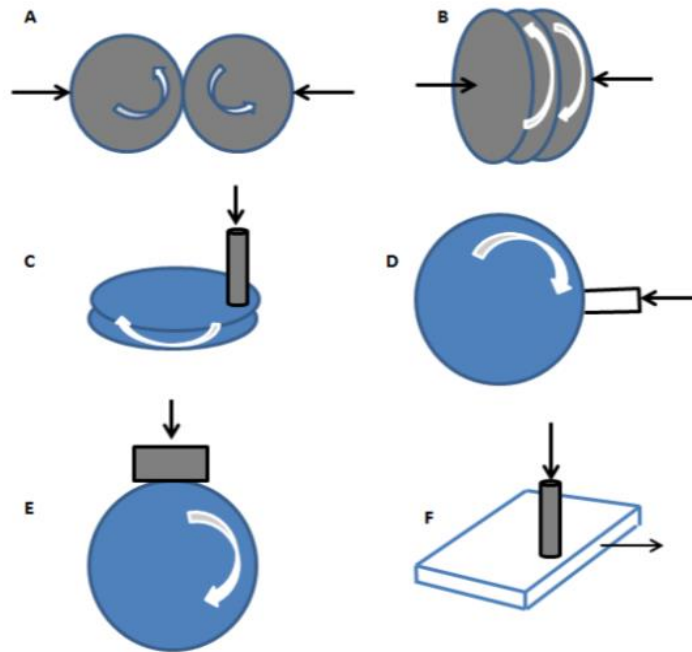


Figure 2 Geometries employed in sliding wear tests [44].

2.5 Unlubricated wear of metals

In the case of unlubricated (dry) sliding, wear mechanisms change as the sliding conditions are varied. The transition in dominant wear mechanism and in the associated wear rate are occurred with the variation of normal loads and sliding speeds and also in a few cases with sliding time or sliding distance. The main factors that control the basic wear mechanisms are mechanical stresses, temperature and oxidation phenomena. Consideration of these factors is must in understanding the sliding wear of metals. These three factors are interrelated and influenced by both normal load and sliding speed, which make sliding wear complicated.

Tribo-corrosion maps for steels, titanium and titanium carbide materials

Fig.3 shows schematically how the normal loads and sliding speeds effect on mechanical damage, due to surface stresses and on interface temperature. With the increase in normal load surface stresses increase that result in more severe mechanical damage. Normal load and sliding speed both effect the interface temperature as they control the energy dissipated at the interface which is product of the sliding speed and frictional force.

Moreover, the sliding speed effects on the heat conduction away from the interface. At low sliding speed, more heat will be conducted away that result in lower temperature of the interface, the sliding process will be in the limit of isothermal in this case. At higher sliding speed less heat will be conducted away from the interface that result in high temperature of the interface and limiting conditions would be adiabatic. A high interface temperature results in high chemical reactivity of the sliding surfaces, which leads to rapid growth of oxide films in the presence of air. It will reduce the mechanical strength of the asperities and of the near surface material, which may in extreme case result in melting of the contact surfaces.

There are two types of stress involve in sliding wear system i.e. normal stress at the surface of the each sliding body, and the shear stresses at and below the surface. The normal stress at the asperity contacts will be close to the indentation hardness of the softer metal and in state of plastic contact. When the contact surfaces are very smooth and conforming or under lower normal load then the asperity contact may be elastic. The applied normal load controls the extent of plastic flow at the asperity contacts. In case of lower normal load or well conformal contact surfaces, wear will occur very slowly due to elastic contact.

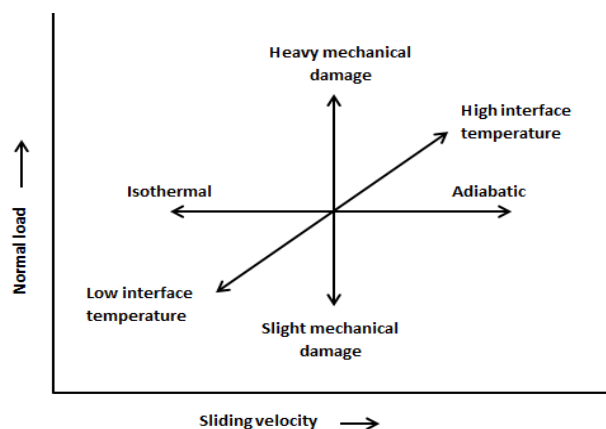


Figure 3 The combined influences of load and sliding speed on the sliding process in metals [62].

On the other hand shear stresses depend on the coefficient of friction. For $\mu \leq 0.3$ the maximum shear stress and plastic flow will be underneath the contact surface, and plastic strain accumulated by each sliding cycle will be low. This situation occurs in the presence of lubrication or for the sliding surface having a protective oxide layer. For $\mu \geq 0.3$, the maximum shear stress will lie at the sliding surface and result in higher shear strains. Plastic flow causes several wear mechanisms to be dominated that involved are adhesion and shear, nucleation of subsurface cracks leading to delamination wear and wear by fatigue. At relatively lower sliding speed and higher normal loads plasticity-dominated wear occurs that leads to severe wear.

Oxidation of the surfaces during sliding wear is important as well, as nearly all metals form oxide films in air. The rate of oxide films growth depends on the temperature between the mating surfaces, which is supposed to be higher than the surrounding and enhanced at the asperity contacts by transient 'flashes' or 'hot spots' . The temperature rise varies with sliding speed because the power dissipation depends on sliding speed and motion of the heat source over the counterface [62].

2.6 Mechanisms of Sliding Wear

Wear occurs by mechanical and/or chemical actions and is generally accelerated by frictional heating. Wear includes six principal and quite distinct phenomena [90]. These are: (1) adhesive, (2) abrasive, (3) fatigue, (4) impact by erosion and percussion, (5) chemical (or corrosive), and (6) electrical-arc-induced wear. Other commonly encountered wear types are fretting and fretting corrosion. These are not different mechanisms, but up to some extent are combinations of the adhesive, corrosive, and abrasive forms of wear. According to some estimates, two-thirds of all wear encountered in industrial environments due to adhesive- and abrasive-wear mechanisms. Wear by all mechanisms, except by fatigue mechanism, occurs by gradual removal of material.

This is to note that of the above mentioned wear mechanisms, one or more may be operating in one particularly machinery. In many cases, wear is initiated by one mechanism and it may proceed by other wear mechanisms, thereby complicating failure analysis [89].

2.6.1. Adhesive Wear

Adhesive wear occurs when two nominally flat solid bodies are in sliding contact. Adhesion or bonding occurs at the asperity contacts at the mating surfaces and these contacts are

sheared by sliding, which may result in detachment of a fragment from one surface and attachment to the other surface. As the sliding continues, the transferred fragments may come off the surface on which they are transferred and be transferred back to the original surface, or else form loose wear particles. Some are fractured by a fatigue process during repeated loading and unloading action resulting in formation of loose particles.

Several mechanisms have been proposed for the detachment of a fragment of a material. In an early theory of sliding wear, it was suggested that shearing can occur at the original interface or in the weakest region in one of the two bodies [29], Fig. 4. In most cases, interfacial adhesion strength is expected to be small as compared to the breaking strength of surrounding local regions; thus, the break during shearing occurs at the interface Fig. 4, (path 1) in most of the contacts and no wear occurs in that sliding cycle. In a small fraction of contacts, break may occur in one of the two bodies Fig. 4, (path 2) and a small fragment (shaded region in the figure) may become attached to the other surface. These transfer fragments are irregular and blocky shaped. In another wear mechanism, plastic shearing of successive layers of an asperity contact result in detachment of wear fragment. According to this theory, plastic shearing of successive layers based on a slip line field occurs in conjunction with the propagation of a shear crack, along which the fragment detaches, Fig. 5, [89]. This process results in thin wedge-shaped transfer fragments. The fragment is detached from one surface and transferred to the mating surface because of adhesion. Further sliding causes more fragments to be formed by either of the two mechanisms.

The formation of wear debris often results from chemical changes in the fragment. The fragments have large surface area and tend to oxidise readily, which reduces adhesive strength, and readily break loose. A second mechanism responsible for formation of loose particles involves the residual elastic energy of adherent fragments. When sandwiched between two surfaces, the fragment is heavily stressed. As the other surface moves on, only residual elastic stresses remain. If the elastic energy is larger than adhesive energy, a fragment breaks loose as a wear particle.

In case of dissimilar materials combinations, wear particles of both materials are formed with more wear particles from the softer material. The size of the softer material wear particles will be larger. Formation of the fragments of the harder material may also be produced by detachment of the material transferred by adhesion to the harder surface by a fatigue process as a result of number of loading and unloading cycles.

The transfer of material from one surface to another has been studied by several investigators. In the early 1950s, an autoradiography technique was used in which one sliding material was made radioactive and the transfer of the radioactive material to the mating surface during sliding was demonstrated by placing a photographic film in contact with the mating surface after rubbing and later developing the film to obtain an autoradiograph of any transferred material [93-95]. Black impressions on the developed film are produced by each fragment.

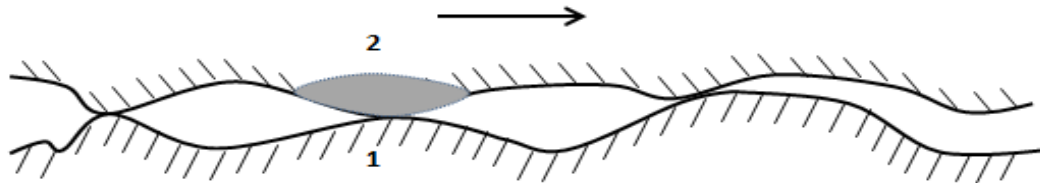


Figure 4 Schematic shows two possibilities of break (1 and 2) during shearing of an interface [89].

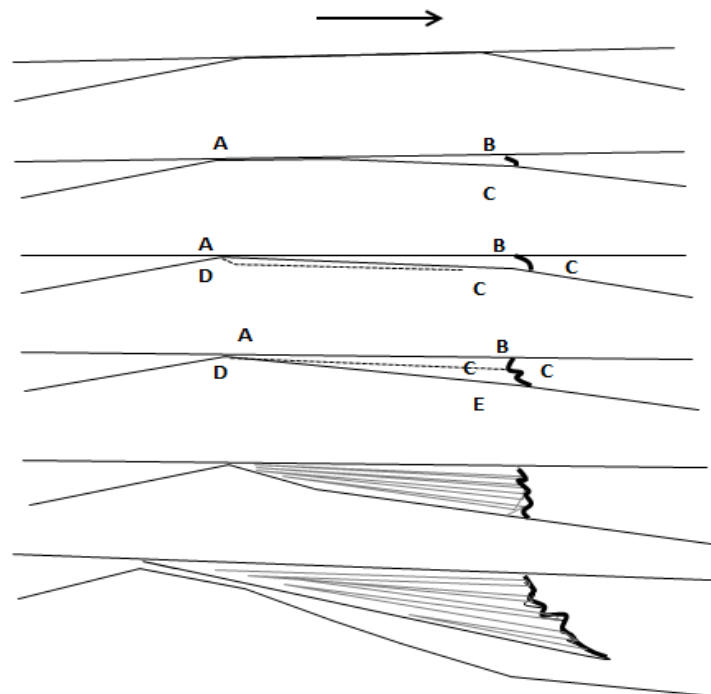


Figure 5 Schematic shows detachment of fragment of a material from plastic shearing of successive layers of an asperity contact [89].

During continuous sliding, surface asperities undergo plastic deformation and /or fracture. The plastic deformation and strain hardening also occurred in the subsurface. The extensive structural changes occurred and the material close to the worn surface may be

Tribo-corrosion maps for steels, titanium and titanium carbide materials

recrystallized from an instantaneous surface temperature rise during sliding. Micro-hardness of the worn layer increases up to 10-80% than that of the original hardness of the material [94-95].

Severe type of adhesive wear is often called galling, scuffing, welding or smearing. These terms are sometimes also used to describe other types of wear [89]. The tendency of the sliding metals to adhere strongly to each other is indicated by their metallurgical compatibility, which is the degree of solid solubility when the two metals are melted together. Increasing the degree of incompatibility reduces wear, leading to lower value of the wear coefficient. This is also true for the coefficient of friction [96].

Simple Theory of Sliding Wear: The Archard Wear Equation

When two surfaces in contact slide over each other, one or both surfaces will suffer wear. A simple theoretical analysis of this type of wear from Holm and Archard is based on experimental data of various unlubricated material pairs, the vast majority being metallic; it is possible to write the laws of adhesive wear as follows:

$$v = \frac{kWx}{H} \quad (2.1)$$

Where v is the amount of wear, W is applied load, x is sliding distance, H is hardness of the softer surface and k is a non-dimensional wear coefficient dependent on the materials in contact and their cleanliness.

Archard [29] presented a theoretical basis for the expression in Eq. 2.1. Consider two surfaces in a sliding contact under applied load W . Assume that during an asperity interaction, the asperities deform plastically under the applied load and that at each unit event there is a definite probability that a wear particle will be produced. Further assume that contact is made up of asperities with an average radius of a , Fig. 6. If the material has yielded under the maximum normal load dW , supported by as asperity,

$$dW = \pi a^2 H \quad (2.2)$$

Where H is mean contact pressure under the condition of full plasticity flow pressure, or hardness of the softer material. We now assume that this asperity contact results in a worn particle of volume dv . The dimension of this worn particle will be directly proportional to

Tribo-corrosion maps for steels, titanium and titanium carbide materials

the contact size. Physical examination of the wear particles shows that particles are generally of roughly equal lengths in three dimensions rather than, say, layers. Thus, dv is expected to be proportional to a^3 . If the particle is assumed to be hemispherical in shape with radius equal to the contact radius, then,

$$dv = \frac{2}{3} \pi a^3 \quad (2.3)$$

Finally, contact is assumed to remain in existence for a sliding distance dx equal to $2a$, after which it is broken and the load is taken up a new contact,

$$dx = 2a \quad (2.4)$$

From Equations 2.2, 2.3, and 2.4

$$\frac{dv}{dx} = \frac{dW}{3H} \quad (2.5)$$

If only a fraction ($= 3k$) of all encounters produce wear particles, then the volume of wear by all asperities is:

$$v \propto \frac{Wx}{3H} = \frac{kWx}{H} \quad (\text{plastic contacts}) \quad (2.6)$$

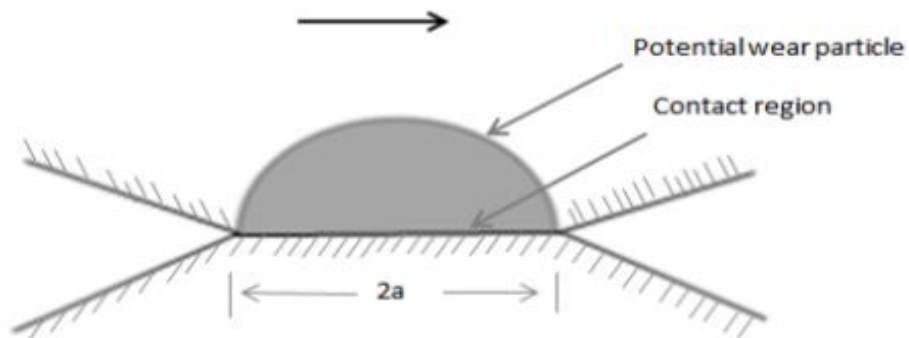


Figure 6 Schematic of a hypothetical model of generation of a hemispherical wear particle during sliding contact [89].

Adhesive wear Equation 2.1 imply that if k is a constant for a given sliding system, then the volume of worn material should be inversely proportional to H .

For a given material combination with primarily plastic contacts, wear rate generally decreases with an increase in hardness. However, in the case of extremely hard and/or brittle materials, fracture toughness generally affects the wear rate, but is not included in the wear equations. For a material combination with primarily elastic contacts, wear rate generally decreases with an increase in the modulus of elasticity. For a material combination with primarily elastic contacts, the wear rate, in adhesive wear mode, should decrease with an increase in surface roughness. However, if the wear occurs by other wear modes, such as abrasive wear, the wear rate may increase with an increase in surface roughness [89].

In many materials combinations, the sliding wear increases linearly with normal load up to certain range of applied load. The wear rate may either increase or decrease abruptly at some critical loads [97]. It is the apparent pressure which determines the critical value of the load. This can be attributed to breaking or formation of oxide layers as a function of pressure or frictional heating Fig. 7. Experimental data suggest that the wear volume increases with the sliding distance or sliding time at a constant velocity [11]. The wear rate may be either higher or lower during the running-in period, followed by steady-state wear rate until failure of the contact surfaces. As per Equation 2.1, the wear rate should be independent of the sliding velocity. For many sliding combinations, this assumption holds for a range of values of sliding velocity. However, sharp transitions in wear rate are seen at critical sliding velocities and apparent pressures.

For sliding wear, some analogies may be made between the effects of increasing applied load Fig. 7, [13] and sliding speed Fig. 8, [12] on the material surface. Increase in either parameter increase the level of frictional heating on the contact surfaces. In such conditions, if the material being tested for sliding wear is metallic, e.g. steel, then the oxidation rate on the contact surface will increase. This result in the wear increases initially with increasing sliding speed and normal load through an oxidation-scrape-re-oxidation process [37]; at higher sliding speeds and normal loads when frictional heating results in higher flash contact temperatures the oxides on the surface become increasingly soft and a rapid decrease in the wear rate is observed [4].

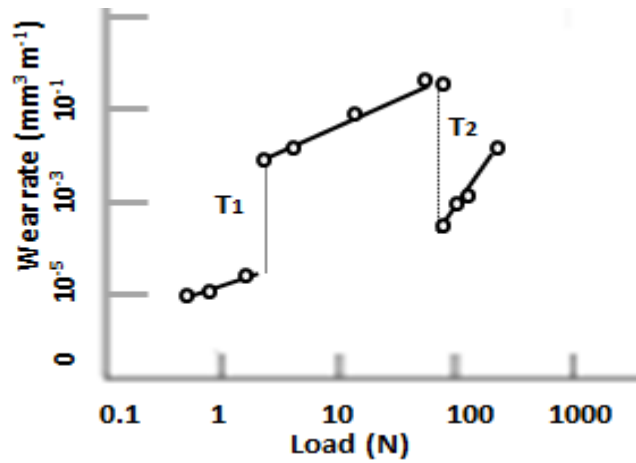


Figure 7 The variation of wear rate with load for 0.5% plain carbon steel pin sliding at 1 m s^{-1} in air against tool steel in a pin-on-ring test [13]

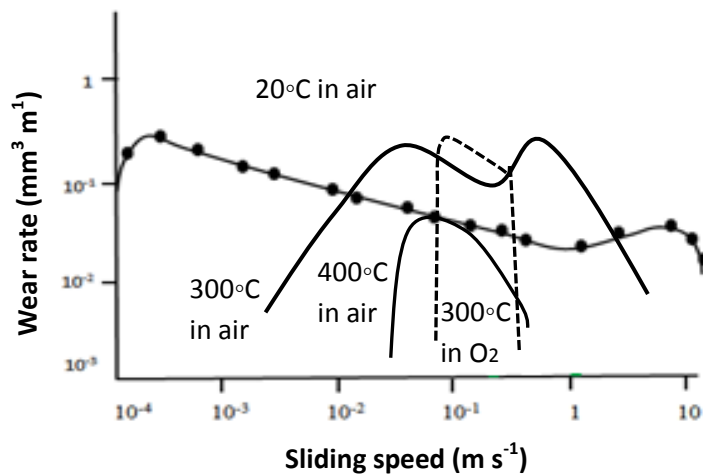


Figure 8 The variation of wear rate with sliding speed for α/β brass sliding against steel at various temperatures in air and in pure oxygen [12]

2.6.2. Abrasive Wear

In abrasive wear, material is removed or displaced from a surface by hard particles or some times by hard protuberances on a counterface, forced against and sliding along the surface. Several qualifying terms can be used in describing abrasion. The distinction in abrasion process is made by two-body abrasive wear Fig. 9(a) or three-body abrasive wear Fig 9(b). In two-body abrasive wear caused by hard protuberances on the counterface for example, in mechanical operations, such as grinding, cutting and machining. In three-body abrasive wear hard particles are free to roll and slide between two sliding surfaces for example, in free-abrasive lapping and polishing. In many cases, the wear mechanism at the start is adhesive, which generates wear particles that get trapped at the inter-face, resulting in a

Tribo-corrosion maps for steels, titanium and titanium carbide materials

three-body abrasive wear [95]. In most abrasive wear situations, scratching (of mostly the softer surface) is observed as a series of grooves parallel to the direction of sliding (ploughing).

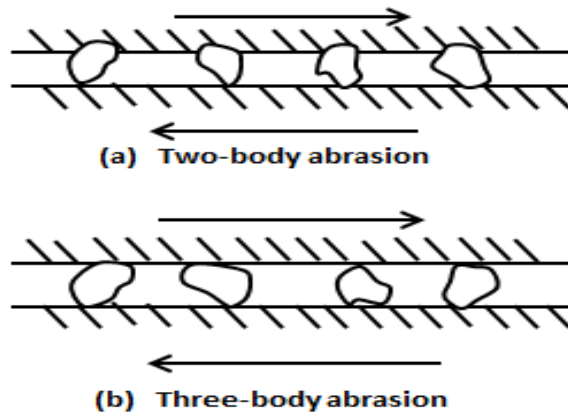


Figure 9 Illustration of the differences between (a) two-body abrasion; and (b) three-body abrasion [62]

The abrasive wear can also be described by the terms of high-stress and low-stress abrasion. In high-stress abrasion, the crushing strength of the abrasive particles is exceeded to break them up during the wear process. In low-stress abrasion the particles remain unbroken. The term gouging abrasion is often used to describe high-stress abrasion by large lumps of hard abrasive material, for example in rock crushing machinery.

Abrasive wear by brittle fracture

During sliding process, most metallic and ceramic surfaces show evidence of plastic flow. Even at lower normal load contacting asperities of metals deform plastically. When the material is brittle having low fracture toughness, wear in this case occurs by brittle fracture and the worn zone consists of significant cracking.

Abrasive wear by plastic deformation

In abrasive wear by plastic deformation, material is removed from surface via plastic deformation during abrasion by several deformation modes which include ploughing, wedge formation and cutting Fig. 10. Ploughing results in a series of grooves as a result of the plastic flow of the softer material. In the ploughing (also called ridge formation) process, material is displaced from a groove to the sides without removal of material Fig. 10(a). However, after the surface has been ploughed several times, material removal can occur by a low-cycle fatigue mechanism. When ploughing occurs, ridges form along the

sides of the ploughed grooves regardless of whether or not wear particles are formed. These ridges become flattened, and eventually fracture after repeated loading and unloading cycles, Fig. 11 [97]. Ploughing process also causes subsurface plastic deformation and may contribute to the nucleation of surface and subsurface cracks [98]. Further loading and unloading (low-cycle, high-stress fatigue) cause these cracks and pre-existing voids and cracks to propagate (in the case of subsurface cracks to propagate parallel to the surface at some depth) and join neighbouring cracks, which eventually shear to the surface leading to thin wear platelets Fig. 11. In very soft metals, such as indium and lead, the amount of wear debris produced is small and the deformation material is displaced along the sides of the groove.

In the wedge formation type of abrasive wear, an abrasive tip ploughs a groove and develops a wedge on its front. It generally occurs when the ratio of shear strength of the interface relative to the shear strength of the bulk is high (about 0.5-1). In this situation, only some of the material displaced from the groove is displaced to the sides and the remaining material shows up as a wedge, Fig. 10(b).

In the cutting form of abrasive wear, an abrasive tip with large attack angle ploughs a groove and removes the material in the form of discontinuous or ribbon-shaped debris particles similar to that produced in a metal cutting operation, Fig. 10(c). This process results in generally significant removal of material and the displaced material relative to the size of the groove is very little.

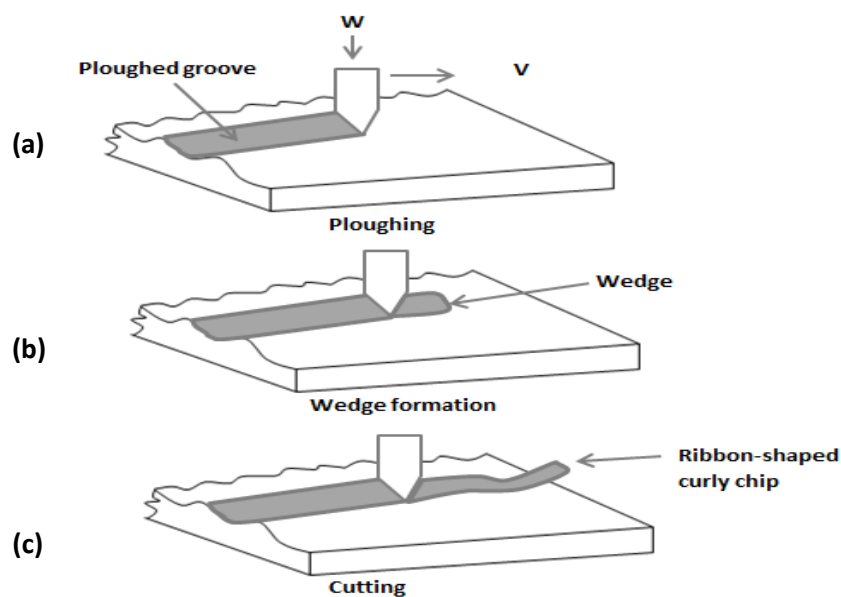


Figure 10 Schematics of abrasive wear processes as a result of plastic deformation by three deformation modes [89].

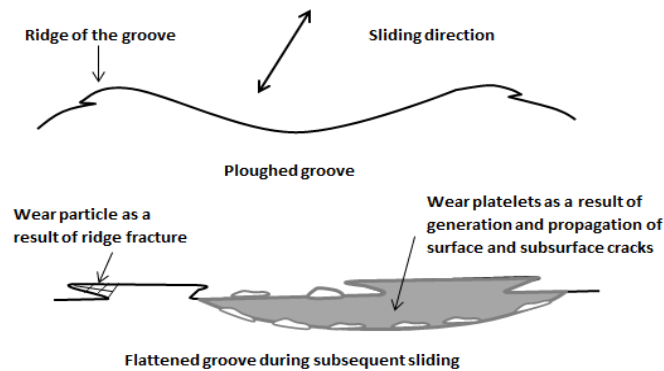


Figure 11 Schematics of ploughed groove and formation of wear particle due to ploughing as a result of fracture of flattened ridge and propagation of surface and subsurface cracks [89].

Effects of hardness

In two-body [99-100] and three-body [101] abrasive situations, if the abrading medium is softer than the work piece, the wear coefficient either remains or does not remain constant. It is known that when the hardness ratio of the work piece to the abrasive particles is less than unity, the wear coefficient remains approximately constant; however, if the ratio is equal to or greater than unity, the wear coefficient decreases rapidly with an increase in the hardness ratio [101]. When the hardness of the work piece is of same order of magnitude as the hardness of the abrasive particles, the wear of the work piece is not rapid, since the deformation occurs both in the abrasive particles and the work piece, and wear generally occurs in both. When the work piece is significantly harder than that of abrasive particles, negligible deformation, and consequently wear, occurs. Accompanying the change in hardness ratio from less than unity to greater than unity, there is a significant change in the roughness of the worn surface because the wear mechanism has changed. The wear coefficient from the wear tests with work pieces with varying hardness against an abrasive can be used to estimate hardness of the abrasive [102].

There is significant experimental evidence in literature that the wear rate in two-body abrasion is generally inversely proportional to the hardness and proportional to the normal load and sliding distance for many pure metals; alloys often exhibit more complex behaviour [103-106]. Hardness is an important parameter for abrasive wear resistance. Wear resistance (proportional to $1/\text{wear rate}$) of annealed pure metals is generally directly proportional to their hardness but is more complex for alloys [103,107]. These authors

reported that prior work hardening of pure metals and alloys had no effect on the wear rate. Cold working of the 0.4% carbon steel resulted in a significant increase in bulk hardness but had no effect on its wear resistance. These and other experiments show that a metal surface strain hardens by plastic flow during abrasion to a maximum value, and it is this value of hardness which is important for abrasion resistance. Also note that if a material is hardened, it generally become more brittle. Brittle materials can produce larger particles, resulting in high wear rates.

Effects of normal load, sliding speed, particle size and sliding distance

Volume of Wear generally increases linearly with an increase of applied normal load; often the linear relationship is not maintained at high loads. Wear rate changes as a function of sliding velocity and the particle size of an abrasive paper or roughness of the abrading surface. The effect of the particle size on the wear rate in two-body and three-body abrasion is dependent of sliding velocity and abrasive grit size [108]. The wear rate is not very sensitive to the sliding velocity. Increase in wear resistance with sliding velocity is due to presumably to the increase in strain rate which increases the yield stress of the material. At very high sliding velocities, high interface temperatures as a result of frictional heating result in a decrease in the yield stress of the material being abraded, which counter acts the effect due to increased strain rate.

The dependence of abrasive wear rate as a function of sliding distance is more complex. If wear takes place with fresh abrasive paper (in two-body wear) or fresh abrasive particles (in three-body wear), wear continues at a steady rate [96,109]. However, if a limited amount of abrasive is used with the sliding continues, the wear rate generally decreases as a function of time. For example in the work of Mulhearn and Samuels, wear rate decreases as a function of sliding distance when steel is abraded on silicon carbide abrasive paper [104]. A decrease in the wear rate as a function of sliding distance is believed to occur as a result of blunting of abrasive surfaces in two-body wear or abrasive particles in three-body wear, Fig. 12(a). In addition, clogging of the abrasive surface by abraded debris occurs during wear, Fig. 12(b), [96]. If at any instance, wear debris is larger than abrasive particles, it may leave the material being abraded above the level of the abrasive grains and result in no additional wear. One can see that abrasive action should cease much more rapidly in wear with fine grades of abrasive paper than with coarse grades.

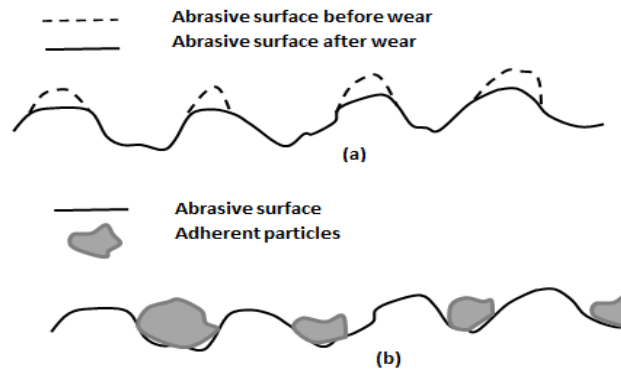


Figure 12 Schematics of, (a) an abrasive surface before and after wear, showing blunting, and (b) an abrasive surface clogged by wear [89].

2.6.3. Fatigue Wear

Fatigue wear of a material is caused by a cycling loading during friction. It is the progressive and localized structural damage that occurs when a material is subjected to cyclic loading. Fatigue occurs if the applied load is higher than the fatigue strength of the material.

Subsurface and surface fatigues are observed during repeated rolling and sliding respectively. The repeated loading and unloading cycles may lead to formation of cracks in subsurface or surface of the material. After a critical number of cycles the damage of the surface occurs, leaving large pits in the surface. This process is called pitting as well. Prior to this critical point negligible wear takes place, contrast to the wear caused by an adhesive or abrasive wear mechanism, where wear causes a gradual deterioration from the start of running. Therefore, the amount of material removed by fatigue wear is not a useful parameter. Much more relevant is the useful life in terms of the number of revolutions, cycles or time before fatigue failure occurs.

In rolling contact, cracks initiate below the surface, until a region of metal is separated to some extent from the base metal by the crack and ultimately becomes detached and spalls out. With passage of time these cracks grow to emerge at the surface and produce wear particles, these particles may become large spalls or flakes. A typical example of spalling of a ball bearing race due to subsurface fatigue is shown in Fig. 13. In rolling contact applications surface hardened materials are used and contact surface could be brittle. Therefore cracks may be initiated at the surface as a result of tensile stresses and lead to surface fatigue.



Figure 13 Spalling of a 52100 ball bearing race by subsurface fatigue [89].

One of the types of fatigue wear is fretting wear, caused by cycling sliding of two surfaces across each other with small amplitude (oscillation). The friction force produces alternating compression-tension stresses, which result in surface fatigue. The direction of motion is usually tangential to the surfaces. When the amplitude of the motion lies in a range typically from 1 to 100 μm , surface degradations occur which are called fretting damage or fretting wear [62].

Although fretting wear can be regarded formally as reciprocating sliding wear with very small displacements. The difference between is, sliding wear usually results from deliberate movement of the surfaces, fretting often arises between surfaces which are intended to be fixed in relation to each other. These small displacements often originate from vibration. Typical examples of locations where fretting may occur are in hubs and discs press-fitted to rotate shafts, in riveted or bolted joints, between the strands of wire ropes, and between the rolling elements and their tracks in stationary ball and roller races. It may also occur between items packed inadequately for transport, where vibration can lead to fretting damage at the points of contacts between the items. Since the debris formed by fretting wear is predominantly oxide, which in most metals occupies a larger volume than the metal from which it originates. On the other hand fretting wear can also lead to seizure of parts which are designed to slide or rotate with a small clearance. Whether fretting leads to increased clearance or to seizure depends on the ease with which the wear debris can escape from the contact region.

2.6.4. Impact Wear

Two broad types of wear phenomena belong under this heading: erosive and percussive wear. Erosion can occur by jets and streams of solid particles, liquid droplets, and implosion of bubbles formed in the fluid. Percussive occurs from repetitive solid body impacts. Repeated impacts result in progressive loss of solid material.

Erosion by Solid Particles

This wear process occurs when discrete solid particles strike a surface Fig. 14. It differs from three-body abrasion, as it involves loose particles, primarily in the origin of the forces between the particles and the wearing surface. In abrasion the particles are pressed against the surface and move along it, usually because they are trapped between two sliding surfaces. In erosion, several forces of different origins may act on a particle in contact with a solid surface [62]. The particle velocity and impact angle combined with the size of the abrasive give a measure of the kinetic energy of the impinging particles, that is, of the square of the velocity. Wear debris formed in erosion occurs as a result of repeated impacts.

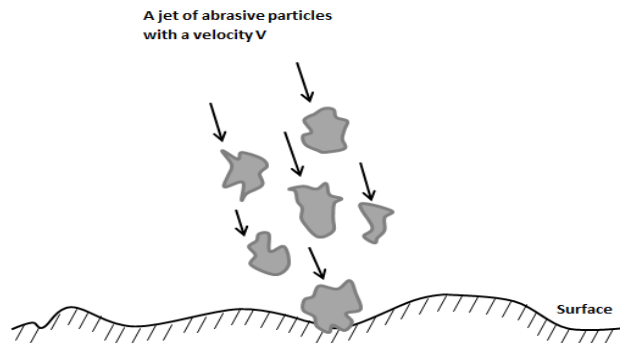


Figure 14 Schematic of a jet of abrasive particles hitting a surface at a high velocity [89].

As in the case of abrasive wear, erosive wear occurs by plastic deformation and/or brittle fracture, dependent upon material being eroded away and upon operating parameters. Wear rate dependence on the impact angle for ductile and brittle materials is different, as shown in Fig. 15, [110]. Ductile materials will undergo wear by a process of plastic deformation in which the material is removed by the displacing or cutting action of the eroded particle. In brittle material, on the other hand, material will be removed by the formation and intersection of cracks that extend out from the point of impact of the eroded particle [111]. The shapes of the abrasive particles affect the pattern of plastic deformation

Tribo-corrosion maps for steels, titanium and titanium carbide materials

around each indentation, consequently the proportion of the material displaced from each impact. In the case of brittle materials, the degree and severity of cracking will be affected by the shape of the abrasive particles.

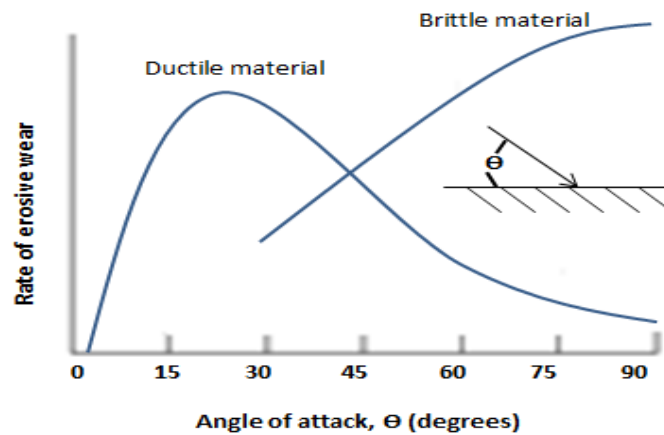


Figure 15 Rate of erosive wear as a function of angle of attack (with respect to the material plane) of impinging particles [89].

Solid particle erosion is a problem in machinery such as by ingested sand particles in gas turbine blades, helicopter and airplane propellers, windshields of airplanes, nozzles for sand blasters, coal turbines, hydraulic turbines and centrifugal pumps used for coal slurry pipelines. It has useful application in process such as sand blasting, abrasive de-burring, and erosive drilling of hard materials.

Liquid Impingement Erosion

This process occurs when small drops of liquid strike the surface of a solid at high speeds (as low as 300m s^{-1}). The pressures are experienced that exceed the yield strength of most materials. Thus plastic deformation or fracture can result from a single impact, and repeated impact leads to pitting and erosive wear. In many cases, the probable impact velocities and impact angle are such that pure liquid impingement erosion is an unlikely mechanism; an erosion-corrosion mechanism usually does more damage [112]. The damage by this process is important in the so-called moisture erosion of low-pressure steam turbine blades operating with wet steam, rain erosion of aircraft or missile surfaces and helicopter rotors, nuclear power plant pipes, and heat exchanger.

Cavitation Erosion

Cavitation is defined as the repeated nucleation, growth and violent collapse of cavities or bubbles in a liquid. Cavitation erosion arises when a solid and fluid are in relative motion, and bubbles formed in the fluid become unstable and collapse against the surface of the solid. The bubbles, which are in contact with or very close to a solid surface, will collapse asymmetrically, forming a micro-jet of liquid directed toward the solid. The solid material will absorb the impact energy as elastic deformation, plastic deformation or fracture. The latter two processes may cause localized deformation and/or erosion of the solid surface [112]. Damage by this process is found in components such as ships' propellers and centrifugal pumps.

All liquids contain gaseous, liquid impurities, which act as nucleation sites for the bubbles or vapour-filled voids. When a liquid is subjected to sufficiently high tensile stresses, bubbles are formed at weak regions within the liquid. Subsequently if this liquid is subjected to compressive stresses, i.e. to higher hydrostatic pressures, these bubbles will collapse. In practice, cavitation can occur in any liquid in which the pressure fluctuates either because of flow patterns or vibration in the system. If, at some location during liquid flow, the local pressure falls below the vapour pressure of the liquid, then cavities may be nucleated, grow to a stable size and be transported downstream with the flow. When these cavities reach the high-pressure region, they become unstable and collapse [113]. The stability of a bubble is dependent on the difference in pressure between the inside and outside of the bubble and the surface energy of the bubble. The damage created is a function of the pressures produced and the energy released by collapse of the bubble. Thus reduction of surface tension of the liquid reduces damage, as does an increase in vapour pressure.

Materials that are resistant to fatigue wear, namely, hard but not brittle materials, are also resistant to cavitation. Resistance to corrosive attack by the liquid, however, is an additional requirement for cavitation resistance [89].

Percussion

Percussion is a repetitive solid body impact, such as experienced by print hammers in high-speed electrochemical applications and high asperities of the surfaces in a gas bearing. In most practical machine applications, the impact is associated with sliding i.e. the relative approach of the contacting surfaces has both normal and tangential components known as compound impact [113]. Percussion wear occurs by hybrid wear mechanisms which

Tribo-corrosion maps for steels, titanium and titanium carbide materials

combine several of the following mechanisms: adhesive, abrasive, surface fatigue, fracture, and tribo-chemical wear.

2.7 Corrosion

In chemistry, a process in which a solid, especially a metal, is eaten away and changed by a chemical action, as in the oxidation of iron in the presence of water by an electrolytic process. Corrosion is the gradual destruction of materials (usually metals) by chemical reaction with its environment. Dry corrosion, oxidation, occurs when there is no moisture or water to aid chemical reaction. The metal in such a situation oxidizes with only the atmosphere. This process is very sensitive to temperature. At high temperature, dry corrosion occurs at a much faster rate as compared to normal conditions.

Corrosive wear in aqueous conditions occurs because of a chemical reaction accompanied by the passage of an electric current (electrochemical reaction), and for this to occur, a potential difference must exist between two regions. The region at low potential is known as an anode and the region at high potential is known as a cathode. If there is a current flow between the anode and cathode through an electrolyte (any conductive medium), at the anode the metal dissolves in the form of ions and liberates electrons. The electrons migrate through the metal to the cathode and reduce either ions or oxygen [89]. Corrosion degrades the useful properties of materials and structures including strength, appearance and permeability to liquids and gases.

2.8 Tribo- corrosion

Tribo-corrosion involves the interaction between mechanical wear processes and electrochemical and/or chemical corrosion processes and leads to a material loss that is a summation of these effects, as shown below:

Wear–corrosion = mechanical wear processes + electrochemical (and/or chemical, oxidative) response

In dry conditions, corrosive wear occurs when sliding takes place in atmosphere (in air). Oxygen is the most dominant corrosive medium in air. The chemical wear occurs in air is generally called oxidative wear. In the absence of tribological-action, the chemical products of the corrosion (e.g. oxides) would form a film typically less than a μm thick on the surfaces, which would tend to slow down the corrosion. During the dry sliding action the chemical protective film is removed from the surface and the chemical action can continue

Tribo-corrosion maps for steels, titanium and titanium carbide materials

due to high temperature at the contact point. In sliding process flash temperatures of several hundred degrees can readily be generated. The magnitude of these temperatures depends on the sliding speed. Only moderate sliding speeds are required for most of the metals for these hot-spot temperatures become high enough to cause significant surface oxidation. Therefore oxide films formation will continue during rubbing due to flash temperatures.

Friction modifies the kinetics of chemical reactions of sliding bodies with each other and with the gaseous or liquid environment. To the extent that reactions which occur at high temperatures the same reactions can occur at moderate, even ambient, temperatures during sliding at the contact point of the sliding bodies. Chemistry dealing with this modification of chemical reaction by friction or mechanical energy is referred to as tribo-chemistry, and wear controlled by this reaction is referred to as tribo-chemical wear [114-115]. The most obvious mechanism by which friction increases the rate of chemical reaction is frictional heat produced at contacting asperities. Beside the frictional heat, other mechanisms are: removal of product scale resulting in fresh surfaces, accelerated diffusion and direct mechano-chemical excitation of surface bonds. The tribo-chemical reactions result in tribo-oxidative wear of metals. During friction the adhesive dissipation of energy is often influenced by chemical effects, Fischer and Mischler [116].

Additional factors associated with coatings

Understanding the tribo-corrosion of coatings is complicated as compared with the metals. Coating processes used can degrade (without intention) the coating microstructure by adding a considerable amount of porosity and pockets of oxides into the coating. Coating process can affect the substrate properties as well. During the pre-coating substrate treatment, such as shot or grit blasting; remnant from this process can be embedded into the surface of the substrate and then coated which affect the adhesive properties of the coating/substrate interface. These add to the already complex interactions that can occur during wear contacts [150].

Multiple phases of coatings can lead to micro-galvanic activity and selective phase corrosion. Examples of such surfaces include composites or surfaces that undergo tribological induced compositional changes. As the presence of carbides in a metallic surface, added to improve wear resistance, establishes a micro-corrosion cell as the carbide

is likely to be cathodic with respect to the surrounding metallic matrix. This can result in anodic dissolution of the metallic matrix close to or at the matrix/carbide interface and thereby accelerate carbide removal from surfaces and reduce the anti-wear properties of the coated surface [150].

2.8.1. Mild- oxidation

The oxide layers on the sliding wear surfaces effect the wear behaviour in different manners. As found in literature, the very lower sliding speeds (smaller than 1 m s^{-1}) do not generate a high enough flash temperature during sliding to make oxidation the dominant wear mechanism. Under such a condition, the very thin oxide film effectively separates the asperities up till the contact pressure at the asperities remain low. In this case fine oxide particles are produced and wear mechanism is mild wear [11-117]. These fine particles could also come from small metallic fragments which may occasionally be removed probably through delamination wear mechanism and oxidised. The damaged surface quickly re-oxidises, preventing further direct metallic contact, maintaining the mild wear condition [118]. With the increase in sliding speed results in higher oxidation rate due to increase in frictional heat and flash temperature between sliding surfaces. Oxidation therefore becomes dominated mechanism of generating wear particles.

When normal load is higher to penetrate the thicker but brittle oxide layers generated by increased frictional heating on the soft substrate, direct metal to metal contacts takes place. Within a small range of sliding condition, severe oxidative wear occurs with much damage on the sliding surfaces. In this situation the rate of oxide removal is greater than that of formation of oxide. With the further increase in sliding speed and normal load, a hard surface layer is formed on mating surfaces as a result of higher flash temperatures, followed by rapid quenching as the heat is conducted quickly into the underlying bulk material. The higher flash temperature increased the local oxidation rate as well. A thicker layer of oxide is supported by the hardened substrate in this situation and prevents further metallic contacts, despite of the higher contact pressure at the asperities. In this range of sliding speeds and normal loads mild oxidative wear occurs. In this situation, the rate of oxide removal is lower than that of oxide formation. Mild oxidative wear results in reduction in wear rate significantly [119].

2.8.2. Severe-oxidation

At higher sliding speed more than 10 m s^{-1} , the rate of oxidation on the sliding surfaces is increased from the isolated patches to a plastically deformed continuous film of oxide covering the entire sliding surface [120-121]. The oxide formed under such conditions is thicker than those formed under the condition of mild-oxidation, more continuous, and almost certainly hotter and more plastic as compared to the brittle nature of the 'colder' oxide [122]. The characteristics of the wear process are different and the rates of wear are generally lower. The mechanism is one of melting of thick oxide layer formed under the much hotter environment resulting from the more severe sliding conditions [122]. The prefixes of 'mild' and 'severe' refer to the extent of oxidation at the sliding surfaces as a result of flash temperatures generated at the sliding contacts, these are not a reflection of the wear rates. In fact, the wear rates when severe-oxidation dominates are usually low [119].

2.8.3 Modes of wear

Archard and Hirst [11] identified two modes of wear which they termed as 'mild' and 'severe'. Quinn [123-124] considered Burwell and Strang's classification and those of Tabor [125] and Ludema [126] to be special cases of the mild and severe wear classification of Archard and Hirst. The more recent trend of classifying wear into regimes according to the types of debris produced [127-128] is also regarded by Quinn [24] as related to the more general classification of Archard and Hirst. The classification of wear is, of course, linked to the mechanisms by which it occurs. A survey of the literature on wear mechanisms reveals a rather confusing picture. Part of the confusion lies with the variety of terms used to describe the wear mechanisms. Lim S.C. et al. related the 'mild' and 'severe' wear classification of the Archard and Hirst to this newer classification [129].

Mild Wear

Mild wear gives a smooth and dark surface Fig. 16. It takes place in the situations as below:

(i) When contact pressure and sliding speed are both very low, a thin tough oxide layer may prevent direct metal to metal contact between the asperities of the sliding surfaces. This thin layer may deform elastically without rupture. The black powdered oxide wear debris may generate from this thin oxide layer and perhaps from tiny metallic fragments which may be sometime removed and oxidised. The damaged surface quickly re-oxidises,

Tribo-corrosion maps for steels, titanium and titanium carbide materials

preventing metal-to-metal contact between the sliding surfaces. This is the mild wear regime of Archard and Hirst [11].

(ii) At higher sliding speeds, a thicker and more brittle layer of oxide is continuously generated at the asperity contacts due to high flash temperatures. The rate of oxidation is higher than the rate of removal from the contact surfaces due to break away of oxide fragments as wear debris. In this way direct metal-to-metal contact is prevented. This is Quinn's mild-oxidational wear mechanism [130].

(iii) At higher loads, a hard surface layer (most likely martensitic) is formed on carbon-steel surfaces due to high flash temperatures, followed by rapid quenching as the heat is conducted into the underlying bulk material. The higher flash temperatures also increase the local oxidation rate at the contacts areas. A thicker layer of oxide now supported by the hardened substrate and is able to prevent further direct metal-to-metal contact despite the higher pressure at the contacting asperities. This reduces the wear rate by about two orders of magnitude and results in a transition from a severe wear to mild wear [89].

(iv) At higher sliding speeds, the increased interfacial temperature now cause of continuous oxide to deform plastically [120-121]. The metal is partly insulated from the higher temperatures by this thick and continuous layer of oxide [121], but the oxide itself is hot enough that it can flow or even melt. This has been as severe oxidation above [69]. The prefix 'severe' refers to the extent of oxidation, not the wear rate, which is low when severe oxidational wear occurs [131].

Severe Wear

Severe wear produces rough and deeply torn surfaces with higher wear rate Fig. 16. It takes place in the situations as below:

(i) When at lower sliding speeds, contact pressure is high enough to rupture the thin oxide layer and direct metal-to-metal contact can occur, wear is severe. The resultant frictional traction causes a sudden increase in the plastic shear strain accumulated in the subsurface layer where cracks nucleate and grow parallel to the surface, eventually breaking out to give flake-like debris. This is the delamination mechanism first proposed by Suh [118].

Tribo-corrosion maps for steels, titanium and titanium carbide materials

(ii) When the load is high enough to penetrate the thicker but brittle oxide layers generated by asperity heating on a soft subsurface layer, metal-to-metal contacts result. This causes deep tearing of the surfaces, giving severe metallic wear.

(iii) When the sliding conditions are so severe that the local temperatures reach the melting point of the steel or other couple of metals, a liquid film forms at the contact. In this case Wear is determined by the flow and expulsion of the molten layer [120]. Even though some surfaces may appear smooth because of the way the molten layer has flowed and the rate of wear is very higher [129].

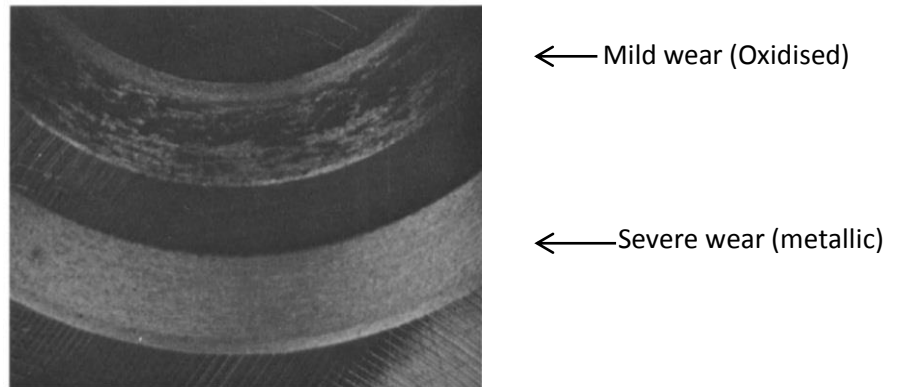


Figure 16 Wear tracks on steel disk [33]

Medium (mixed) Wear

As discussed by A. F. Smith [34] that there is some confusion in the literature regarding the types of wear. There have been moves [133-134] to revert to essentially the severe and mild wear classification originally proposed by Archard and Hirst [11]. It is also proposed that a mixed regime can exist [134], where both severe and mild wear is occurring either simultaneously or alternately. The wear rate in this regime could be intermediate between the severe and mild wear rates with the production of both metallic and oxide debris [34].

2.9 Wear-regime maps

The development of wear maps is a useful tool to study and predict the wear behaviour of materials sliding against each other at different sliding speeds and normal loads [73]. The concept of generating wear maps for metals is not new. It is since 1941 when the attempt was made to present wear data in map form in their work on the wear of cast iron and steel by Okoshi and Sakai [142]. More than two decades later, welsh presented a diagram

Tribo-corrosion maps for steels, titanium and titanium carbide materials

summarising the sliding conditions corresponding to the mild wear and severe wear transitions observed in the wear of steels [68].

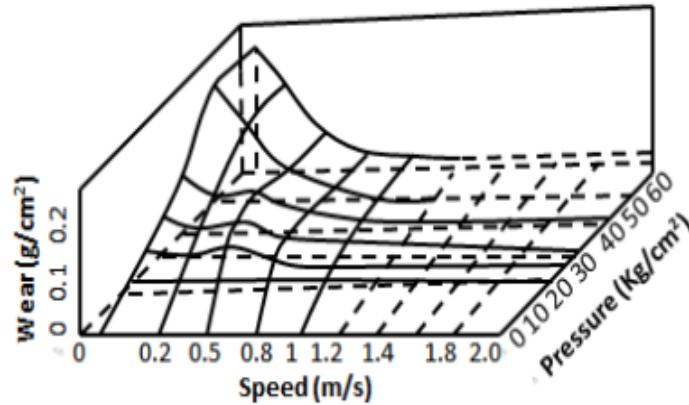


Figure 17 The wear-rate surface for steel proposed by Okoshi and Sakai [142]

In the early 1980s, a number of wear maps, mostly included for the unlubricated wear of steels with different tests methods were generated. These include the work of Child [144], Eyre [145], Marciniak and Otimianowski [146] and Egawa [147]. These diagrams show the boundaries drawn between mild and severe wear regimes except from Marciniak and Otimianowski diagram, which gives wear-rate surface as that of Okoshi and Sakai work Fig. 17.

In the Childs wear map not only the mode of wear is described but expected dominant wear mechanisms in five different regimes (A to E) are also mentioned Fig 18. Childs wear mechanisms map shows the effects of sliding speed and normal load on wear mechanisms during the dry sliding of soft steels on soft steels [144]. In region A, surface work hardening and smoothing can occur under a protective oxide layer. Wearing is occurring in this region either by removal of oxide layer or by metal fatigue i.e. delamination. In regime B, at slightly higher loads and sliding speeds, oxide protective layer may break down leads to severe metallic transfer and wear. In region C, at the same range of normal load that of A, but at higher sliding speeds, enhanced oxidation due to frictional heating and surface transformation hardening of steels can restore the oxide protective layer. In hotter condition, region D, gross surface softening can be cause of wear mode transition from mild to severe wear again. In the even more-hot region E, again oxidative dominated wear regimes have been observed. The positions of the boundaries in this map depend strongly

Tribo-corrosion maps for steels, titanium and titanium carbide materials

on the materials of the sliding couple. For example the tongue, in this case, with which region B separate region A and C can be retracted by hardening the steels [144].

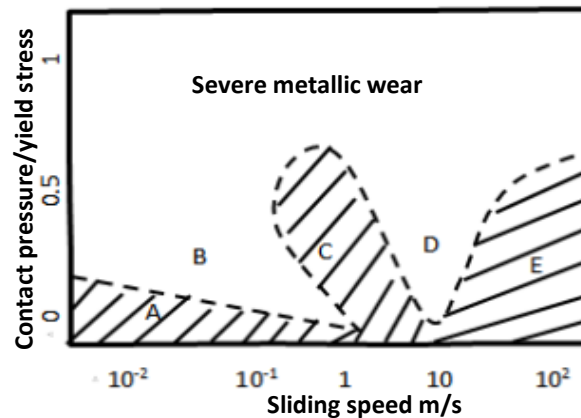


Figure 18 Wear regimes mapped on a base of load and sliding speed for soft steels sliding on soft steels [144].

The wear maps available so far except Childs wear map had limited range of operating conditions covered and the lack of information on the dominant mechanisms of wear. The information provided was limited to whether mild wear, severe wear or transition observed between these wear modes. These limitations were addressed by Lim and Ashby [135] by developing the wear-mode map for unlubricated sliding of steel on steel in the pin-on-disc configuration Fig. 19. This map presenting the various wear regimes, in which different modes of wear dominate. It defined a mathematical method of establishing boundaries between regimes, and importantly, superimposed contours of wear rates on the surface. This map was an important advance in describing the interactions between wear regimes where oxidation occurring due to frictional heating affected the wear mechanism [4].

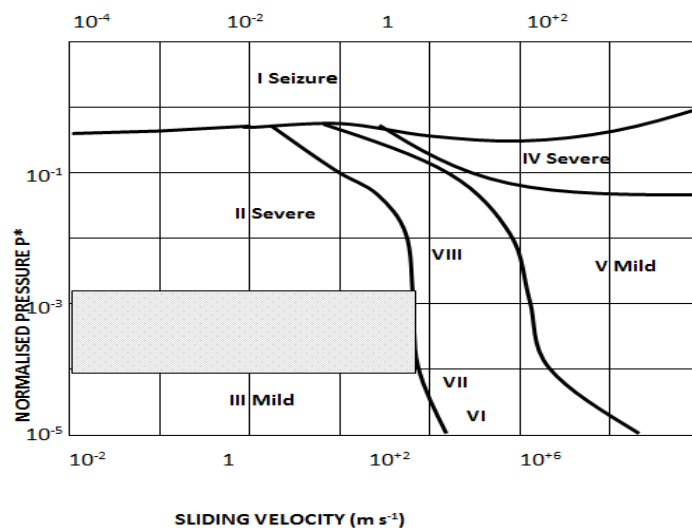


Figure 19 Wear mode-mode map for unlubricated sliding of steel on steel in the pin-on-disc configuration [135].

This map is specific for steels but the general form will be similar for the unlubricated sliding of most metals in air. In this map dimensionless variables are employed: a normalized contact pressure (defined as the normal load on the specimen pin, divided by the normal contact area times the indentation hardness of the softer material), and a normalized velocity (which can be thought of as the sliding velocity divided by the velocity of the heat flow). Representative values of sliding velocity are also given along the upper x-axis, for typical steel.

The dominant modes of wear, and resulting regions on the diagram are represented by plotting empirical data collected from different experiments and by using a simple analytical models for wear rates due to the various wear mechanisms. Eight distinct regimes can be identified in Fig. 19. Regime (I) represents very high contact pressure result in seizure of the contact surfaces. This regime corresponds to extensive growth of asperity junctions and the real area of contact becomes equal the apparent area. Regime (II) is a severe wear region, related to high normal load and relatively low sliding speeds. Thin surface oxide layer is penetrated at asperity contacts, high adhesive friction results in metallic wear debris. In regime (III) the oxide layer is not penetrated and low wear rate results in mild wear. In regimes (II) and (III) thermal effects are negligible.

In regime IV, the frictional power dissipation is high due to higher loads and sliding speeds results in no heat removal from the interface leads to melting occurs. Although this lead to a low friction coefficient, viscous forces in the molten layer continue to dissipate energy and severe wear occurs. In regime V the interface temperature is high at lower normal loads and higher sliding speeds but does not reach the melting point of the metal. Severe oxidation, results in lower wear rate, mild wear occurs in this region due to high rate of surface oxidation at higher surface temperature.

Regimes (VI), (VII) and (VIII) are consisted of narrow range of sliding speed. Different types of wear mode transitional behaviour occurs in this region i.e. the extreme of low sliding speed, isothermal conditions and high sliding speed, adiabatic conditions. With increase in sliding speed these three wear regimes are observed at lower normal loads. In regime (VI), thermal effects begin to play a role through the action of hot-spots at the asperity contacts. The flash temperature leads to generation of patchy oxide layer and mild wear debris produces in this regime, comes from the oxide layer. In regime (VII), metallic contact between asperities occurs due to higher load and severe wear occurs with metallic wear

debris. In regime (VIII), at higher flash temperatures martensite is formed at the contact surface due to local heating of the asperities, followed by quenching by conduction of heat into the bulk. The higher flash temperatures also increase the local oxidation rate at the contacts areas. A thicker layer of oxide now supported by the hardened substrate and is able to prevent further direct metal-to-metal contact despite the higher pressure at the contacting asperities and results in mild wear [62].

Later on Liu et al. [136] constructed a qualitative wear mechanism map for Al alloys by collecting data from the literature. Their work obtained reasonable agreement with the above mentioned Lim and Ashby map. Another wear map approach was adopted by Kato et al. involving pin-on-disk unlubricated sliding wear tests over a wide range of normal loads and sliding speeds carried out on untreated and gas nitride steels [137]. They classified mild and severe wear regimes on load and speed axis on the basis of wear debris produced during tests. It was found that gas nitriding not only reduced steel wear rates but also expanded the mild wear regime region towards higher normal load and sliding speed.

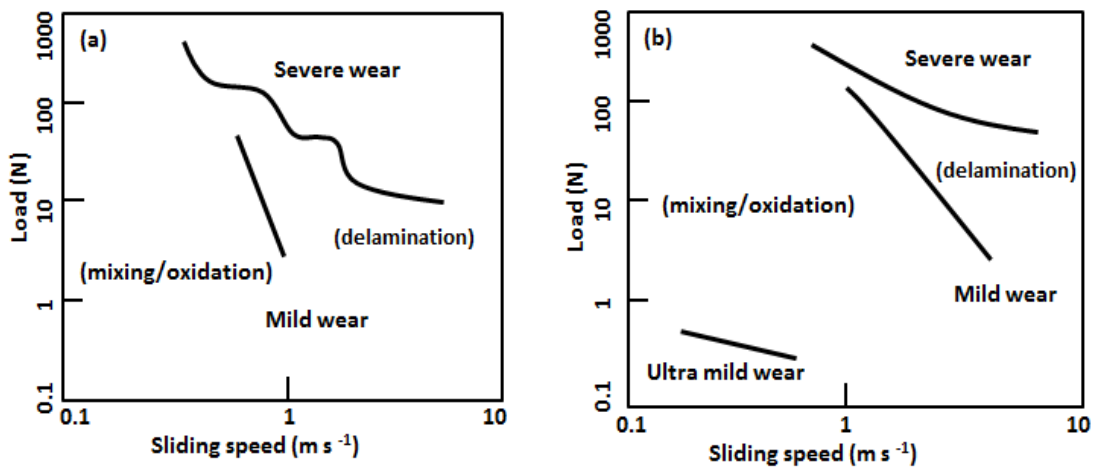


Figure 20 Wear rate maps (a) for A356 Al worn against SAE 52100 steel counterface, (b) for A356 Al-20% SiC composite worn against SAE 52100 steel counterface [73].

Zhang and Alpas constructed an empirical wear transition map on normal load versus sliding speed axis for the aluminium alloy sliding against steel [72]. They observed that the transition from mild to severe occurred when the bulk surface temperature T_b exceeded a critical temperature and provided a practical approach by which the onset of severe wear for a given tribo-system can be predicted for Al alloys sliding against steel, using a single bulk temperature measurement. Other wear maps have been developed are included TiN and Al₂O₃ coated steels [70] and ceramic sliding pairs [138].

S. Wilson and A.T. Alpas [73], developed wear mechanism maps for metal and metal matrix composites (A356 Al and A356 Al-20% SiC) against SAE (AISI) 52100 bearing steel counterface Fig. 20. The boundaries of mild and severe wear were drawn on the basis of wear rates on these maps. As shown in the Fig. 20(b) the composite has an additional ultra-mild wear regime where an order of magnitude drop in wear rate occurs at very low normal loads and sliding speeds. The ultra-mild wear is due to the load bearing capacity of the SiC reinforcing particles at very low loads. An iron oxide layer forms on the contact surface of the composites. Negligible particle fracture occurs in this regime that protects the matrix alloy from removal during sliding against the steel [139]. At the extreme of normal load and sliding speed conditions, severe wear occurs and wear rate increases. This is more pronounced in the case of A356 Al Fig. 20(a). The addition of SiC to A356 Al extends the transition to severe wear to the higher range of sliding speeds and normal loads.

For both materials, within the mild wear regime, wear occurs by two different wear mechanisms which are 'mechanical mixing/oxidation' at low normal loads and sliding speeds, whereas by 'delamination' at higher sliding speeds. Mechanical mixing/oxidation produces a compacted layer comprised of mechanically mixed Al and Fe particles together with amorphous Al and aluminium oxide [72]. The delamination wear occurs at higher sliding speed due to the frictional heating effects. Debris produced during delamination above the critical speed range was shiny metallic and plate-like in shape. Due to addition of SiC particulates in A356 Al the boundary between mixing/oxidation and delamination wear regimes is extended to a higher range of sliding speeds Fig. 20.

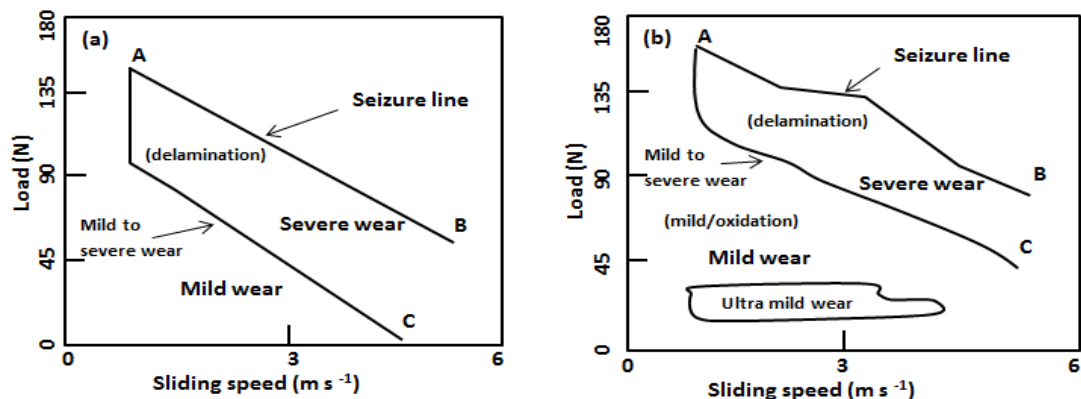


Figure 21 Wear mechanism map (a) for 7010 alloy, (b) for 7010 -25% SiCp [148].

Recently, the wear maps developed by R. N. Rao, et al. for dry sliding wear of AA7010 (Al-Zn-Mg-Cu) aluminium matrix composite are shown in Fig. 21 [148]. The effects of the

change in sliding speeds and normal loads on the wear rates are represented on these wear maps in terms of mild wear, severe wear (delamination) and seizure for the bulk and composite material. For aluminium alloys, mild wear is dominated at low sliding speeds and normal load. The line AB is the upper boundary line for the delamination wear after that seizure occurs. Line AC shows the upper boundary of the mild wear and then wear mode transition occurs mild to severe (delamination) Fig. 21(a). For the composite material, Fig. 21(b), It is clear that both line AB and AC shifted upward significantly i.e. the range of sliding speed and normal load has extended to higher side for the composite materials. The observations of this work are in agreement with S. Wilson and A.T. Alpas wear maps [73].

The usefulness of wear-mechanism maps is not restricted to bulk materials. It has been suggested that these maps can be employed to understand the wear of coatings deposited on different substrate [140]. These maps can be used for modelling wear mechanisms and the design of coating systems to provide enhanced performance [63]. Wear characteristics of TiN and TiC coatings on tool inserts were also examined by using mapping techniques Fig. 22,[140].

Fig. 22 shows the coated tool and flank-wear map for TiN-coated HSS tool inserts. Coating results in expansion of the safety zone and least-wear regimes as compared to uncoated one. This map shows that the amount of tool wear reduction which such a coating may provide is dependent on the machining conditions employed. This type of wear map will help the end users to employ these coated inserts in the cost effective manner [63].

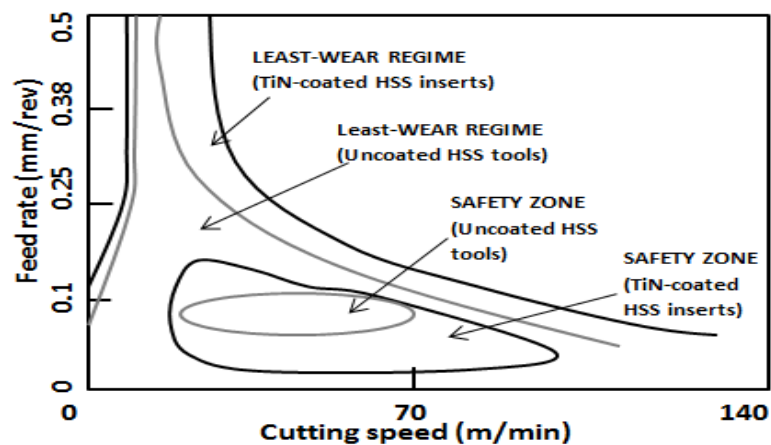


Figure 22 Map showing the expansion of safety zone and least-wear regimes as a result of the application of TiN coatings on the crater wear of HSS tools during dry turning operations [63].

By using the similar wear mapping approach to that of [73], for metal matrix composites, Wilson and Alpas developed the wear mechanism maps for TiN-coated high speed steel Fig. 23, [74]. Four wear regimes are presented on this map. In regime (I) rapid coating wear occurs at low sliding speeds and normal loads and coating worn through to the substrate due to rapid polishing of the coatings. Regime (II) shows the behaviour of coating, mild wear of TiN coating occurs along with mass gain for a few combinations of sliding speeds and normal loads and oxidised HSS transfer from pin.

In wear regime (III) high wear of TiN occurs above the 100 N normal loads due extensive coating damaged and exposure of substrate. At higher sliding speeds and normal loads, region (IV), same wear trend seen as that of in region (I).

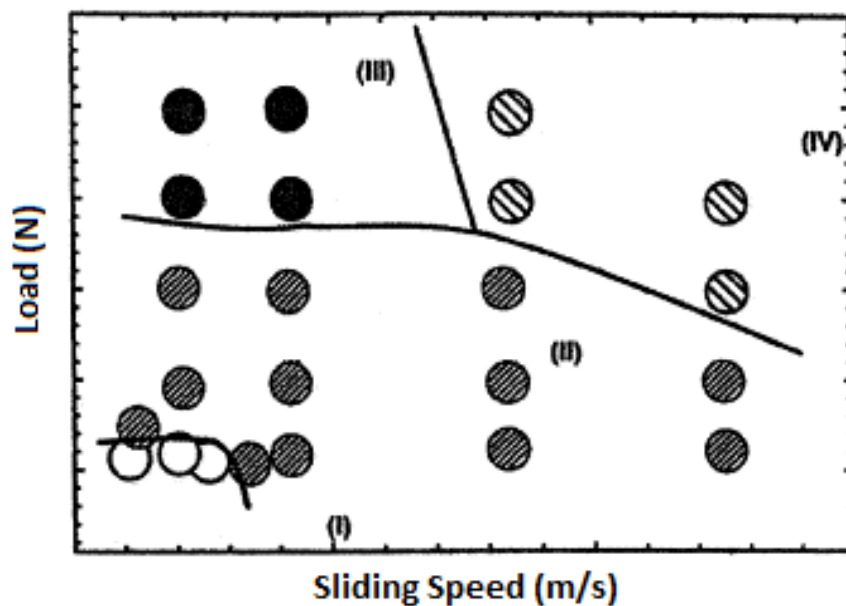


Figure 23 Wear map for TiN sliding on steel [74].

2.10 wear of coatings

For tribological applications, the wear resistance of the materials can be increased and their frictional properties can be changed by using surface engineering techniques. The only microstructure of the surface material can be modified without changing its composition, as in transformation hardening or melting followed rapid solidification. Both the composition and the microstructure can be changed as well, by thermally-enhanced diffusion of a different chemical species into the surface. The changes in composition and microstructure which can be carried out by these methods are not limited and for many specific purposes coatings of completely different materials can be carried out [62]. When

the surface of a tribo-element has a coating that is much harder than that of the substrate, wear of the substrate much reduced due to coating as long as it exists on the surface, because hard materials generally are more wear resistance than soft materials under the same frictional conditions [155], Fig. 24.

In the case of TiC composite coating, it is assumed that the wear process proceeds by preferentially abrading the matrix pick and dig up the matrix progressively. This action gradually raises the hard TiC particles in the coating and then these particles carry the load of abrasive particles. Generally, the two components of wear resistant materials (matrix and hard TiC particles) perform different roles. The metal matrix supply sufficient toughness for hard particles, the hard particles provide a barrier against indentation, grooving and cutting of abrasive materials as well as reducing the contact area of the matrix with the abrading counterface. Thus, the amount, size and distribution of hard particles and also the hardness and fracture toughness of both components and the bond between them are significant parameters in the resistance of material against wear [158].

Wear mechanism typically classifies into four types of interactions between abrasive particle and the wearing material. These are microploughing, microfatigue, microcutting and microcracking. Microploughing does not lead to any material separation from the wearing surface because of a single pass of one abrasive particle. A plough is produced ahead of the abrading particle and the material is successively moved sideways to create ridges adjacent to the groove. The material may break off by microfatigue as a result of ploughing aside repeatedly by passing particles. Microcutting produces a volume loss by chips equal to the volume of wear grooves. Microcracking takes place when abrasive particles impose on highly concentrated stress, especially on the surface of brittle materials. Generally, microploughing and microcutting are major wear mechanisms that occur on ductile materials while microcracking is dominated on brittle materials [195].

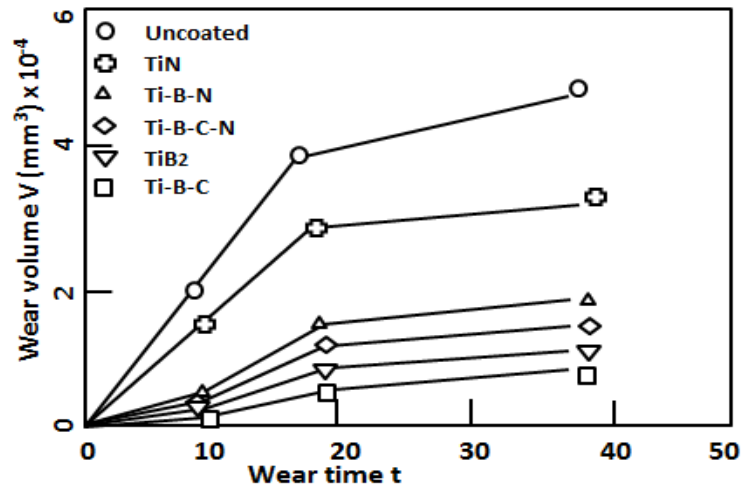


Figure 24 Wear volume as a function of time for different coatings and uncoated substrate [62].

2.11. Friction

Friction may be defined as the resistance encountered by one body in moving over another. The relation between normal load and frictional force is represented by the friction coefficient, μ .

$$\mu = F/W$$

μ - values describe the magnitude of the frictional force. Values between around 0.001 and around 10 are encountered in a lubricated bearing under light loads and when clean metals rub against each other in vacuum respectively. The most μ -values, for sliding surfaces in air, fall between 0.1 and 1.0 [62].

2.11.1 The Laws of Friction

Law 1:

Friction force is proportional to normal load.

This law, which can be expressed as $F = \mu W$ means that the friction coefficient, μ is independent of the normal load.

The most of metals, in both lubricated and unlubricated conditions, obey the first law, while the most of polymeric materials do not. Fig. 25 shows the change in coefficient of friction with the increase in normal load of steel against alumina under unlubricated sliding conditions, which is in agreement of 1st. law of friction.

Tribo-corrosion maps for steels, titanium and titanium carbide materials

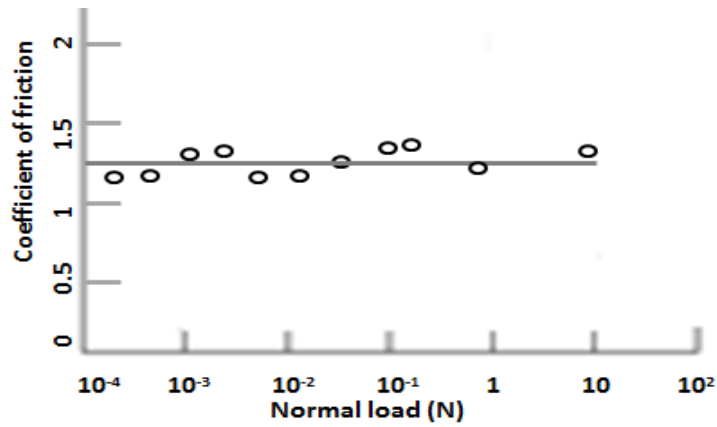


Figure 25 The variation of the coefficient of friction with normal load for the unlubricated sliding of steel on aluminium in air [62].

Law 2:

The frictional force is independent of the apparent contact area.

Again, this law normally is held for metals and do not frequently for polymers. Fig. 26 shows the change in coefficient of friction with the change in apparent area of contact for wooden sliders on an unlubricated steel surface, which is in agreement of 2nd law of friction.

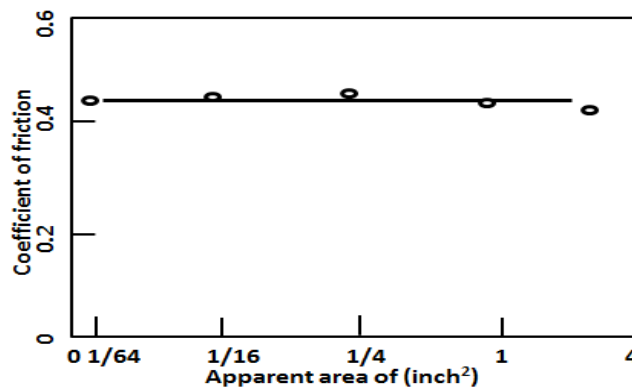


Figure 26 The variation of the coefficient of friction with apparent area of contact for wooden sliders on an unlubricated steel surface [62].

Law 3:

The frictional force is independent of the sliding speed.

This law does not hold as frequently as the first two laws.

It is almost always observed that the frictional force needed to be overcome in order to start a body moving is higher than the force needed to be overcome in order to maintain

Tribo-corrosion maps for steels, titanium and titanium carbide materials

the body in motion (i.e. the static friction coefficient μ_s is larger than the dynamic friction coefficient μ_d). Fig. 27 shows coefficient of friction as a function of sliding velocity for titanium sliding on titanium at a normal load 3N.

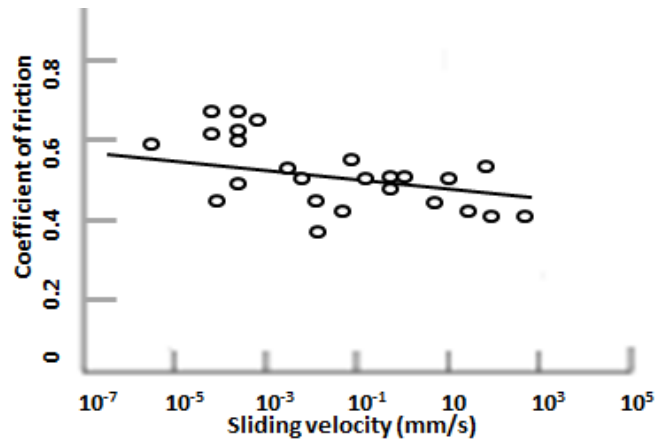


Figure 27 The coefficient of friction as a function of sliding velocity [96].

Moreover, the coefficient of kinetic friction as a function of sliding speed generally has a negative slope Fig. 27. The small slope of friction-sliding velocity curve shows that the coefficient of friction changes very slowly with respect to the change in velocity of an order of magnitude. Changes in the sliding speeds result in change in the shear rate and surface temperature that can both affect the mechanical properties of the mating surfaces [89].

2.11.2 Causes of Friction

Friction is because of interactions between asperities at the contact area. The energy produced by the motion is dissipated as heat in the near-surface region. In steady state, the energy produced per unit time is the product of the frictional force and the sliding speed. Adhesion and deformation play a major role in the dissipation of heat.

Adhesion

Adhesion arises from the attractive forces operating between the asperities. Clean, oxide-free metal surfaces show significant adhesion effects that can be observed under high vacuum conditions, which result in an increase of coefficient of friction between sliding partners as compared to the normal environments.

Deformation

Tribo-corrosion maps for steels, titanium and titanium carbide materials

Apart from the interactions between asperities of both sliding partners, there is also the possibility that an asperity ploughs its way through the surface of the other partner, leading to a groove. In this case one of the partners is significantly harder than that of the other. Therefore deformation also contribute to the coefficient of friction

It is found in the literature that adhesion and deformation both contribute around 0.3 to the value of friction coefficient [62]. Work hardening and junction growth play the biggest role in this situation. Work hardening lead to higher value of the adhesion component than one would expect from normal shear strength values. Junction growth occurs when an asperity is plastically deformed by means of shear force, thereby leading to an increase in contact area. This process is limited either by the tensile strength of the material or the presence of a boundary film of low shear strength. The presence of such a film is one of the principles of lubrication [62].

2.12 Friction of Materials

The coefficient of friction of a material is dependent upon the counterface material, surface preparation and operating conditions.

2.12.1 Friction of Metals and Alloys

As mentioned above, the clean metal and alloy surfaces in contact present high adhesion, and consequently high friction and wear due to strong metallic bonds across the interface and significant transfer of metal between tribo-couple and results in loose wear debris. Even very low contamination or formation of chemical film reduces the adhesion that results in reduction of friction [11, 117].

Most metals oxidise in air to some extent and oxide film of 1 to 10nm thick forms on the metals surfaces within a few minutes of exposure to air. The oxide film acts as a low shear-strength film and due to its ductility offer low friction. The oxide film may effectively reduce metal to metal contact of the mating surfaces [62].

The coefficient of friction in case of soft and ductile metals such as Pb and Sn is high because of large contact areas even at lower normal load and small elastic recovery. Hexagonal metals such as Co and Mg as well as non-hexagonal metals such as Mo and Cr offer low friction. Co, Mo and Cr are common alloying elements in steel to reduce friction, wear and corrosion. Generally alloys exhibit lower coefficient of friction as compared to its pure metals.

2.12.2 Effect of Operating Conditions

The coefficient of friction of metals and alloys is affected by sliding speed, normal load, temperature, environment, and relative humidity as well.

Effect of sliding speed

High sliding speed results in surface frictional heating. Surface heating at high speeds may result in formation of a thin molten layer at the asperity contacts in case of low-melting point metals, which reduces its shear strength and friction drop to a low value determined by viscous forces in the liquid. Generally formation of oxide layers at high temperature results in lower friction. At low sliding speeds a molten film does not form and the friction is controlled by the interaction of the solid surfaces Fig. 28, [62].

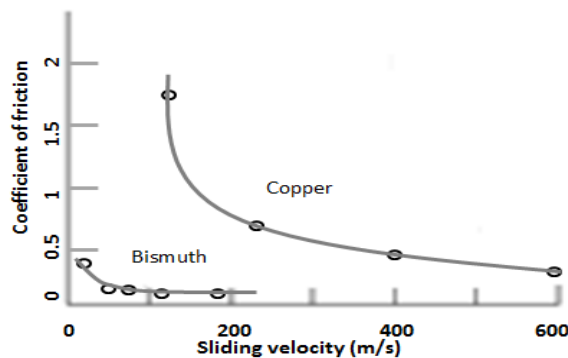


Figure 28 The variation of the coefficient of friction with sliding speed for pure bismuth and copper sliding against themselves [62].

Effect of normal load

Fig. 29(a) shows the coefficient of friction as a function of normal load for a steel slider on unlubricated aluminium in air, which stays constant despite the normal load is varied by a factor of 10^2 [151]. Fig. 29(b) shows the coefficient of friction may not remain constant during sliding as a function of normal load. As in the case of copper sliding on copper in air, the coefficient of friction is low at low loads and a transition occurs to a higher value with an increase in normal load. This because of (1) that copper readily oxidises in air and thin oxide layer effectively separate the two metal surfaces and there is little or no metal to metal contact between mating surfaces at low normal loads; (2) that the oxide layer has low shear strength. With an increase in normal loads, the oxide layer breaks down, result in metal to metal contact between mating surfaces at high loads, which is responsible for high friction and surface damage [151]. This type of behaviour of friction has been observed in

Tribo-corrosion maps for steels, titanium and titanium carbide materials

other metals as well [96]. On the other hand the coefficient of friction decrease with increase in normal load for many metals Fig. 29(c). Increased surface roughness and a large quantity of wear debris are attributed to the decrease in friction [152].

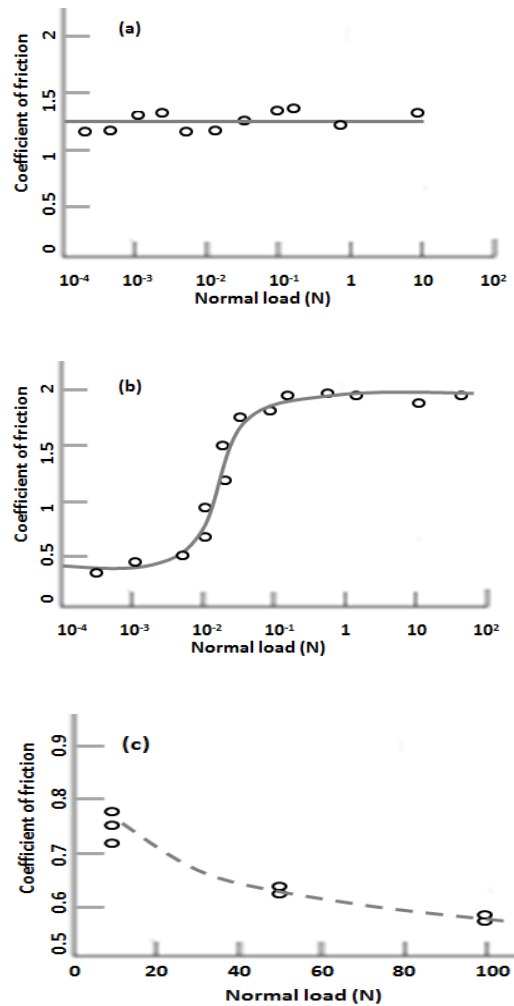


Figure 29 The effect of normal load on the coefficient of friction for (a) steel on aluminium in air, (b) a copper on copper in air, and (c) AISI 440C stainless steel on Ni3Al alloy in air [89].

In case of dissimilar metals and alloys, the coefficient of friction tends to be low than that for its pure components. The sliding friction of steels has been widely studied: coefficient of friction varies with composition as well as with microstructure, and often depends on normal load. In Fig. 30, the solid curve, for 0.4% carbon steel shows a transition from relatively high value of μ at low loads to lower value at high loads.

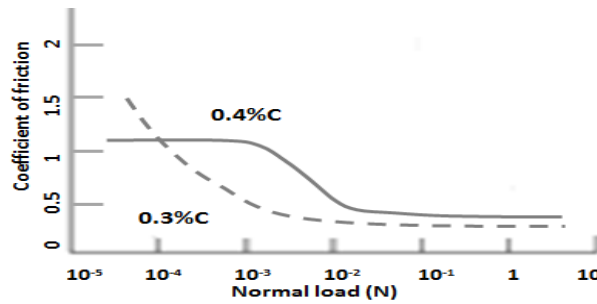


Figure 30 The variation of coefficient of friction with normal load for steels sliding against themselves in air, showing the results for two different plain carbon steels, with carbon contents of 0.4% (full curve) and 0.3% (broken curve) [62].

Effect of Temperature

With the increase in temperature of the sliding metal, several effects occur. Its mechanical properties will change, its rate of oxidation will increase, and phase transformations may take place. All these factors will affect its frictional behaviour.

2.12.3 Friction of Ceramic Materials

Engineering ceramics have low density with excellent mechanical properties i.e. high strength, hardness and stiffness, up to high temperatures. The major difference in mechanical behaviour between the engineering ceramics and metals arise from the different nature of the interatomic forces: ionic or covalent in ceramics, rather than metallic bonding. Ionic bonding, in ceramics such as MgO or Al₂O₃, leads to crystal structures with only a small number of independent slip systems available for dislocation. Covalent bonding, as in SiC, TiC or diamond, leads to very narrow dislocations which move only under high stress [62].

Ceramic materials show only limited plastic flow and much less ductility than metals. The asperity contact between ceramics is more likely to be elastic than in metals. The larger plastic strains associated with junction growth in metals do not therefore occur in ceramics except at high temperature. Despite adhesive forces are present between ceramic materials in contact, the coefficient of friction never reaches the very high values as found in clean metals sliding in the absence of oxygen. The value of μ for ceramic-ceramic contacts lies in the range from 0.25 to 0.8 which is equal to the value of the μ for metallic couple sliding in air in the presence of intact oxide films. The μ for engineering ceramics vary due to change in environment. Despite the engineering ceramics are considered to be chemically inert, the surfaces of most ceramics are susceptible to tribo-chemical reactions

which lead to formation of surface films and thus modify their frictional behaviour. These reactions take place much more rapidly at a sliding contact due to flash temperature than on a free surface at the same bulk temperature.

It has been found that non-oxide ceramics like silicon nitride, silicon carbide, titanium nitride and titanium carbide have reacted with oxygen significantly after sliding in air. Oxide ceramics like alumina and zirconia will react with water and form hydrated surface layers on sliding in humid air. While in the case of non-oxide ceramics, oxidation followed by hydration.

In a few ceramics the effect of surface films and the extent of surface fracture can be important in the friction of ceramics. Surface film can reduce the friction and surface fracture leads to an increase in friction, since it provides an additional mechanism for the dissipation of energy at the sliding contact. Fig. 31 shows the results of experiment, found in literature, in which a diamond cone was slid over a single crystal of silicon carbide. At low normal loads, the value of the μ is small due to plastic grooving of the silicon carbide with no fracture. With the increase in load, brittle fracture results in higher coefficient of friction [62].

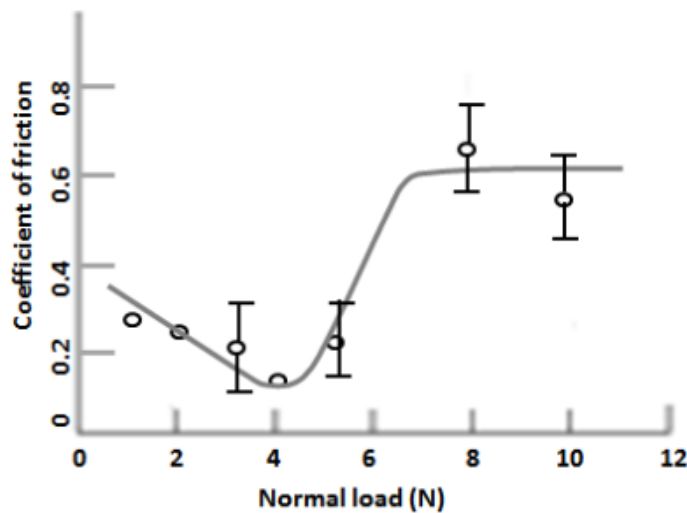


Figure 31 The variation of coefficient of friction with normal load for a 60° diamond cone sliding over the (0001) face of a silicon carbide single crystal. The increase for loads above ~ 4N is associated with fracture along the sliding path [62].

As observed for metals, the effects of environment composition, temperature, load, sliding speed and time of sliding on the frictional behaviour of ceramics occur in shape of tribo-chemical surface film and the extent of the fracture in the contact area. Fig. 31 and Fig. 32

Tribo-corrosion maps for steels, titanium and titanium carbide materials

show the effects of normal load and sliding speed on friction during sliding of ceramics. Both load and sliding speed will also affect the rate of frictional energy dissipation that results in change of temperature at the interface. Sufficiently high temperatures increase the plasticity in most ceramics as well and will also affect the frictional behaviour.

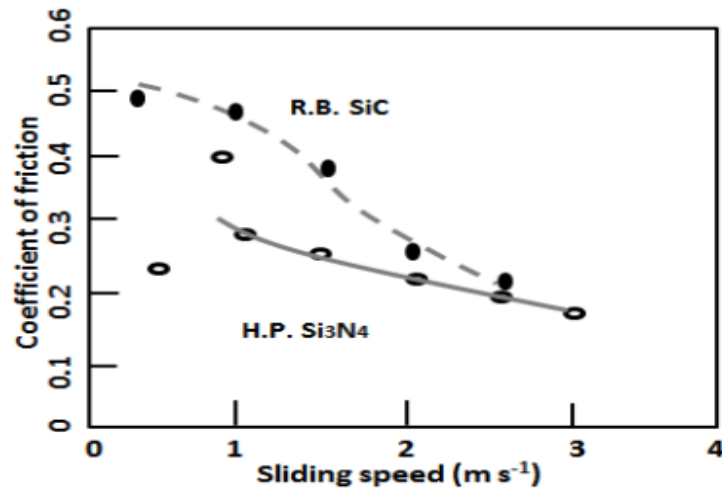


Figure 32 The variation of coefficient of friction with sliding speed reaction-bonded silicon carbide and hot-pressed silicon nitride sliding in self-mated couples in air [62].

2.13 Wear in relation to friction

Friction and wear are responses of a tribo-system. Coefficient of friction and wear are parameters describing the state of contact of bodies in a tribo-system, and they are not material constants of the bodies in contact [153]. Friction and wear, as two kinds of responses from one tribo-system, need to be exactly related with each other for every state of contact in a tribo-system, although a comprehensive simple relationship should not be expected [154].

Chapter 3

Experimental Methodology

3.1. Pin-on-Disk sliding wear testing rig (ASTM G99)

3.1.1. Introduction

Pin-on-disk apparatus is the most widely used wear testing process. This configuration is commonly used for wear tests in laboratories because of its simple arrangement. The applications of the pin-on-disk tests include investigation of the wear and friction properties of bulk materials, surface coatings, ceramics and cemented carbides etc. under ambient conditions at room temperature, at elevated temperatures, in controlled atmosphere, under wet and lubricated conditions [156]. Materials are tested in pairs under nominally non-abrasive conditions. The principal area of experimental attention in using this type of apparatus is to measure the sliding wear. The coefficient of friction during sliding can also be measured. Fig. 33 shows the schematic of the pin-on-disk sliding wear testing rig.

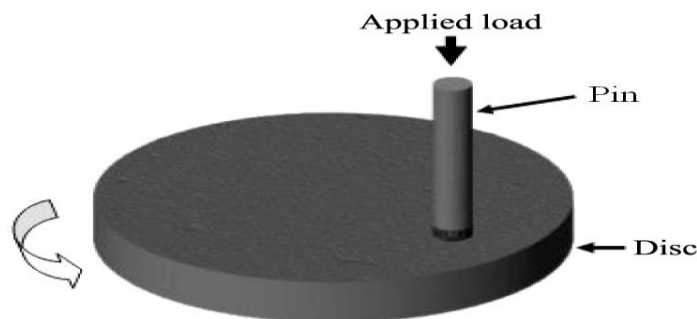


Figure 33 Schematic of Pin-on-Disk wears test apparatus.

For the pin-on-disk wear test, two specimens are required. One, a pin with smaller radius, is positioned perpendicular to the other and a flat circular disk. A ball, rigidly held, can also be used as pin specimen. The test machine causes either the disk specimen or the pin specimen to revolve about the disk centre. In either case, the sliding path is a circle on the disk surface. The plane of the disk may be oriented either horizontally or vertically.

3.1.2. General apparatus description

The Schematic drawing of a typical Pin-on-Disk wear testing apparatus is shown in Fig. 33. This system consists of a driven spindle and disk holding arrangement to hold the revolving disk, a lever-arm device to hold the pin, and the attachments to allow the pin specimen to

Tribo-corrosion maps for steels, titanium and titanium carbide materials

be forced against the revolving disk specimen with a controlled load. The system may have a friction force measuring arrangement, for example a load cell that allows the coefficient of friction to be determined.

A variable speed motor, capable of maintaining constant speed ($\pm 1\%$ of rated full load motor speed) under load is required. The motor should be mounted in such a manner that its vibration does not affect the test. The machine shall be equipped with a revolution counter that will record the number of disk revolutions, and preferably have the ability to shut the machine after a pre-selected number of revolutions. The stationary specimen holder is attached to a lever arm that has a pivot. Adding weights, as one option of loading, produces a test force proportional to the mass of the weights applied. Ideally, the pivot of the arm should be located in the plane of the wearing contact to avoid extraneous loading forces due to sliding friction. The pin holder and arm must be of substantial construction to reduce vibration motion during the test.

3.1.3. Significance and use

The amount of wear in any system will, in general, depend upon the number of system factors such as the applied load, machine characteristics, sliding speed, sliding distance, the environment, and material properties. The value of any wear test method lies in predicting the relative ranking of material compositions. Since the pin-on-disk test method does not attempt to duplicate all the conditions that may be experienced in service (for example; lubrication, load, pressure, contact geometry, removal of wear debris, and presence of corrosive environment), there is no insurance that the test will predict the wear rate of a given material under conditions differing from those in the test.

3.1.4. Testing apparatus (pin-on-disk sliding wear testing rig)

Fig. 34 shows the pin-on-disk wear testing rig, which was used for experimental work of the present project. In this rig the plane of the disk was oriented horizontally, which was revolving and the stationary pin was held rigidly in a pin holder which was subjected to required variable normal loads in this arrangement. This apparatus was mainly consisted of:

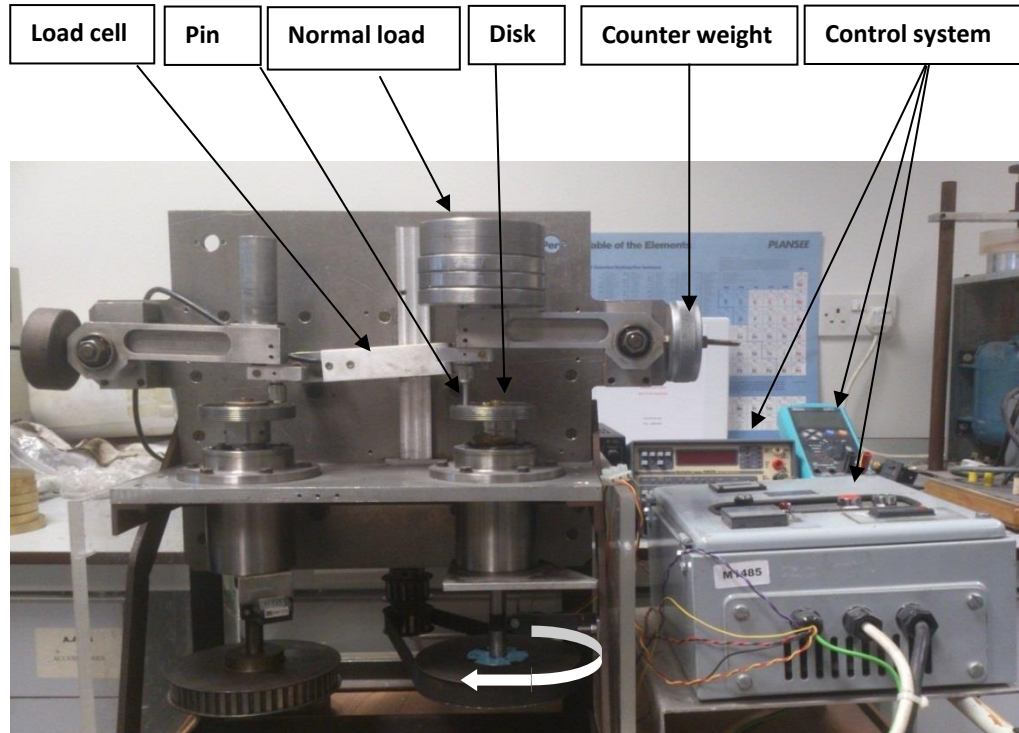


Figure 34 Pin-On-Disk dry sliding wear testing rig.

- **Load cell:** a 20kg load cell was installed to measure the friction force between the mating surfaces of rotating disk and stationary pin during sliding.
- **Pin:** was used as a test specimen and was rigidly held in pin holder.
- **Normal load:** this arrangement shows that variable loads can be applied.
- **Disk:** was used as counterface and was rigidly held in the disk holder.
- **Counter weight:** was used to balance the weight of the pin specimen holder and lever arm prior to applying tests normal loads.
- **Control system:** was consisted of, a) a frequency meter, to control the sliding speed, b) a revolution counter, to control the number of revolutions and c) timer, to control the experimental time for constant sliding distance for the various combinations of sliding speeds and normal loads.

3.1.5. Function and calibration of load cell

The load cell is mounted on rigid plate that locates it behind the pin holder. When the horizontally held disk is rotated under the stationary normally loaded pin by overcoming the frictional force, the pin holder arm push the sensor of the load cell in the tangential

Tribo-corrosion maps for steels, titanium and titanium carbide materials

(rotating) direction of the disk. Load cell send signal through the cable connection to dc bridge / transducer amplifier. This amplifier transmit signal to the multi-meter in volts.

Calibration of load cell to record friction force:

- Select coarse gain on dc-bridge / transducer amplifier and set at 1volt.
- Select fine gain on dc bridge / transducer amplifier to get 00 (zero) reading at no load position and lock.
- Select – V (volt) position on Black Star 4503 Intelligent Multimeter and then select button No. 4, i.e. range 0- 0.4volt.

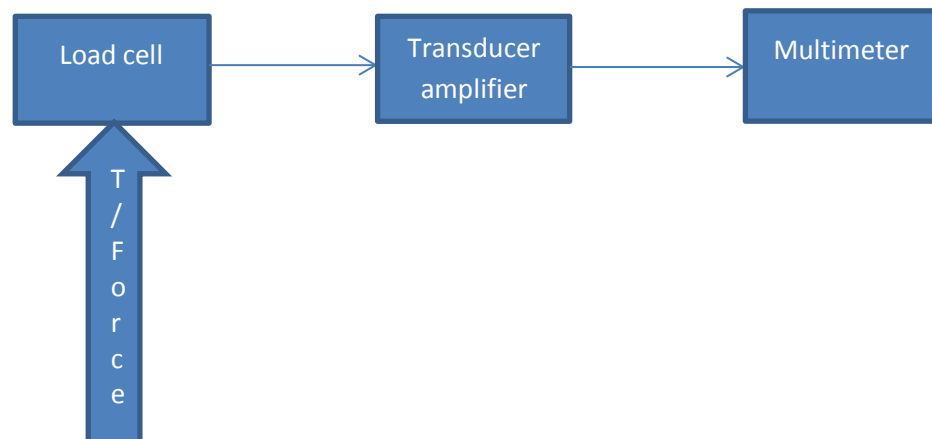
Dismantled the load cell from the testing rig and then calibrated this by applying 1 to 5N normal load as under:

Load (N)	1	2	3	4	5
Meter Reading (V)	0.00135	0.00270	0.00405	0.00540	0.00675

Table 1 Variation in multimeter reading with increase in loads

1N load = 0.00135volts (1 N frictional force = 0.00135 volts at multimeter display)

Fig. 35 shows the working of load cell to measure friction force between the mating surfaces of the mater under testing.



Tangential force to overcome friction

Figure 35 Schematic diagram of the load cell function.

3.1.6. Control system

The control system of this dry sliding wear testing rig was developed in view of the parameters and conditions of the experimental work. As mentioned above, sliding speed, number of revolutions and sliding distance (experiment time) were controlled by frequency meter, revolution counter and timer respectively. Frequency meter and revolution counter worked on the base of a focused reflective object sensor, which was installed against the rotating spindle that revolved the disk chuck. The speed of the dc motor was controlled manually by maintaining the calculated frequency for required sliding speed. The frequency counter was connected to the focused reflective object sensor to count the number of revolutions per second. The timer was introduced between the on – off switch and dc motor which turn off the motor as per pre- setting time for the constant sliding distance of the experiment. Fig. 36 shows the working of the control system of the sliding wear testing rig to count the revolutions per second i.e. frequency and number of revolutions.

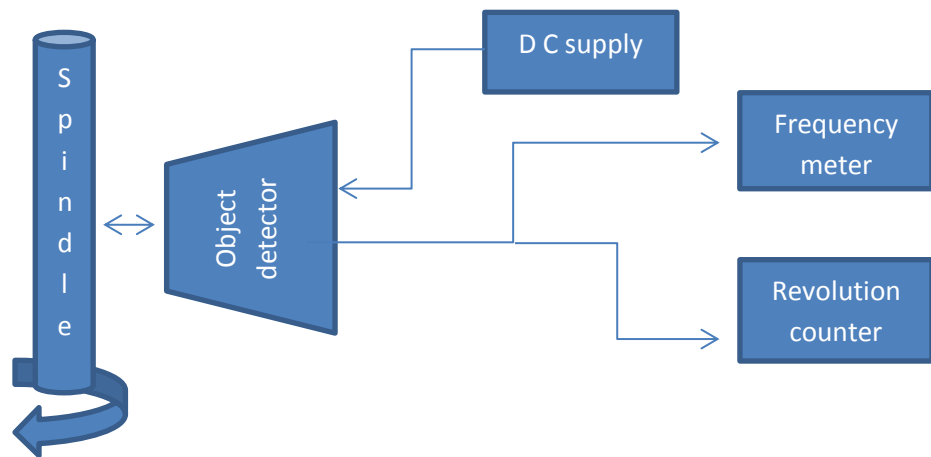


Figure 36 Schematic diagram of the sliding speed control and revolution counter.

Fig. 37 shows the working of the timer to control experimental duration for constant sliding distance in connection with DC motor and On/Off switch.

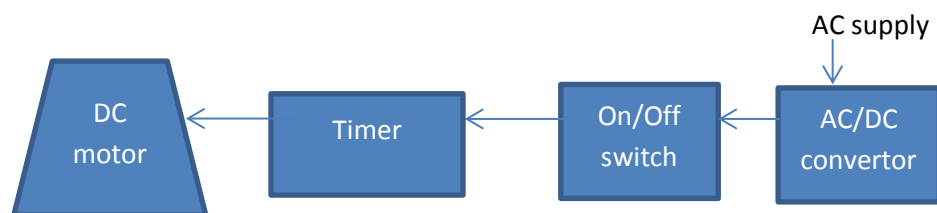


Figure 37 Schematic of the timer control and motor connections.

3.2. Experimental

For the dry sliding wear behaviour of 303 stainless steel disks against 8620 low alloy steel pins (Chapter 4), wear tests were carried out at sliding speeds 0.38, 0.5, 0.86, 1.2, and 1.5 m s⁻¹ and normal loads 10, 20, 30, 40, and 50 N. The sliding distance 5740 m and number of revolutions 30,000 were kept constant for each test. The dry sliding wear tests of 303 stainless steel and 303 stainless steel base titanium carbide composite coatings against alumina (Chapter 5) were carried out at sliding speeds 3, 7, 11, and 15 cm s⁻¹ and normal loads 2, 4, 6, 8, and 10 N. The sliding distance 500 m and number of revolutions 26,526 were kept constant for each test. For the dry sliding wear behaviour of commercially pure (CP) titanium and commercially pure (CP) titanium base titanium carbide composite coatings pins against hardened steel (A.I.S.I. 0-1-Ground Flat Stock) disk (Chapter 6 to 8) wear tests were carried out at sliding speeds 0.38, 0.5, 0.86, 1.2, and 1.5 m s⁻¹ and normal loads 10, 20, 30, 40, and 50 N. The sliding distance 5560 m and number of revolutions 30,000 were kept constant for each test. All tests were carried out under ambient conditions at room temperatures.

3.2.1. Calculations of frequency and experimental times

We know that Angular velocity $\omega = \frac{2\pi}{\text{time of 1 rev.}}$

Linear velocity $v = \omega r = \frac{2\pi}{\text{time of 1 rev.}} \times r$

Experimental times for dry sliding wear tests, carried out on pin-on-disk sliding wear testing rig Fig. 34, were calculated from the above relation between angular velocity and linear velocity; circumference of the wear track and frequency (revolutions per second) of the revolving disk holder spindle as below:

$$\text{Circumference of the wear track} = 2\pi r \text{ ----- (1)}$$

Where r is the average radius of the wear track in metre

We know frequency = rev s⁻¹

When revolution frequency = 1 = 1 rev s⁻¹

$$\text{Then sliding speed } v = 2\pi r \text{ m s}^{-1} \text{ ----- (2)}$$

From equation (2), we can find the required frequency for any sliding speed as follow:

Tribo-corrosion maps for steels, titanium and titanium carbide materials

Required frequency = required sliding speed dividing by the speed at frequency 1.

$$\text{Required frequency} = \text{required test sliding speed, } m \text{ s}^{-1} \div 2\pi r \text{ m s}^{-1} \text{ ---- (3)}$$

For calculation of experimental time for the different sliding speed use the following equation:

$$\text{We know that the distance covered, } s = v t \text{ ----- (4)}$$

Where v is speed and t is the time taken to cover distance s

$$\text{From equation (2), } t = s v^{-1} \text{ ----- (5)}$$

As the sliding distance is constant for each test therefore by using equation (5) we can calculate test duration for each sliding speed to cover constant sliding distance. Table 2 and 3 show the revolutions frequencies and tests duration for the experimental work carried out on pin-on-disk sliding wear testing rig Fig. 34 (chapter 4, 6-8).

Sliding speed (m s ⁻¹)	Circumference of the wear track (m)	Frequency (rev. per sec.) from equation (3)	Sliding distance (m)	Test duration (minutes) from equation (5)	Number of revolution
0.38	0.191	1.99	5,740	252	30,000
0.5	0.191	2.62	5,740	191	30,000
0.86	0.191	4.5	5,740	111	30,000
1.2	0.191	6.26	5,740	80	30,000
1.5	0.191	7.9	5,740	64	30,000

Table 2 Tests frequency and tests duration for 303SS disks against 8620 low alloy steel pins (chapter 4).

Sliding speed (ms ⁻¹)	Circumference of the wear track (m)	Frequency (rev. per sec.) from equation (3)	Sliding distance (m)	Test duration (minutes) from equation (5)	Number of revolution
0.38	0.185	2.1	5,560	244	30,000
0.5	0.185	2.7	5,560	185	30,000
0.86	0.185	4.65	5,560	108	30,000
1.2	0.185	6.5	5,560	77	30,000
1.5	0.185	8.1	5,560	62	30,000

Table 3 Tests frequency and tests duration for Ti and Ti base TiC composite coatings pins against hardened steel disks (chapter 6-8).

Note: The tests carried out to investigate the wear behaviour of 303SS and 303SS base TiC composite coatings (chapter 5) on +CSM Tribometer. This apparatus was computerised

Tribo-corrosion maps for steels, titanium and titanium carbide materials

controlled. There was no need of calculations for revolutions frequencies and tests durations.

3.2.2. Test specimens

This test method may be applied to variety of materials. The only requirement is that specimens having the specified dimensions can be prepared and can withstand the stresses imposed during the test without failure or excessive flexure. The materials being tested shall be described by dimensions, surface finish, material type, form, composition, microstructure, processing treatments, and indentation hardness (if appropriate).

The typical pin specimen shall be cylindrical or spherical in shape with diameters range from 2 to 10mm. The typical disk specimen diameters range from 30 to 100 mm and have thickness in the range of 2 to 10 mm. A ground surface roughness of 0.8 μm arithmetic average or less is usually recommended as the rough surfaces make wear scar measurement difficult. Care must be taken in surface preparation to avoid subsurface damage that alters the material significantly.

3.2.3 Test parameters

- Normal Load - Values of the force in Newton at the wearing contact.
- Sliding Speed – The relative sliding speed between the contacting surfaces in metres per second.
- Distance – Sliding distance in metres.
- Atmosphere – The atmosphere surrounding of the wear contact.

3.2.4. Test procedure

Prior to testing, weighing (10 min), the specimens were cleaned by using acetone to remove any type of dirt and contamination and dried.

- After cleaning and drying the specimens, weighed the both pin and disk test samples on an analytical balance with accuracy of 0.01 mg to the nearest 0.0001 g.
- Inserted the disk securely in the holding device perpendicular to the axis of the resolution.
- Inserted the pins specimen securely in its holder and checked that the specimens were perpendicular and maintaining the necessary contact conditions.
- Started the motor and adjusted the frequency for the desired sliding speed holding the pin specimen out of contact with the disk.

- Fixed the timer to the desired test time.
- Added the required proper mass (normal load) to lever arm to develop the selected force pressing the pin against the disk.
- Began the tests with specimens (pins) in contact under load.
- Recorded the reading of the multimeter after interval during the tests run.
- No test was interrupted and restarted.
- Timer stopped the tests automatically when the pre-fixed times were over.
- Removed the specimens and cleaned off any loose wear debris with acetone. Noted the existence of features on or near the wear scar such as; protrusions, displaced metal, discoloration, cracking or spotting with eyes.
- Reweighed the specimens to the nearest 0.0001 g, as appropriate.
- Performed the tests for the different combination of sliding speeds and normal load under the tests conditions including repeat tests to obtain sufficient data for significant results.
- Wear debris collected for further investigation of the sliding wear behaviour of the specimens.
- SEM and EDX tests of the worn surfaces and wear debris were carried out.
- Volume losses of the dissimilar tribo-couple were calculated from the densities of the specimen and counterface.

3.2.5. Calculation of wear and reporting

The wear measurements should be reported as volume loss in cubic millimetres or cubic metre for the pin and disk separately (in case of dissimilar pin and disk materials). While mass loss results may be used internally in laboratories to compare materials of equivalent densities. Take care to use and report the best available density value for the materials tested when calculating volume loss from measured mass loss.

Use the following equation for conversion of mass loss to volume loss:

$$\text{Volume loss, mm}^3 = (\text{mass loss g} \div \text{density g cm}^3) \times 10^3 \text{ ----- (6)}$$

$$\text{Volume loss, m}^3 = (\text{mass loss g} \div \text{density g cm}^3) \div 10^6 \text{ ----- (7)}$$

$$\text{Wear rate, (m}^3 \text{ m}^{-1}) = \text{volume loss} \div \text{sliding distance} \text{ ----- (8)}$$

$$\text{Or specific wear rate, (mm}^3 \text{ N}^{-1} \text{m}^{-1}) = \text{volume loss} \div (\text{sliding distance} \times \text{normal load}) \text{ ----- (9)}$$

Tribo-corrosion maps for steels, titanium and titanium carbide materials

If the materials being tested exhibit considerable transfer between specimens without loss from the system, volume loss may not be adequately reflect the actual amount or severity of wear. In these cases, this test method for reporting wear should not be used.

3.3 303stainless steel against 8620 low alloy steel

3.3.1 Experimental conditions

A 303SS (stainless steel) disk of 75 mm outer diameter, 3 mm thickness and a 8620 low alloy steel pins of 6mm diameter, 35mm height flat ends, apparent area of contact ($2.83 \text{ m}^2 \times 10^{-5}$) were used as tests specimens. The dry sliding wear tests were carried out under ambient conditions at room temperature on a Pin-On-Disk sliding wear testing apparatus Fig. 34. The (normally loaded) stationary pins were slid against rotating disks. The sliding distance was kept constant for all tests. The tests were carried out at different constant sliding speeds, 0.38, 0.5, 0.86, 1.2 and 1.5 m s^{-1} by varying normal loads in increments of 10 N, from 10 to 50N, apparent contact pressure range of 354 to 1,768kPa respectively, for 25 combinations of sliding speeds and normal loads. The sliding distance was 5740 m and the numbers of revolution were 30,000 for each combination of sliding speed and normal load. The same disk and pin were used for all tests at a constant sliding speed for variable normal loads i.e. from 10 to 50 N for total sliding distance 28,700 m. After each test, the mass loss of disk and pin for sliding distance 5740 m was calculated on an analytical balance with an accuracy of 0.01 mg to the nearest 0.0001 g. The reproducibility of tests were checked which was varied from 10-20 %. Table 2 shows the sliding speeds frequencies and test duration for each combination of sliding speed and normal load.

3.3.2 Materials

Chemical composition of 303 stainless steel disk and 8620 low alloy steel pin materials

Table 4 shows the chemical compositions of the 303stainless steel and 8620 low alloy steel. The chemical compositions of these materials were checked on X-ray Fluorescence Spectrometer (XRF). 303SS has high percentage of Cr i.e. 18.7 % and 8620 low alloy steel has no Cr contents.

Element	303 stainless steel disk	8620 low alloy steel
Ti	0.201 %	
V	0.207 %	
Cr	18.7 %	
Mn	1.44 %	0.544 %
Fe	71.1 %	97.9 %
Co	0.254 %	
Ni	7.76 %	0.519 %
Cu	0.188 %	0.125 %
Ag	0.104 %	0.112 %
Mo	0.0548 %	0.0143 %
Al		0.769 %

Table 4 The chemical composition of the 303 stainless steel disk and 8620 low alloy steel pin materials

Hardness

Hardness value of 303stainless steel; Hardness, Vickers: 167HV10 and hardness value of 8620 low alloy steel; Hardness, Vickers: 207HV10.

3.4 303stainless steel uncoated and coated with titanium carbide composite coating against alumina

3.4.1 Experimental conditions

The experiments were carried out under ambient conditions at room temperature for dry sliding wear in pin-on-disc test method on CSM Tribometer for both uncoated and coated materials. The wear rates of 303SS and 303SS base TiC composite coatings produced by TIG process were measured against an alumina (99.6% Al₂O₃, hardness 1800 HV) ball of diameter 3mm in sliding contacts. The ball was rigidly held at the contacting face of the pin. Sliding speeds were 3, 7, 11 and 15 cm s⁻¹ and normal loads increased in increments of 2 N from 2 to 10 N, with the wear track diameter being 6 mm. Table 5 shows the test duration for each test for a constant sliding distance 500 m for various combinations of sliding speeds and normal loads. The total numbers of revolutions were 26,526 for each test. New disk and alumina ball were used for each test. Total 20 combinations of sliding speeds and normal loads were tested. An analytical balance with accuracy of 0.0001 g was used to evaluate mass loss after each test carried out. The wear rates were calculated by dividing the mass loss by the sliding distance. SEM micrographs and EDX analysis of the wear tracks were carried out after each test to identify predominant wear mode, wear mechanisms and wear mode transitions.

Sliding speed (cms ⁻¹)	Circumference of the wear track (cm)	Sliding distance (m)	Test duration (minutes) from equation (5)	Number of revolution
3	18.85	500	278	26,526
7	18.85	500	119	26,526
11	18.85	500	76	26,526
15	18.85	500	56	26,526

Table 5 Tests frequency and tests duration for 303SS disks (uncoated and coated with TiC composite coatings) against alumina ball (chapter 5)

3.4.2 Materials

Table 6 and 7 show the chemical compositions of the 303SS and 303SS base composite coatings respectively. The 303SS composition shown on Table 6 shows a high proportion of Cr (18.7%) and Ni (7.8%). The alumina balls (99.6% Al₂O₃) were used as counterface. The hardness values of the 303 stainless steel and Alumina counterface were 172HV10 and Alumina 1800 HV respectively. The average hardness of the 303 stainless steel base titanium carbide composite coatings was 347HV10.

Element	Wt. %	Element	Wt. %
Ti	0.201	Co	0.254
V	0.207	Ni	7.76
Cr	18.7	Cu	0.188
Mn	1.44	Ag	0.104
Fe	71.1	Mo	0.0548

Table 6 The composition of the 303 stainless steel disk

Element	Wt. %
Ti	74.05
Cr	7.55
Fe	18.40

Table 7 The composition of the 303 stainless steel base TiC coating disk surface

3.5 Titanium uncoated and coated with titanium carbide composite coatings against hardened steel (A.I.S.I. 0-1-Ground Flat Stock)

3.5.1 Experimental conditions

The dry sliding wear tests were carried out under ambient conditions at room temperature on a Pin-On-Disk (ASTM 99-05) apparatus Fig. 34. Cylindrical pins of Ti and Ti base TiC coatings produced by TIG welding torch melting process of 4.3mm diameter, with flat ends, apparent area of contact ($1.44\text{m}^2 \times 10^{-5}$), were used as tests specimens. Hardened steel disks of 75mm outer diameter, 3.8mm thickness were used as the counterface for testing of

Tribo-corrosion maps for steels, titanium and titanium carbide materials

pins specimens. The normally loaded stationary pin was slid against unidirectional rotating disk under dry sliding conditions at room temperature. The sliding distance was kept constant for all tests. The tests were carried out at different constant sliding speeds, 0.38, 0.5, 0.86, 1.2 and 1.5m s⁻¹ by varying normal loads in increments of 10 N, from 10 to 50N, apparent contact pressure range of 694 to 3,472kPa respectively, for 25 combinations of sliding speeds and normal loads for uncoated and coated specimens separately. The sliding distance was 5560m and the numbers of revolutions were 30,000 for each test. A new disk and pin pair was used for each test. A 20kg load cell was used to measure the frictional force between pin and disk mating surfaces during the test. An analytical balance with accuracy of 0.01 mg was used to evaluate mass loss following exposure. The wear rates (m³ m⁻¹) were calculated by converting mass loss to volume loss from the densities of both materials and then dividing the volume loss by the total sliding distance.

SEM micrograph and EDX analysis of the wear surfaces and wear debris were carried out after each test to study the wear modes and wear mechanisms of these materials against each other. The density of Ti, TiC composite coatings and hardened steel were 4.51g cm⁻³, 4.92g cm⁻³ and 7.8g cm⁻³ respectively. Volume wear rates (m³ m⁻¹) were calculated on the basis of these values. Table 3 shows the sliding speeds frequencies and test duration for each combination of sliding speed and normal load for Ti uncoated and coated with TiC composite coatings against hardened steel tests.

3.5.2 Materials

Table 8 shows the chemical compositions of the steel (A.I.S.I. 0-1-Ground Flat Stock) disk. The hardness value of hardened steel (A.I.S.I. 0-1-Ground Flat Stock) was: 701HV5. Titanium pins were used as reference material and as substrate for TiC composite coatings. Prior to start work titanium was checked to confirm its purity by doing EDX analysis tests Fig. 38. The hardness value of Titanium was: 184HV5.

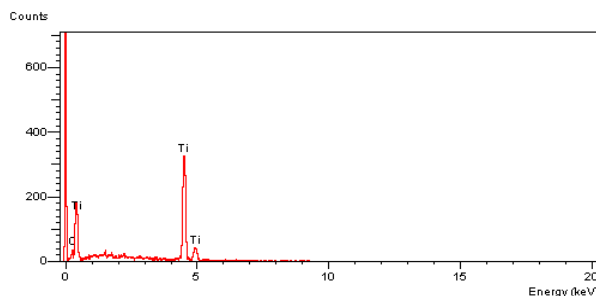


Figure 38 EDX analysis of titanium.

Tribo-corrosion maps for steels, titanium and titanium carbide materials

For sliding wear tests of the coatings, titanium substrate, pins, coated with titanium carbide composite were used as specimens against hardened steel. Titanium carbide has very high melting point and thermal stability, low coefficient of friction, high electrical and thermal conductivities, low density, high hardness and high wear and corrosion resistance. The hardness value of titanium base titanium carbide composite coatings was: 383HV5.

Element	Wt. %
C	0.95
W	0.50
Cr	0.50
Mn	1.20
V	0.20
Si	0.25
S&P up to	0.035
Fe	96.37

Table 8 The chemical composition of the steel (A.I.S.I. 0-1-Ground Flat Stock) disk

3.6 Tungsten Inert Gas (TIG) Melting Coatings procedure

TIG welding torch was used as heat source. The coating was carried out on TIG 165 DC/HF welding machine. For this project, all material was provided by our collaborator IIUM and coatings were carried out over there.

3.6.1. TiC powder pre-placement process

303 stainless steel and titanium substrates were hydraulically sheared to the dimension of 75 x 75 mm² and grounded with Grit 120 emery paper by using grinding machine to make rough surface. Then these samples were washed / cleaned by using water and acetone to remove any type of dirt and contamination and dried by using electric dryer machine.

3.6.2. TiC powder placement

Titanium carbide powder, TiC – 140, + 325 mesh, typically 99.5% pure, with amount of 1 mg mm⁻² per substrate surface area was used for coating. A few drops of alcohol (to wet enough the powder) along with 5 drops of PVA (polyvinyl acetate) binder were added to that powder and mixed them by adding a few drops of water. The paste was spread equally on the substrate surface and flattens by using hard plastic sheet. Samples were dried with electric dryer to evaporate the alcohol leaving PVA binder in the paste only. Then those samples were put in an oven at 80 centigrade for one hour to remove all moisture from the powder mixture on the surface of the substrate.

3.6.3 303SS base titanium carbide composite coating by TIG welding torch melting method

Metal matrix composite melt tracks were produced using TIG 165 machine with a 2.4 mm in diameter of tungsten thoriated electrode. A working distance of 1mm was measured at the end of electrode tip to the surface of dried coating before the melting commenced. The input energy of 30 V at 90 ampere with the table travelling speed at 2 mm s^{-1} was used to produce 50% overlapped tracks of the coatings. These overlapped/multi-pass tracks were produced in one single direction until the melted layers cover the whole surface area of the sample. The direction of the multi-pass tracks and distance of travel were controlled using simple numerical control. TIG melting efficiency is considered to be at 48% [157]. The samples were shielded using argon gas at the rate of 20 litres per minute, which were streamed while producing the track layers to prevent excessive oxidation. The average thickness of the coating was 0.5-0.6 mm after grinding.

3.6.4 Optical Micrographs and EDX analysis of the specimens

Figs. 39 and 40 show the microstructures and EDX analysis of the uncoated 303SS and 303SS base TiC composite coatings respectively. Fig. 40(c) shows the thickness of the coatings after grinding the coated surface of the sample

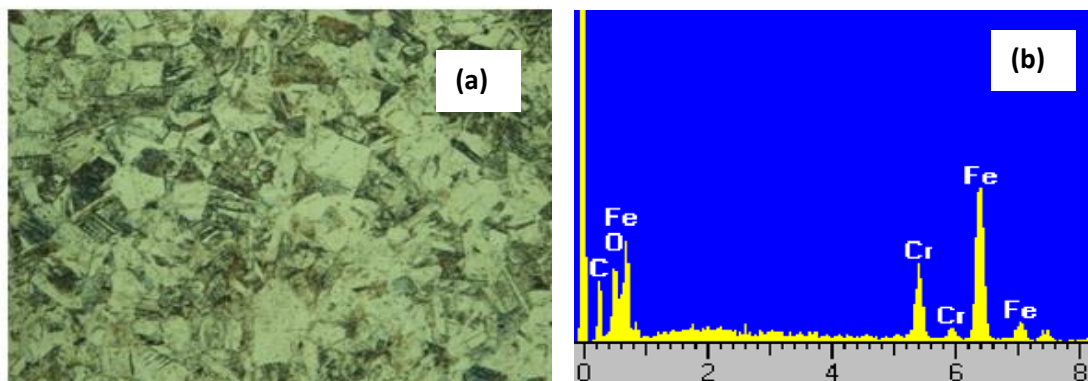
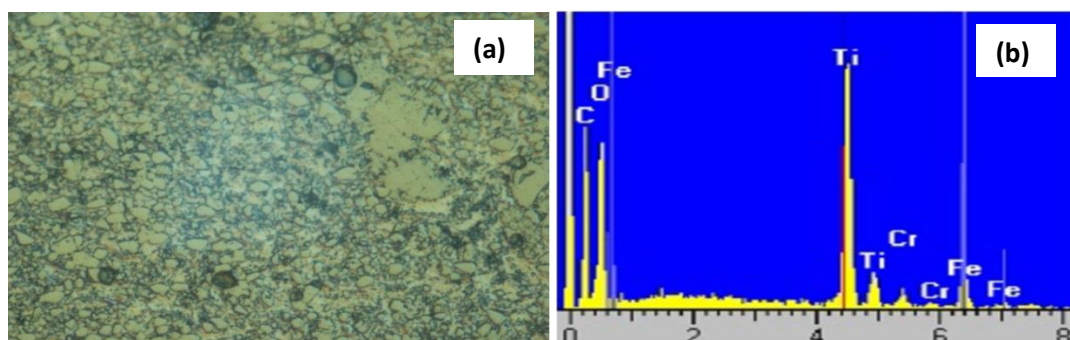


Figure 39 (a) Microstructure of 303 stainless steel 200X and (b) EDX analysis of 303stainless steel.



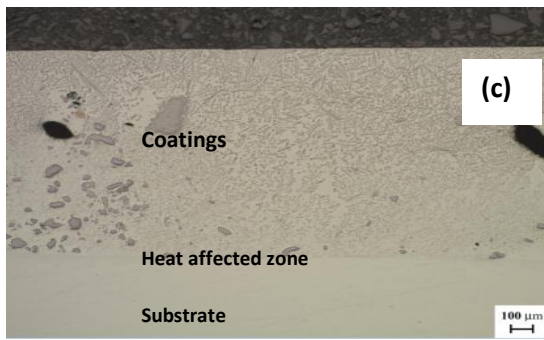


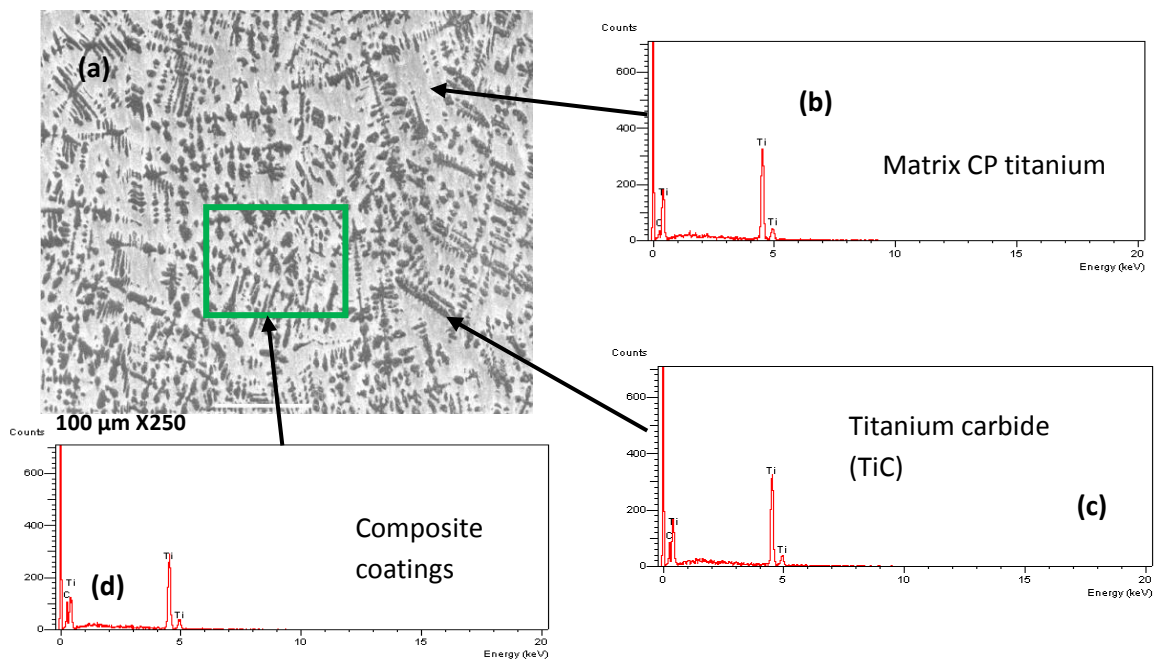
Figure 40 (a) Microstructure of 303stainless steel base TiC coating surface magnification X500, (b) the EDX analysis of the coated surface and (c) thickness of the 303SS base titanium carbide composite coatings after grinding the surface

3.6.5. Titanium base titanium carbide composite coatings by TIG welding torch melting method

The same conditions and procedure were used to produce Ti base TiC composite coatings as that of 303SS base TiC composite coatings, Section 3.6.3, except the table travelling speed, which was at 1 mm s^{-1} instead of 2 mm s^{-1} in this case. After coating carried out, the samples were ground on grinder machine and then cut into pin size 4.3 mm diameter on EDM wire cut machine.

3.6.6 Optical Micrographs and EDX analysis of the coated surface

Fig. 41 shows the micrograph and EDX analysis and the thickness of the coatings after grinding sample surface of the titanium base titanium carbide composite coatings.



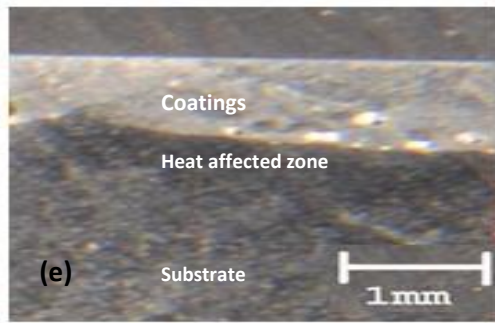


Figure 41 (a) The micrograph of the CP titanium base TiC coating surface, (b) the EDX analysis of the CP titanium matrix (substrate), (c) the EDX analysis of the Titanium carbide (TiC), (d) the EDX analysis of the titanium carbide composite coatings and (e) thickness of the coatings after grinding the surface.

3.6.7 Integrity of the coatings

The integrity of the Ti base TiC composite coatings produced by TIG welding torch melting process was checked by using a number of analytical techniques. The coated surface was ground and checked for surface cracks using the microscope. The thickness of the coating and coating defects such as cracks, pores and pockets of oxygen were checked on a microscope as well by cross-sectionally shearing the coated surface. An EDX analysis of the coatings was carried out to check the weight percentage of coating on the composite surface. The hardness of the coating surfaces was checked in the Hardness Vickers test at 5 Kg and 10 Kg. The dry sliding wear tests were used to obtain the wear rates and the coefficients of friction of the examined coatings. These tests were conducted at a range of sliding speeds and normal loads. After the tests were carried out, SEM, EDX and micrographic analysis of the worn surfaces were carried out to check for surface cracks, stability and coating thickness respectively.

3.6.8 Mapping tribo-corrosion

Tribo-corrosion has led to the description of the wear-corrosion process in terms of regimes. These regimes enable the degradation to be classified in terms of wear or corrosion dominated behaviour. Such an analysis provides a means of generating tribo-corrosion maps of the overall regimes encountered.

The development of wear maps is a useful tool to study and predict the wear behaviour of metals in tribological contact. Wear maps can represent the mechanistic changes on the worn surfaces of material and the counterpart over a range of operating conditions. Wear mode maps identify the mode of degradation and establish the level of wastage rate and potential “safe” and “unsafe” operation conditions for materials. On the other hand, wear

Tribo-corrosion maps for steels, titanium and titanium carbide materials

mechanistic maps show the different wear mechanisms, for various combinations of sliding speeds and normal loads for different materials sliding against each other under dry sliding conditions. These maps demonstrate clearly that transitions from one dominant wear mechanism to another may also be identified by changes in measured wear rates. Mapping wear mode and wear mechanisms of the material against which a coating is worn is also essential, since any changes in its wear behaviour will directly influence coating performance and vice versa.

Wear mode maps and wear mechanism maps have been constructed for uncoated and coated materials on the basis of main parameters, sliding speed and normal load, of this experimental work. These maps developed on normal loads versus sliding speeds data plot for the tested combinations of sliding speeds and normal loads on the basis of tests results, mass loss, wear rate, physical analysis of worn surfaces and wear debris; SEM and EDX analysis of the worn surfaces and wear debris. The boundaries on the wear maps are only approximations and it is assumed that the transitions in wear modes and wear mechanisms are occurring between these lines.

3.7. Experimental Error and Uncertainty

Whenever data is collected in an experiment, there is always some error and uncertainty. It is important to quantify that error so that the accuracy of the conclusion can be estimated for the validity of the experimental results. The experimental error is a difference between measurement and true value or between two measured values. Experimental error, itself, is measured by its accuracy and precision [193, 194].

Accuracy measures how close a measured value is to true value or accepted value. Since a true and accepted value for physical quantity may be unknown, it is some time impossible to determine the accuracy of the measurement.

Precision measures how closely two or more measurements agree with the other. Precision sometimes referred to as “repeatability” or “reproducibility.” A measurement which is highly reproducible tends to give values which are very close to each other.

Standard Error

Standard error is a measurement of random error in a set of data. Random errors are “two sided” errors that affect the precision of the measurement. It shows the scatter of the data of repeat measurements in an experiment about the mean value.

Percent Error

Percent error measures the accuracy of a measurement by the difference between a measured or experimental E and true or accepted value A. The percent error can be measured by the following equation:

$$\% Error = \frac{|E - A|}{A} \times 100\% \text{ -----10}$$

Experimental error for 8620 low alloy steel pins against 303SS disks

Fig. 42 shows the percent experimental error of 8620 low alloy steel pins against 303SS disks. The experimental error for this tribo-couple was calculated at sliding speed 0.86 m s^{-1} and at normal load 20N. Three repeat tests were carried out and mass losses of the low alloy steel pins were found as 0.0504, 0.0693 and 0.0684g. Average value of mass loss 0.0627 g was been taken as acceptable value ‘A’ [193, 194]. Experimental error for this tribo-couple calculated by using equation 10, which was in the range of 10 -20% (chapter - 4).

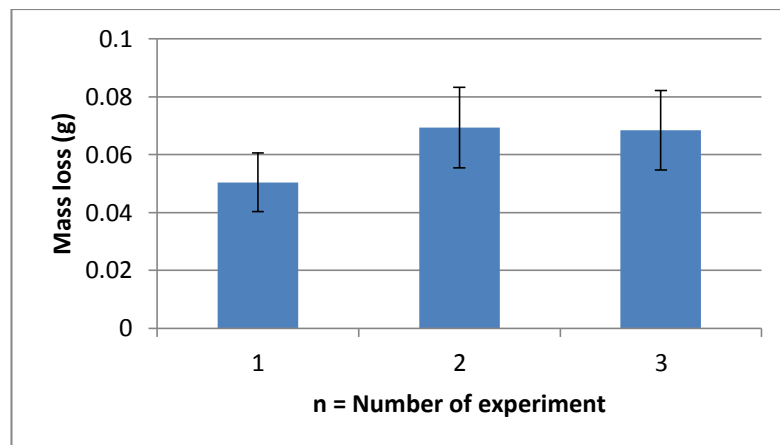


Figure 42 Experimental errors (20%) for the 8620 low alloy steel pins against 303SS disks.

Experimental error for 303SS base TiC coatings disks against alumina balls

Tribo-corrosion maps for steels, titanium and titanium carbide materials

Fig. 43 shows the percent experimental error of 303SS base TiC coatings disks against alumina balls. The experimental error for 303SS base TiC coatings disks against alumina balls were calculated at sliding speed 15cm s^{-1} and at normal load 8N. Three repeat tests were carried out and mass losses of the TiC coated disks were found as 0.0059, 0.0068 and 0.0071g. Average value of mass loss 0.0066g was been taken as acceptable value 'A' [193, 194]. Experimental error for 303SS base TiC was calculated by using equation 10, which was in the range of 10.6% (chapter - 5).

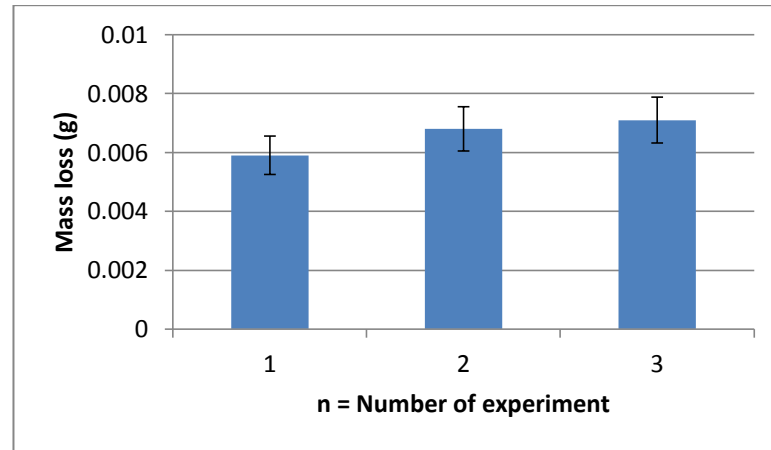


Figure 43 Experimental errors (11%) for 303SS base TiC coatings disks against alumina balls.

Experimental error for Ti base TiC coatings pins against hardened steel disks

For experimental error, Refer to chapter – 7, page number 152, Fig. 138.

Chapter 4

High and zero Cr contents steel in dry sliding contact

4.1. Introduction

In this experimental base study, investigations have been carried out on the basis of tests results of the wear behaviour of both components of the tribological contact, i.e. the pin and disk. This work addresses this issue, by investigating the sliding wear mode and wear mechanisms of both 8620 low alloy steel and 303stainless steel by using a tribo-system approach. Both metals have different hardness and oxidation resistance. The differences in the maps are discussed with reference to the change in oxidative wear mechanisms for both pin and disk materials.

4.2. Tests results

Dry sliding wear tests were carried out on pin-on-disk sliding wear testing rig Fig. 34 at different combinations of sliding speeds and normal loads as per experimental conditions mentioned in section 3.3, chapter 3. The wear behaviour of 303SS and 8620 low alloy steel were investigated for 25 combinations of sliding speeds and normal loads. The sliding distance 5,740 m and numbers of revolutions 30,000 were kept constant for all tests. At the end of each sliding test mass loss was measured and worn surfaces of the disks and pins were examined to decide the wear mode and mechanism regimes. At the end of test dark and smooth worn surface; lower mass loss and dark grey powdery wear debris were found due to oxidation of mating surfaces which results in mild wear. On the other hand bright, rougher worn surfaces and larger metallic wear debris, and higher mass loss results in medium and severe wear. SEM micrographs and EDX analysis of the worn surfaces were also carried out. The dry sliding wear tests results of 303SS disks and 8620 low alloy steel pins, sliding against each other, are as follows:

4.2.1. Wear at 0.38 m s^{-1} sliding speed for the range of normal loads

Table 9 and Fig. 44 show the mass loss of 303SS disks and 8620 low alloy steel pins against each other at 0.38 m s^{-1} sliding speed for the range of normal loads.

Normal Load (N)	Mass loss of disk (g)	Mass loss of pin (g)
10	0.0037	0.0124
20	0.0163	0.0349
30	0.0081	0.0583
40	0.0897	0.1709
50	0.0043	0.0853

Table 9 Mass loss of 303SS disks and 8620 low alloy steel pins at 0.38m s^{-1} sliding speed.

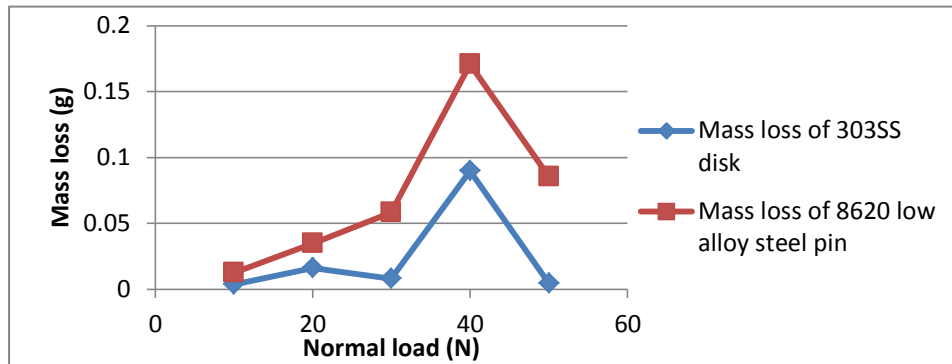


Figure 44 Mass loss of 303SS disk and 8620 low alloy steel pin at 0.38m s^{-1} sliding speed.

For the 303SS disk, at a sliding speed of 0.38m s^{-1} , for normal loads from 10 to 30 and 50 N, mild wear, while at 40 N medium (mixed) wear occurred i.e. transitions of wear regime occurred at normal load 40 and 50 N, Table 9 and Fig. 44. For the 8620 low alloy steel pin, the wear mode transitions shifted to lower velocities, with mild wear observed at 10 and 20 N, medium (mixed) wear occurred at normal loads 30 and 50 N while severe wear occurred at 40 N, table 9 and Fig. 44. At the end of the tests, for these conditions, a dark and smooth wear track surface was observed, indicative of a mild wear regime.

4.2.2. Wear at 0.5m s^{-1} sliding speed for the range of normal loads

Table 10 and Fig. 45 show the mass loss of 303SS disk and 8620 low alloy steel pin against each other at 0.5m s^{-1} sliding speed for the range of normal loads.

Normal Load (N)	Mass loss of disk (g)	Mass loss of pin (g)
10	0.0979	0.1135
20	0.0051	0.0249
30	0.0242	0.0835
40	0.0797	0.1615
50	0.0088	0.0621

Table 10 Mass loss of 303SS disks and 8620 low alloy steel pins at 0.5m s^{-1} sliding speed.

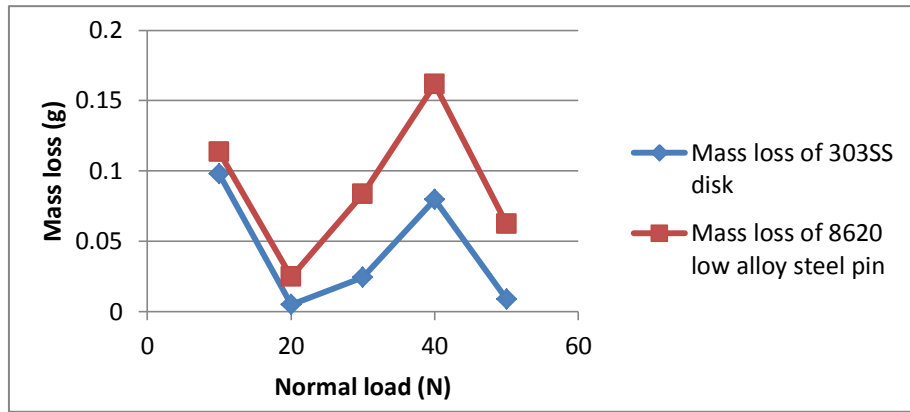


Figure 45 Mass loss of 303SS disks and 8620 low alloy steel pins at 0.5 m s^{-1} sliding speed.

At sliding speed 0.5 m s^{-1} for the 303SS material, the wear mode transitions appeared to occur at higher loads but the trend was far from clear, with mild wear observed at normal loads 20, 30 and 50 N while medium wear was found at 10 and 40 N, Table 10, Fig. 45. For the 8620 low alloy steel pin, in these conditions, there were several transitions in wear modes i.e. mild wear at normal load 20 N, medium wear at 10, 30 and 50 N and severe wear at 40 N, Table 10 and Fig. 45. As it is evident from SEM micrographs and EDAX analysis Fig. 54(b)-55(b) that an oxide layer was observed on the wear track, which resulted in a mild wear phenomenon of the disk material at 20, 30 and 50 N normal loads. In this case more oxide was found at 50 N, probably arising from the increase in interfacial temperature between sliding surfaces, due to higher sliding speed. At the end of the tests, for these conditions, a dark and smooth wear track surface was observed, indicative of a mild wear regime.

4.2.3. Wear at 0.86 m s^{-1} sliding speed for the range of normal loads

Table 11 and Fig. 46 show the mass loss of 303SS disk and 8620 low alloy steel pin against each other at 0.86 m s^{-1} sliding speed for the range of normal loads.

Normal Load (N)	Mass loss of disk (g)	Mass loss of pin (g)
10	0.0998	0.0841
20	0.0881	0.0627
30	0.1419	0.0889
40	0.1333	0.0739
50	0.1833	0.0902

Table 11 Mass loss of 303SS disk and 8620 low alloy steel pin at 0.86 m s^{-1} sliding speed.

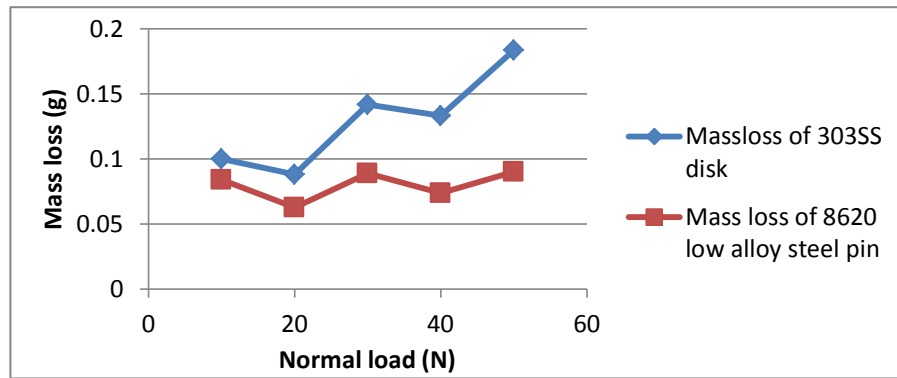


Figure 46 Mass loss of 303SS disks and 8620 low alloy steel pins against at 0.86 m s^{-1} sliding speed.

At sliding speed 0.86 m s^{-1} , a change in wear trend occurred for both the 303SS disk and 8620 low alloy steel pin:

- 1- For the 303SS disk, medium wear was observed from normal loads 10 to 40 N whereas severe wear was found at 50 N.
- 2- For the 8620 low alloy steel pin, medium wear was found at all normal loads.
- 3- At sliding speed 0.38 m s^{-1} & 0.5 m s^{-1} , the wear of 8620 low alloy steel pins was higher than the 303 stainless steel disks whereas this reversed at 0.86 m s^{-1} , Table-11 and Fig. 46.

4.2.4. Wear at 1.2 m s^{-1} sliding speed for the range of normal loads

Table 12 and Fig. 47 show the mass loss of 303SS disk and 8620 low alloy steel pin against each other at sliding speed 1.2 m s^{-1} for the range of normal loads.

Normal Load (N)	Mass loss of disk (g)	Mass loss of pin (g)
10	0.1352	0.0576
20	0.1935	0.0820
30	0.2786	0.1474
40	0.3418	0.1303
50	0.4608	0.2088

Table 12 Mass loss of 303SS disks and 8620 low alloy steel pins at 1.2 m s^{-1} sliding speed.

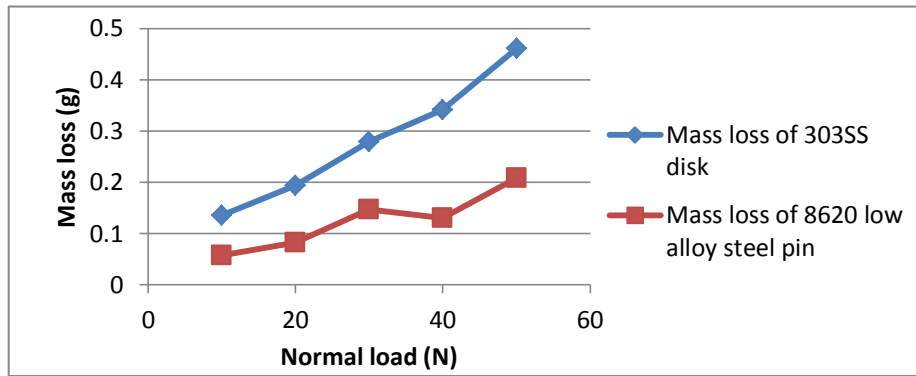


Figure 47 Mass loss of 303SS disks and 8620 low alloy steel pins at 1.2 m s^{-1} sliding speed.

At sliding speed 1.2 m s^{-1} , there was increased wear for all normal loads i.e. severe wear for 303SS disk except normal load 10 N while the wear of 8620 low alloy steel pin was mainly in the medium wear mode at 10 to 40 N, with severe wear at 50 N Table 12 and Fig. 47. At normal load 50 N, the 8620 low alloy steel pin exhibited severe wear.

4.2.5. Wear at 1.5 m s^{-1} sliding speed for the range of normal loads

Table 13 and Fig. 48 show the mass loss of 303SS disks and 8620 low alloy steel pin against each other at 1.5 m s^{-1} sliding speed for the range of normal loads.

Normal Load (N)	Mass loss of disk (g)	Mass loss of pin (g)
10	0.1615	0.0693
20	0.2329	0.0909
30	0.3056	0.1229
40	0.3381	0.1098
50	0.2854	0.0525

Table 13 Mass loss of 303SS disk and 8620 low alloy steel pin against each other at 1.5 m s^{-1} sliding speed.

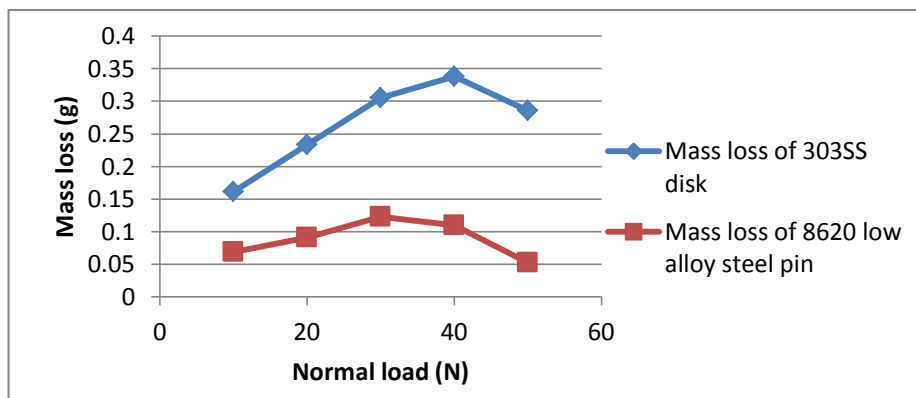


Figure 48 Mass loss of 303SS disks and 8620 low alloy steel pins against each other at 1.5 m s^{-1} sliding speed.

At sliding speed 1.5 m s^{-1} , severe wear was found for the 303SS disks at all normal loads and medium wear for the 8620 low alloy steel pin at all normal loads Table 13 and Fig.48. Though the 8620 low alloy steel is harder than 303SS, at sliding speeds 0.38 and 0.5 m s^{-1} ,

higher wear of the steel pin observed. However, by contrast, for sliding speed 0.86 to 1.5 m s⁻¹, the wear rate of 303 stainless steel disks was greater than the 8620 low alloy steel pins. Hence, the relative wear rates of both steel pins and disks depended on the normal load and sliding speed.

4.2.6. Mass loss of 303SS disks against 8620 low alloy steel pins at different constant sliding speeds and various normal loads

Table 14 shows the mass loss of 303SS disks against 8620 low alloy steel pins and Fig. 49 shows the data plots on the graphs of mass loss of 303SS disks against 8620 low alloy steel pin due to dry sliding wear at different constant sliding speed and various normal loads.

Normal load (N)	Mass loss (g) x 10 ⁻³ at 0.38 m s ⁻¹	Mass loss (g) x 10 ⁻³ at 0.5 m s ⁻¹	Mass loss (g) x 10 ⁻³ at 0.86 m s ⁻¹	Mass loss (g) x 10 ⁻³ at 1.2 m s ⁻¹	Mass loss (g) x 10 ⁻³ at 1.5 m s ⁻¹
10	3.7	97.9	99.8	135.2	161.5
20	16.3	5.1	88.1	193.5	232.9
30	8.1	24.2	141.9	278.6	305.6
40	89.7	79.7	133.3	341.8	338.1
50	4.3	14.2	183.3	417.0	318.1

Table 14 Mass loss of 303 stainless steel disks against 8620 low alloy steel pins.

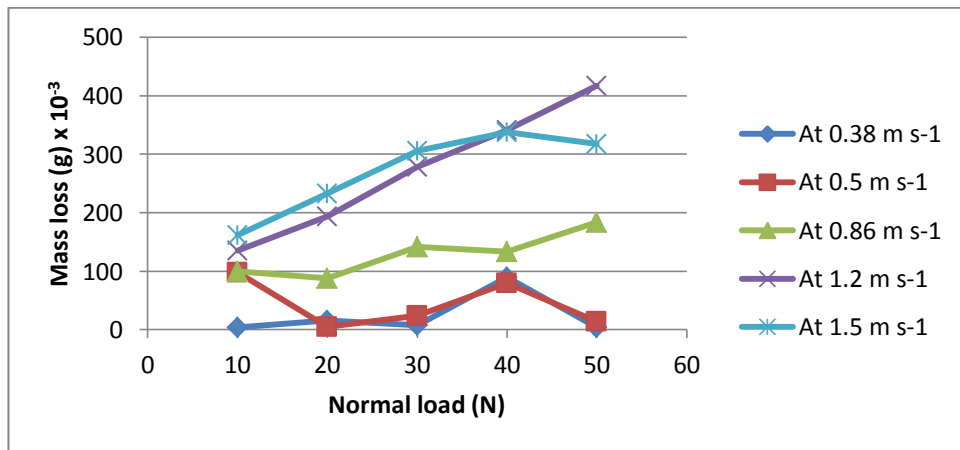


Figure 49 Mass loss vs normal load of 303 stainless steel disks against 8620 low alloy steel pins.

4.2.7. Mass loss of 303SS disks against 8620 low alloy steel pins at different constant normal loads and various sliding speeds

Table 15 shows the mass loss of 303SS disks against 8620 low alloy steel pins and Fig. 50 shows the data plots on the graphs of mass loss of 303SS disks against 8620 low alloy steel pins due to dry sliding wear at different constant normal loads and various sliding speeds.

Sliding speed m s ⁻¹	Mass loss (g) x 10 ⁻³ at 10N	Mass loss (g) x 10 ⁻³ at 20N	Mass loss (g) x 10 ⁻³ at 30N	Mass loss (g) x 10 ⁻³ at 40N	Mass loss (g) x 10 ⁻³ at 50N
0.38	3.7	16.3	8.1	89.7	4.3
0.5	97.9	5.1	24.2	79.7	14.2
0.86	99.8	88.1	141.9	133.3	183.3
1.2	135.2	193.5	278.6	341.8	417.0
1.5	161.5	232.9	305.6	338.1	318.1

Table 15 Mass loss of 303 stainless steel disks against 8620 low alloy steel pins.

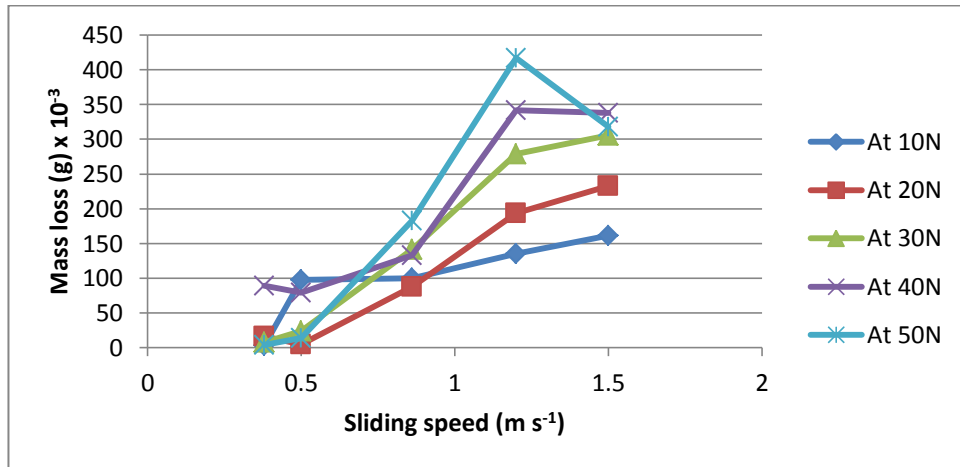


Figure 50 Mass loss vs sliding speed of 303 stainless steel disks against 8620 low alloy steel pins.

4.2.8. Mass loss of 8620 low alloy steel pins against 303SS disks at different constant sliding speeds and various normal loads

Table 16 shows the mass loss of 8620 low alloy steel pins against 303SS disks and Fig. 51 shows the data plots on the graphs of mass loss of 8620 low alloy steel pins against 303SS disks due to dry sliding wear at different constant sliding speeds and various normal loads.

Normal load (N)	Mass loss (g) x 10 ⁻³ at 0.38 m s ⁻¹	Mass loss (g) x 10 ⁻³ at 0.5 m s ⁻¹	Mass loss (g) x 10 ⁻³ at 0.86 m s ⁻¹	Mass loss (g) x 10 ⁻³ at 1.2 m s ⁻¹	Mass loss (g) x 10 ⁻³ at 1.5 m s ⁻¹
10	12.4	113.5	84.1	57.6	69.3
20	34.9	24.9	62.7	82.0	90.9
30	58.3	83.5	88.9	147.4	122.9
40	170.9	161.5	73.9	130.3	109.8
50	85.3	63.0	90.2	180.1	99.3

Table 16 Mass loss of 8620 low alloy steel pins against 303 stainless steel disks.

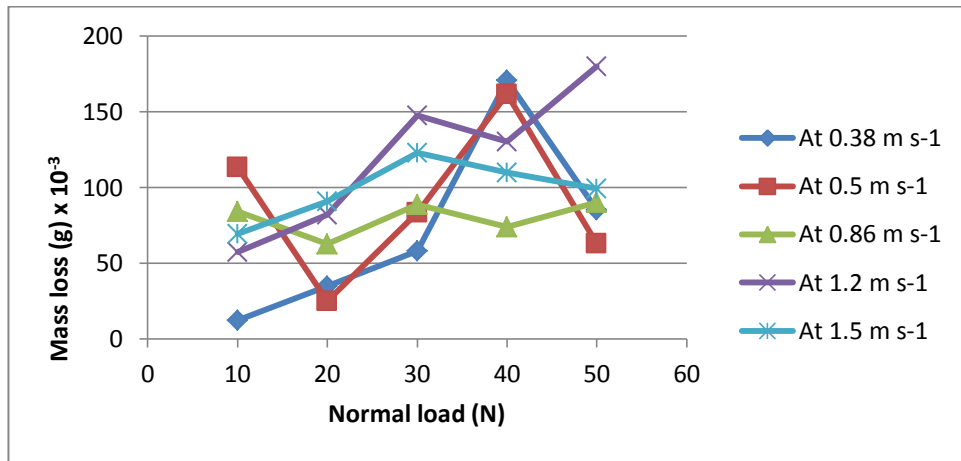


Figure 51 Mass loss vs. normal load 8620 low alloy steel pins against 303 stainless steel disks.

4.2.9. Mass loss of 8620 low alloy steel pins against 303SS disks at different constant normal loads and various sliding speeds

Table 17 shows the mass loss of 8620 low alloy steel pins against 303SS disks and Fig. 52 shows the data plots on the graphs of mass loss of 8620 low alloy steel pins against 303SS disks due to dry sliding wear at different constant normal loads and various sliding speeds.

Sliding speed m s ⁻¹	Mass loss (g) x 10 ⁻³ at 10N	Mass loss (g) x 10 ⁻³ at 20N	Mass loss (g) x 10 ⁻³ at 30N	Mass loss (g) x 10 ⁻³ at 40N	Mass loss (g) x 10 ⁻³ at 50N
0.38	12.4	34.9	58.3	170.9	85.3
0.5	113.5	24.9	83.5	161.5	63.0
0.86	84.1	62.7	88.9	73.9	90.2
1.2	57.6	82.0	147.4	130.3	180.1
1.5	69.3	90.9	122.9	109.8	99.3

Table 17 Mass loss of 8620 low alloy steel pins against 303 stainless steel disks.

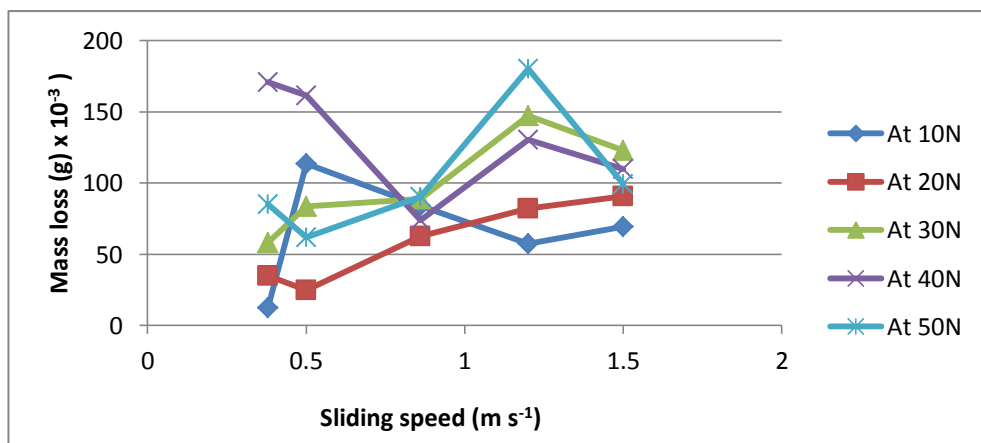


Figure 52 Mass loss vs normal load of 8620 low alloy steel pins against 303 stainless steel disks.

4.2.10. Total mass loss comparison

Table 18 and Fig. 53 show the total mass loss (on the average bases for the repeated tests) of the 303SS disk and 8620 low alloy steel pin at each constant sliding speed for the range of normal loads i.e. at variable loads from 10 to 50 N, and increasing in 10 N increments for the total sliding distance 28,700 m.

Sliding speed (m s ⁻¹)	Total mass loss of 303 stainless steel disk (g)	Total mass loss of 8620 low alloy steel pin (g)
0.38	0.12	0.36
0.5	0.22	0.45
0.86	0.65	0.40
1.2	1.37	0.57
1.5	1.36	0.48

Table 18 The total mass loss of 303 stainless steel disks and 8620 low alloy steel pins.

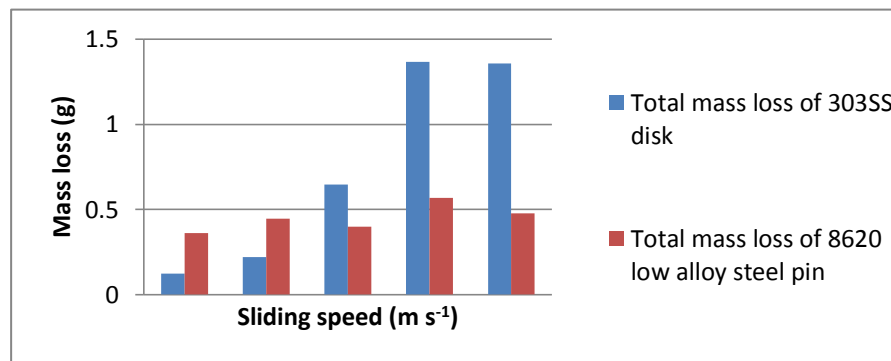


Figure 53 The total mass loss comparison of 303 stainless steel disks and 8620 low alloy steel pins.

4.2.11. SEM micrographs of the worn surfaces

Fig. 54 shows the SEM micrographs of the wear tracks on the 303SS disks against 8620 low alloy steel pins at 0.38 and 0.5 m s⁻¹ sliding speeds and 50 N normal load. Fig. 55 shows the EDX analysis of the wear tracks on the 303SS disks against 8620 low alloy steel pins at s⁻¹ 0.38 and 0.5 m s⁻¹ and normal load 50 N.

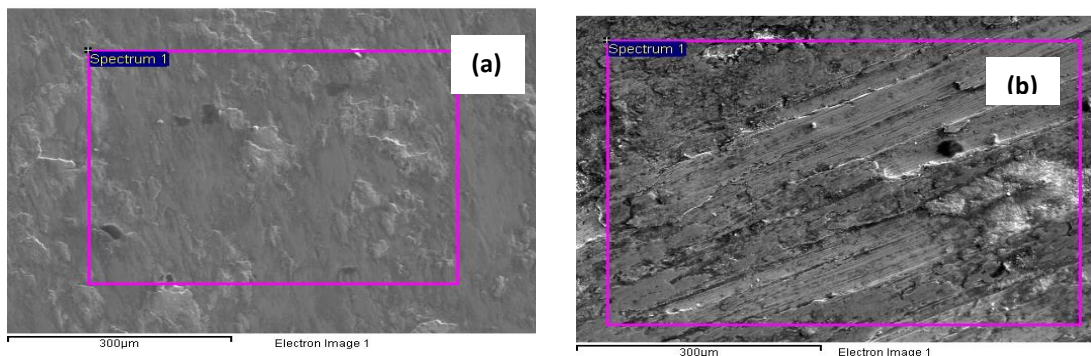


Figure 54 SEM micrograph of 303SS disk (a) at sliding speed 0.38 m s⁻¹ and normal load 50N and (b) at 0.5 m s⁻¹ and 50 N.

4.2.12. EDX analysis of the worn surfaces

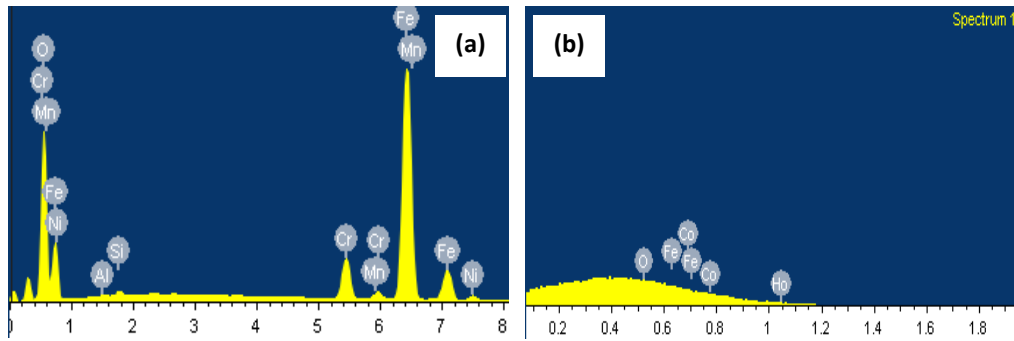


Figure 55 EDX analysis of 303SS disk (a) at sliding speed 0.38 m s^{-1} and normal load 50 N and (b) at 0.5 m s^{-1} and 50 N.

It was observed for these materials that wear curves for 303SS disks and 8620 low alloy steel followed the parallel paths even after the change in wear trends of 303SS disks and 8620 low alloy steel pins after sliding speed 0.5 m s^{-1} Fig. 44-48. The mass loss of 8620 low alloy steel was greater than 303SS at sliding speeds 0.38 m s^{-1} & 0.5 m s^{-1} , whereas it changed to lower than 303SS from 0.86 m s^{-1} - 1.5 m s^{-1} Fig.53. The fluctuation in mass loss of the tribo-couple occurred due to strain hardening or thermal softening and oxidation of the mating surfaces during dry sliding against each other Figs. 49-52.

4.3. Discussion

4.3.1. Wear Mechanisms

It is clear from the tests results, Tables 14-15 & Figs. 49-50, and from Tables 16-17 & Figs.51-52, that the wear of both materials varies with increases in normal load and sliding speed. Moreover, it was observed that the wear rates showed sharp transitions and a non-linear wear trend with respect to the changes in load and speed. The inverse linear relationship with respect to hardness was also found to break down at low loads and high speeds [25]. This behaviour was also noted by Hirst and Lancaster for brass [159] and for steel i.e. by Saka et al. [160], Welsh [13], and was attributed to a competition between strain hardening and thermal softening that may occur simultaneously at the surface of the material as sliding speed increases [72]. Similarly, it can be postulated that in the case of the 303 stainless steel and 8620 low alloy steel, strain hardening effects may have been resulted in a reduction in wear, and softening of surface layers as a result of frictional heating also interacts with such mechanisms.

The effects of hardness on sliding behaviour are not well understood [163]. For sliding speed up to 0.5 m s^{-1} , the 303SS disks mass loss was less than that of 8620 low alloy steel pins, Fig. 53, and oxidative wear occurred, Figs. 54-55. This might have been due to the strain hardening effect or transfer of material and effect of mechanical mixing layer. Material transfer between tribo-couple occurs due to adhesion or bonding at the asperity contacts at the mating surfaces and these contacts are sheared by sliding, which may result in detachment of a fragment from one surface and attachment to the other surface. The stainless steel (highly alloy steel) has strong tendency to adhere to other metals, ceramics and work hardened property which make it particularly difficult to form as well. As the sliding continues, the transferred fragments may come off the surface on which they are transferred and be transferred back to the original surface, or else form loose wear particles.

During continued sliding, the initial transferred fragments are deformed, fractured and blended, leading to formation of mechanically mixed material on the sliding surfaces. Typical sliding wear debris particles come from this modified material [41]. The transferred layer becomes oxidized due to frictional heating. The wear process consist of three stages: transfer of metal, oxidation of transferred layer, and the subsequent removal of the oxide to form a loose wear-product [42]. The hardness of the mechanically mixed material can be greater or less than that of the underlying substrate, and this directly determines whether it forms a compressed layer or remains as patches or plateaus on the surface. The mechanically mixed material can have a wide range of hardness values, depending on the volume fraction of component phases and on the grain size. The material can also be heterogeneous, especially early in the mixing process, so its hardness can vary locally, [27]. It was also observed by M. Kerridge that the hardness of the mating surface of annealed steel pin rubbing against a hardened steel ring was considerably higher than the original pin material and this might have been due to the intense, localized, thermal effects which, as is well known, accompany rubbing under unlubricated conditions [42]. In earlier studies by Welsh [13], similar shifts in transitions to the above were observed, but that time also, with steel carbon content which affected the relative hardness values.

For sliding wear, some analogies may be made between the effects of increasing applied load and sliding velocity on the material surface. Increases in either parameter increase the level of frictional heating on the surface; in such cases, if the material undergoing sliding is

metallic in nature, e.g. steel, then the oxidation rate on the surface will increase. As a result, the wear increases initially with increasing velocity or applied load through an oxidation-wear process, at higher velocities or loads, when frictional heating results in higher flash contact temperatures [4]. At the end of the tests, for these conditions, a dark and smooth wear track surface, indicative of a mild wear regime, and the bright and rougher wear track surface demonstrating severe wear is consistent with earlier studies and reports from other work [11, 31, 32, 165].

In this sliding pair, the 303SS is significantly more oxidation resistant due to the high Cr content, with Cr additions essentially lowering the oxidation rate due to the fact that the parabolic growth rate of Cr based oxides is significantly lower than that for Fe based oxides and this is reflected in different transitions as has been found for alloys of varying Cr content in erosion-oxidation [164]. This means that there will be less oxide scale likely to form at the contact and less available oxide film and thickness to provide a solid lubricant or an oxide “glaze”, to protect the surface from further wear, in the more highly alloyed material, the 303SS [8].

As indicated in the work of Welsh, published in 1957 [4], for each steel, sliding at constant speed, there should be some critical value of load at which the steady state wear regime shifts from severe wear to mild wear and this is also observed in the literature on other tribo-oxidative processes i.e. erosion-oxidation of steels [164]. This prediction is confirmed through further experiments, with a new feature i.e. a second critical load is detected, below which mild wear again prevails. This is illustrated in Fig. 56(b) which shows the change of equilibrium wear rate with load for the 0.52 % C steel, sliding at a speed of 100 cm s^{-1} , [23]. To correlate the present work Fig. 56(a), with that of Welsh work [13, 23], Fig. 56(b), a plot of the 303SS disk sliding against 8620 low alloy steel pin at sliding speed 1.2 m s^{-1} and normal load 10 to 50 N, Fig. 47, is taken from the present work for comparison. The range of normal load of the present work covers is the highlighted portion on X-axis of the data plot [23], Fig. 56(b). The trend of wear observed in the present work is thus seems to be in agreement with the earlier work [13, 23] for the range of sliding speed and normal load of the present work.

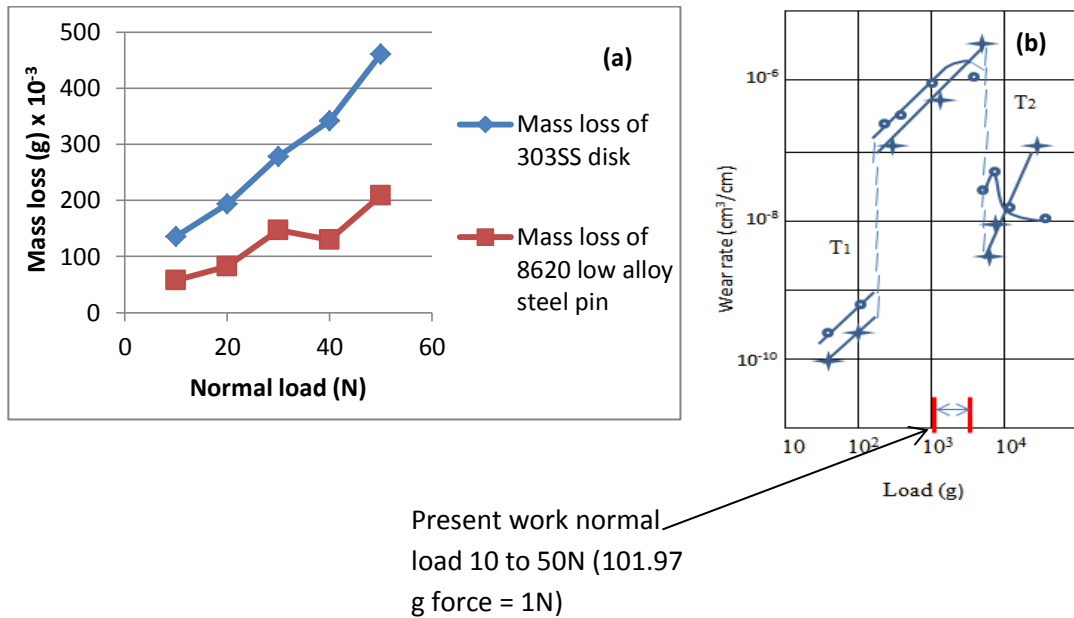


Figure 56 (a) Mass loss of 303SS disk and 8620 low alloy steel pin against each other at sliding speed 1.2 m s^{-1} and normal load 10 to 50 N, from the present work, and (b) wear rate plotted against load for the 0.52 % C steel at sliding speed 100 cm s^{-1} (1 m s^{-1}) and 50 g to 25 Kg (0.5 N to 250 N) load, x, for pin.; o, for ring, from [23].

The transition loads vary widely with the sliding speed, composition and hardness of the steel; if these factors are selected arbitrarily one or more transitions may not appear within the range of load investigated and this is also observed in the later erosion-oxidation research [8]. An increase in sliding speed lowers all the transition loads and, for a fixed load, there must be critical values of speed at which equivalent changes in the wear rate occur [23]. Fig. 57(b) shows the wear rates of 0.52% C steel at loads 1 and 5 Kg plotted as function of speed taken from Welsh work [23]. Fig. 58 shows the variation of wear rate with sliding speed of brass sliding against steel at 20°C in air taken from Lancaster work [162]. It is clear from the Fig. 57(b) and Fig. 58 that wear rate is increasing with sliding speed and there is sudden transition in wear mode i.e. from severe wear to mild wear, for a metal pair in sliding contact, at higher speeds.

It should be noted that in the present work, the ranges of sliding speed and normal load are very narrow compared to those for the Welsh [13, 23] and Lancaster [162] work, but nevertheless, the present studies can be correlated with their work for these ranges. A further comparison between the present study and that of Welsh [13, 23] can be made, with the range of the sliding speed of the present work. Fig. 57(a) a plot of mass loss of 303SS against 8620 low alloy steel at normal loads 10 and 50 N as a function of sliding speed taken from Fig. 50 of the present work is highlighted on the X-axis of Welsh data plot Fig. 57(b). The wear trends are similar i.e. wear is increasing with the increase in sliding

speed. The transition in wear mode of the 303SS disk against 8620 low alloy steel pin i.e. from severe wear toward mild wear at 50N normal load with increase in sliding speed is also seems to be in agreement with the Welsh work [13, 23]. Similarly the present work can be correlated with the Lancaster work [162] for the range of sliding speed Fig. 57(a) and Fig. 58, albeit that the 303SS has a higher Cr content than for the Welsh studies [13].

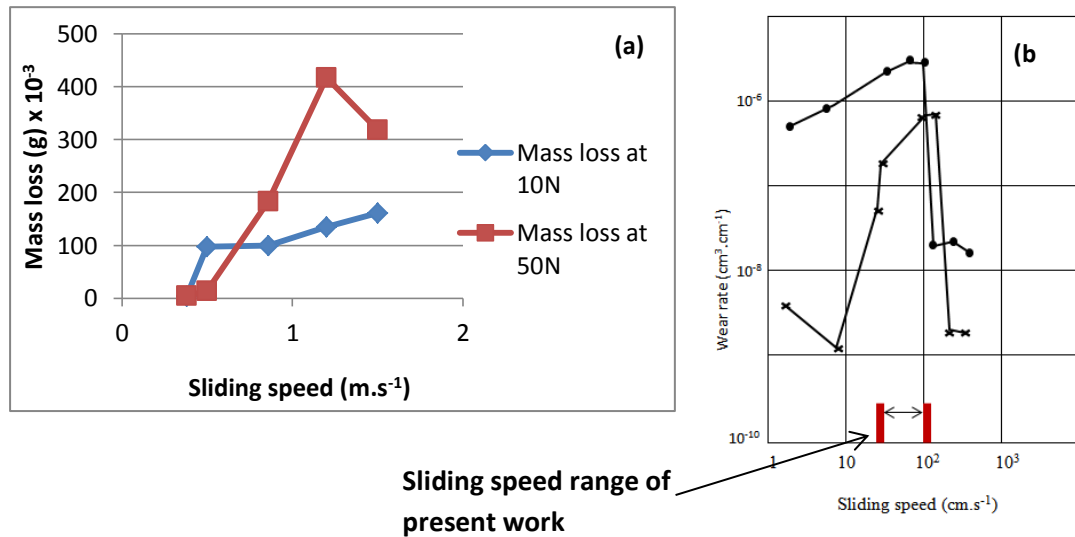


Figure 57 (a) The comparison of change of wear trend of 303 stainless steel disk against 8620 low alloy steel pin at constant normal load 10 and 50 N in the range of sliding speed i.e. 0.38 to 1.5 m s⁻¹ taken from Fig. 4.7 above, and (b) the trend of change of wear rate with sliding speed for the 0.52 % C steel. Loads: x, 1Kg (10 N equivalent) and ●, 5 Kg (50 N equivalent), from [23].

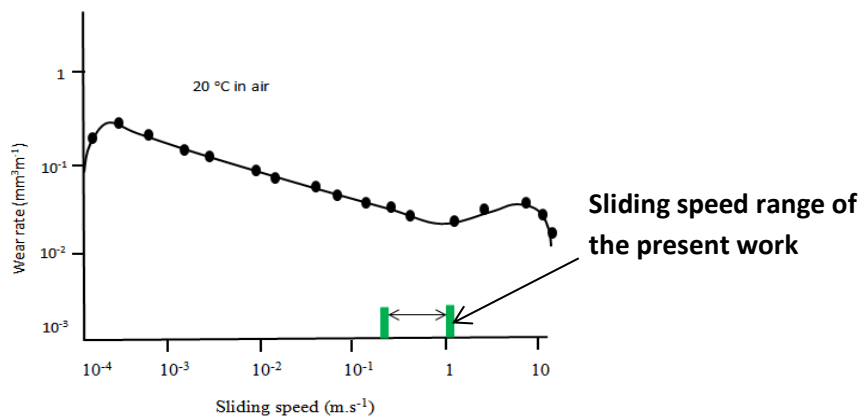


Figure 58 Variation in wear rate of brass with increase in sliding speeds against steel at 20°C in air [162].

During dry sliding, oxidation of the metals is dependent mainly on the oxygen level available in the atmosphere. In the case of 303SS, chromium rich oxides, (Cr₂O₃) are formed

on the 303SS surface. During sliding, the continuous removal of oxide and higher temperature is experienced between the mating surfaces. The higher thermal expansion rate of the 303SS can also result in problems such as distortion and may lead to scale/layer loss (spalling) during thermal cycling. The broken oxide scale particles can trap in wear track and result in reduce coefficient of friction due to reduce in actual contact area at the interface of the mating surfaces.

It should be noted that for the two materials, the role of oxidation in modifying the wear rate will be significant. As discussed above, the high Cr content of the 303SS means that the instantaneous oxidation rate, at the contact, will be significantly lower than for the low alloy steel [8]. This meant that there is less possibility of establishing a wear resistant oxide layer for the higher alloyed material and may be the reason why higher wear rates are observed for the Cr content material at higher speeds.

4.3.2. Wear regimes and wear maps

The development of wear maps is a useful way to study and predict the wear behaviour of materials sliding against each other at different sliding speeds and normal loads. The generalized classification of mass loss into three distinct regimes, mild, medium and severe wear are found in literature [11, 31, 32, 34, 165]. In the present work the wear mode regimes, namely (a) mild wear (b) medium wear and (c) severe wear are defined consistent with previous research work found in literature [34, 72], tests results, mass loss data, physical observations of the worn surfaces, SEM and EDX of the worn surfaces and wear debris at the end of the test.

The various wear mode regimes are identified for the 303SS disk and 8620 low alloy steel pin, as a function of sliding speed and normal load, showing distinctive differences in the wear mode regimes transitions, as addressed above Figs. 49-52. Furthermore, if such wear modes regimes are presented in a wear mode map, Fig. 59, it can be clearly seen that severe wear is more prevalent in the relatively high load and speed regimes, for the more highly alloyed material, 303SS, whereas for the 8620 low alloy steel, medium wear is predominant than mild wear at low speeds and high loads. Moreover, in Fig. 59(a-b) the mild wear regions can be regarded as the safe operation regime for these materials for practical applications. The boundary line of this regime represents the upper limit of the service life of 303SS against 8620 low alloy steel and vice versa [72]. The boundaries of the wear mode regimes are as follows:

Tribo-corrosion maps for steels, titanium and titanium carbide materials

- a) Mild wear \leq [0.05 g]
- b) [0.05 g] < medium wear \leq [0.15 g]
- c) Severe wear > [0.15 g]

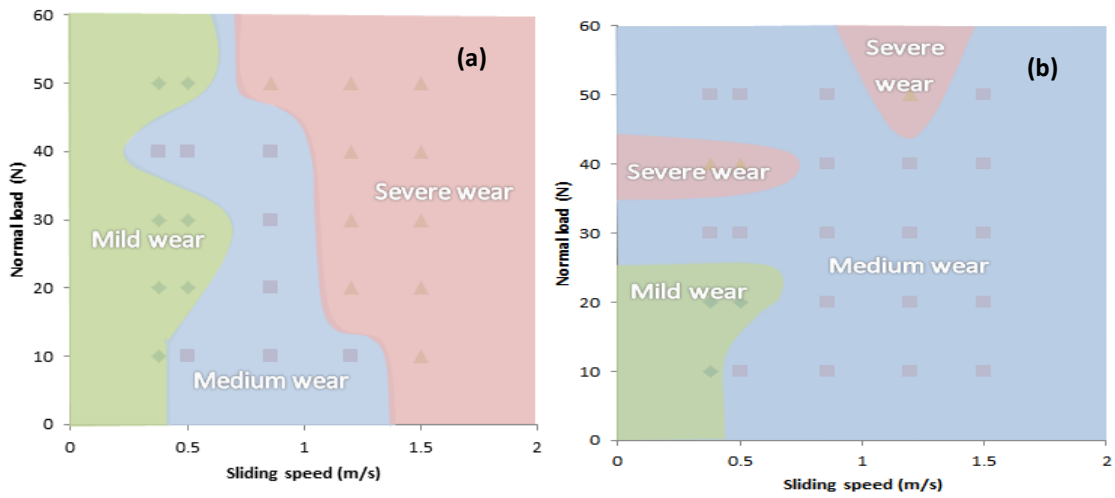


Figure 59 Wear mode maps (a) 303stainless steel disk against 8620 low alloy steel pin and (b) 8620 low alloy steel pin against 303stainless steel disk.

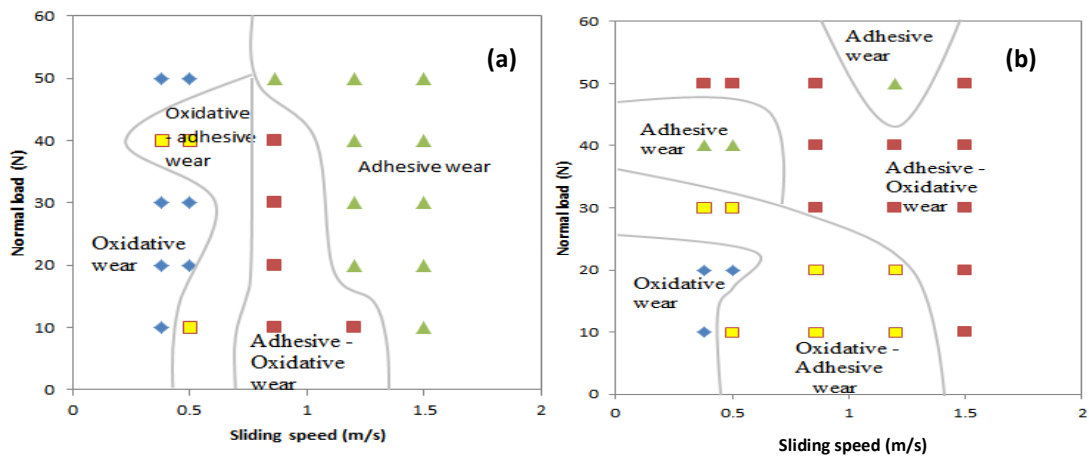


Figure 60 Wear mechanism maps (a) 303 stainless steel disk against 8620 low alloy steel pin and (b) 8620 low alloy steel pin against 303 stainless steel disk.

Fig. 60 shows the wear mechanism map for 303SS and 8620 low alloy steel. The wear mechanism regimes suggested are as follows, are based on the experimental results and observations above. For both tribological components of the couple, with oxidative wear being more prevalent for the low alloy steel at higher loads and sliding speeds and adhesive wear being more predominant for the high Cr containing steel, in the same load regime. The wear mechanisms regimes are as follows:

- Oxidative wear
- Oxidative – adhesive
- Adhesive – oxidative
- Adhesive wear

4.4. Links between Lim and Ashby [69] wear diagram and present work

The Lim and Ashby approach, Fig. 61, is based on a wide data base, of published wear rates, and providing a mathematical basis for charting the transition between regimes. This wear map assigned different regimes where wear occurred through different mechanisms [69]. The primary data is derived from dry sliding wear, pin-on-disk experiments, from the literature and plotted on a diagram. These data are plotted based on dimensionless parameters i.e. normalised wear rate on axis of normalized sliding velocity and normalized pressure. The results suggest that data from various sources, using specimens of differing shapes and sizes, can best be correlated by using a normalised wear rate, force and sliding velocity [69].

Fig. 61 shows the redrawn Lim and Ashby wear-mechanism map. To correlate present work with the Lim and Ashby wear-mechanism map, wear rate, normal load and sliding speed of the present work were converted to normalised values.

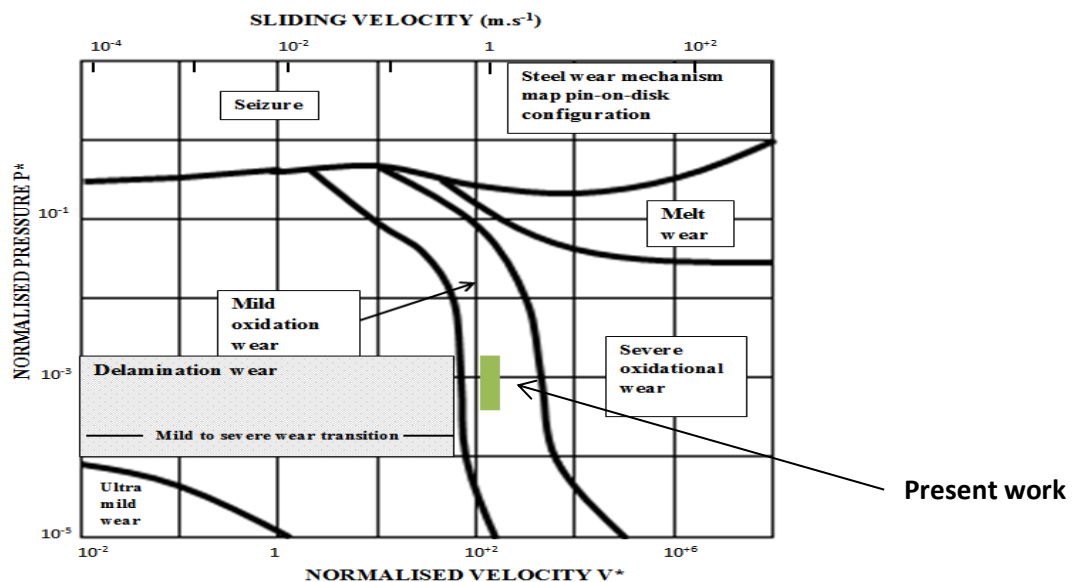


Figure 61 Wear-mechanism map for a steel sliding pair using the pin-on-disk configuration [69].

By normalising normal loads and sliding speeds as per [69], the normalising ranges of the present work as below:

Tribo-corrosion maps for steels, titanium and titanium carbide materials

- Sliding speed $0.38 - 1.5 \text{ m s}^{-1}$ converted to $1.25 \times 10^2 - 4.95 \times 10^2$
- Normal load (force) $10 - 50 \text{ N}$ converted to $5.80 \times 10^{-4} - 2.9 \times 10^{-3}$

Note: For these conversions, the diameter of the pin = 6mm, Hardness 190HV (average hardness of the 303 stainless steel disk and 8620 low alloy steel pin), Thermal diffusivity

= $9.1 \times 10^{-6} \text{ m}^2 \text{ s}^{-1}$ has been used.

The highlighted area of the Fig. 61 shows the boundaries of the field studied by the present work. The window of conditions in the present work represents mild-oxidative wear i.e. oxidation-affected wear. Hence, the work above focuses on the various transitions over a small window of the wear map above, where oxidation interacts with wear and thus the findings of the present work can be compared to those of Lim and Ashby wear maps for steels [69, 135, 119]. This confirms that the wear maps for more highly alloyed materials such as stainless steel, as examined in the present study Fig. 60(a), involves a larger adhesive wear portion of the map, Fig. 61, compared to the original maps for low alloy steel [69] and this is consistent with improved oxidation resistance due to the increased levels of Cr in the higher alloyed steel.

Hence, the results from the current study indicate by mapping the transitions of both pin and disk, an important overview can be generated of mechanistic changes on both the pin and disk in the tribological contact. This provides further insights into wear mechanism changes as a function of increases of alloying additions.

4.5. Conclusions

1. Fluctuation in wear of both materials with increases in normal load and sliding speed is attributed to strain hardening, thermal softening and oxidation effects of the mating surfaces due to frictional heating.
2. For highly alloyed material, 303SS, severe wear is more prevalent in the relatively high load and speed regimes, whereas for the 8620 low alloy steel, medium wear is predominant than mild wear for the range of speeds and normal loads.
3. Such observations are interpreted in the role of wear-oxidation mechanisms, material transfer, and the development of a mechanically mixed layer in modifying the wear process in the tribological contact.

4. The differences of the tribo-oxidation area of the map for the stainless steel compared with the low alloy steel are attributed to the role of Cr in reducing the oxidative wear process for the latter material.

Chapter 5

Wear maps for titanium carbide composite based coatings deposited on 303stainless steel

5.1 Introduction

In this experimental base study, the effects of applied load and sliding speed on the wear behaviour of 303SS (uncoated and coated with titanium carbide composite coatings) against alumina were investigated. The use of austenitic/ferritic stainless steel is limited in tribological application due to its low sliding wear resistance. In tribo-engineering applications, especially where components undergo sliding wear, steels may exhibit poor tribological properties such as low sliding wear resistance; unstable friction qualities; surface damage and formation of strong adhesion; delaminated wear; ploughing wear and plastic deformation. Surface treatments such as depositing coatings on the surfaces of different substrates susceptible to wear increase the operating life and range of conditions for which the substrates may be used. Several methods are used for coating surfaces. The dry sliding wear behaviour of titanium carbide composite coatings produced by the Tungsten Inert Gas (TIG) welding torch melting method has been discussed in the contents of the wear behaviours of different coatings made by other methods.

5.2. Wear tests results of 303stainless steel (uncoated and coated with TiC composite coatings) disks against alumina balls

Sliding wear tests were carried out in air under ambient conditions at room temperature on pin-on-disk CSM Tribometer for both uncoated and coated materials at different combinations (20 combinations for each uncoated and coated substrate) of sliding speeds and normal loads as per experimental conditions mentioned in section 3.4, chapter 3. The coating was carried out as per procedure mentioned in Section 3.6, chapter 3. The effects of change in change of sliding speeds and normal loads on wear behaviour of 303SS (uncoated and coated with TiC composite coatings) against alumina were investigated. SEM micrograph and EDX analysis of the worn surfaces were carried out for each combination of sliding speed and normal load. At the end of test dark and smooth worn surfaces; and low wear loss rate results in mild wear while bright and rougher worn surfaces; and high wear rate results in severe wear. The tests results of this tribo-system are as under:

5.2.1. Wear rate of 303SS against alumina at 3 cm s⁻¹ for the range of normal loads

Fig. 62 shows the sliding wear and coefficient of friction trends of 303SS against alumina ball at 3cm s⁻¹ at various normal loads.

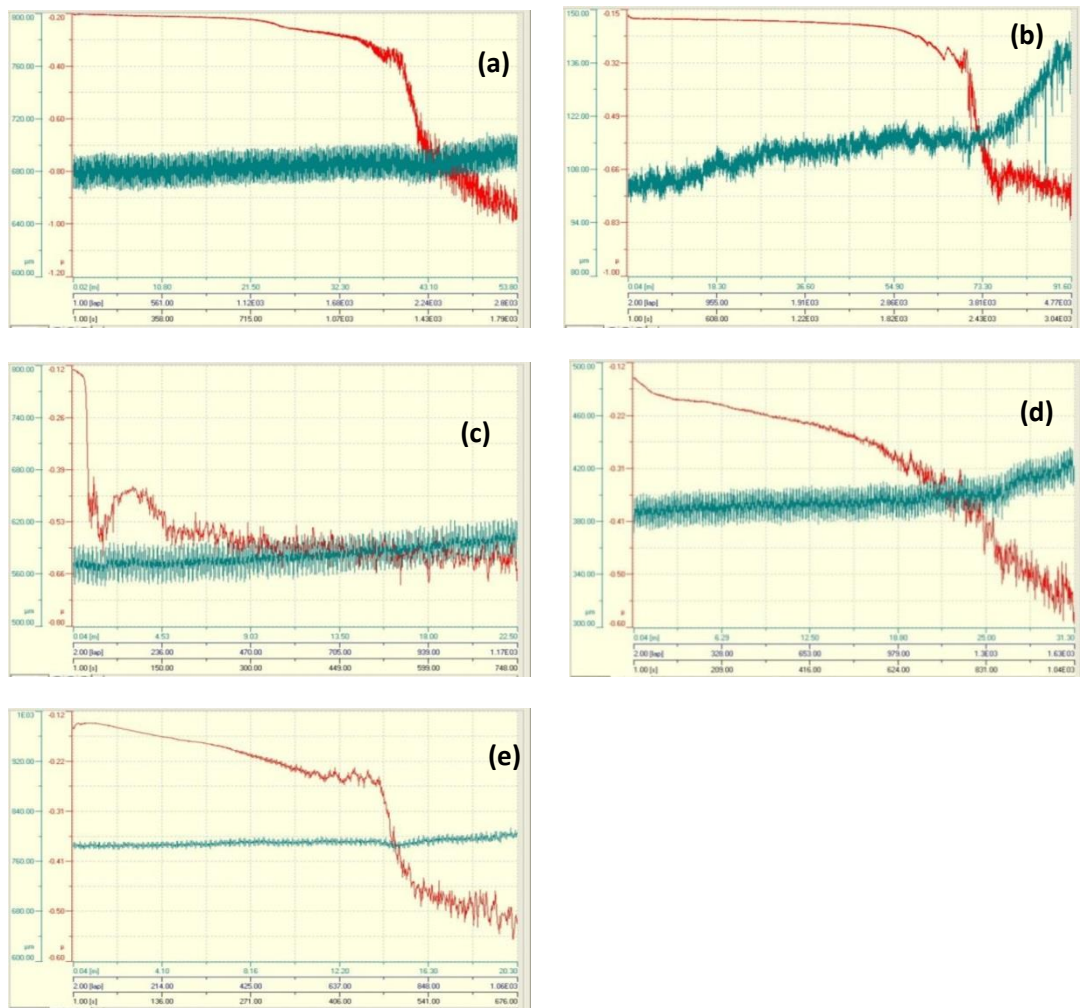


Figure 62 Sliding wear and coefficient of friction trends of 303SS against alumina ball at sliding speed 3 cm s⁻¹ and (a) normal load 2 N, (b) at 4 N, (c) at 6 N, (d) at 8 N and (e) at 10 N.

Table 19 shows the sliding distance covered and wear rate of 303SS against alumina at 3 cm s⁻¹ and various normal loads.

Normal loads (N)	Sliding distance of the test (m)	Total mass loss (g)	Wear rate (g.m ⁻¹) x10 ⁻⁷
2	53.80	0.0005	93
4	91.60	0.0004	44
6	22.50	0.0004	178
8	31.30	0.0009	288
10	20.30	0.0008	394

Table 19 Wear rate of 303SS disks against alumina ball at 3 cm s⁻¹ and various normal loads.

Tribo-corrosion maps for steels, titanium and titanium carbide materials

Fig. 63 shows the wear rate of 303SS disks sliding against alumina ball at sliding speed 3 cm s⁻¹ for the range of normal loads.

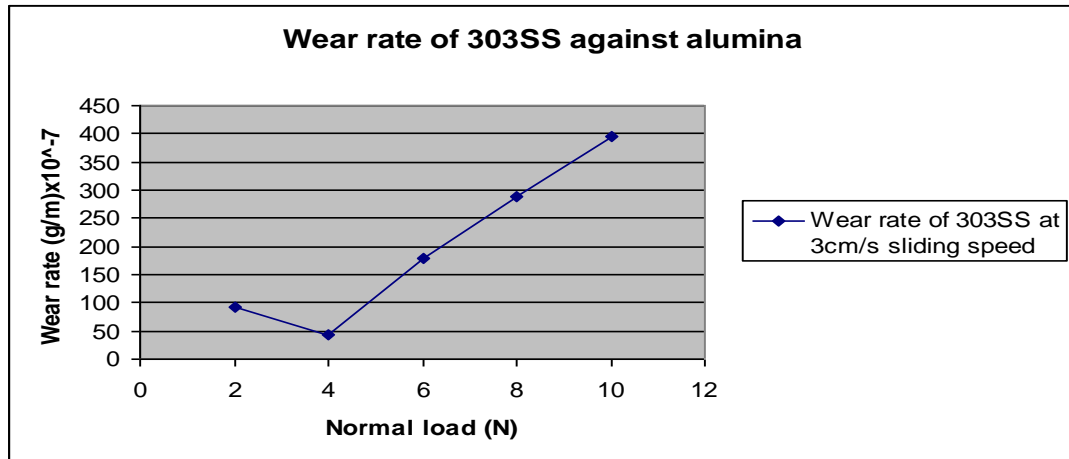


Figure 63 Wear rate of 303SS disks against alumina ball at 3 cm s⁻¹ and various normal loads.

5.2.2. Wear rate of 303SS against alumina at 7 cm s⁻¹ for the range of normal loads

Fig. 64 shows the sliding wear and coefficient of friction trends of 303SS against alumina ball at 7 cm s⁻¹ at various normal loads.

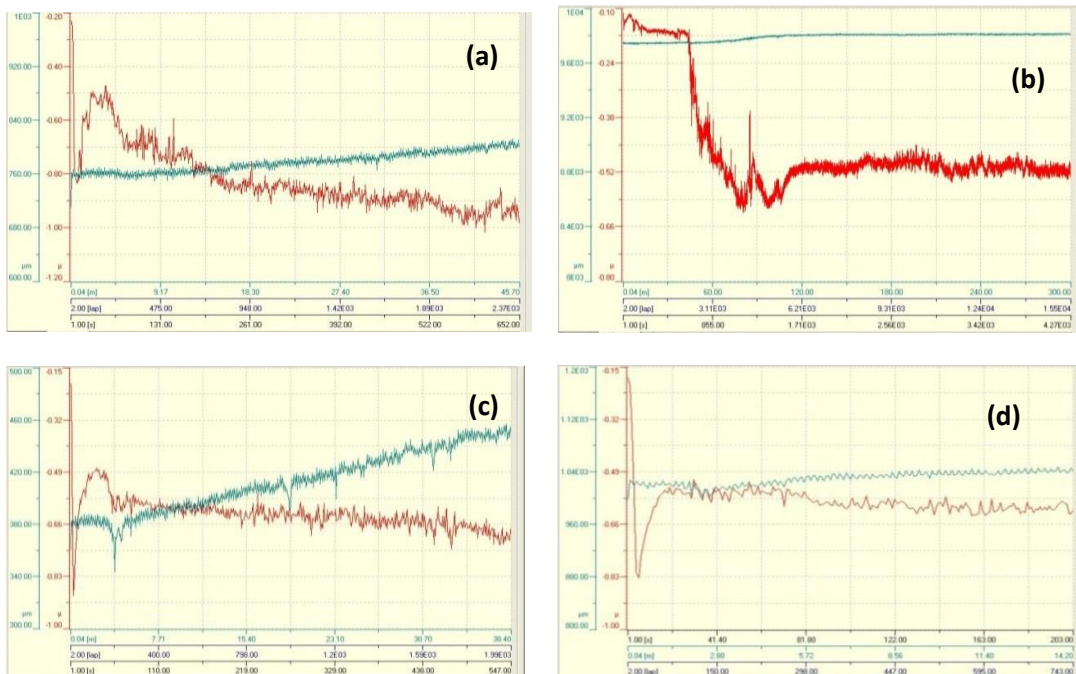




Figure 64 Sliding wear and coefficient of friction trends of 303SS against alumina ball at sliding speed 7 cm s^{-1} , and (a) at normal load 2 N, (b) at 4 N, (c) at 6 N, (d) at 8 N, and (e) at 10 N.

Table 20 shows the sliding distance covered and wear rate of 303SS against alumina at 7 cm s^{-1} and various normal loads.

Normal loads (N)	Sliding distance covered (m)	Total mass loss (g)	Wear rate (g m^{-1}) $\times 10^{-7}$
2	45.70	0.0010	219
4	300	0.0025	83
6	38.40	0.0019	495
8	14.20	0.0006	422
10	5.60	0.0008	1429

Table 20 Wear rate of 303SS disks against alumina ball at 7 cm s^{-1} and various normal loads.

Fig. 65 shows the wear rate of 303SS disks sliding against alumina ball at sliding speed 7 cm s^{-1} for the range of normal loads.

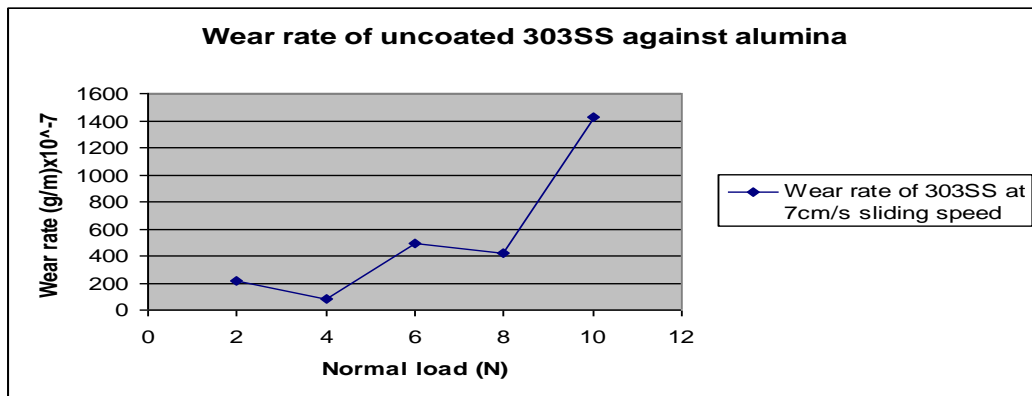


Figure 65 Wear rate of 303SS disks against alumina ball at 7 cm s^{-1} and various normal loads.

5.2.3. Wear rate of 303SS against alumina at 11 cm s^{-1} for the range of normal loads

Fig. 66 shows the sliding wear and coefficient of friction trends of 303SS against alumina ball at 11 cm s^{-1} at various normal loads.

Tribo-corrosion maps for steels, titanium and titanium carbide materials

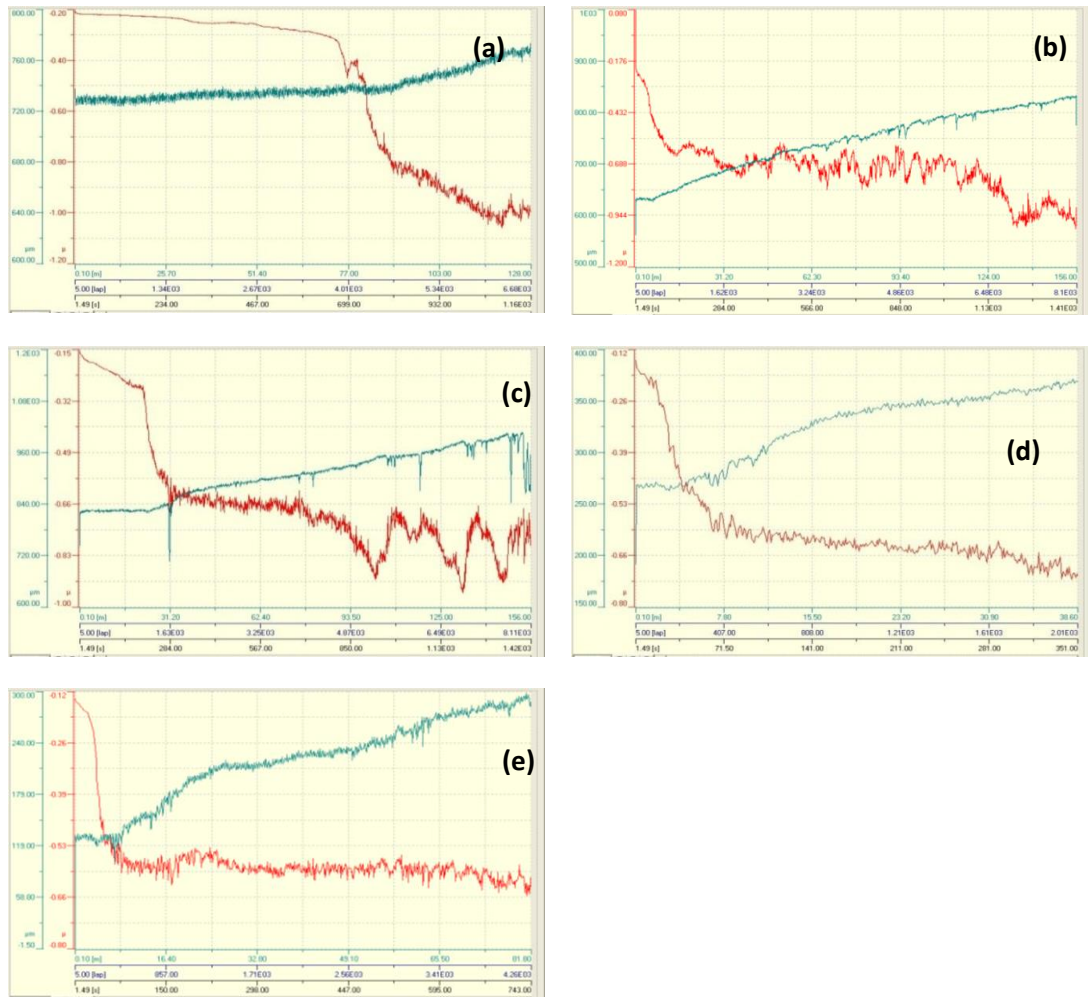


Figure 66 Sliding wear and coefficient of friction trends of 303SS against alumina ball at 11cm s^{-1} and (a) at normal load 2N, (b) at 4N, (c) at 6N, (d) at 8N, and (e) at 10N.

Table 21 shows the sliding distance covered and wear rate of 303SS against alumina at 11cm s^{-1} and various normal loads.

Normal loads (N)	Sliding distance covered(m)	Total mass loss (g)	Wear rate (g m^{-1}) $\times 10^{-7}$
2	128	0.0008	63
4	156	0.0026	167
6	156	0.0029	186
8	38.60	0.0010	259
10	81.80	0.0028	342

Table 21 Wear rate of 303SS disks against alumina ball at 11cm s^{-1} and various normal loads.

Fig. 67 shows the wear rate of 303SS disks sliding against alumina ball at sliding speed 11cm s^{-1} for the range of normal loads.

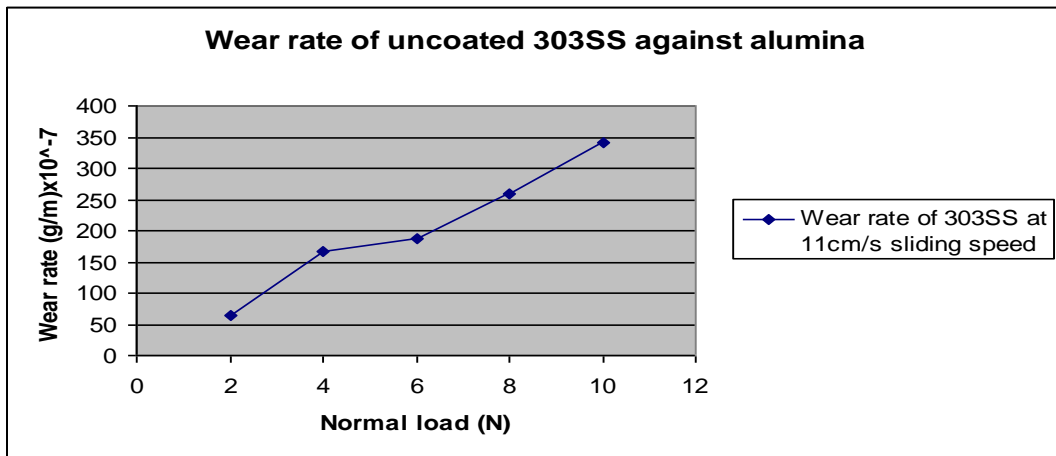
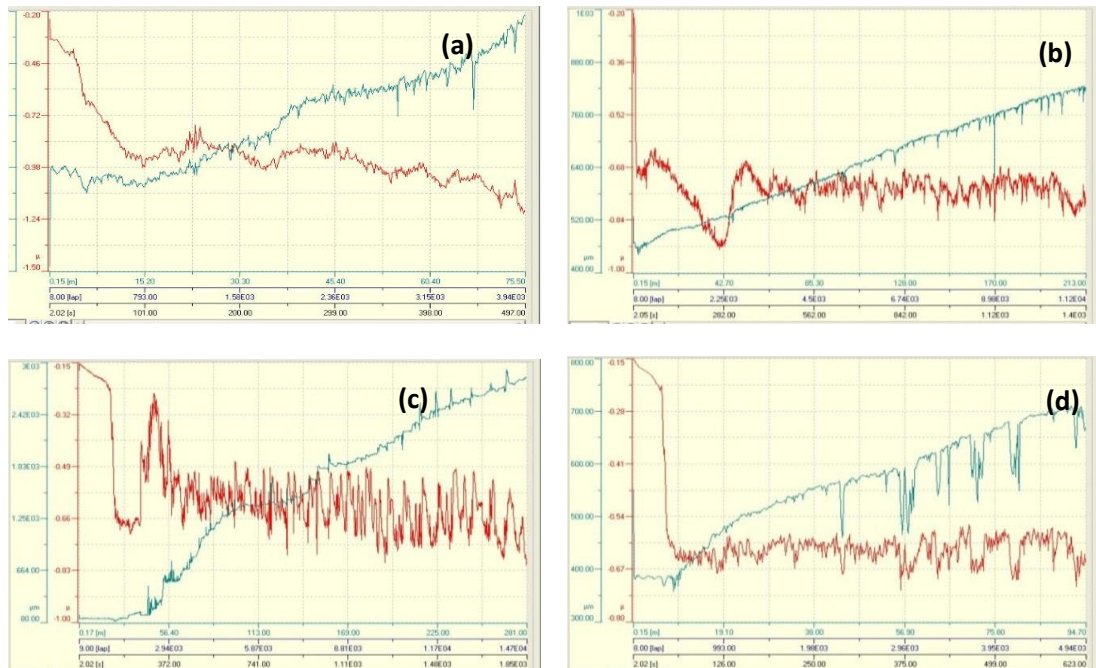


Figure 67 Wear rate of 303SS disks against alumina ball at 11cm s⁻¹ and various normal loads.

5.2.4. Wear rate of 303SS against alumina at 15cm s⁻¹ for the range of normal loads

Fig. 68 shows the sliding wear and coefficient of friction trends of 303SS against alumina ball at 15cm s⁻¹ at various normal loads.



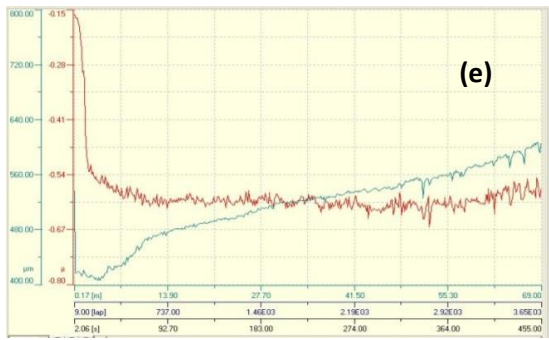


Figure 68 Sliding wear and coefficient of friction trends of 303SS against alumina ball at sliding speed 15cm s^{-1} and (a) at normal load 2N, (b) at 4N, (c) at 6N, (d) at 8N, and (e) at 10N.

Table 22 shows the sliding distance covered and wear rate of 303SS against alumina at 15cm s^{-1} and various normal loads.

Normal loads (N)	Sliding distance covered (m)	Total mass loss (g)	Wear rate (g m^{-1}) $\times 10^{-7}$
2	75.50	0.0007	93
4	213	0.0037	174
6	281	0.0045	160
8	94.70	0.0026	275
10	69	0.0041	599

Table 22 Wear rate of 303SS disks against alumina ball at 15cm s^{-1} and various normal loads.

Fig. 69 shows the wear rate of 303SS disks sliding against alumina ball at sliding speed 15cm s^{-1} for the range of normal loads.

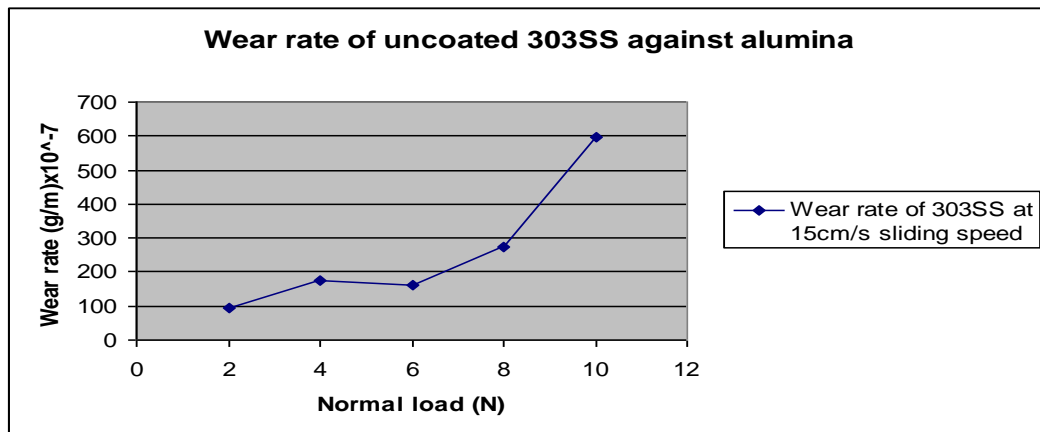


Figure 69 Wear rate of 303SS disks against alumina ball at sliding speed 15cm s^{-1} and various normal loads.

5.2.5. Wear rate of 303stainless steel against alumina at constant sliding speeds and various normal loads

Table 23 shows the wear rate of 303SS against alumina at constant sliding speeds and various normal loads.

Normal load (N)	Wear rate (g m^{-1}) $\times 10^{-7}$ at 3 cm s^{-1}	Wear rate (g m^{-1}) $\times 10^{-7}$ at 7 cm s^{-1}	Wear rate (g m^{-1}) $\times 10^{-7}$ at 11 cm s^{-1}	Wear rate (g m^{-1}) $\times 10^{-7}$ at 15 cm s^{-1}
2	93	219	63	93
4	44	83	167	174
6	178	495	186	160
8	288	422	259	275
10	394	1429	342	599

Table 23 Wear rate of 303stainless steel against alumina at constant sliding speeds and various normal loads.

Fig. 70 shows the wear rate of 303SS against alumina at constant sliding speeds and various normal loads.

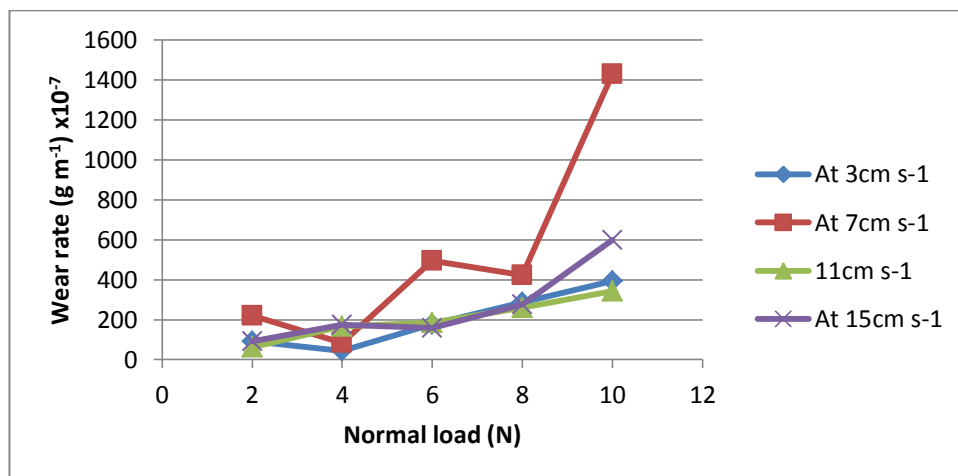


Figure 70 Wear rate vs normal load of 303stainless steel against alumina.

5.2.6. Wear rate of 303stainless steel against alumina at constant normal loads and various sliding speeds

Table 24 shows the wear rate of 303SS against alumina at constant normal loads and various sliding speeds.

Sliding speed (cm s ⁻¹)	Wear rate (g m ⁻¹) x10 ⁻⁷ at 2N	Wear rate (g m ⁻¹) x10 ⁻⁷ at 4N	Wear rate (g m ⁻¹) x10 ⁻⁷ at 6N	Wear rate (g m ⁻¹) x10 ⁻⁷ at 8N	Wear rate (g m ⁻¹) x10 ⁻⁷ at 10N
3	93	44	178	288	394
7	219	83	495	422	1429
11	63	167	186	259	342
15	93	174	160	275	599

Table 24 Wear rate of 303stainless steel against alumina at constant normal loads and various sliding speeds.

Fig. 71 shows the wear rate of 303SS against alumina at constant normal loads and various sliding speeds.

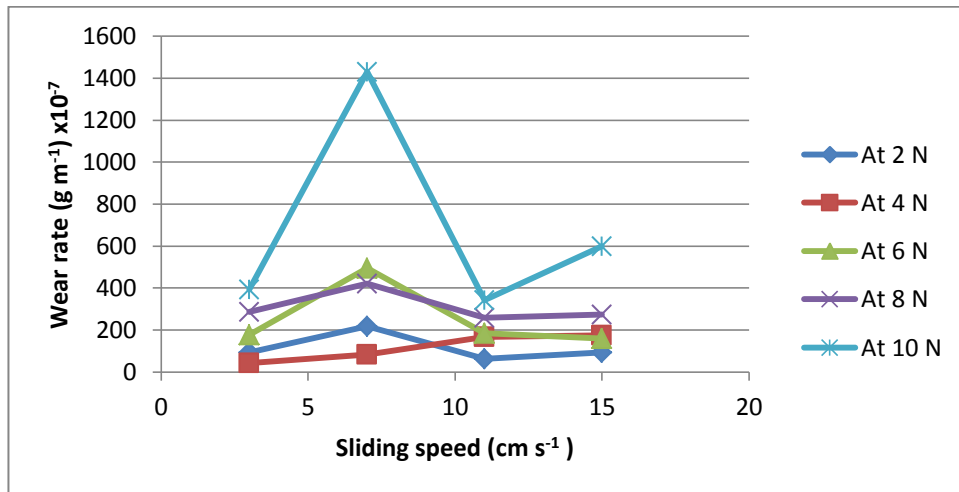


Figure 71 Wear rate vs sliding speed of 303stainless steel against alumina.

5.2.7. SEM micrographs and EDX analysis of worn surfaces of 303SS against alumina

Fig. 72 shows the SEM micrograph, and EDX analysis of the worn surface at sliding speed 3 cm s⁻¹ and 2 N normal load.

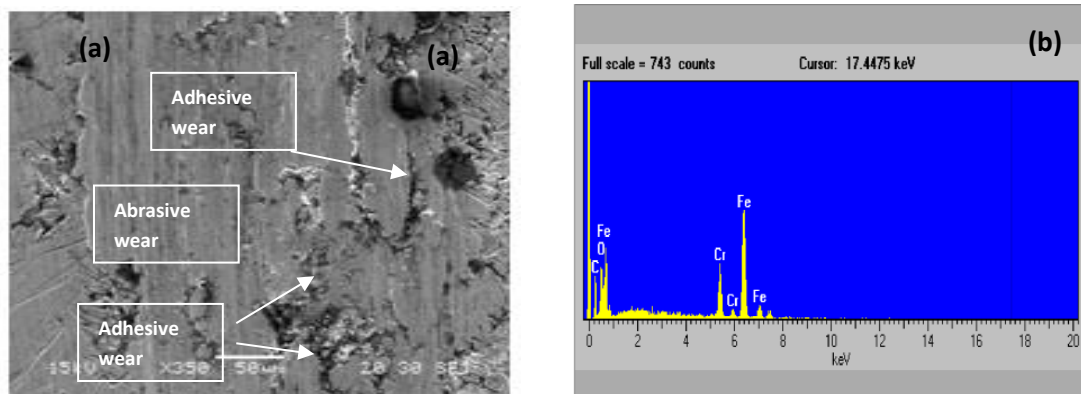


Figure 72 303SS against alumina, (a) SEM micrograph of the worn surface and (b) EDX analysis of the worn surface; at sliding speed 3cm s⁻¹ and normal load 2N.

Tribo-corrosion maps for steels, titanium and titanium carbide materials

Fig. 73 shows the SEM micrograph, and EDX analysis of the worn surface at sliding speed 7cm s^{-1} and 4N normal load.

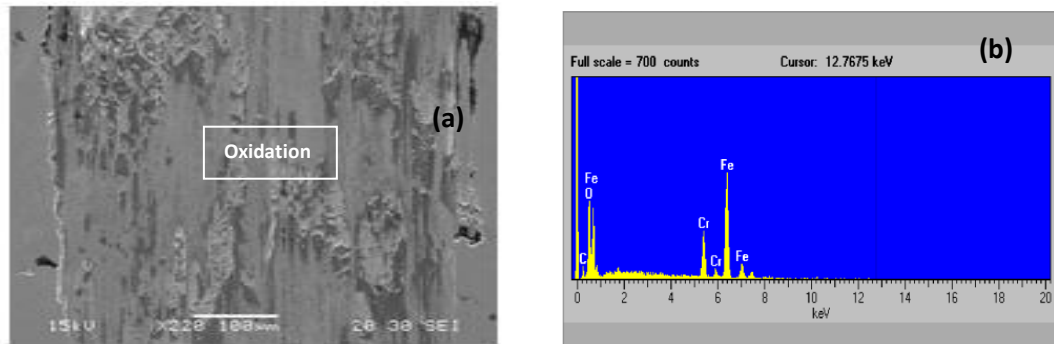


Figure 73 303SS against alumina, (a) SEM micrograph of the worn surface and (b) EDX analysis of the worn surface; at sliding speed 7cm s^{-1} and normal load 4N.

Fig. 74 shows the SEM micrograph, and EDX analysis of the worn surface at sliding speed 11cm s^{-1} and 4 N normal load.

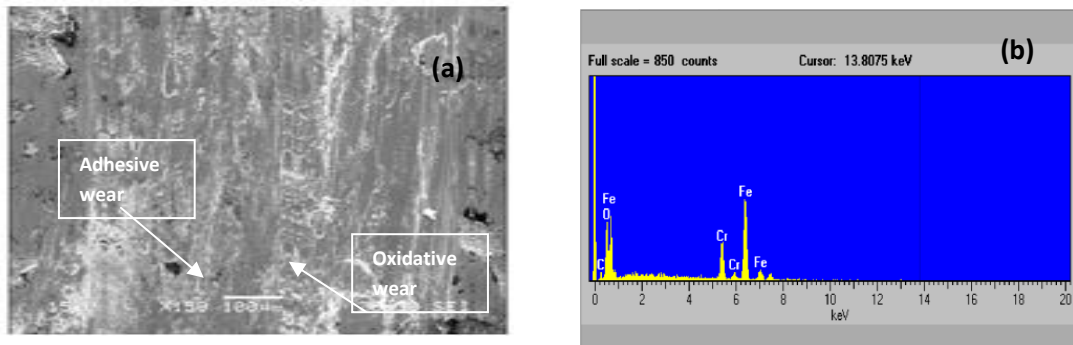


Figure 74 303SS against alumina, (a) SEM micrograph of the worn surface and (b) EDX analysis of the worn surface; at sliding speed 11cm s^{-1} and normal load 4N.

Fig. 75 shows the SEM micrograph, and EDX analysis of the worn surface at sliding speed 15cm s^{-1} and 8N normal load.

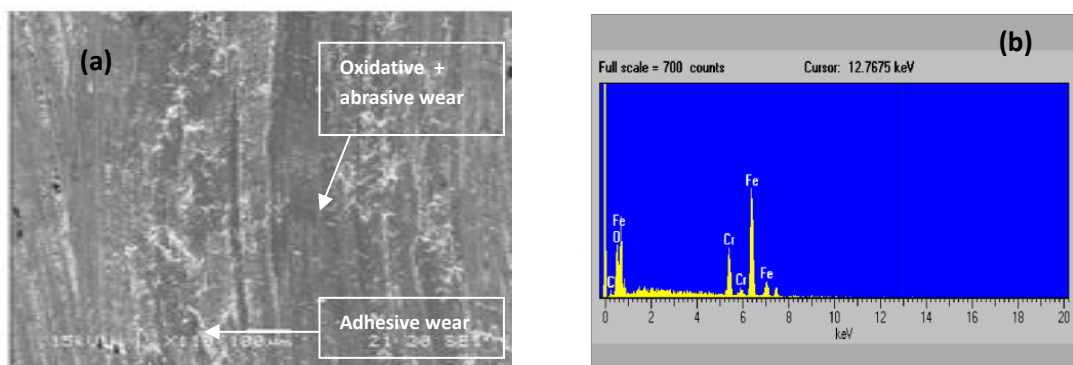


Figure 75 303SS against alumina, (a) SEM micrograph of the worn surface and (b) EDX analysis of the worn surface; at sliding speed 15cm s^{-1} and normal load 8N.

5.2.8 Wear behaviour of 303SS against alumina

All tests were terminated in between without completing constant sliding distance, which was 500 m, due to high wear rate and friction force at the mating surfaces of 303SS disks and alumina balls Tables 19-22 and Figs. 62-69.

At sliding speed 3 cm s^{-1} and normal load 2 & 6 N, the worn surfaces were very rough, adhesive wear, cracks on worn surfaces Fig. 72 and increased wear rate Table 23 results in medium wear. At 4 N mild wear was found due to the oxidation of wear track result in dark and smooth wear track surface at the end of test. At 8 and 10 N severe wear was found due to high wear rate, worn surface very rough, oxidation and adhesive wear occurred. The medium wear mode to mild wear mode, mild wear mode to medium wear mode and then medium to severe wear mode transitions occurred for the range of normal loads Table 19 and Fig. 63.

At sliding speed 7 cm s^{-1} the same wear trend was observed as that of at 3 cm s^{-1} for normal load 2 and 4 N Figs. 72-73. At 6 to 10 N severe wear was found due to high wear rate, worn surface very rough, oxidative and adhesive wear. The medium wear mode to mild wear mode and then mild wear mode to severe wear mode transitions occurred for the range of normal load Table 20 and Fig. 65.

At sliding speed 11 cm s^{-1} and normal load 2 N mild wear was found due to oxidative wear as in the case of 3 and 7 cm s^{-1} at 4 N. At 4 to 8 N medium wear was found due to the worn surfaces rough, adhesive, plastic deformation, delamination and oxidative wear of the wear track Fig. 74. At 10 N severe wear was found due to high wear rate, worn surface very rough, adhesive and oxidative wear and delamination of wear track. From the mild wear to medium wear and then medium to severe wear mode transitions occurred for the range of normal loads Table 21 and Fig. 67.

At sliding speed 15 cm s^{-1} and normal load 2 to 6 N medium wear was found as the worn surfaces rough and due to plastic deformation, adhesive and oxidative wear. At 8 and 10 N severe wear was found due to high wear rate, worn surface very rough, adhesive, oxidative wear and delamination of wear track Fig. 75. At this sliding speed no mild wear was found for the range of normal loads. From medium wear to severe wear mode transitions occurred between 6 and 8 N normal loads Table 22 and Fig. 69.

5.3. Wear tests results of 303SS base TiC composite coatings disks against alumina balls

5.3.1. Wear rate of 303SS base TiC coatings against alumina at 3cm s^{-1} for the range of normal loads

Fig. 76 shows the sliding wear and coefficient of friction trends of 303SS base TiC composite coatings against alumina ball at 3cm s^{-1} and various normal loads.

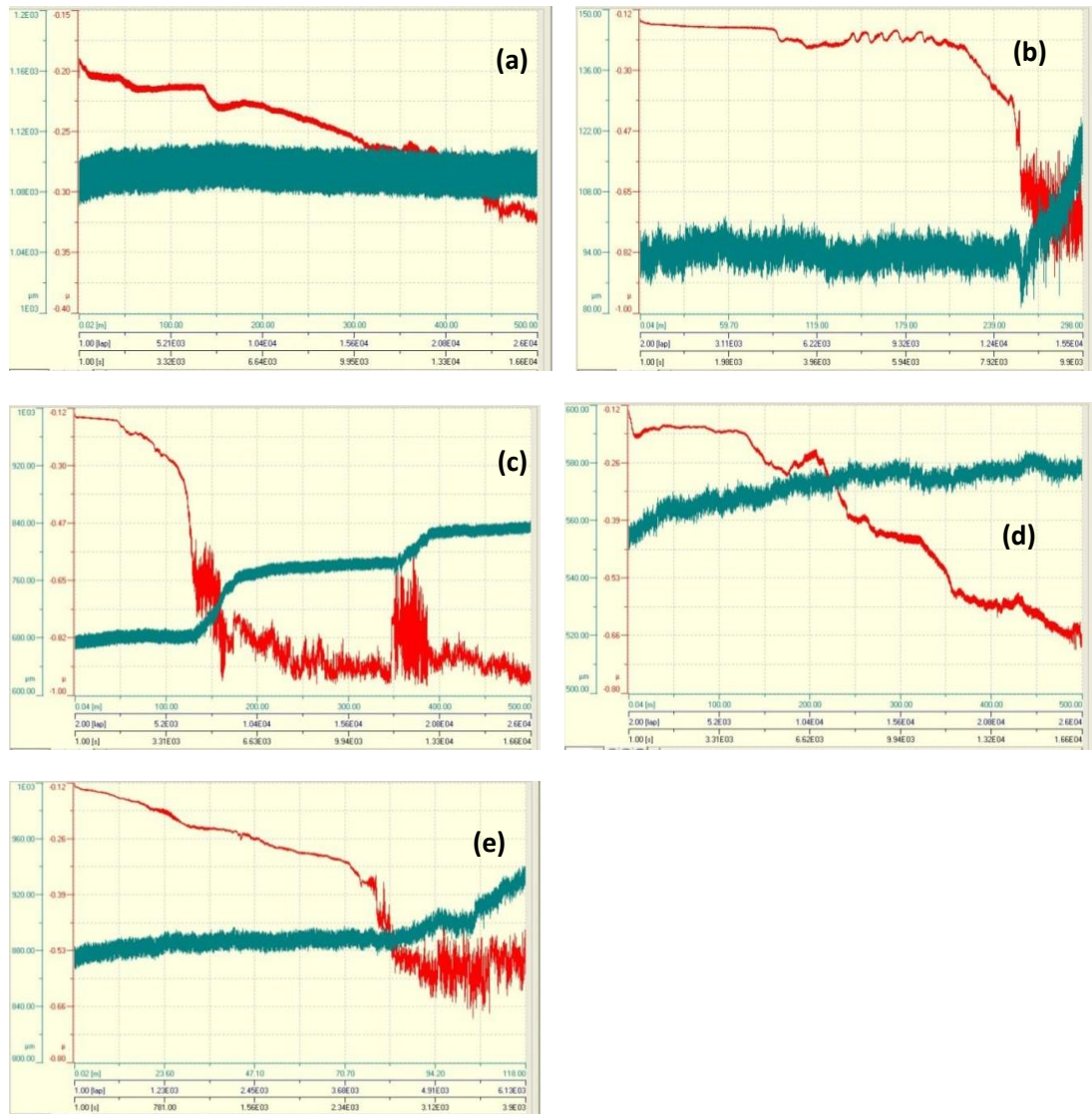


Figure 76 Sliding wear and coefficient of friction trends of 303SS base TiC coatings disks against alumina balls at sliding speed 3cm s^{-1} and (a) at normal load 2N, (b) at 4N, (c) at 6N, (d) at 8N and (e) at 10N.

Table 25 shows the sliding distance covered before termination of test and wear rate of 303SS base TiC composite coatings against alumina at 3cm s^{-1} and various normal loads.

Normal loads (N)	Sliding distance of the test (m)	Total mass loss (g)	Wear rate (g m ⁻¹) x10 ⁻⁷
2	500	0.0001	2
4	298	0.0005	17
6	500	0.0003	6
8	500	0.0003	6
10	118	0.0001	8.5

Table 25 Wear rate of 303SS disks against alumina ball at 3cm s⁻¹ and various normal loads.

Fig. 77 shows the wear rate of 303SS base TiC coatings disks sliding against alumina ball at sliding speed 3cm s⁻¹ for the range of normal loads.

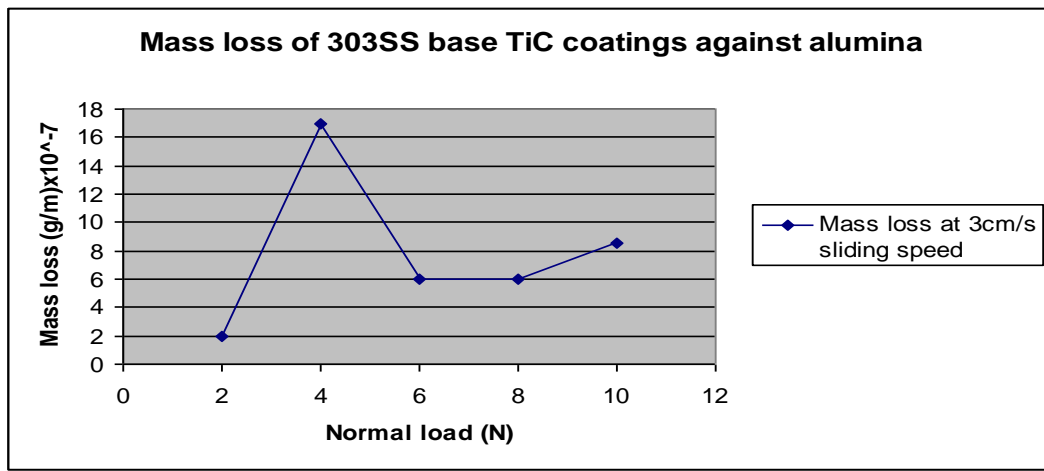
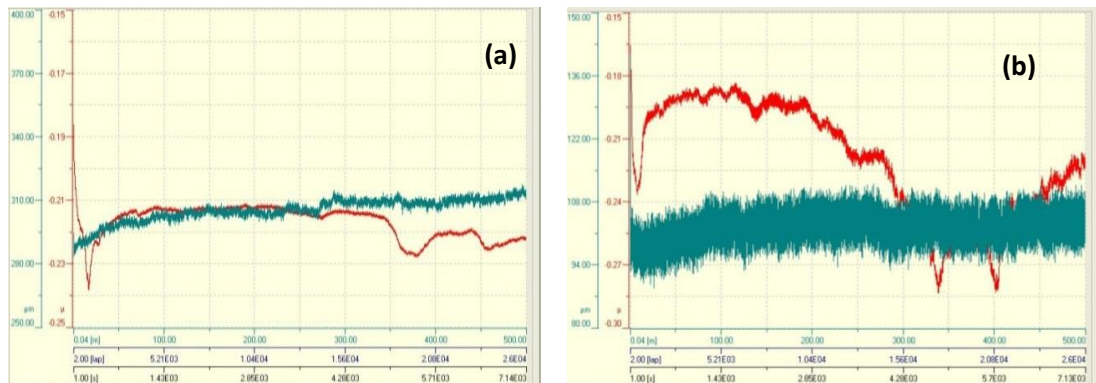


Figure 77 Wear rate of 303SS disks against alumina ball at sliding speed 3cm s⁻¹ and various normal loads

5.3.2. Wear rate of 303SS base TiC coatings against alumina at 7cm s⁻¹ for the range of normal loads

Fig. 78 shows the sliding wear and coefficient of friction trends of 303SS base TiC composite coatings against alumina ball at 7cm s⁻¹ at various normal loads.



Tribo-corrosion maps for steels, titanium and titanium carbide materials

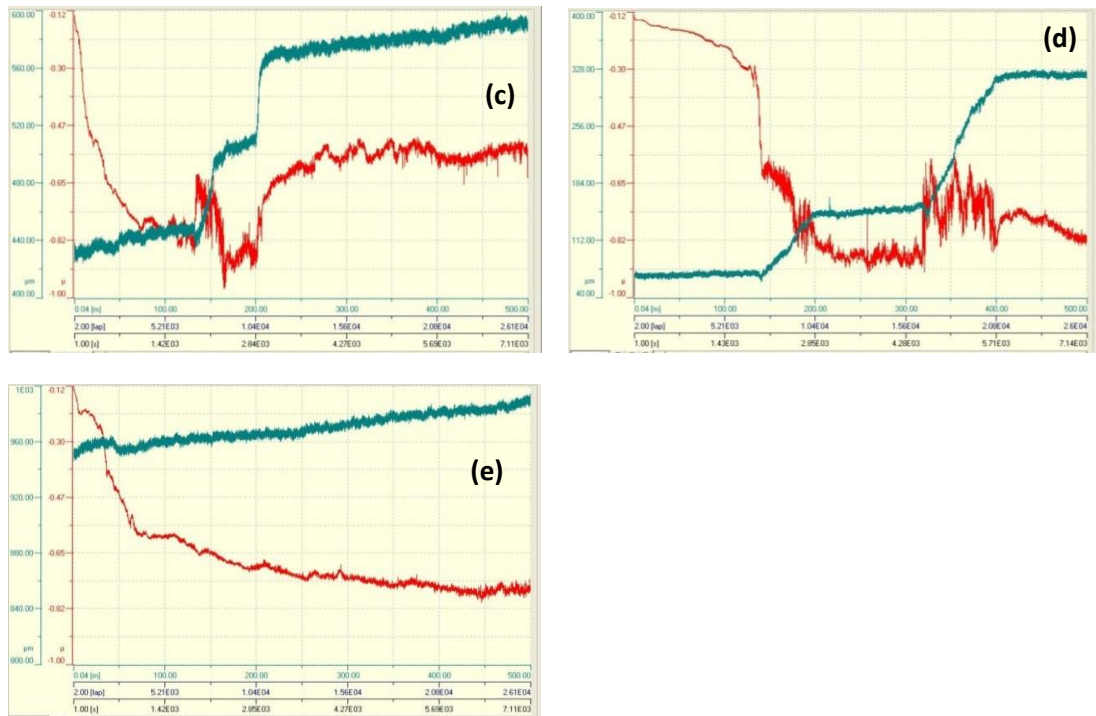


Figure 78 Sliding wear and coefficient of friction trends of 303SS base TiC coatings disks against alumina balls at sliding speed 7 cm s^{-1} and (a) at normal load 2N, (b) at 4N, (c) at 6N, (d) at 8N and (e) at 10N.

Table 26 shows the sliding distance covered before termination of test and wear rate of 303SS base TiC composite coatings against alumina at 7 cm s^{-1} and various normal loads.

Normal loads (N)	Sliding distance of the test (m)	Total mass loss (g)	Wear rate (g m^{-1}) $\times 10^{-7}$
2	500	0.0001	2
4	500	0.0001	2
6	500	0.0002	4
8	500	0.0011	22
10	500	0.0010	20

Table 26 Wear rate of 303SS base TiC coatings disks against alumina ball at sliding speed 7 cm. s^{-1} and various normal loads.

Fig. 79 shows the wear rate of 303SS base TiC coatings disks sliding against alumina ball at 7 cm s^{-1} sliding speed for the range of normal loads.

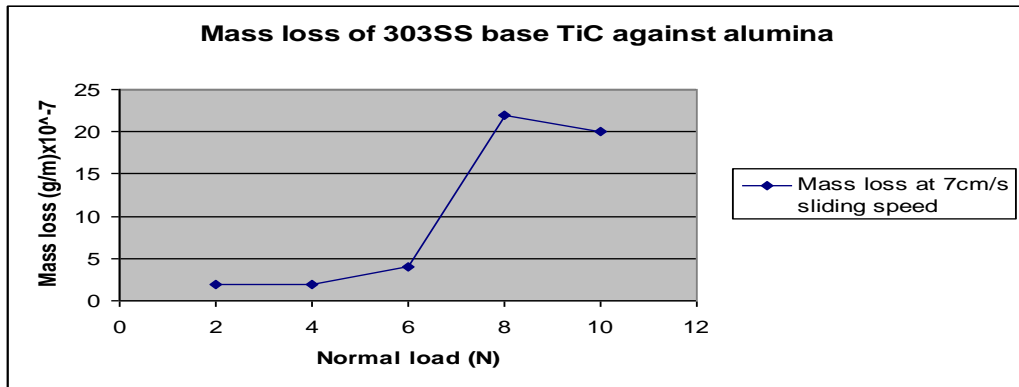
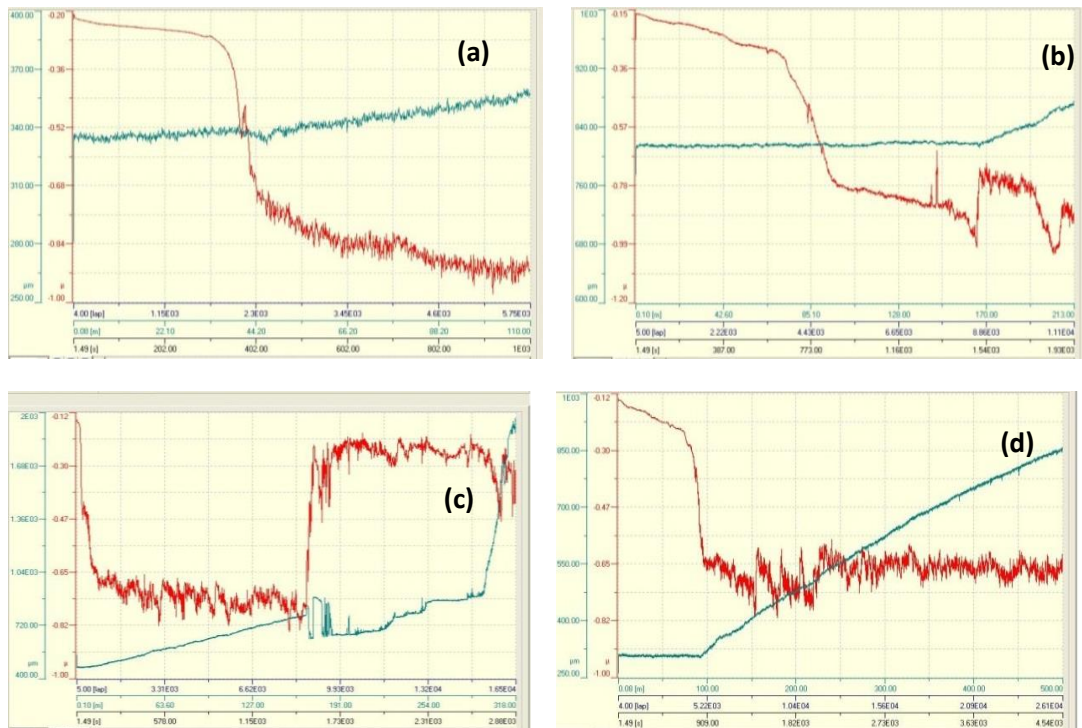


Figure 79 Wear rate of 303SS disks against alumina ball at sliding speed 7cm s⁻¹ and various normal loads.

5.3.3. Wear rate of 303SS base TiC coatings against alumina at 11cm s⁻¹ for the range of normal loads

Fig. 80 shows the sliding wear and coefficient of friction trends of 303SS base TiC composite coatings against alumina ball at 11 cm s⁻¹ and various normal loads.



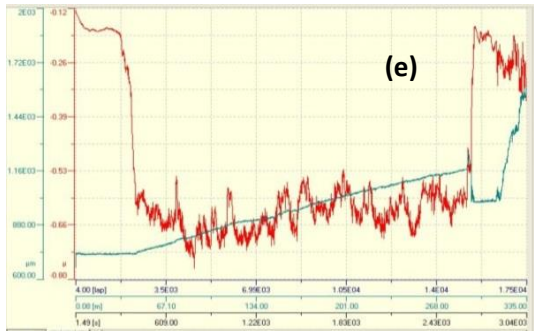


Figure 80 Sliding wear and coefficient of friction trends of 303SS base TiC coatings disks against alumina balls at 11 cm s^{-1} and (a) at normal load 2N, (b) at 4N, (c) at 6N, (d) at 8N, and (e) at 10N.

Table 27 shows the sliding distance covered before termination of test and wear rate of 303SS base TiC composite coatings against alumina at 11 cm s^{-1} and various normal loads.

Normal loads (N)	Sliding distance of the test (m)	Total mass loss (g)	Wear rate (g m^{-1}) $\times 10^{-7}$
2	110	0.0005	45
4	213	0.0007	32
6	318	0.0015	47
8	500	0.0048	96
10	335	0.0032	96

Table 27 Wear rate of 303SS base TiC coatings disks against alumina ball at 11 cm s^{-1} and various normal loads.

Fig. 81 shows the wear rate of 303SS base TiC coatings disks sliding against alumina ball at sliding speed 11 cm s^{-1} and various normal loads.

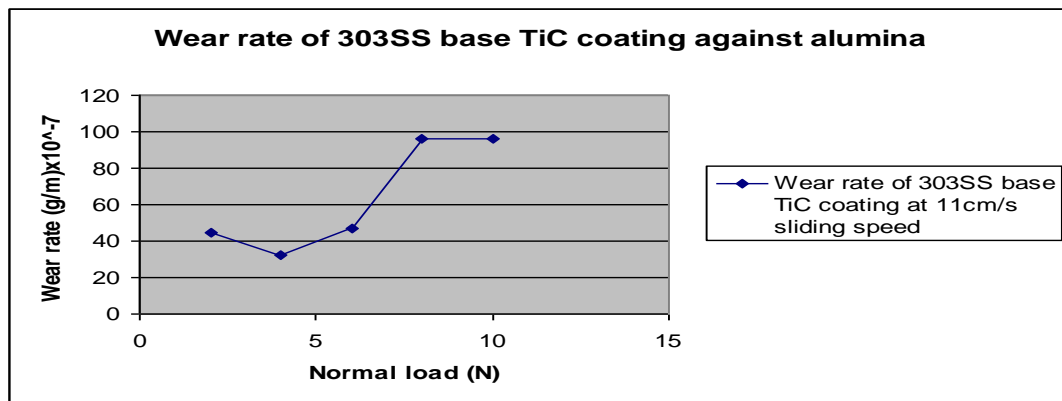


Figure 81 Wear rate of 303SS base TiC coatings disks against alumina ball at sliding speed 11 cm s^{-1} and various normal loads

5.3.4. Wear rate of 303SS base TiC coatings against alumina at 15 cm s^{-1} for the range of normal loads

Fig. 82 shows the sliding wear and coefficient of friction trends of 303SS base TiC composite coatings against alumina ball at 15 cm s^{-1} and various normal loads.

Tribo-corrosion maps for steels, titanium and titanium carbide materials

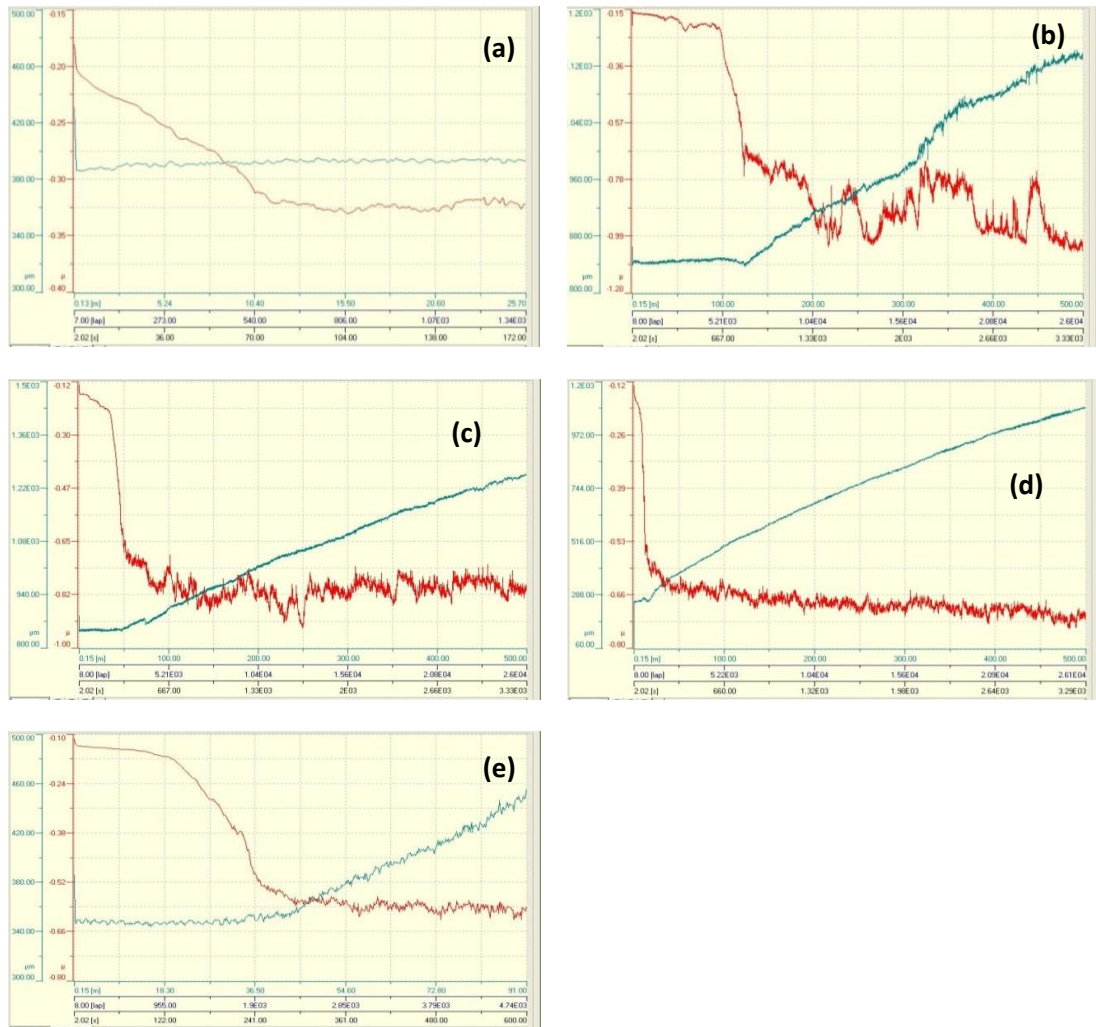


Figure 82 Sliding wear and coefficient of friction trends of 303SS against alumina ball at sliding speed 15 cm s^{-1} and (a) at normal load 2N, (b) at 4N, (c) at 6N, (d) at 8N, and (e) at 10N.

Table 28 shows the sliding distance covered before termination of test and wear rate of 303SS base TiC composite coatings against alumina at sliding speed 15 cm s^{-1} and various normal loads.

Normal loads (N)	Sliding distance of the test (m)	Total mass loss (g)	Wear rate (g m^{-1}) $\times 10^{-7}$
2	25.70	0.0002	78
4	500	0.0034	68
6	500	0.0038	76
8	500	0.0066	132
10	91	0.0010	110

Table 28 Wear rate of 303SS base TiC coatings disks against alumina balls at 15 cm s^{-1} and various normal loads.

Fig. 83 shows the wear rate of 303SS base TiC coatings disks sliding against alumina ball at 15cm s⁻¹ sliding speed for the range of normal loads.

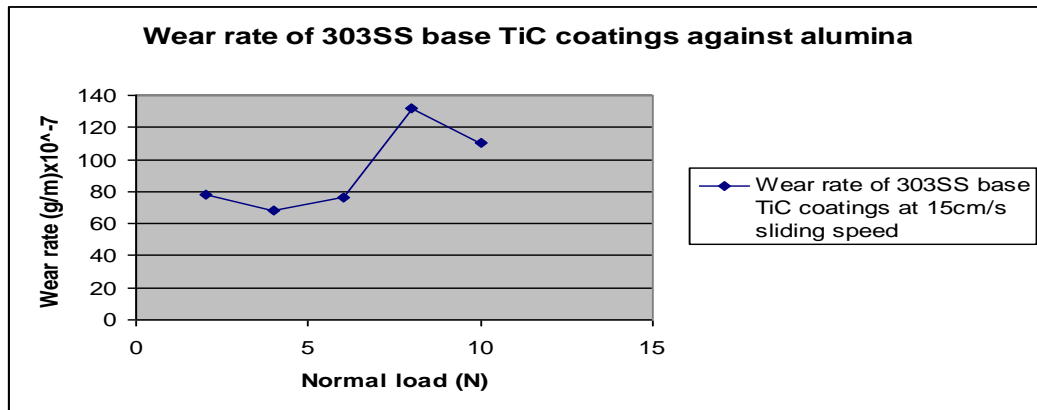


Figure 83 Wear rate of 303SS base TiC coatings disks against alumina ball at sliding speed 15cm s⁻¹ and various normal loads

5.3.5. Wear rate of 303SS base TiC against alumina at constant sliding speeds and various normal loads

Table 29 shows the wear rate of 303SS base TiC composite coatings against alumina at constant sliding speeds and various normal loads.

Normal load (N)	Wear rate (g m ⁻¹) x 10 ⁻⁷ at 3cm s ⁻¹	Wear rate (g m ⁻¹) x 10 ⁻⁷ at 7cm s ⁻¹	Wear rate (g m ⁻¹) x 10 ⁻⁷ at 11cm s ⁻¹	Wear rate (g m ⁻¹) x 10 ⁻⁷ at 15cm s ⁻¹
2	2	2	45	78
4	17	2	32	68
6	6	4	47	76
8	6	22	96	132
10	8.5	20	96	110

Table 29 Wear rate of TiC coatings against alumina at constant sliding speeds and various normal loads.

Fig. 84 shows the wear rate of 303SS base TiC composite coatings against alumina at constant sliding speeds and various normal loads.

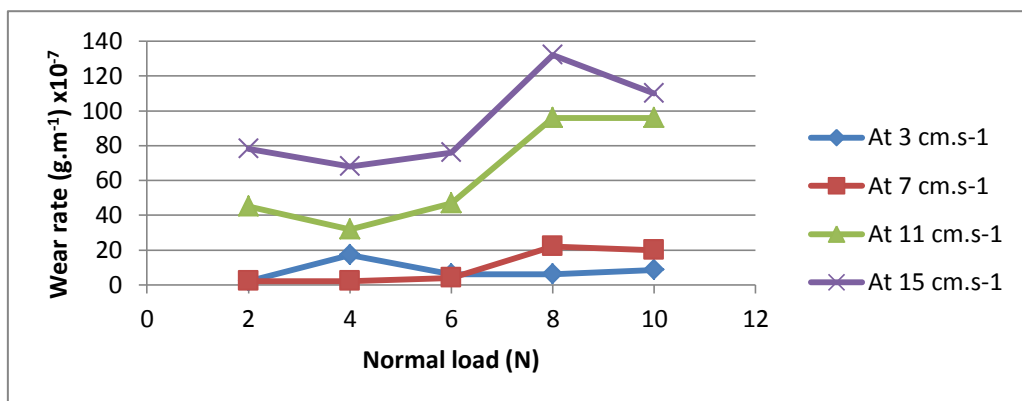


Figure 84 Wear rate vs normal load of 303SS base TiC coatings against alumina

5.3.6. Wear rate of 303SS base TiC coatings against alumina at constant normal loads and various sliding speeds

Table 30 shows the wear rate of 303SS base TiC composite coatings against alumina at constant normal loads and various sliding speeds.

Sliding speed (cm s ⁻¹)	Wear rate (g m ⁻¹) x10 ⁻⁷ at 2N	Wear rate (g m ⁻¹) x10 ⁻⁷ at 4N	Wear rate (g m ⁻¹) x10 ⁻⁷ at 6N	Wear rate (g m ⁻¹) x10 ⁻⁷ at 8N	Wear rate (g m ⁻¹) x10 ⁻⁷ at 10N
3	2	17	6	6	8.5
7	2	2	4	22	20
11	45	32	47	96	96
15	78	68	76	132	110

Table 30 Wear rate of TiC coating against alumina at constant normal loads and various sliding speeds.

Fig. 85 shows the wear rate of 303SS base TiC composite coatings against alumina at constant normal loads and various sliding speeds.

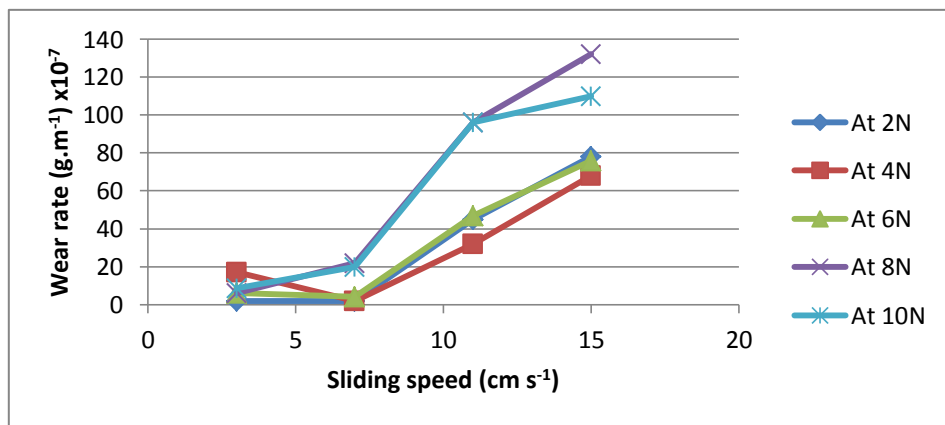


Figure 85 Wear rate vs sliding speed of 303SS base TiC coatings against alumina.

5.3.7. SEM micrographs of the worn surface of 303SS base TiC coatings against alumina

Fig. 86 shows the SEM micrograph and EDX analysis of the worn surface at sliding speed 3 cm s⁻¹ and normal load 2 N.

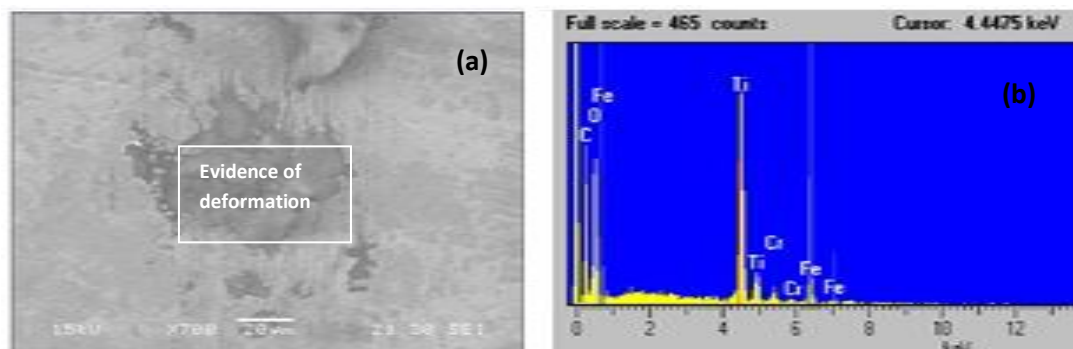


Figure 86 303SS base TiC coatings against alumina, (a) SEM micrograph of the worn surface and (b) EDX analysis of the worn surface; at 3 cm s⁻¹ and 2 N.

Tribo-corrosion maps for steels, titanium and titanium carbide materials

Fig. 87 shows the SEM micrograph, and EDX analysis of the worn surface at sliding speed 3 cm s^{-1} and normal load 8 N.

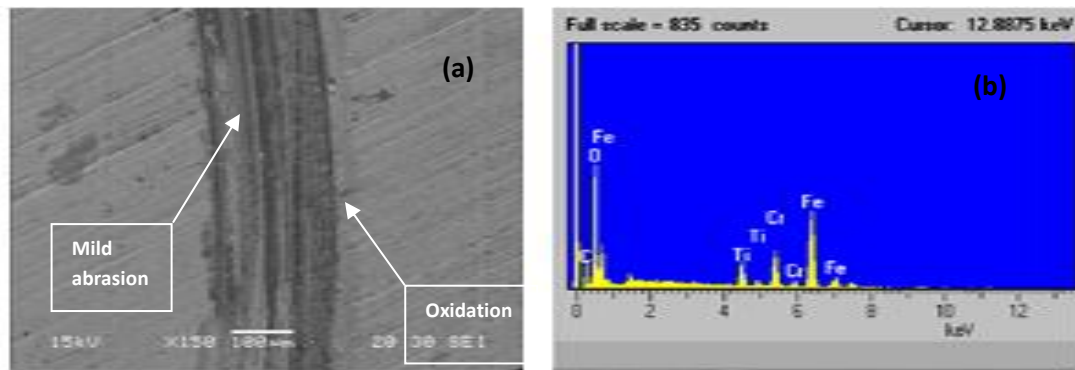


Figure 87 303SS base TiC coatings against alumina, (a) SEM micrograph of the worn surface and (b) EDX analysis of the worn surface; at 3 cm s^{-1} and 8 N.

Fig. 88 shows the SEM micrograph, and EDX analysis of the worn surface at sliding speed 7 cm s^{-1} and normal load 10 N.

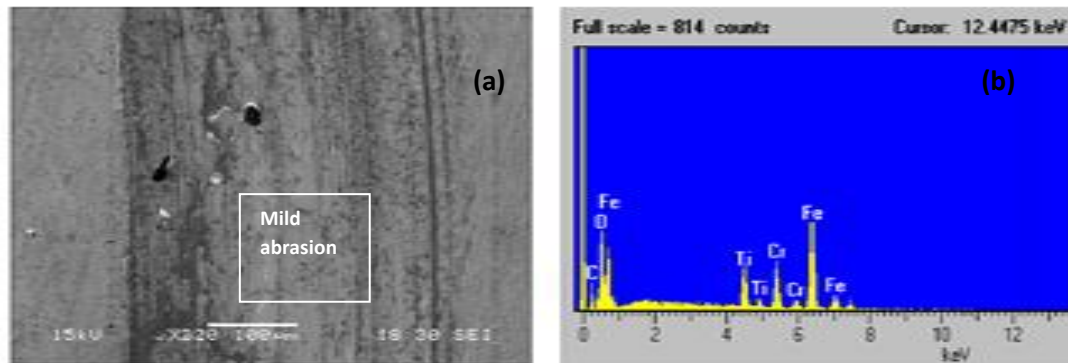


Figure 88 303SS base TiC coatings against alumina, (a) SEM micrograph of the worn surface and (b) EDX analysis of the worn surface; at 7 cm s^{-1} and 10 N.

Fig. 89 shows the SEM micrograph, and EDX analysis of the worn surface at sliding speed 15 cm s^{-1} and normal load 6 N.

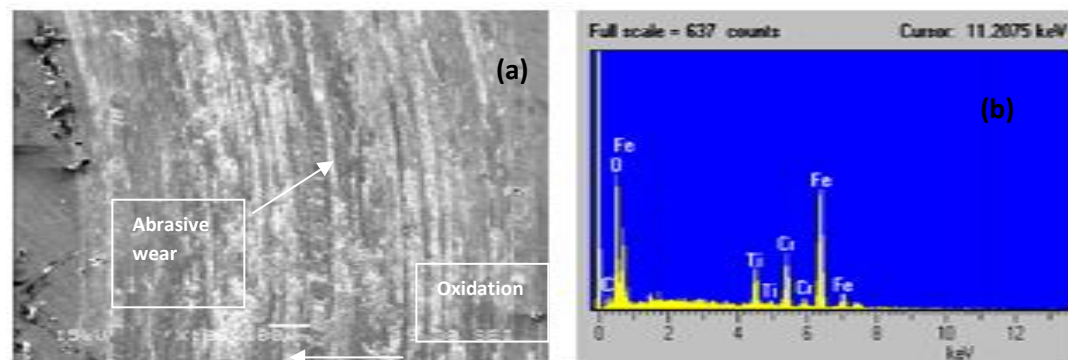


Figure 89 303SS base TiC coatings against alumina, (a) SEM micrograph of the worn surface and (b) EDX analysis of the worn surface; at 15 cm s^{-1} and 6 N.

Tribo-corrosion maps for steels, titanium and titanium carbide materials

Fig. 90 shows the SEM micrograph, and EDX analysis of the worn surface at sliding speed 11cm s^{-1} and normal load 8 N.

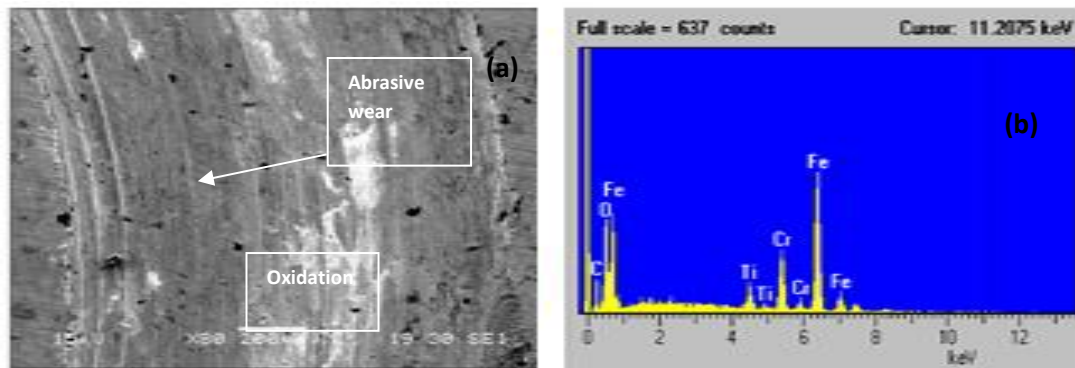


Figure 90 303SS base TiC coatings against alumina, (a) SEM micrograph of the worn surface and (b) EDX analysis of the worn surface; at 11cm s^{-1} and 8N.

Fig. 91 shows the SEM micrograph, and EDX analysis of the worn surface at sliding speed 7cm s^{-1} and normal load 8 N.

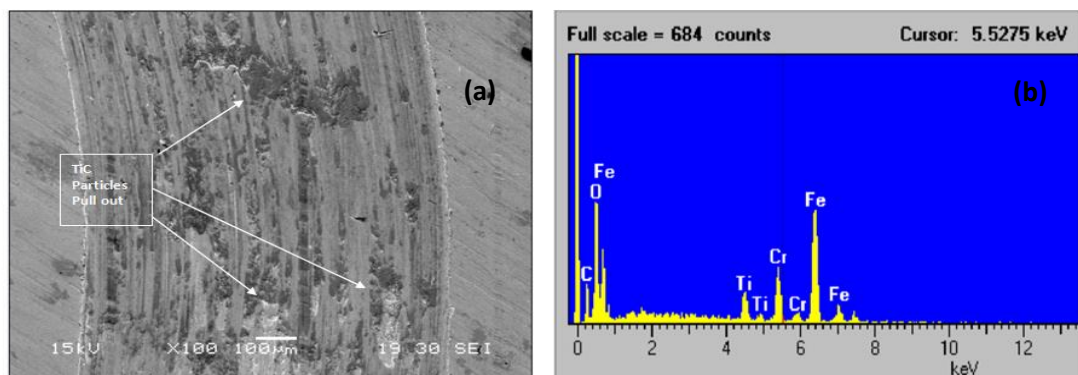


Figure 91 303SS base TiC coatings against alumina, (a) SEM micrograph of the worn surface and (b) EDX analysis of the worn surface; at 7cm s^{-1} and 8N.

5.3.8 Wear behaviour of 303SS base TiC composite coatings against alumina

Most of the tests completed constant sliding distance, which was 500 m, due to low wear rate and friction force at the mating surfaces of 303SS base TiC coatings disks and alumina balls Tables 25-28 and Figs. 76-83. At sliding speed 3cm s^{-1} for the range of normal loads very mild wear rate found due to the very light abrasion and oxidation of the wear tracks Table 25 and Figs. 77, 86-87.

At sliding speed 7cm s^{-1} and normal loads 2 to 6 N very mild wear was found due to very light abrasive mark and oxidation on the wear track. At 8 & 10 N mild wear were found due to mild abrasive and oxidation of wear tracks Table 26 and Figs. 79, 88.

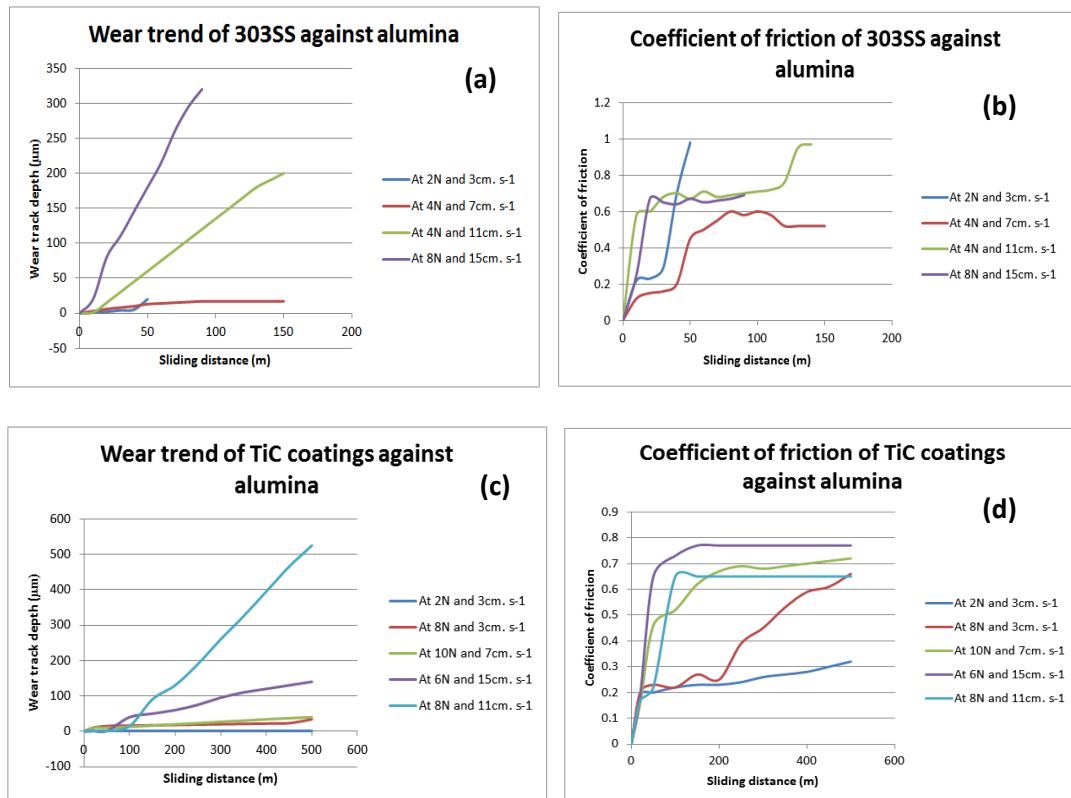
Tribo-corrosion maps for steels, titanium and titanium carbide materials

At sliding speed 11 cm s^{-1} and normal loads 2 to 6 N mild wear was found due to plastic deformation and oxidation on the wear track. At 8 & 10 N medium wear was found due to increased wear rate, ploughing grooves and oxidative wear Fig. 90. From mild wear to medium wear mode transitions occurred between normal load 6 and 8 N at this speed Table 27 and Fig. 81. At sliding speed 15 cm s^{-1} , the same wear behaviour was found for the range of normal loads as that of 11 cm s^{-1} Table 28 and Figs. 83, 89.

5.4. Dry sliding wear behaviour of 303SS (uncoated and coated with TiC) against alumina

5.4.1 Wear trend and coefficient of friction of 303SS (uncoated and coated with TiC) against alumina

Fig. 92 shows the wear trends and coefficient of frictions for 303SS (uncoated and coated with TiC) against alumina on separated XL data plots for various sliding speeds and normal loads combinations. Figs. 92(a, c) show the wear trends and Figs. 92(b, d) show the comparison of coefficient of frictions versus sliding distance of the substrate and of the coatings respectively. Figs. 92(e-f) show the comparison between coefficient frictions versus normal loads at various constant sliding speeds for the range of normal loads.



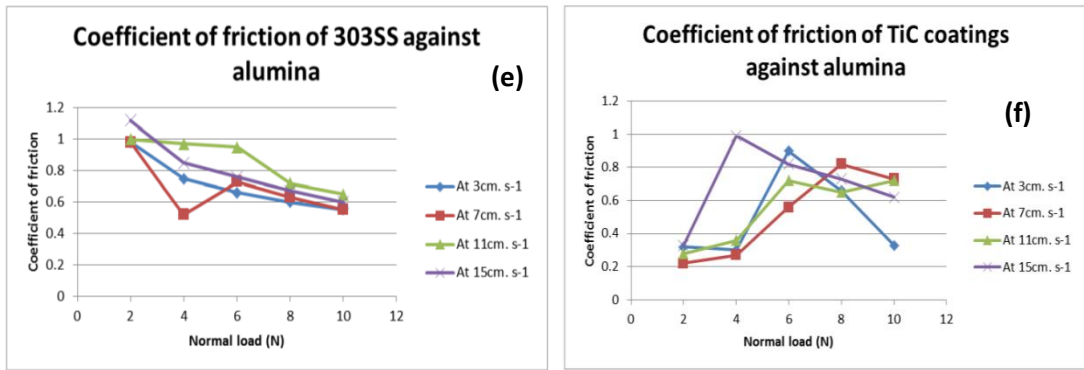


Figure 92 Wear trends and coefficient of friction comparison of 303 stainless steel and TiC coatings against alumina, (a) wear trend of 303SS against alumina, (b) coefficient of friction of 303SS against alumina, (c) wear trend of TiC coatings against alumina, (d) coefficient of friction of TiC coatings against alumina, (e) coefficient of friction of 303SS against alumina for the range of normal loads and sliding speeds and (f) coefficient of friction of TiC coatings against alumina for the range of normal loads and sliding speeds

5.4.2. Wear rate comparison of 303SS (uncoated and coated with TiC) against alumina at 3 cm s⁻¹

Table 31 shows the wear rate comparison of 303SS (uncoated and coated with TiC) against alumina at sliding speed 3 cm s⁻¹ for the range of normal loads.

Normal loads (N)	Wear rate 303SS (g m ⁻¹) x 10 ⁻⁷ at 3cm s ⁻¹	Wear rate of 303SS base TiC coatings (g m ⁻¹) x10 ⁻⁷ at 3cm s ⁻¹
2	93	2
4	44	17
6	178	6
8	288	6
10	394	8.5

Table 31 Wear rate of 303SS and 303SS base TiC coatings disks against alumina balls.

Fig. 93 shows the wear rate data plot of 303SS (uncoated and coated with TiC) against alumina at sliding speed 3 cm s⁻¹ for the range of normal loads.

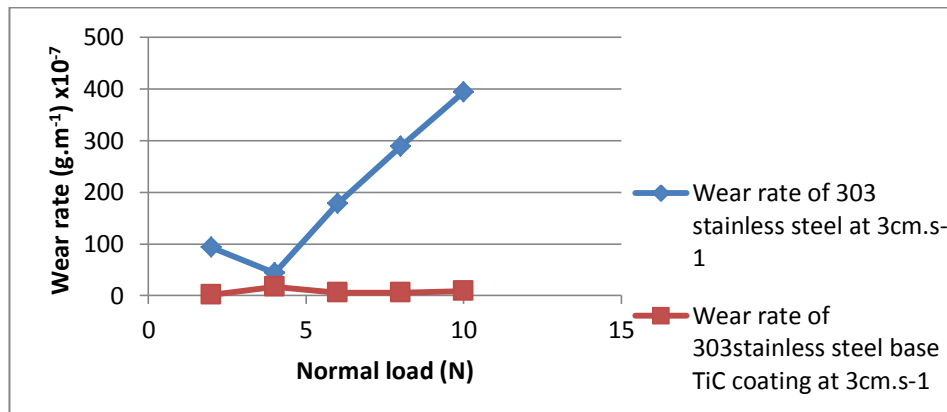


Figure 93 Wear rate of 303SS and 303SS base TiC coatings disks against alumina balls.

5.4.3. Wear rate comparison of 303SS (uncoated and coated with TiC) against alumina at 7 cm s⁻¹

Table 32 shows the wear rate comparison of 303SS (uncoated and coated with TiC) against alumina at sliding speed 7 cm s⁻¹ for the range of normal loads.

Normal loads (N)	Wear rate of 303SS (g m ⁻¹) x10 ⁻⁷ at 7cm s ⁻¹	Wear rate of 303SS base TiC coatings (g m ⁻¹) x10 ⁻⁷ at 7cm s ⁻¹
2	219	2
4	83	2
6	495	4
8	422	22
10	1429	20

Table 32 Wear rate of 303SS and 303SS base TiC coatings disks against alumina balls.

Fig. 94 shows the wear rate data plot of 303SS (uncoated and coated with TiC) against alumina at sliding speed 7 cm s⁻¹ for the range of normal loads.

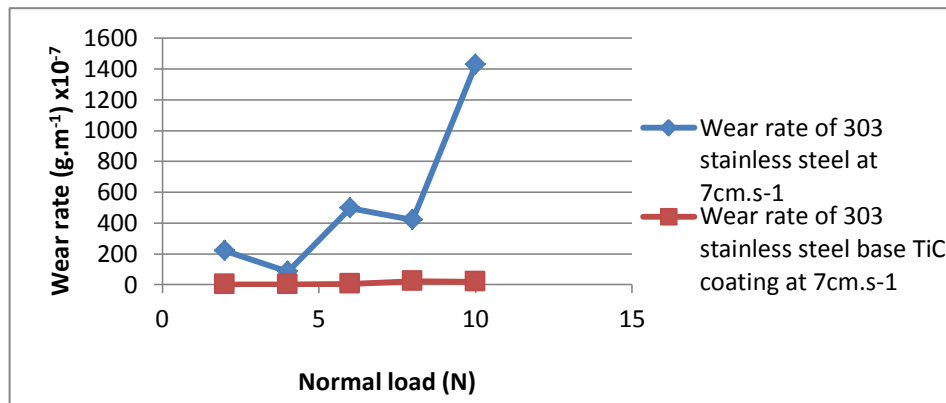


Figure 94 Wear rate of 303SS and 303SS base TiC coatings disks against alumina balls.

5.4.4. Wear rate comparison of 303SS (uncoated and coated with TiC) against alumina at 11 cm s⁻¹

Table 33 shows the wear rate data plot of 303SS (uncoated and coated with TiC) against alumina at sliding speed 11 cm s⁻¹ for the range of normal loads.

Normal loads (N)	Wear rate of 303SS (g m ⁻¹) x10 ⁻⁷ at 11cm s ⁻¹	Wear rate of 303SS base TiC coatings (g m ⁻¹) x10 ⁻⁷ at 11cm s ⁻¹
2	63	45
4	167	32
6	186	47
8	259	96
10	342	96

Table 33 Wear rate of 303SS and 303SS base TiC coatings disks against alumina balls.

Fig. 5.34 shows the wear rate data plot of 303SS (uncoated and coated with TiC) against alumina at sliding speed 11 cm s^{-1} for the range of normal loads.

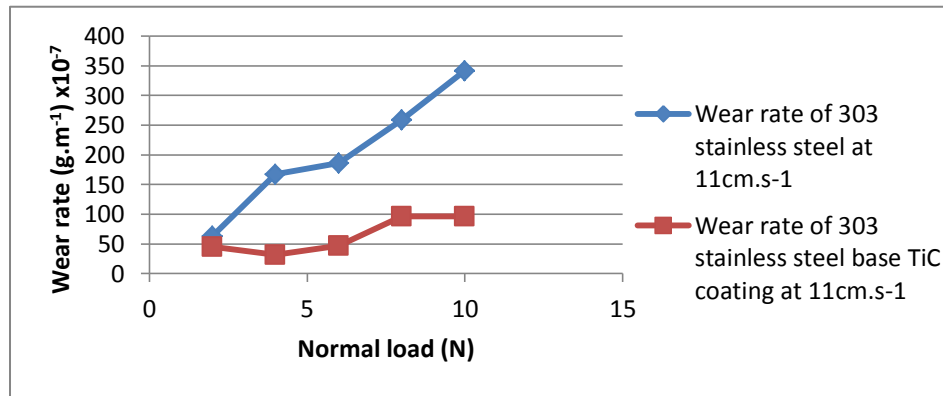


Figure 95 Wear rate of 303SS and 303SS base TiC coatings disks against alumina balls.

5.4.5. Wear rate comparison of 303SS (uncoated and coated with TiC) against alumina at 15 cm s^{-1}

Table 34 shows the wear rate of 303SS (uncoated and coated with TiC) against alumina at sliding speed 15 cm s^{-1} for the range of normal loads.

Normal loads (N)	Wear rate of 303SS (g m^{-1}) $\times 10^{-7}$ at 15 cm s^{-1}	Wear rate of 303SS base TiC coatings (g m^{-1}) $\times 10^{-7}$ at 15 cm s^{-1}
2	93	78
4	174	68
6	160	76
8	275	132
10	599	110

Table 34 Wear rate of 303SS and 303SS base TiC coatings disks against alumina balls.

Fig. 96 shows the wear rate data plot of 303SS (uncoated and coated with TiC) against alumina at sliding speed 15 cm s^{-1} for the range of normal loads.

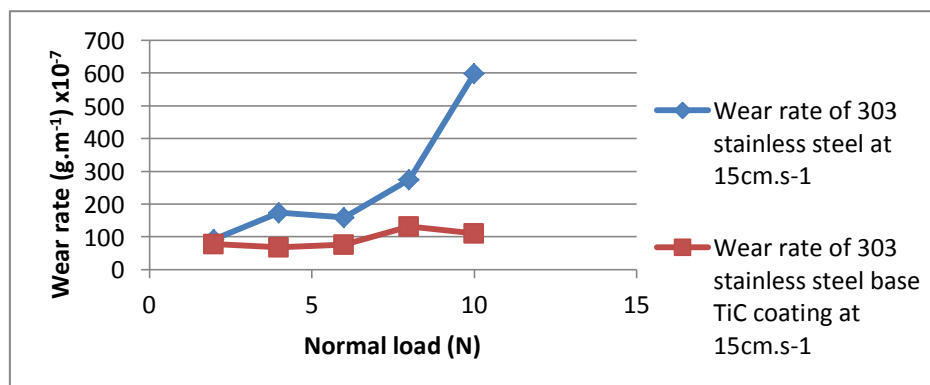


Figure 96 Wear rate of 303SS and 303SS base TiC coatings disks against alumina balls.

5.4.6 Total mass loss comparison of 303SS uncoated and coated against alumina

For each test, different disk was used for a combination of sliding speed and normal load for 500 m sliding distance. Five tests were carried out for each constant speed at variable loads from 2 to 10 N, and increasing in 2 N increments. The table 35 shows the total mass loss of the 303SS and 303SS base TiC coatings disks against alumina balls at each constant sliding speed for the range of normal loads for the total sliding distance 2,500 m. Wear resistance of the 303SS substrate is increased by over 7 times because of surface composite coatings.

Sliding speed (cm s ⁻¹)	Total mass loss (g) of 303stainless steel uncoated disks	Total mass loss (g) of 303stainless steel base TiC coating disks
3	0.05	0.002
7	0.132	0.003
11	0.051	0.016
15	0.065	0.023

Table 35 The total mass loss of 303SS and 303SS base TiC coatings against alumina.

Fig. 97 shows the data plot of total mass loss comparison of 303SS and 303SS base TiC coating against alumina at various constant sliding speeds for 2 to 10N normal loads.

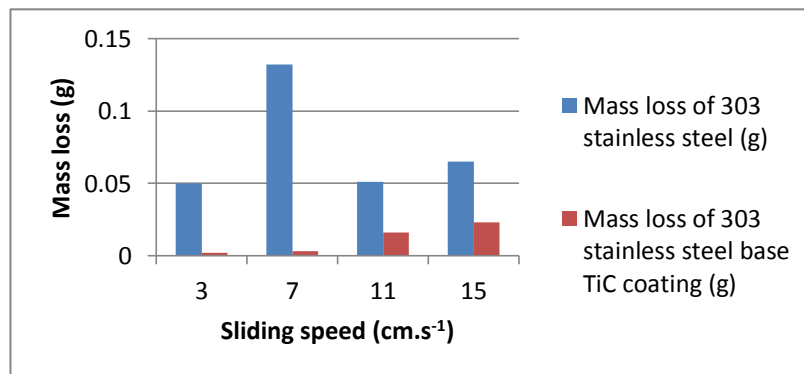


Figure 97 Total mass loss comparison of 303SS and 303SS base TiC coatings against alumina.

5.4.7. Optical micrograph of 303SS base TiC composite coatings worn surfaces against alumina

Fig. 98 shows the cross-sectional optical micrograph of the worn surfaces of 303SS base TiC coating against alumina for various combination of sliding speeds and normal loads.

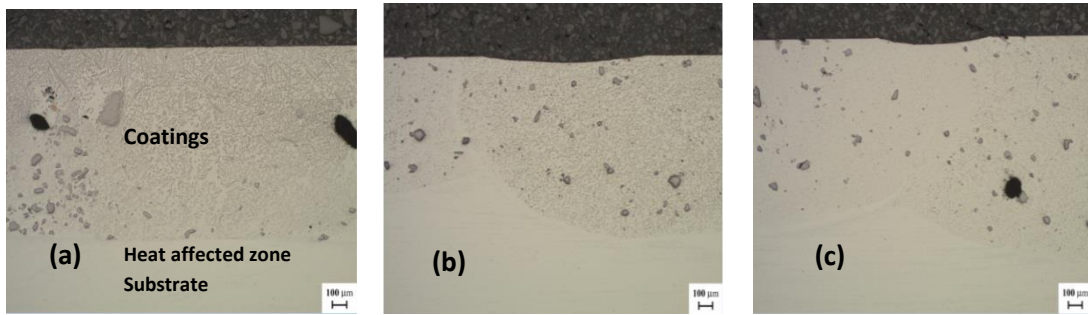


Figure 98 The optical micrograph of the cross-section of the wear tracks of TiC coating against alumina, (a) sliding speed 7 cm s^{-1} and normal load 10 N, (b) 11 cm s^{-1} and 10 N and (c) 15 cm s^{-1} and 10 N.

5.4.8. Sliding wear comparison of 303SS (uncoated and coated with TiC composite coatings) against alumina

For the uncoated 303SS, generally for the range of sliding speeds and normal loads higher wear rate was found Tables 23-24 and Figs. 70-71, 92(a) and all tests were terminated without completing constant sliding distance Figs. 62, 64, 66, 68, 92(a); worn surfaces showed evidence of adhesion, plastic deformation and abrasion with delamination evident on the wear tracks Figs. 72-75, and higher wear rate and mass loss occurred as compare to the wear rate and mass loss of TiC coatings Figs. 93-97. Mild wear observed due to oxidation of the wear tracks Figs. 72(a)-75(a). It was interesting that there were observed peaks in the wear rate with increases in applied load and sliding speed, indicative of transitions in wear regimes, Figs. 70-71, 92(a). EDX analysis, Figs. 72(b)-75(b), indicate traces of oxidation on the surfaces, suggesting that oxidation was influencing the wear in these conditions. The coefficient of friction was unstable for all combination of sliding speeds and normal loads during the course of tests Figs. 62, 64, 66, 68, 92(b).

On the contrary for the 303SS base TiC composite coatings, at lower sliding speeds and normal loads there was very mild wear rate Tables 29-30, significantly less degradation on the surfaces, with only very mild abrasive marks evident on the wear track and only minor evidence of abrasion and oxidation of the wear tracks Figs. 86-88. At higher loads, there was evidence of oxidation on the surface and this was confirmed by EDX analysis Figs. 89-91 and by the stability of the coefficient of friction Fig. 92(d). The effects of increase in normal load and sliding speed on the wear rate trends indicated transitions in wear regimes, Figs. 84-85, with the wear rates peaking at intermediate loads. A comparison between the mass loss data for the coated and uncoated steel indicated little difference at lower loads, but change in mechanism as the load increased, with a sharp rise in wear rate for the uncoated

Tribo-corrosion maps for steels, titanium and titanium carbide materials

material Figs. 93-97. Optical microscopy of the cross-section of the worn surfaces, Fig. 98 shows the stages in deformation of the coating surface with increments in sliding speed, with significant deformation at higher speeds.

5.5. Discussion

5.5.1. Wear mechanisms of 303SS (uncoated and coated with TiC composite coatings) against alumina

During the dry sliding wear tests of 303SS against alumina, it is clear from Tables 19-22 and Figs. 62, 64, 66, 68 that no test completed its total sliding distance i.e. 500 m. The termination of the each test occurred because of the high wear rates and high coefficient of frictions Figs. 92(a-b). This observation is in consistent with the work of other author found in the literature [166]. The hardness of 303SS is significantly lower compared to that of its counterpace alumina, therefore 303SS exhibited very poor wear resistance against alumina during dry sliding wear under ambient conditions, resulting in high wear rates for the range of sliding speed and normal load tested Table 23. Similar phenomena is observed in literature for the dry sliding wear behaviour of group of composite materials based on alumina short fibre reinforced Al-Si alloy against steel. As found in this case the abrupt wear rate occurred when un-reinforced Al-Si was tested against steel [167].

The 303SS disks against alumina show the increase in wear rate with the increase in normal loads Fig.70 due to changes in mechanical stresses and temperature between mating surfaces. Fig. 71 shows the wear rate of 303SS against alumina remains almost same for the range of sliding speeds. This is attributed to the strong tendency of 303SS (high alloy steel) to adhere to other metals, ceramics and work hardened during dry sliding. A material transfer event is treated as depending on interface separation and junction adhesion. The amount of material transferred varied for each combination of sliding speed and normal load. The time taken to reach the steady conditions is inversely proportional to the normal load. At steady state the material transfer from the soft metals to its hard counterpart is equal to the wear rate. M. Kerridge observed this in his experiment where annealed steel pin was rubbed against a hardened steel ring [42]. During dry sliding, material transfer occurs due to adhesion or bonding at the asperity contacts at the mating surfaces. These contacts are sheared by sliding, which may result in detachment of a fragment from one surface and attachment to the other surface. The transferred 303SS formed a mechanical layer on the contact surface of the alumina ball. As the sliding continues, the transferred

Tribo-corrosion maps for steels, titanium and titanium carbide materials

fragments come off the surface on which they are transferred and form loose wear particles. Subsequently, further sliding occurred between the similar material i.e. 303SS substrate at steady state under severe wear conditions [71].

On the other hand during the dry sliding wear tests of the 303SS base TiC coating against alumina, almost all tests completed total sliding distance Tables 25-28 and Figs. 76, 78, 80, 82. Due to the presence of the TiC coating, the surface hardness of the substrate was increased, thereby enhancing the sliding wear resistance of the substrate significantly, which resulted in a substantial decrease in the wear rates and stable coefficient of frictions of the substrate against alumina Table 29 and Figs. 84, 92(c-d) [168].

The wear rates comparison of substrate and TiC coatings, Tables 31-34 and Figs. 93-96, show the wear rates of coatings are very low compared to that of the uncoated material. Hence, the wear resistance of the substrate was improved significantly due to the TiC composite coatings [14], resulted in a new wear mode regime i.e. very mild wear at the lower sliding speed. SEM micrographs and EDX analysis of the wear tracks Figs. 86-91, 98 are evident of the presence of TiC coatings on the worn surfaces of the 303SS base TiC coatings disks after the tests carried out. This suggest that the coatings were chemically and physically stable under dry sliding conditions.

The total mass loss comparison between substrate and TiC coatings against alumina ball show a significant increase in wear resistance due to coatings Fig. 97, [55]. The sliding wear tests results show the relative wear resistance of the TiC composite coatings is significantly higher than that of substrate Figs. 93-96, which result in different wear rate, wear modes and wear mechanisms of uncoated and coated materials. Similar findings are available in the case of wear of TiC-coated carbide tools in dry turning for flank and crater in the literature [65].

Tables 29-30 and Figs. 84-85 show the increase in the wear rates of TiC coating against alumina with the increase in sliding speed and normal load. This increase in wear rates occurred due to the thermal softening effects of frictional heat, which increased with the increase in sliding speed and normal load at interface. The increase in wear rates with the increase in sliding speed and normal load are also found in literature in the other studies i.e. for TiN coating against high speed steel at 0.7 m s^{-1} [171], PVD-TiAlN coated carbide [75], plasma sprayed TiC-NiCrBSi coatings [161], under dry sliding wear behaviour of TiC

Tribo-corrosion maps for steels, titanium and titanium carbide materials

welding clad WC composite coatings [143], friction and wear behaviour of tungsten and titanium carbide coatings [55] and for other titanium coatings [172].

It is interesting that the 303SS and 303SS base TiC coated disks exhibited a substantial amount of one-way transfer of material from disk to ball. This material transfer resulted in a smoothing of counterface. As a result strong adhesion occurred between the transferred material on alumina balls and the surface of the disks, resulted in back transfer, mutual transfer, production of a mechanically mixed layer and finally waste as loose wear fragments [166]. This type of material transfer was also observed in the case of HSS base TiN-coated disk against HSS pin [74].

The coefficient of friction for both 303SS uncoated and coated with TiC Figs. 92(b & d) was fluctuating considerably with increase in sliding speed and normal load. Upto normal load 4 N the coefficient of friction of the TiC was about 60% lower than that of the uncoated 303SS against alumina for all sliding speeds. The higher value of the coefficient of friction of the 303SS uncoated was due to adhesion, plastic deformation and abrasive wear by the harder counterpart Fig. 72(a). The higher value of coefficient of friction for TiC at higher load at all sliding speed Fig. 92(f) was because of abrasive wear that results in pulling of TiC particles in few tests from coated surface as well Fig. 91(a). The higher coefficient of friction contributed to higher temperature rise which was presumably responsible for the higher wear rate with increase in sliding speed and normal load Figs. 84-85. The same situation was also found in other studies i.e. for friction and wear behaviour of tungsten and titanium carbide coatings [55]. The coefficient of friction of TiC coating found stable during the course of the tests Fig. 92(d) and this is evident of oxidation of wear tracks.

The results above indicate several transitions in the wear rate versus normal load and sliding velocity. This behaviour was also noted by Hirst and Lancaster in brass [159] and by Saka et al. [160] in steel and was attributed to a competition between strain hardening and thermal softening that might have occurred concomitantly at surface of the material as sliding speed increases [72]. Similarly, it can be postulated that in this case, following transfer of material to the alumina ball, the strain hardening effect dominates at first reducing the wear, but this was counterbalanced by the softening of surface layers as a result of frictional heating and the effects of oxidation.

5.5.2. Wear regimes and maps

Fig. 99 shows the wear mode maps of 303SS uncoated and coated against alumina and the boundaries on the diagrams are only approximate. The wear mode regimes are classified on the basis of wear rates Table 3 & 5, our previous work and in consistent with the research work found in literature [34, 72]; then these are correlated with wear mechanistic regimes:

a-1) Very mild wear $< [20 \times 10^{-7} \text{ (g m}^{-1}\text{)}]$

a) $[20 \times 10^{-7} \text{ (g m}^{-1}\text{)}] = \text{mild wear} \leq [91 \times 10^{-7} \text{ (g m}^{-1}\text{)}]$

b) $[91 \times 10^{-7} \text{ (g m}^{-1}\text{)}] < \text{medium wear} \leq [274 \times 10^{-7} \text{ (g m}^{-1}\text{)}]$

c) Severe wear $> [274 \times 10^{-7} \text{ (g m}^{-1}\text{)}]$

5.5.3. Wear mode maps

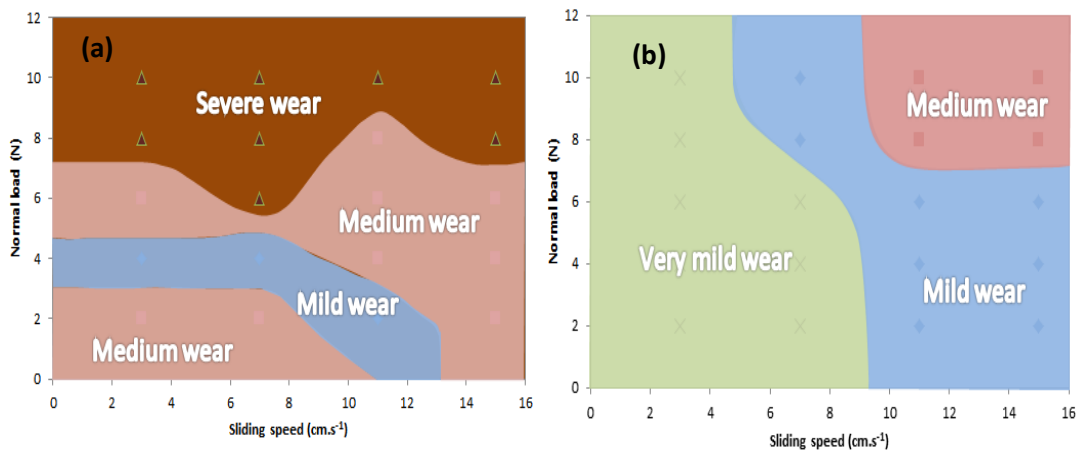


Figure 99 Wear mode map, (a) 303SS against alumina and (b) 303SS base TiC coating against alumina.

In Fig. 99(a), the wear mode map of 303SS against alumina shows that the severe wear is more prevalent at all sliding speeds and at relatively high normal loads. In the case of the 303SS base TiC coating against alumina Fig. 99(b), mild wear is prevalent for the range of sliding speeds and normal loads. It is clear that due to the presence of the coatings, the mild wear regime is expanded to a higher range of sliding speeds and normal loads with an additional wear mode i.e. very mild wear and with an elimination of the severe wear mode, a similar scenario is found in the case of wear of metal matrix composite [73]. Moreover, in Fig. 99(a-b), the combination of the very mild and mild wear zone can be regarded as the safe operation zone for the uncoated and coated steels against alumina respectively [65].

5.5.4. Wear mechanism maps

Wear mechanism maps are useful tools for analysing the change in wear regime over a multi-parameter space. The wear mechanism regimes below are based on the wear rate, physical observations, SEM micrographs and EDX analysis of the worn surfaces. For 303SS against alumina, Fig. 100(a), these can be summarized as:

- Adhesive wear
- Adhesive - oxidative wear
- Oxidative-adhesive wear
- Oxidative- abrasive wear

The maps for the coated and uncoated steel exhibit significant transitions with similar regimes in the low load – sliding speed window but adhesive wear predominating the maps for steel at higher normal loads and sliding speeds, Fig. 100(a), with oxidative and deformation mechanisms predominating the wear mode at intermediate normal loads and high sliding speeds.

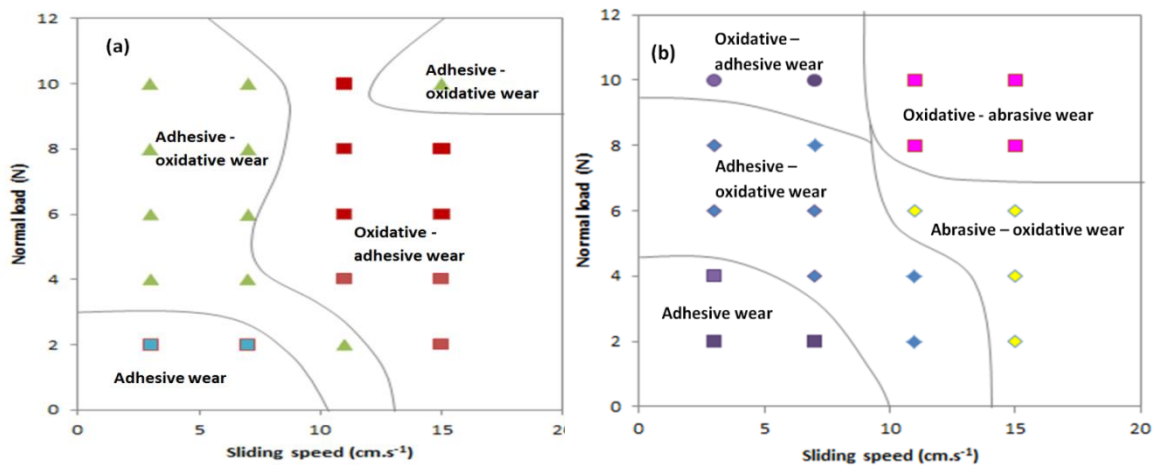


Figure 100 The wear mechanism map, (a) 303SS against alumina and (b) 303SS base TiC coating against alumina.

5.5.5. Wear mechanisms and regimes for 303SS base TiC coatings

For the TiC coatings, Fig. 100(b), the wear regimes suggested are as follows:

- Abrasive wear
- Adhesive –oxidative wear
- Oxidative- adhesive wear
- Abrasive-oxidative wear
- Oxidative- abrasive wear

Figs. 100(a-b), indicate very different wear maps configurations for both materials. With ploughing and oxidation predominates the wear map at higher loads and speeds, and very little evidence of abrasive wear for the coating, which indicates that in this window of conditions, the coatings provides resistance to the environment. In particular, adhesion dominates the upper part of the map for the steel, with some oxidation affected areas apparent, whereas for the more wear resistant coatings, this window of conditions is characterized by oxidative wear mechanisms. Clearly, the transitions between the regimes are identified through SEM analysis of surface morphologies and therefore are a relatively arbitrary method of defining regime transitions; however, the extent of oxidation and thus oxidative wear are much higher for the steel, Fig. 100(a) compared to the coating, Fig. 100(b), at lower loads. The various transitions at intermediate loads and velocities can be attributed to the competition between oxidation, wear resistance, and extent of frictional heating between both surface and counterface materials.

5.6. Comparison between wear mechanism maps for 303SS sliding against low alloy steel

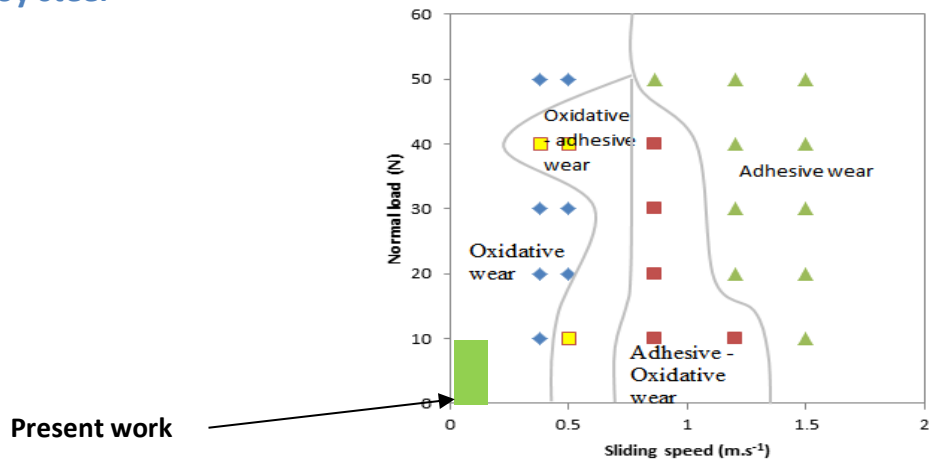


Figure 101 Wear mechanism map for 303 stainless steel disk against 8620 low alloy steel (taken from chapter 4).

Highlighted area on Fig. 101 shows the range of sliding speed and normal load involved in the present study, which can be compared with previous work by the current authors (chapter 4). It is clear from this figure that the wear mechanism of the 303 stainless steel against 8620 low alloy steel is dominated by oxidative wear; while from Fig. 100(a) above, against an alumina counterface, a very different mode is observed i.e. adhesive dominated, and this is possibly due to lower frictional heating in the latter case.

Clearly, the wear maps developed above indicate many possible wear regime transitions between coated and uncoated materials against different counterface materials. Further work will be to investigate the wear mechanisms of coatings of varying such as volume fraction and size to provide a basis for coating optimization in such conditions.

5.7. Conclusions

1. Uncoated 303SS exhibited poor wear resistance which was increased by applying a TiC composite coating. The coating was applied with a TIG welding torch melting process and it substantially increased the wear resistance of the substrate for the tested range of sliding speeds and normal loads.
2. Significant differences in wear regimes were identified for both materials, with more evidence of oxidation for the coated material in these conditions. Adhesive wear was predominated wear mechanisms for the steel, in particular at higher normal loads and sliding speeds. Oxidation wear influenced the wear mechanisms at intermediate normal loads and sliding speeds in each case.
3. Wear maps are indicating many possible wear regimes and significant differences in material degradation mechanisms for the substrate and TiC coatings.
4. The presence of the coatings expanded the mild wear regime to a higher range of sliding speeds and normal loads with an additional wear mode i.e. very mild wear and with an elimination of the severe wear mode.

Chapter 6

Titanium against hardened steel (A.I.S.I. 0-1-Ground Flat Stock) in dry sliding

6.1. Introduction

The purpose of this study is to investigate the wear behaviour of titanium against hard metal with respect to sliding speed and normal load and to develop wear mode and wear mechanistic maps to understand and predict the wear behaviour for the both materials in dry sliding contact under ambient conditions at room temperature. This is the advancement in the work done on Ti against hard metal found in the literature. Moreover, to produce a base line data to investigate the wear behaviour of titanium base titanium carbide coatings produced by TIG process against the same hard metal to compare the wear behaviour of the coatings with respect to substrates and coatings produced other than TIG process.

6.2. Sliding wear tests results

Dry sliding wear tests were carried out on pin-on-disk sliding wear testing rig Fig. 34 for 25 combinations of sliding speeds and normal loads as per experimental conditions mentioned in section 3.5, chapter 3. The sliding distance 5,560m and numbers of revolutions 30,000 were kept constant for all tests. At the end of each sliding tests worn surfaces of the disks and pins and wear debris were examined to investigate the wear mode and wear mechanism regimes. The effects of change in sliding speeds and normal loads on wear behaviour of Ti against hardened steel (A.I.S.I. 0-1-Ground Flat Stock) have been investigated. At the end of test dark and smooth worn surface; lower mass loss and dark grey powdery wear debris were found due to oxidation of mating surfaces which resulted in mild wear. On the other hand bright, rougher worn surfaces and larger metallic wear debris, and high mass loss resulted in medium and severe wear. The dry sliding wear results of Titanium against hardened steels are as below:

6.2.1. Wear rate at 0.38 m s⁻¹ sliding speed for the range of normal loads

Table 36 and Fig. 102 show the wear rate of Ti pins and hardened steel disks against each other at sliding speed 0.38 m s⁻¹ for the range of normal loads.

Normal load (N)	Wear rate of Ti pin ($\text{m}^3 \text{m}^{-1}$) $\times 10^{-12}$ at 0.38 m s^{-1}	Wear rate of hardened steel disk ($\text{m}^3 \text{m}^{-1}$) $\times 10^{-12}$ at 0.38 m s^{-1}
10	2.23	0.64
20	1.63	0.15
30	3.6	0.64
40	6.16	1.70
50	9.88	2.73

Table 36 wear rate of Ti pins and hardened steel disks against each other.

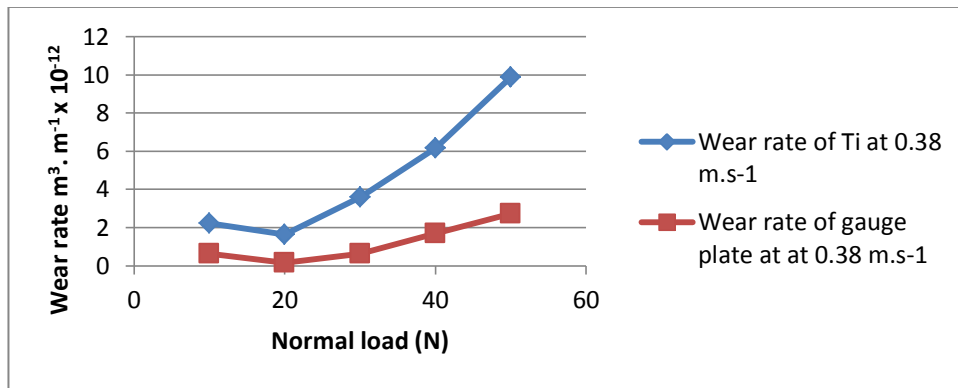


Figure 102 Wear rate of Ti pins and hardened steel disks against each other.

6.2.2. Wear rate at 0.5 m s^{-1} sliding speed for the range of normal loads

Table 37 and Fig. 103 show the wear rate of Ti pins and hardened steel disks against each other at sliding speed 0.5 m s^{-1} for the range of normal loads.

Normal load (N)	Wear rate of Ti pin ($\text{m}^3 \text{m}^{-1}$) $\times 10^{-12}$ at 0.5 m s^{-1}	Wear rate of hardened steel disk ($\text{m}^3 \text{m}^{-1}$) $\times 10^{-12}$ at 0.5 m s^{-1}
10	1.13	0.19
20	1.28	0.15
30	2.60	0.18
40	2.87	0.22
50	4.42	0.73

Table 37 Wear rate of Ti pin and hardened steel disk against each other.

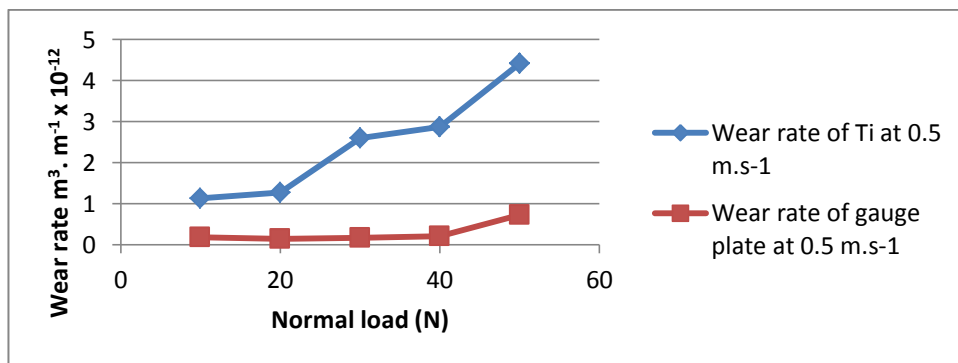


Figure 103 Wear rate of Ti pins and hardened steel disks against each other.

6.2.3. Wear rate at 0.86 m s⁻¹ sliding speed for the range of normal loads

Table 38 and Fig. 104 show the wear rate of Ti pins and hardened steel disks against each other at sliding speed 0.86 m s⁻¹ for the range of normal loads.

Normal load (N)	Wear rate of Ti pin (m ³ m ⁻¹)x 10 ⁻¹² at 0.86 m s ⁻¹	Wear rate of hardened steel disk (m ³ m ⁻¹)x 10 ⁻¹² at 0.86 m s ⁻¹
10	0.75	-0.0051
20	1.25	0.22
30	3.05	0.20
40	4.98	0.21
50	11.92	0.51

Table 38 Wear rate of Ti pin and hardened steel disk against each other.

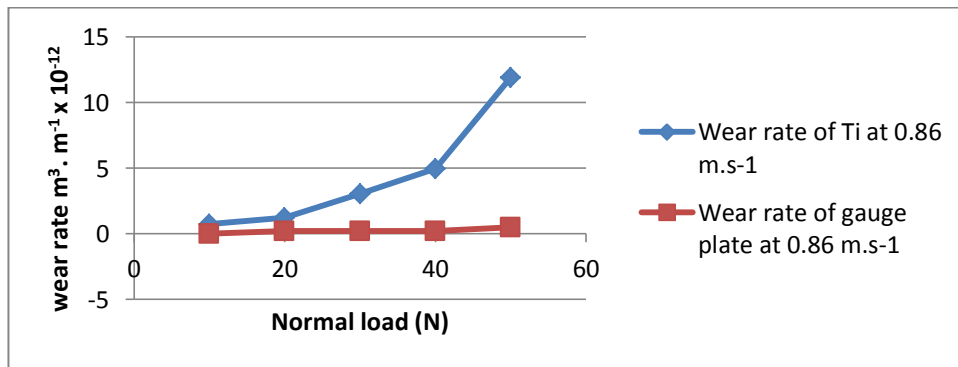


Figure 104 Wear rate of Ti pins and hardened steel disks against each other.

6.2.4. Wear rate at 1.2m s⁻¹ sliding speed for the range of normal loads

Table 39 and Fig. 105 show the wear rate of Ti pins and hardened steel disks against each other at sliding speed 1.2 m s⁻¹ for the range of normal loads.

Normal load (N)	Wear rate of Ti pin (m ³ m ⁻¹)x 10 ⁻¹² at 1.2 m s ⁻¹	Wear rate of hardened steel disk (m ³ m ⁻¹)x 10 ⁻¹² at 1.2 m s ⁻¹
10	0.54	0.005
20	0.88	0.019
30	6.38	0.024
40	8.08	0.027
50	22.36	0.222

Table 39 Wear rate of Ti pin and hardened steel disk against each other.

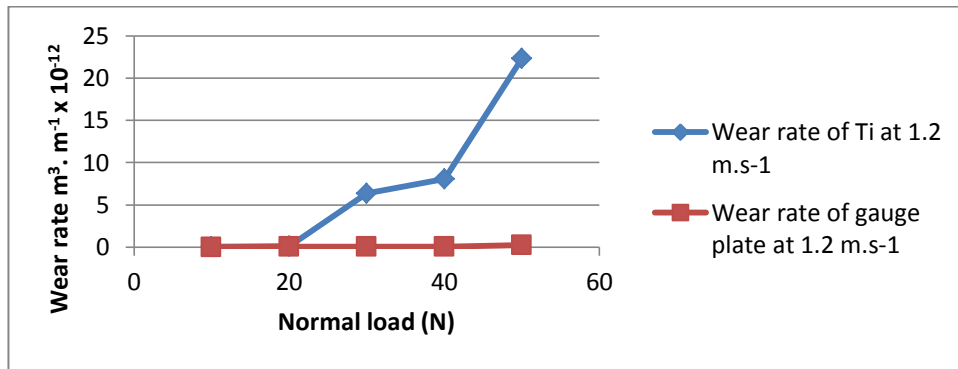


Figure 105 Wear rate of Ti pins and hardened steel disks against each other.

6.2.5. Wear rate at 1.5 m s⁻¹ sliding speed for the range of normal loads

Table 40 and Fig. 106 show the wear rate of Ti pins and hardened steel disks against each other at sliding speed 1.5 m s⁻¹ for the range of normal loads.

Normal load (N)	Wear rate of Ti pin ($\text{m}^3 \text{m}^{-1}$)x 10^{-12} at 1.5 m s ⁻¹	Wear rate of hardened steel disk ($\text{m}^3 \text{m}^{-1}$)x 10^{-12} at 1.5 m s ⁻¹
10	0.76	0.005
20	0.63	0.004
30	6.46	0.10
40	9.25	0.36
50	36.71	0.25

Table 40 Wear rate of Ti pin and hardened steel disk against each other.

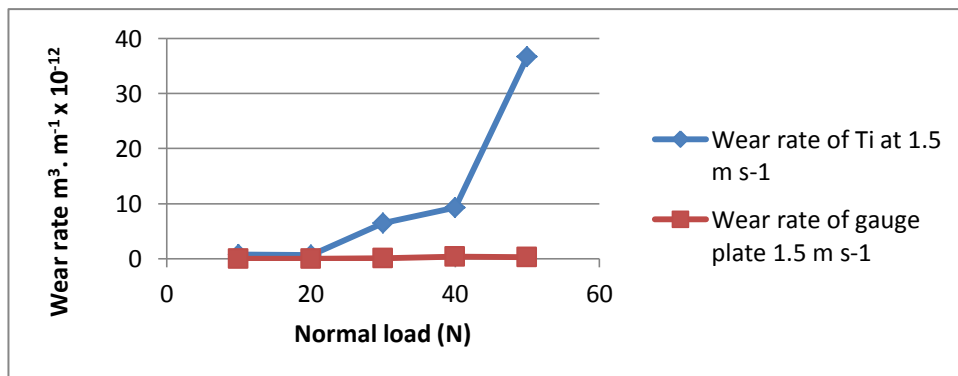


Figure 106 Wear rate of Ti pins and hardened steel disks against each other.

6.2.6. Wear rate of Ti against hardened steel at constant sliding speeds and various normal loads

Table 41 Fig. 107 show the wear rate of Ti pins against hardened steel disks at different constant sliding speed and various normal loads.

Normal load (N)	Wear rate $(\text{m}^3 \text{ m}^{-1}) \times 10^{-12}$ at 0.38 m s^{-1}	Wear rate $(\text{m}^3 \text{ m}^{-1}) \times 10^{-12}$ at 0.5 m s^{-1}	Wear rate $(\text{m}^3 \text{ m}^{-1}) \times 10^{-12}$ at 0.86 m s^{-1}	Wear rate $(\text{m}^3 \text{ m}^{-1}) \times 10^{-12}$ at 1.2 m s^{-1}	Wear rate $(\text{m}^3 \text{ m}^{-1}) \times 10^{-12}$ at 1.5 m s^{-1}
10	2.23	1.13	0.75	0.54	0.76
20	1.63	1.28	1.25	0.88	0.63
30	3.6	2.60	3.05	6.38	6.46
40	6.16	2.87	4.98	8.08	9.25
50	9.88	4.42	11.92	22.36	36.71

Table 41 Wear rate of Ti pins against hardened steel disks.

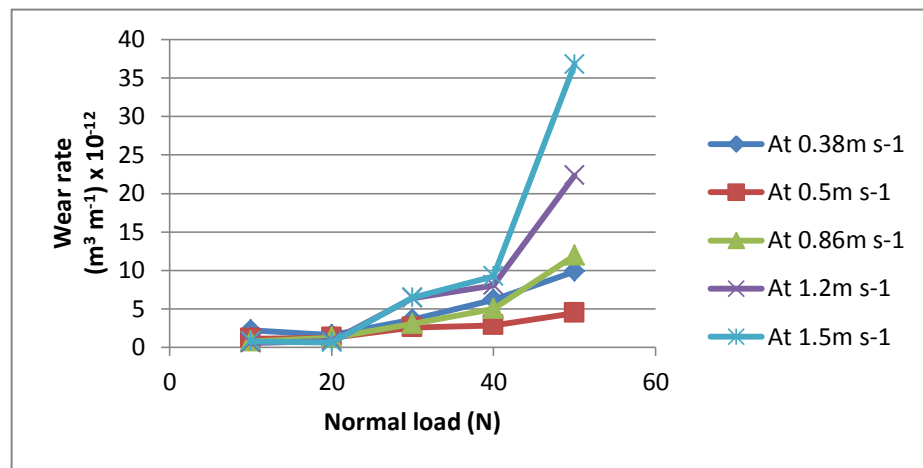


Figure 107 Wear rate of Ti pins against hardened steel disks.

6.2.7. Wear rate of Ti against hardened steel at constant normal loads and various sliding speeds

Table 42 and Fig. 108 show the wear rate of Ti pins against hardened steel at different constant normal loads and various sliding speeds.

Sliding speed (m s^{-1})	Wear rate $(\text{m}^3 \text{ m}^{-1}) \times 10^{-12}$ at 10N	Wear rate $(\text{m}^3 \text{ m}^{-1}) \times 10^{-12}$ at 20N	Wear rate $(\text{m}^3 \text{ m}^{-1}) \times 10^{-12}$ at 30N	Wear rate $(\text{m}^3 \text{ m}^{-1}) \times 10^{-12}$ at 40N	Wear rate $(\text{m}^3 \text{ m}^{-1}) \times 10^{-12}$ at 50N
0.38	2.23	1.63	3.6	6.16	9.88
0.5	1.13	1.28	2.60	2.87	4.42
0.86	0.75	1.25	3.05	4.98	11.92
1.2	0.54	0.88	6.38	8.08	22.38
1.5	0.76	0.63	6.46	9.25	36.71

Table 42 Wear rate of Ti pins against hardened steel disks.

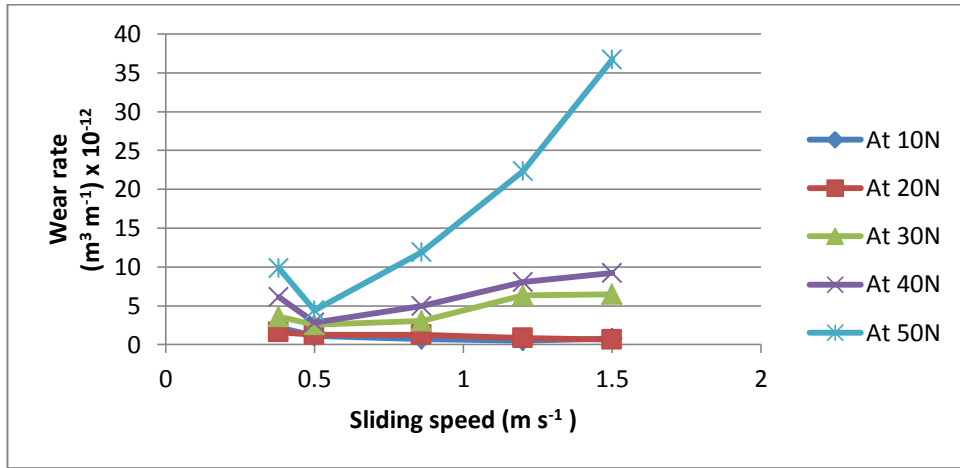


Figure 108 Wear rate of Ti pins against hardened steel disks.

6.2.8. Wear rate of hardened steel against Ti at constant sliding speeds and various normal loads

Table 43 and Fig. 109 show the wear rate of hardened steel disks against Ti pins at different constant sliding speed and various normal loads.

Normal load (N)	Wear rate (m³ m⁻¹) x 10⁻¹² at 0.38 m s⁻¹	Wear rate (m³ m⁻¹) x 10⁻¹² at 0.5 m s⁻¹	Wear rate (m³ m⁻¹) x 10⁻¹² at 0.86 m s⁻¹	Wear rate (m³ m⁻¹) x 10⁻¹² at 1.2 m s⁻¹	Wear rate (m³ m⁻¹) x 10⁻¹² at 1.5 m s⁻¹
10	0.64	0.19	-0.0051	0.005	0.005
20	0.15	0.15	0.22	0.019	0.004
30	0.64	0.18	0.20	0.024	0.10
40	1.70	0.22	0.21	0.027	0.36
50	2.73	0.73	0.51	0.222	0.25

Table 43 Wear rate of hardened steel disks against Ti pins.

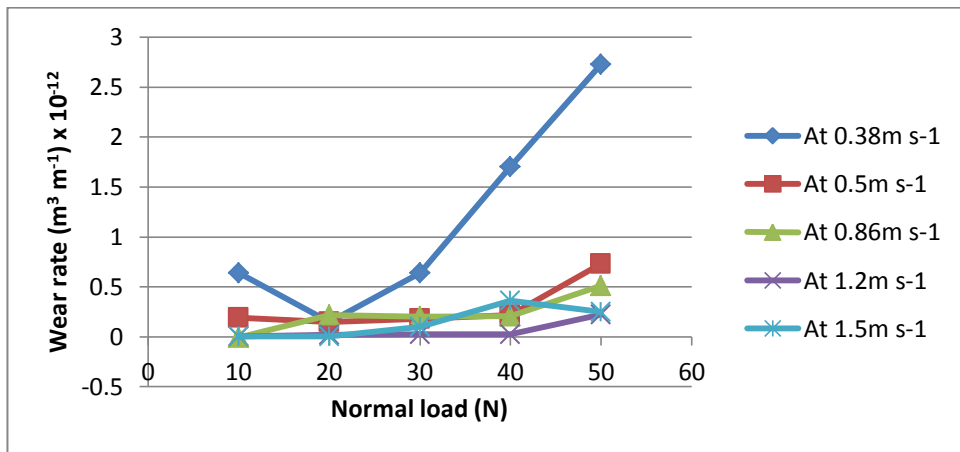


Figure 109 Wear rate of hardened steel disks against Ti pins.

6.2.9. Wear rate of hardened steel against Ti at constant normal loads and various sliding speeds

Table 44 Fig. 110 show the wear rate of hardened steel disks against Ti pins at different constant normal loads and various sliding speeds.

Sliding speed (m s ⁻¹)	Wear rate (m ³ m ⁻¹) x 10 ⁻¹² at 10N	Wear rate (m ³ m ⁻¹) x 10 ⁻¹² at 20N	Wear rate (m ³ m ⁻¹) x 10 ⁻¹² at 30N	Wear rate (m ³ m ⁻¹) x 10 ⁻¹² at 40N	Wear rate (m ³ m ⁻¹)x 10 ⁻¹² at 50N
0.38	0.64	0.15	0.64	1.70	2.73
0.5	0.19	0.15	0.18	0.22	0.73
0.86	-0.0051	0.22	0.20	0.21	0.51
1.2	0.005	0.019	0.024	0.027	0.222
1.5	0.005	0.004	0.10	0.36	0.25

Table 44 Wear rate of hardened steel disks against Ti pins.

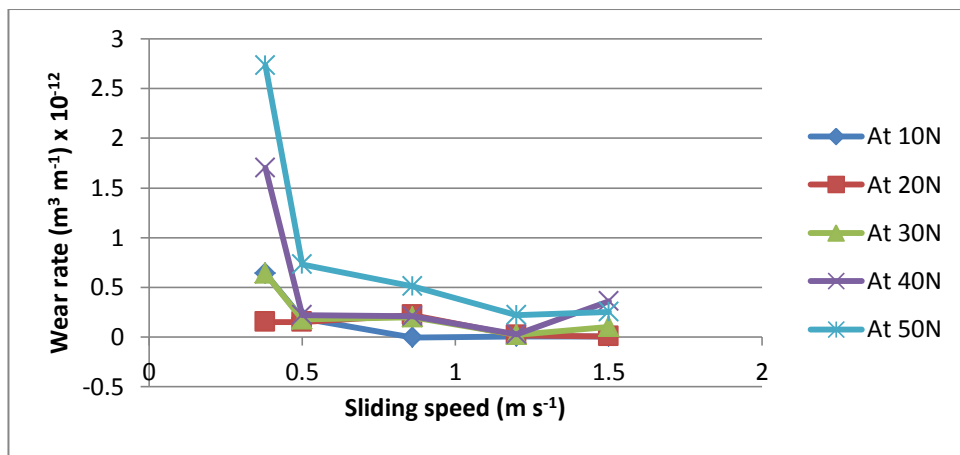


Figure 110 Wear rate of hardened steel disks against Ti pins.

6.2.10. Total mass loss comparison

The table 45 and Fig. 111 show the total mass loss of the Ti pins and hardened steel disks at each constant sliding speed for the range of normal loads i.e. at variable loads from 10 to 50 N, and increasing in 10 N increments for the total sliding distance 27,800 m.

Sliding speed (m s ⁻¹)	Total mass loss of hardened steel disk (g)	Total mass loss of Ti pin (g)
0.38	0.2537	0.5891
0.5	0.0635	0.3083
0.86	0.0477	0.5503
1.2	0.0425	0.959
1.5	0.0348	1.3495

Table 45 The total mass loss of Ti pins and hardened steel disks against each other.

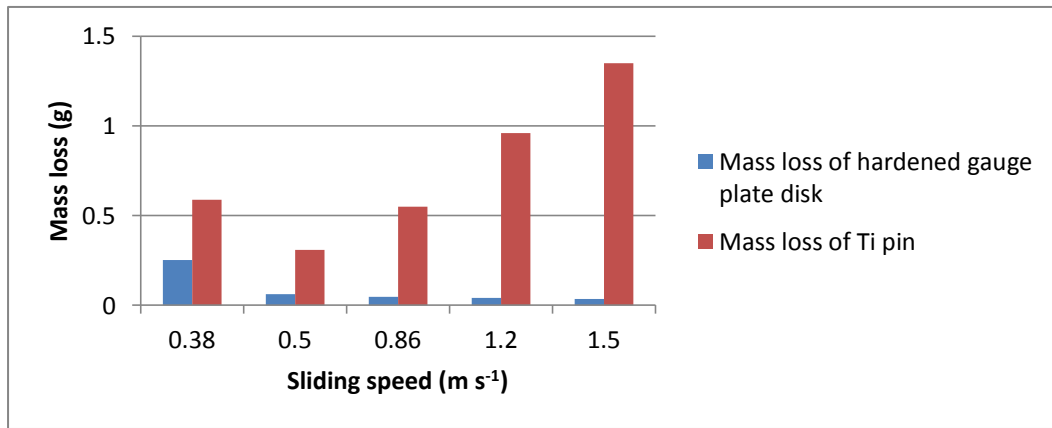


Figure 111 The total mass loss comparison of hardened steel disks and Ti pins.

Tables 36-40 and Figs. 102-106 show the wear resistance of Ti pins is very lower against hardened steel disks. Tables 41-42 and Fig. 107-108 show the wear rate of Ti against hardened steel as function of sliding speed and normal load respectively. Fig. 107 shows that wear rate increased sharply with the increase in applied normal load after 20 N. Fig. 108 shows there are low wear rates up to 20 N normal loads for the range of sliding speeds. Moreover, for each normal load there is a minimum wear rate at an intermediate sliding speed i.e. 0.5 m s^{-1} in this case and with increase in normal load at this sliding speed the minimum become more prominent. It is also observed that the wear rate of Ti is normal load as well as sliding speed dependent as it increased with the increase in normal load and sliding speed and abrupt increase in wear rate is found at the higher normal load Figs. 107-108. Tables 43-44 and Figs. 109-110 show there are higher wear rates of steel against Ti at lower sliding speed. Negative wear rate of hardened steel at sliding speed 0.86 m s^{-1} and normal load 10 N was found due to more pin material transfer rate to disk than that of removal rate as wear products Table 38 and Fig. 104. Table 45 and Fig. 111 show that the total mass loss of Ti is much higher than that of hardened steel. Moreover, the total wear of Ti become prominent with increase in sliding speed and the total wear of hardened steel decrease with increase in sliding speed.

6.2.11. Coefficient of friction of Ti pins against hardened steel disks

Table 46 and Fig. 112 show the trend of friction of Ti pins and hardened steel disks against each other at different constant sliding speeds and various normal loads.

Normal load (N)	Coefficient of friction at 0.38 m s ⁻¹	Coefficient of friction at 0.5 m s ⁻¹	Coefficient of friction at 0.86 m s ⁻¹	Coefficient of friction at 1.2 m s ⁻¹	Coefficient of friction at 1.5 m s ⁻¹
10	0.36	0.26	0.33	0.36	0.41
20	0.22	0.24	0.18	0.25	0.29
30	0.23	0.16	0.28	0.32	0.32
40	0.21	0.30	0.30	0.31	0.30
50	0.24	0.27	0.33	0.26	0.28

Table 46 Coefficient of friction of Ti pins against hardened steel disks.

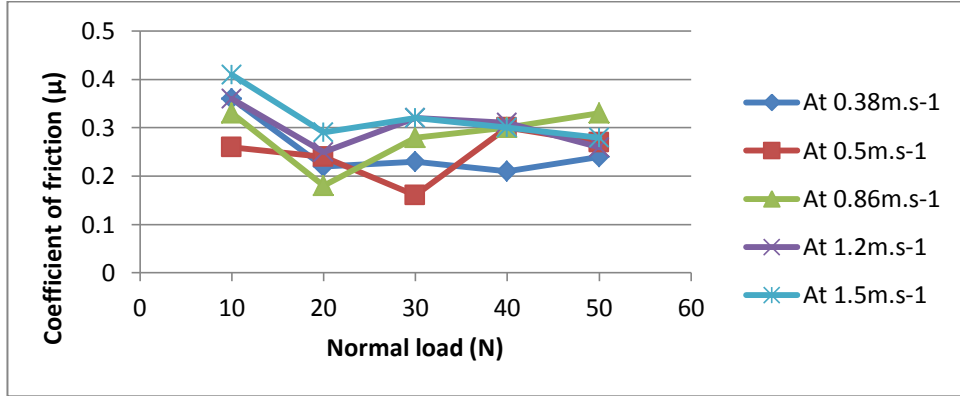


Figure 112 Coefficient of friction of Ti pins against hardened steel disks.

Table 47 and Fig. 113 show the trend of friction of Ti pins and hardened steel disks sliding against each other at different constant normal loads and various sliding speeds.

Sliding speed m s ⁻¹	Coefficient of friction at 10N	Coefficient of friction at 20N	Coefficient of friction at 30N	Coefficient of friction at 40N	Coefficient of friction at 50N
0.38	0.36	0.22	0.23	0.21	0.24
0.5	0.26	0.24	0.16	0.30	0.27
0.86	0.33	0.18	0.28	0.30	0.33
1.2	0.36	0.25	0.32	0.31	0.26
1.5	0.41	0.29	0.32	0.30	0.28

Table 47 Coefficient of friction of Ti pins against hardened steel disks.

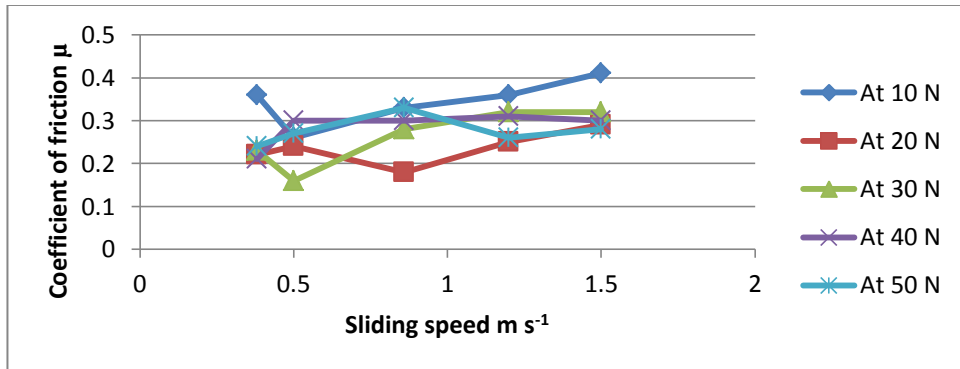
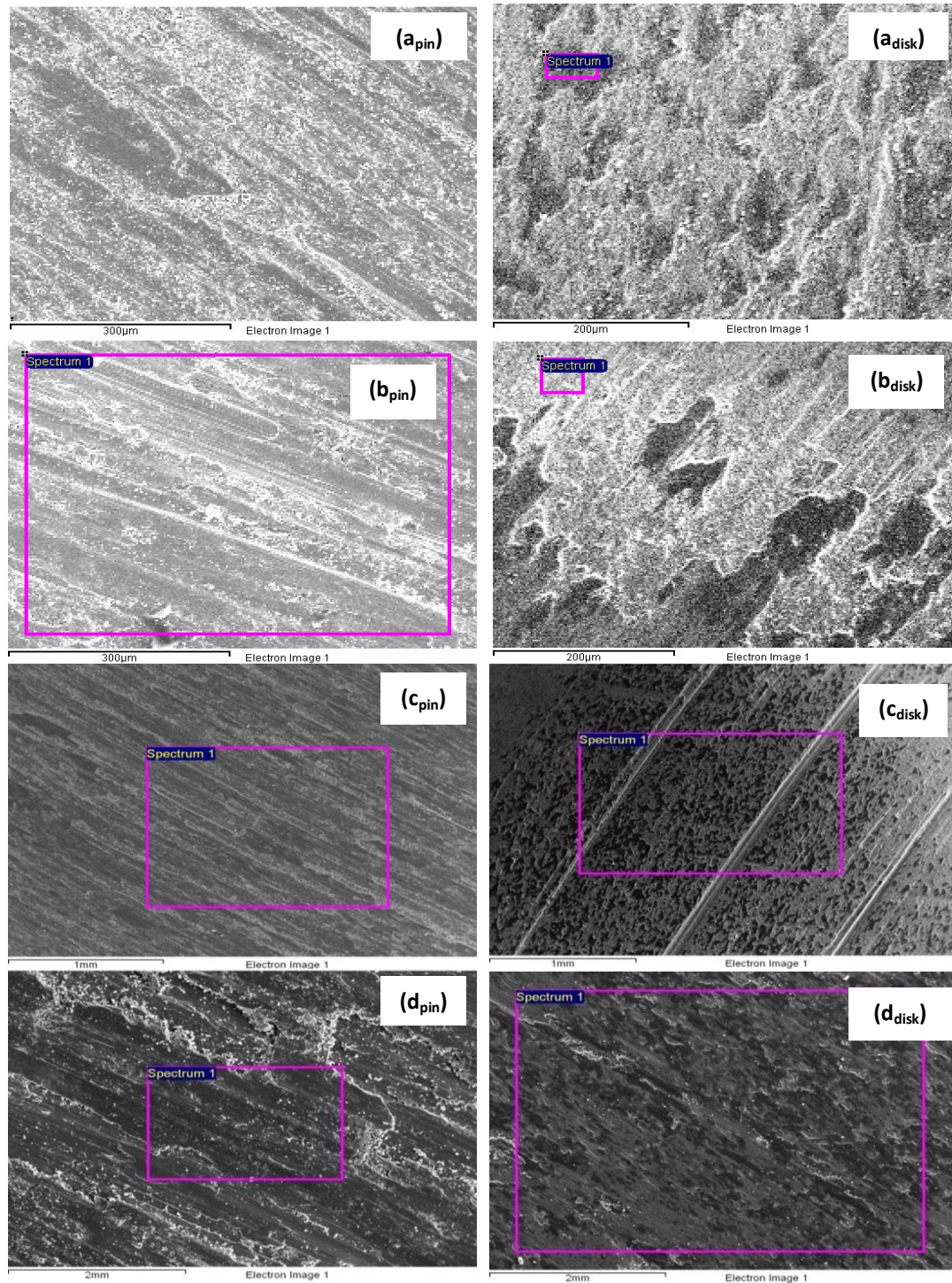


Figure 113 Coefficient of friction of Ti pins against hardened steel disks.

6.2.12. SEM of Ti pins and hardened steel disks against each other

Fig. 114 shows the SEM micrographs of worn surfaces of Ti pins and hardened steel disks. These micrographs have been selected from the 25 combinations of sliding speeds and normal loads on the basis of wear mechanisms observed on the worn surfaces of the pins and disks.



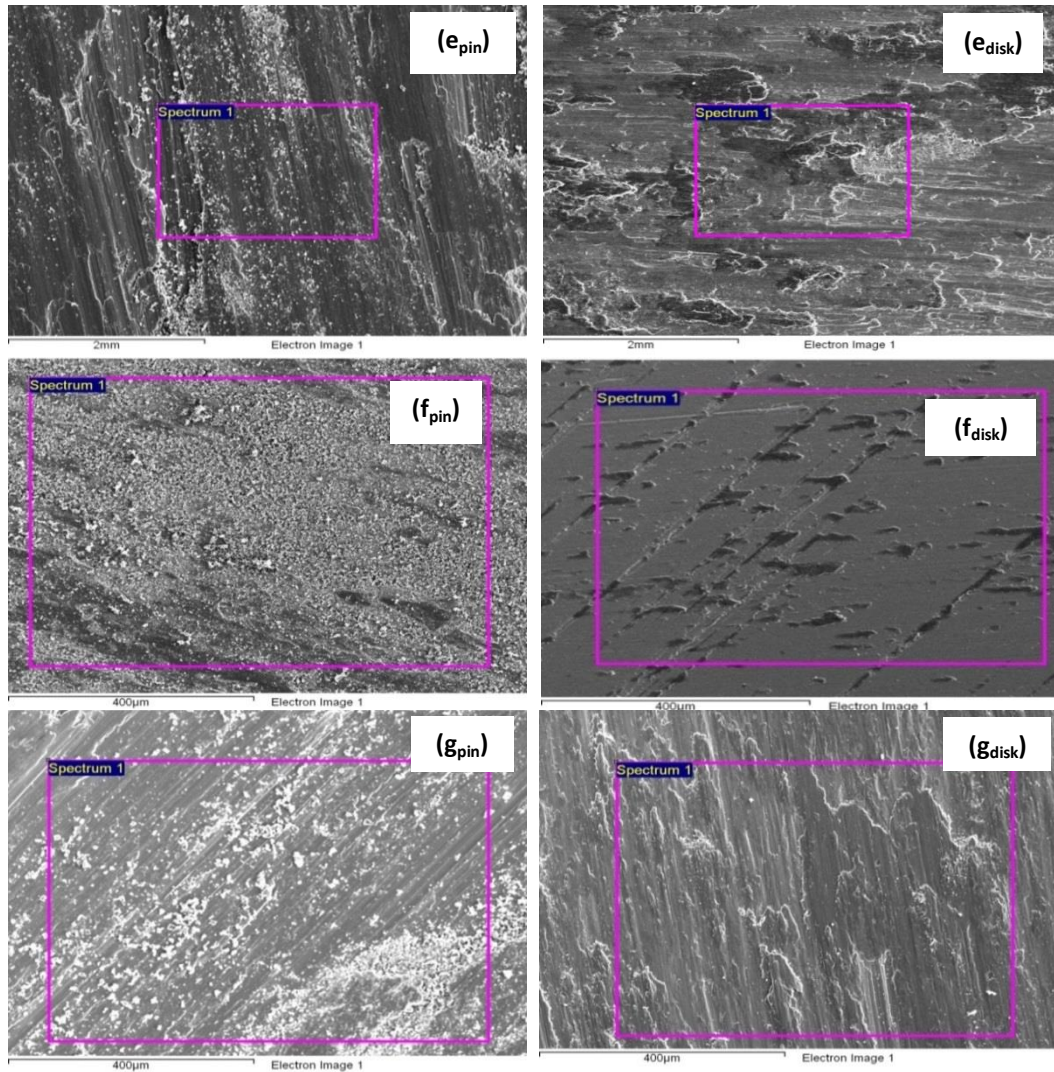
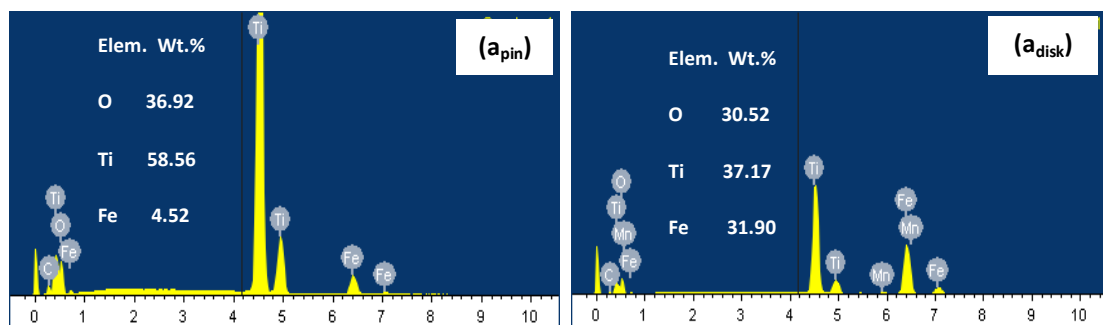


Figure 114 SEM micrographs of the worn surfaces of pins and wear tracks on the disks, (a) at normal load 20N and sliding speed 0.38m s^{-1} , (b) at 40N and 0.38m s^{-1} , (c) at 30N and 0.5m s^{-1} , (d) at 40N and 0.86m s^{-1} , (e) at 50N and 0.86m s^{-1} , (f) at 10N and 1.2m s^{-1} and (g) at 50N and 1.2m s^{-1} .

6.2.13. EDX analysis of Ti pins and hardened steel disks against each other

Fig. 115 shows the EDX analysis of the worn surfaces of Ti pins and hardened steel disks.



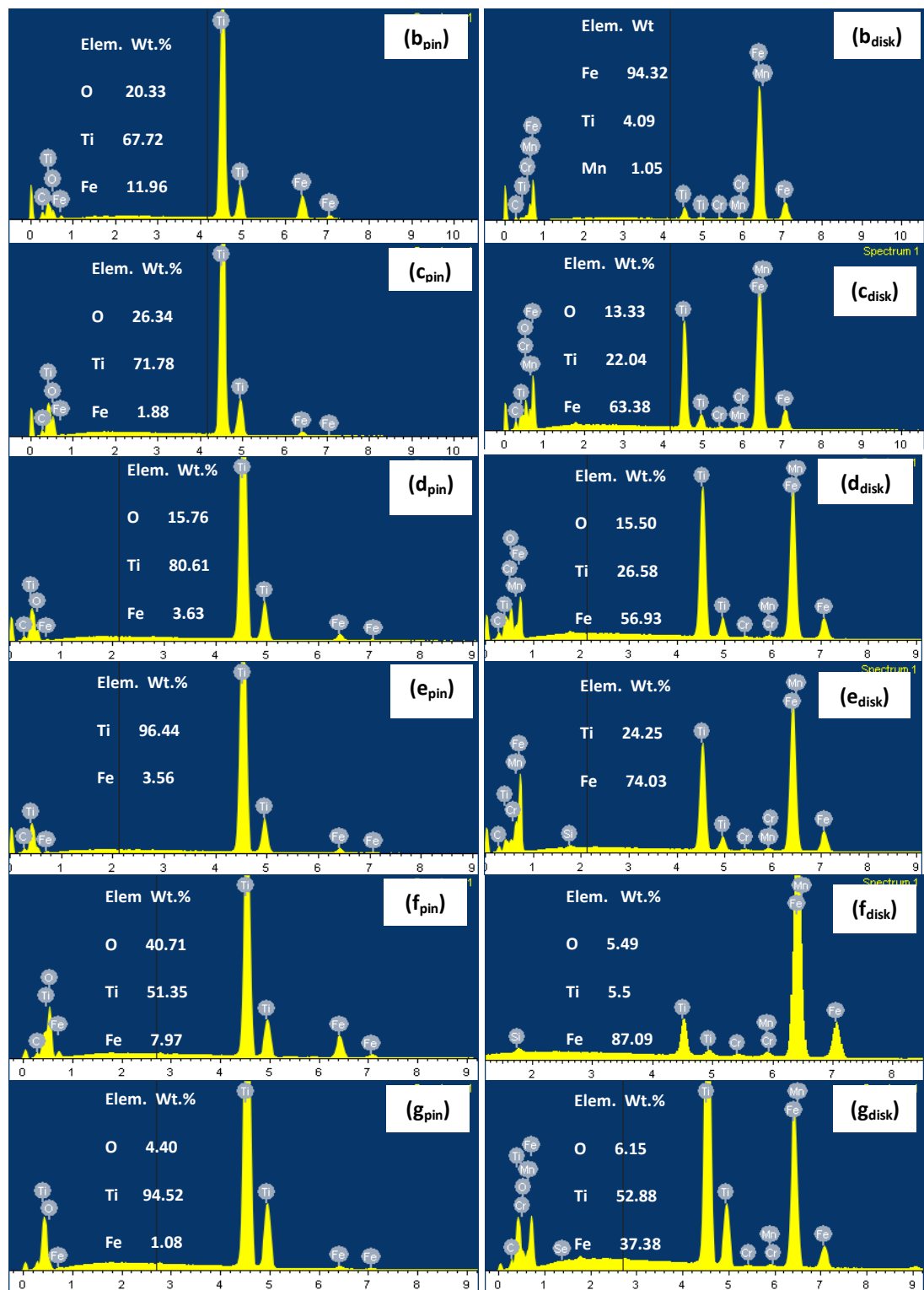


Figure 115 EDX analysis of the worn surfaces of pins and wear tracks of the disks, (a) at normal load 20N and sliding speed 0.38 m s^{-1} , (b) at 40N and 0.38 m s^{-1} , (c) at 30N and 0.5 m s^{-1} , (d) at 40N and 0.86 m s^{-1} , (e) at 50N and 0.86 m s^{-1} , (f) at 10N and 1.2 m s^{-1} and (g) at 50N and 1.2 m s^{-1} .

The Ti pins material was transferred to hardened steel disks during sliding almost for all combinations of sliding speeds and normal loads due to adhesion between mating surfaces, SEM micrographs and EDX analysis Figs. 114-115 respectively. At sliding speed 0.38 m s^{-1} comparatively less pins material was transferred to disks for the range of normal load except 20 N Figs. 114(a-b)-115(a-b). For the rest of sliding speeds and normal loads significant transfer of Ti pins material to the hardened steel counter body occurred as evident from EDX analysis of the disks wear tracks Figs. 115($C_{\text{disk}} - E_{\text{disk}}, g_{\text{disk}}$). As clear from the SEM micrographs of the pins worn surfaces, Fig. 114, that wear occurred by different wear mechanisms i.e. adhesive wear, mild-oxidational wear, plastic deformation, delamination and abrasive wear mechanisms. Up to sliding speed 0.5 m s^{-1} wear occurred by adhesive wear, oxidation of Ti pins mating surfaces and by abrasive wear mechanisms with trace of disks material on pins worn surfaces at lower normal loads Figs. 114($a_{\text{pin}} - C_{\text{pin}}$) - 115($a_{\text{pin}} - C_{\text{pin}}$). In this range of sliding speeds medium wear at lower normal loads while severe wear occurred at higher normal loads Table 41. At higher sliding speeds and lower normal loads the wear of the Ti pins occurred by adhesive and oxidative wear mechanisms with trace of disks material on the worn surfaces of the pins Figs. 114(f_{pin}) -115(f_{pin}). Mild wear of Ti pins was observed at lower normal loads and higher sliding speeds Table 41. At higher sliding speeds and normal loads severe wear occurred due to adhesive wear, plastic deformation and delamination wear mechanisms Figs. 114($d_{\text{pin}}-E_{\text{pin}}, g_{\text{pin}}$)- 115($d_{\text{pin}}-E_{\text{pin}}, g_{\text{pin}}$). Mild wear mode to severe wear mode transitions occurred in this range of sliding speeds and normal loads with abrupt increase in wear rates of Ti pins against hardened steel disks Table 41.

For the hardened steel disk at sliding speed 0.38 m s^{-1} disks material transferred to Ti pin at normal loads 40 & 50N Fig. 115(b) which result in medium wear of hardened steel disks Table 43. Medium wear occurred due to adhesive wear as the SEM micrograph shows the adhesive marks on the wear track, SEM micrograph Fig. 114(b_{disk}) with trace of pins material and there was no trace of oxide, EDX analysis Fig. 115 (b_{disk}). For the rest of sliding speeds and normal loads, the wear tracks were covered to a large extent with transferred pins material Figs. 114($a_{\text{disk}}, C_{\text{disk}}-g_{\text{disk}}$) and 115($a_{\text{disk}}, C_{\text{disk}}-g_{\text{disk}}$). At higher normal loads there was no trace of oxide on the wear tracks therefore the wear occurred by adhesive wear and delamination wear dominated wear mechanisms Figs. 115($b_{\text{disk}}, E_{\text{disk}}$). Disks material was also found on the pins worn surfaces Figs. 115($a_{\text{pin}}-g_{\text{pin}}$), which indicated that mix mechanical layer formed and then loose wear fragments formed. These disks material

Tribo-corrosion maps for steels, titanium and titanium carbide materials

particles seem to be generated in frictional process by pulling out of micro-volumes in places of adhesive bonds from the hardened steel disks surfaces after local frictional heating up and softening. But these particles were still hard enough and behaved abrasively during sliding process in wear of mating surface of the titanium specimen Figs. 114(a_{pin-gpin}). Moreover, the presence of Ti, Fe and O species on the worn surfaces of the Ti pins and on the wear tracks indicates that wear occurred by the oxidation with more oxidation of the pins material (Ti) Figs. 115(a_{pin-gpin}).

6.2.14. SEM micrograph of the wear debris

Fig. 116 shows the SEM micrographs of the wear debris of Ti pins and hardened steel disks sliding against each other

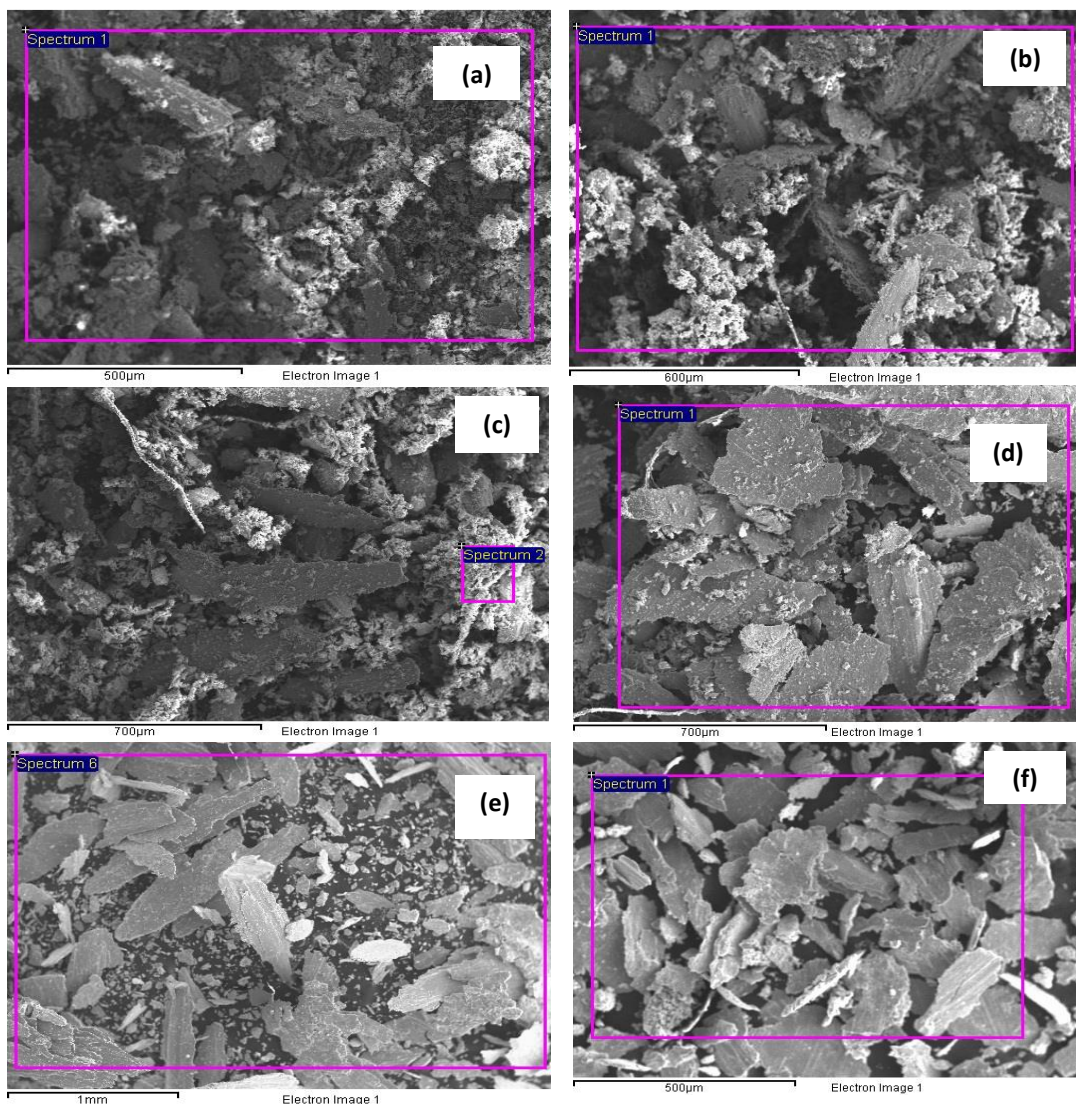


Figure 116 SEM micrograph of wear debris of Ti against hardened steel, (a) at sliding speed 0.38 m s^{-1} and normal load 20N, (b) at 0.38 m s^{-1} and 50N, (c) at 0.5 m s^{-1} and 50N, (d) at 0.86 m s^{-1} and 30N, and (e) at 1.2 m s^{-1} and 50N, and (f) at 1.5 m s^{-1} and 30N.

6.2.15. EDX analysis of the wear debris

Fig. 117 shows the EDX analysis of the wear debris from Ti pins and hardened steel disks sliding against each other.

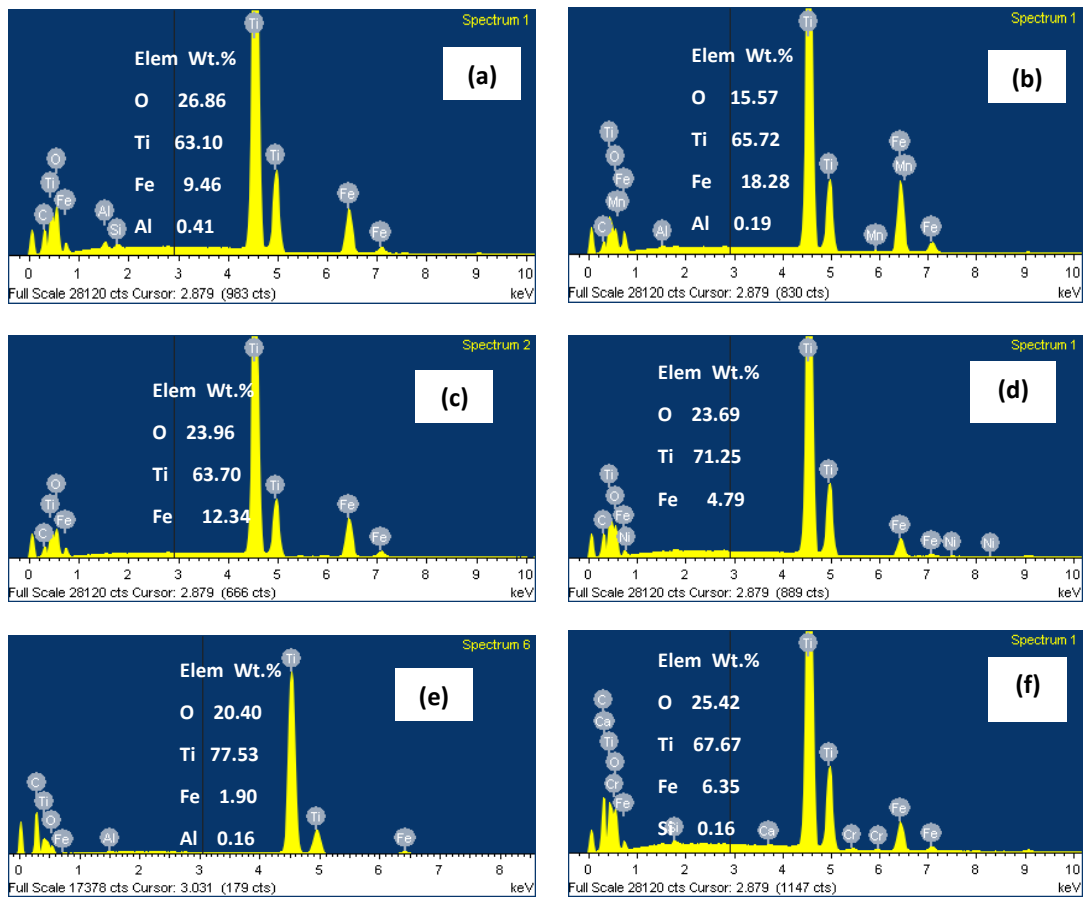


Figure 117 EDX analysis of wear debris of Ti against hardened gauge (a) at sliding speed 0.38 m s^{-1} and normal load 20N, (b) at 0.38 m s^{-1} and 50N, (c) at 0.5 m s^{-1} and 50N, (d) at 0.86 m s^{-1} and 30N, and (e) at 1.2 m s^{-1} and 50N, and (f) at 1.5 m s^{-1} and 30N.

The composition of wear debris mainly consisted of Ti, O and Fe with high percentage of pin material in all cases Fig. 117. This confirms that debris particles came from the hardened steel counter body as well. The shapes of wear debris were different for lower sliding speeds and for the higher sliding speeds irrespective of the normal loads. At lower sliding speeds wear products consisted of fine compact particles, flake shape metallic particles along with fine grey power of titanium oxide, SEM micrographs Figs. 116(a-c) and EDX analysis Figs. 117(a-c); while at higher sliding speeds wear products, mainly, consisted of larger flake-like metallic particles and fine grey power, mainly, of titanium and with trace of ferrous oxide, SEM micrographs Figs. 116 (d-f), EDX analysis Figs. 117(d-f). The shapes of the wear debris are depending on sliding speed i.e. the wear mechanisms are changed with

the change in sliding speed. The wear modes are changed with the change in sliding speeds and normal loads.

6.3. Discussion

6.3.1. Wear mechanisms and regimes

Due to lower value of hardness and poor sliding wear resistance, high wear rate of Ti was found against hardened steel Tables 36-40 and Figs. 102-106. A few tests had to terminate due to very high wear rate before covering total sliding distance i.e. 5,560 m. These observations are in consistence with the previous work (Chapter 5) where 303SS showed similar wear behaviour against alumina and in the others' work found in literature [166]. The pins' mating surfaces were extruded for all combinations of sliding speeds and normal loads. Lower wear rate of the Ti pins against hardened steel disks up to 20 N normal load for the range of sliding speeds, Figs. 107-108, was due to mild oxidative wear of the mating surfaces. The presence of Ti, Fe and O on the worn surface of the Ti pins and wear tracks suggest that the domination of the tribo-oxidation process in the high temperature contact spots between mating surfaces, EDX analysis of the worn surfaces Figs. 115(a, f). This was observed by S. Krol et al. as well that oxidative wear with lower wear rate of the system occurred, typical for mating of metals of diversified mechanical properties at mild friction conditions [50].

At higher normal loads i.e. from 30 to 50 N, severe sliding conditions observed, which was due to adhesive, oxidational, plastic deformation and delamination wear mechanisms, SEM micrographs Figs. 114(b-e, g) and EDX analysis Figs. 115(b-e, g). A transition in wear mode from initial severe wear to a mild wear occurred, which had been widely found for sliding wear of metals [11]. Such a transition is caused by different parameters, like low sliding speed [162], lower normal load [13], and high rates of oxidation [14-15]. Wear mode regimes transitions occurred from medium wear to mild wear at 10N with the increase in sliding speed Table 42 and Fig. 108. The decrease in wear rate and transition in wear mode regimes occurred due to tribo-oxidation process. With the increase in sliding speed more frictional heat generated at the contact point due to increase of flash temperature that led to more oxidation. These observations are in agreement with work of the others' found in the literature [6, 8-9, 174].

With the increase in normal load, rapid increase in wear rate occurred for the Ti pins for the range of sliding speed Table 41 and Figs. 107, 111. The very sharp increase in wear rate suggests severe sliding conditions with plastic deformation and flow of the softer material [50]. The same results were found for Ti and its alloys against hard metals in the experimental work of the other authors [137, 175]. At higher normal load i.e. 30 to 50N for range of sliding speeds mainly adhesive, delamination, wear mechanism was predominated. With the increase in sliding speed the surface temperature and a progressive increase in wear is induced because of thermal softening as soon as the yield point of the material starts decreasing significantly. The effects of an increase in sliding speed results an increased delamination wear [69, 174]. Comparatively lower wear rate of Ti at 0.5 m s^{-1} for the range of normal load, Fig. 111, was due to the mild oxidation of the sliding surfaces contact at this sliding speed Fig. 114(c) and Fig. 115(c), [174]. An oxidative wear can be less severe than that of adhesive, delamination, wear and can result in a decreased wear rate [69]. Garbar explained that, as the normal load increases, tribo-oxidation is accompanied by the mechanism of plastic deformation [40].

Table 46-47 and Figs. 112-113 show the values of the coefficient of frictions for Ti pins against harden steel disks respectively. The coefficient of friction data and plots are on the basis of average values that were observed for each combination of sliding speed and normal load during sliding test. For the Ti and hardened steel tribo couple, Figs. 112-113 show the coefficient of friction was higher at 10 N for the range of sliding speed. A higher coefficient of friction at this normal load might have been due to more actual areas of contact and more adhesion between the mating surfaces. For the rest of the normal loads, the values of μ were found between 0.2-0.3 for the range of sliding speeds. The lower values of μ for those combinations of sliding speeds and normal loads might have been because of more frictional heat at higher normal loads resulted in surface softening effects; lower actual contact area due to rougher contact surfaces [188], poor adhesion between the incompatible pins and disks material [55] and metallic debris trapped in mating surfaces due to severe wear conditions. Moreover, lower coefficient of friction of the substrate might have attributed to the poor frictional wear properties of the Ti. The fluctuation in friction force might have resulted from the wear particles that trapped between the mating surfaces during sliding and changed the contact conditions for various combinations of the sliding speeds and normal loads [181].

When in air, combinations of dissimilar metals i.e. titanium pins and hardened steel disks occurred during the friction process domination of two processes prevailed: the adhesion controlled transfer of the pins material to the disks surfaces and shearing off the adhered titanium layer by the front edge of the moving specimen with accompanying adhesion evoked detachment of small iron particles from the disk working surface and their abrasive action between mating surfaces [50]. From the SEM micrographs of the worn surfaces, Fig. 114 and EDX analysis, Fig. 115, it is clear that a tribo-layer of mixed materials was formed on the wear tracks. Rigney confirmed by the experiments that the sliding of metals can be described by the following basic wear sequence: surface and sub-surface plastic deformation, formation of debris and material transfer, reaction with the environment, mechanical mixing and producing a tribological layer [30]. A transfer event is treated as depending on interface separation and junction adhesion. The amount of material transferred varied for each combination of sliding speed and normal load. The time taken to reach the steady conditions is inversely proportional to the normal load. At steady state the material transfer from the pin is equal to the wear rate. M. Kerridge observed this in his experiment where annealed steel pin was rubbed against a hardened steel ring [42].

At a sliding speed 0.38 m s^{-1} comparatively less pins material transferred to disks for the range of normal load except 20 N Figs. 114(a), 115(a) and from the hardened steel disks comparatively more material transferred to the Ti pins at 40 and 50 N normal loads which resulted in medium wear of hardened steel disk Figs. 114(b), 115(b). This was due to adhesive wear as the SEM micrograph shows that the wear track was not fully covered by the transferred material Fig. 114(b_{disk}) and oxidation of disk mating surfaces and reasonable percentage of disk material on the pins worn surfaces might be oxidised of iron Fig. 115(b_{pin}). For the rest of sliding speeds and normal loads the wear tracks were covered to a large extent with transferred material. Significant transfer of Ti pins material to the hardened steel counter body suggest that severe adhesion took place between Ti and hardened steel Figs. 115 (a_{disk}, c_{disk}-e_{disk}, g_{disk}). The same observation was found in the study of “response of Ti-6Al-4V alloys to dry sliding wear against hardened steel” [137].

During continuous sliding, the initial transferred fragments are deformed, fractured and blended, leading to formation of mechanically mixed material on the wear track. The hardness of this mixed material formed is considerably higher than that of the soft pin material due to the intense, localised, thermal effects which occurred during rubbing under

unlubricated conditions. Typically sliding wear debris particles are made from modified mixed layer [42, 132]. Wear debris at the end of test can be a very useful tool to give clue of wear mechanisms occurred in a sliding system. The SEM micrographs of the wear debris, Fig. 116, acted as a very useful diagnostic tool to confirm the dominated wear mechanism of this dry sliding tribo-system. Various types and sizes of wear debris were found for the range of sliding speed and normal loads which were created as a result of the adhered titanium lumps detachment from the sliding wear tracks together with thin film of counterpart material. EDX analysis Fig. 117 confirm this assumption that during dry sliding, frictional heat generation results in high temperatures at the contact area leading to oxidation of titanium for all combinations of sliding speeds and normal loads. With the increase in temperature usually above 800 °C flake shape titanium debris particles may contain rutile, TiO₂, on their surfaces. Further the exceed in temperature above 1000 °C between the mating surfaces leads to the formation of sub-stoichiometric oxides of general formula Ti_nO_{2n-1}, known as Magnéli phases, which are characterised by extended planar defects and crystallographic shear planes that accommodate the oxygen loss[196].

The wear debris collected after tests, at lower sliding speed 0.38 & 0.5 m s⁻¹, irrespective of the normal load, consisted of fine compact particles and strip shape particles identified as metallic titanium along with grey oxide powder Fig. 116(a-c) – 117(a-c), were resulted from adhesive and oxidation wear [50]. At higher sliding speed 0.86-1.5 ms⁻¹ larger flake types metallic wear particles indicate that severe adhesive and delamination wear occurred during dry sliding [132]. The large quantity of Ti metallic particles in the wear debris suggested that severe adhesive and delamination wear of Ti against hardened steel occurred. Similar wear mechanisms were suggested by Straffelini and Molinari [174], Ohidul Alam and Haseeb, [137], for the Ti-6Al-4V alloy against hardened steel and R. Sahoo et al. for Ti-6Al-4V Alloy Consisting of Bimodal Microstructure, [189]. In this plasticity-dominated wear mechanism, unidirectional sliding of the metal surfaces nucleates surface or subsurface voids/cracks. These extend and link resulting in crack beneath and parallel to the surface. When the crack is large enough, it breaks out to yield flaky debris [137]. At severe conditions, material transfer, wear rate and surface damage are higher. Metallic wear debris produced rapidly and the particles from the soft metals are large [43]. The wear equation based on a delamination theory [118] predicts that wear rate increase as the applied load increases, which is seem to being satisfied in this tribo system.

6.3.2. Wear regimes and wear maps

The development of wear maps is a useful way to study and predict the wear behaviour of metals sliding against each other at different sliding speeds and normal loads. The generalized classification of wear rate into three distinct wear mode regimes, mild, medium and severe wear are found in literature [11, 31, 32, 34, 165]. In this study, the wear mode regimes, namely (a) mild wear (b) medium wear and (c) severe wear, are defined in consistent with previous research work found in literature [34, 72], our previous work (dealt with in Chapters 4 and 5), tests results, mass loss data, wear rate, physical observations of the worn surfaces, SEM and EDX of the worn surfaces and the wear debris.

A tribo-system approach has been adopted to study the wear behaviour of Ti against hardened steel. The wear modes regimes limits are as below:

- a) Mild wear $\leq [1.12 \times 10^{-12} (\text{m}^3 \text{m}^{-1})]$
- b) $[1.12 \times 10^{-12} (\text{m}^3 \text{m}^{-1}) < \text{medium wear} \leq [3.35 \times 10^{-12} (\text{m}^3 \text{m}^{-1})]$
- c) Severe wear $> [3.35 \times 10^{-12} (\text{m}^3 \text{m}^{-1})]$

6.3.3. Wear mode maps

Fig. 118 shows the wear mode maps of the Ti pins and hardened steel disks against each other.

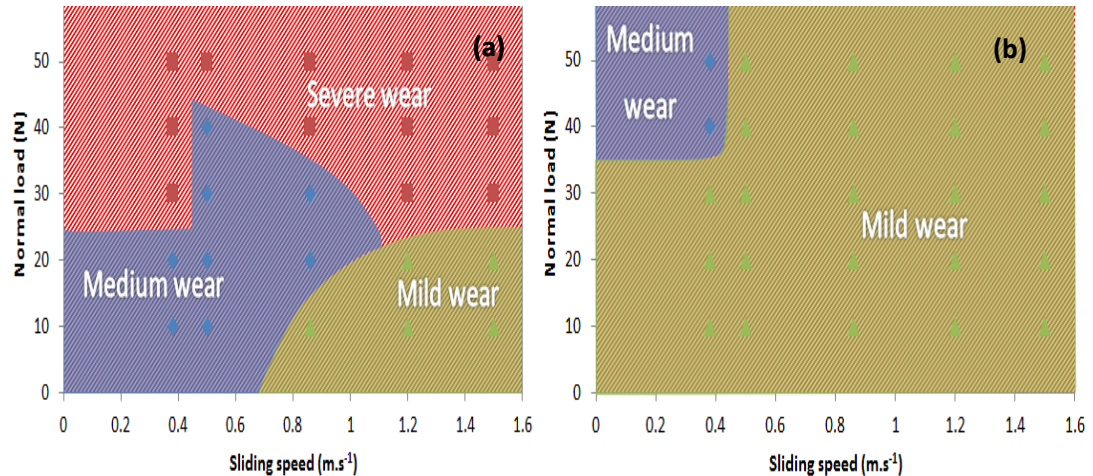


Figure 118 Wear mode maps (a) Ti pins against hardened steel disks and (b) hardened steel disks against Ti pins.

In the Fig. 118 the various wear mode regimes are identified for the Ti pins and hardened steel disks, as a function of sliding speeds and normal loads. These maps show the distinctive differences in the wear mode transitions, as addressed above. It can be clearly seen in Fig. 118(a) that severe wear is more prevalent with respect to normal load for Ti

pins (soft metal). Moreover, the medium wear dominates at lower sliding speeds and normal loads and severe wear predominates at higher normal loads. For the hardened steel disks sliding against Ti pins, wear mode map Fig. 118(b), mild wear is dominant for the range of sliding speeds and normal loads due to the formation of transferred material layer on the wear tracks, which protected the counterface from wearing. In Fig. 118(a-b), the combination of the mild wear zone can be regarded as the safe operation zone for the Ti and hardened steel against each other respectively for this range of sliding speeds and normal loads [65].

6.3.4. Wear mechanism maps

Wear mechanism maps are useful tools for analysing the change in wear mechanism regimes over a multi-parameter space. Fig. 119 shows the wear mechanism maps of the Ti and hardened steel against each other that exhibits significant transitions in wear mechanism regimes. The boundaries of the wear mechanisms regimes on the diagrams are only approximate. The wear mechanisms regimes below are based on the experimental observations as mentioned above.

These can be summarized as:

- Abrasive-oxidative wear
- Adhesive-oxidative wear
- Oxidative-adhesive wear
- Oxidative-abrasive wear

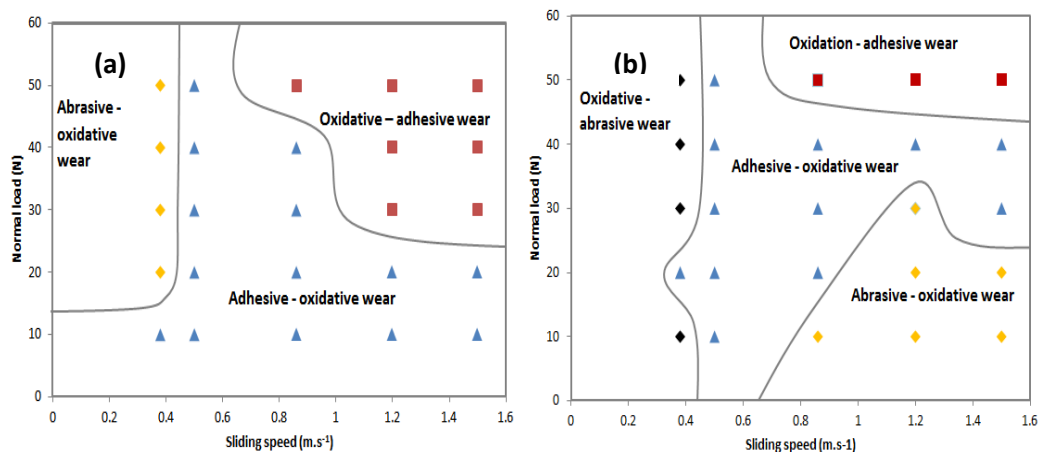


Figure 119 Wear mechanism maps, (a) Ti pins against hardened steel disks and (b) hardened steel disks against Ti pins.

From Fig. 119(a), in the “adhesive-oxidative wear” regime, wear fragments were generated due to adhesion between mating sliding surfaces. The mechanically mixed layer formed which comprises oxidative- wear products, Figs. 114(c - d) and 115(c - d) respectively, with the presence of oxide particles clearly in evidence. Analysis of wear debris shows fine compact powder of titanium oxide and metallic particles of titanium, Figs. 116(c-d) - 117(c-d) [50]. With the increase in sliding speed, frictional heat leads to further oxidation of the surfaces in contact [6, 8, 9, 174]. In this regime, with the high contact temperatures, there is more evidence of adhesion than abrasion.

For the “oxidative-adhesive wear” regime, Fig. 119(a), severe adhesive wear and plastic deformation led to the higher wear rate of the titanium pins in this region, Figs. 114(e, g) and 115(e, g), due to high contact temperatures at higher sliding speeds and normal loads. The flake like shape of metallic wear debris Figs. 116(e-f) and the presence of higher proportions of titanium and oxygen in the wear products, Figs. 117(e-f) indicate that oxidative wear was followed by adhesive wear. In such severe sliding conditions, material transfer, wear, and surface degradation rates are higher. Metallic wear debris are produced rapidly and the particles generated from the wear process are larger in size [43]. Similar wear mechanisms are suggested by Straffelini and Molinari [174] and Ohidul Alam and Haseeb [137] for Ti-6Al-4V alloy against hardened steel.

For the “abrasive-oxidative wear” regime, Fig. 119, oxide scale together with metallic Ti and Fe acts as an abradent on the surfaces, Figs. 114(a, f) and 115(a, f). Adhesion is less evident due to the lower contact temperatures. The nature and shape of the wear debris for this and the above regimes, Figs. 116(a-b) and 117(a-b), identify the major difference between the interaction of oxidation with the abrasive and adhesive wear mechanisms.

6.4. Wear mechanisms Comparison between Ti sliding against hardened steel counterface and 303SS sliding against alumina counterface [Chapter 5]

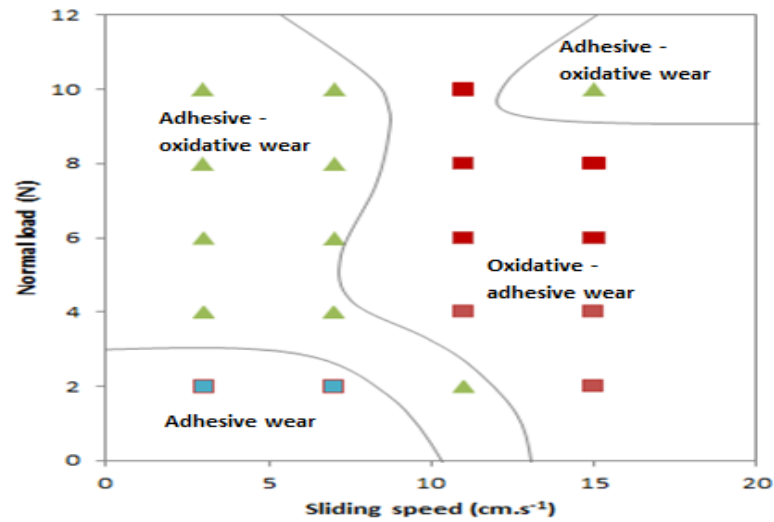


Figure 120 Wear mechanistic maps for 303 SS against alumina (taken from chapter 5).

Fig. 120 shows the wear mechanistic map for 303SS against alumina taken from chapter 5, for comparison with the wear mechanism map of Ti against hardened steel Fig. 119(a). It is clear through comparing (although against different counterface materials) that the oxidative wear mechanism is more prevalent for titanium against the steel counterface.

Clearly, the wear maps developed above indicate many possible wear regime transitions between titanium and steel. Further work will be to investigate the wear mechanisms of Ti base TiC composite coatings against hardened steel to provide a basis for coating optimization in such conditions.

6.5. Conclusions

1. For titanium sliding against steel, oxidative wear predominates for the range of normal loads and sliding speeds and is associated with relatively high wear rates indicating the non-protective nature of the oxide formed and decrease in yield strength with the increase in temperature between mating surfaces.
2. The titanium/steel sliding couple results in severe sliding conditions with adhesive wear, delamination, plastic deformation, material transfer and abrasive wear of the pins material.

- 3.** A mechanically mixed metal layer develops under various combinations of sliding speeds and normal loads on the wear tracks. However, the protective role of this layer depends on the oxide morphology, the contact conditions and crystallographic structure i.e. rutile – type structure.

- 4.** Due to poor tribological properties, the use of uncoated Ti in the wear-resistant situation is unwarranted.

Chapter 7

Titanium base titanium carbide composite coatings in tribological contact

7.1. Introduction

The purpose of this study is to investigate the wear behaviour of titanium base TiC composite coatings sliding against hardened steel in air with respect to change in sliding speeds and normal loads. The integrity of the composite coatings was checked for tribo-corrosion behaviour and wear modes and wear mechanistic maps were constructed to understand and predict the wear behaviour for the both materials in dry sliding contact under ambient conditions at room temperature. Titanium base titanium carbide coatings was produced by TIG welding torch melting process. The tribo-corrosion behaviour of Ti base TiC composite coatings has been compared with respect to 303SS base TiC composite coatings produced by this method (dealt with in chapter 5) and coatings produced other than TIG process.

7.2. Dry sliding wear tests results

Dry sliding wear tests were carried out on pin-on-disk sliding wear testing rig Fig. 34 for 25 combinations of sliding speeds and normal loads for TiC coatings against hardened steel as per experimental conditions mentioned in Section 3.5, chapter 3. The sliding distance 5,560m and numbers of revolutions 30,000 were kept constant for all tests. The coatings were carried out by TIG welding torch melting method as mentioned in Section 3.6, Chapter 3. The effects of change in sliding speeds and normal loads on wear behaviour of Ti base TiC composite coatings against hardened steel (A.I.S.I. 0-1-Ground Flat Stock), were investigated. At the end of each sliding tests worn surfaces of the disks and pins and wear debris were examined to investigate the wear mode and wear mechanism regimes. SEM micrographs and EDX analysis of the worn surfaces and wear debris were carried out. The dry sliding wear results are as follows:

7.2.1. Wear rate at 0.38m s^{-1} sliding speed for the range of normal loads

Table 48 and Fig. 121 show the wear rate of Ti base TiC composite coatings pins and hardened steel disks against each other at sliding speed 0.38m s^{-1} for the range of normal loads.

Normal load (N)	Wear rate of Ti base TiC coatings pin ($\text{m}^3 \text{m}^{-1}$) $\times 10^{-12}$ at 0.38 m s^{-1}	Wear rate of hardened steel disk ($\text{m}^3 \text{m}^{-1}$) $\times 10^{-12}$ at 0.38 m s^{-1}
10	0.004	0.062
20	0.098	0.235
30	0.018	0.244
40	0.095	0.692
50	0.084	0.960

Table 48 Wear rate of Ti base TiC coatings pins and hardened steel disks.

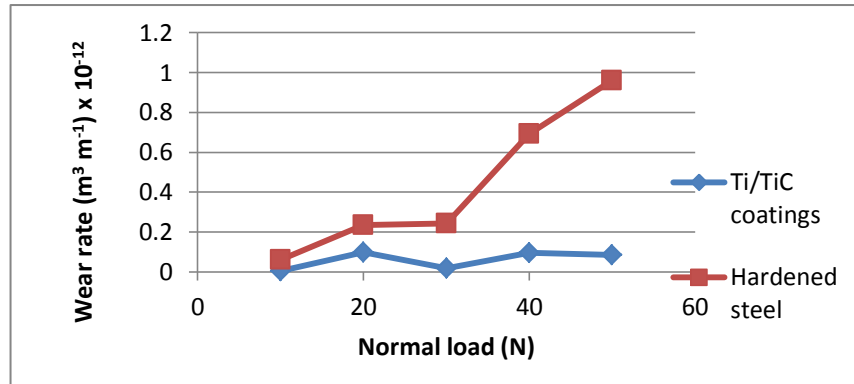


Figure 121 Wear rate of Ti base TiC composite coatings pins and hardened steel disks.

7.2.2. Wear rate at 0.5 m s^{-1} sliding speed for the range of normal loads

Table 49 and Fig. 122 show the wear rate of Ti base TiC composite coatings pins and hardened steel disks against each other at sliding speed 0.5 m s^{-1} for the range of normal loads against each other.

Normal load (N)	Wear rate of Ti/TiC coatings pin ($\text{m}^3 \cdot \text{m}^{-1}$) $\times 10^{-12}$ at 0.5 m s^{-1}	Wear rate of hardened steel disk ($\text{m}^3 \cdot \text{m}^{-1}$) $\times 10^{-12}$ at 0.5 m s^{-1}
10	0.011	0.131
20	0.040	0.302
30	0.102	0.400
40	0.885	0.404
50	1.641	0.120

Table 49 Wear rate of Ti base TiC coatings pins and hardened steel disks.

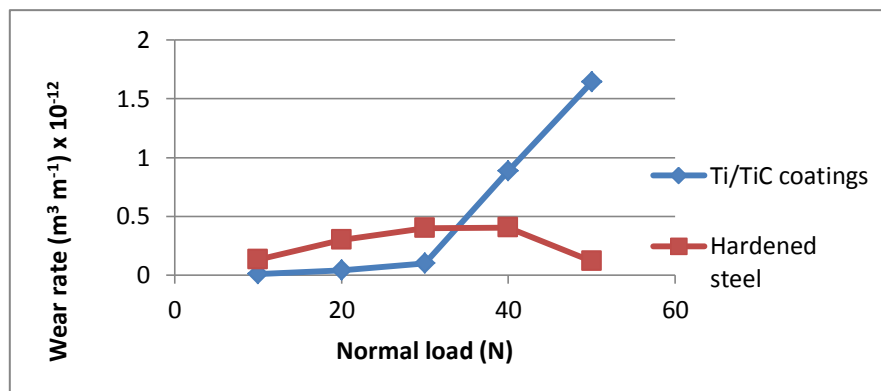


Figure 122 Wear rate of Ti base TiC coatings pins and hardened steel disks.

7.2.3. Wear at 0.86m s⁻¹ sliding speed for the range of normal loads

Table 50 and Fig. 123 show the wear rate of Ti base TiC composite coatings pins and hardened steel disks against each other at sliding speed 0.86m s⁻¹ for the range of normal loads.

Normal load (N)	Wear rate of Ti/TiC coatings pin (m ³ m ⁻¹) x 10 ⁻¹² at 0.86 m s ⁻¹	Wear rate of hardened steel disk (m ³ m ⁻¹) x 10 ⁻¹² at 0.86 m s ⁻¹
10	0.091	0.148
20	0.161	0.323
30	0.954	0.115
40	0.113	0.579
50	0.994	0.221

Table 50 Wear rate of Ti base TiC coatings pins and hardened steel disks.

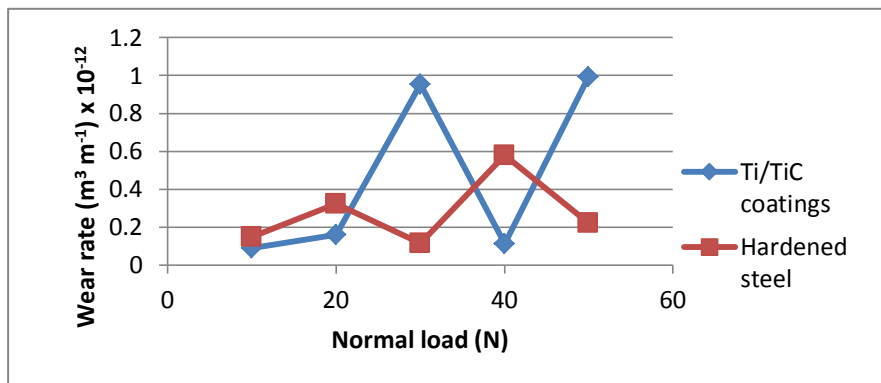


Figure 123 Wear rate of Ti base TiC coatings pins and hardened steel disks.

7.2.4. Wear at 1.2m s⁻¹ sliding speed for the range of normal loads

Table 51 and Fig. 124 show the wear rate of Ti base TiC composite coatings pins and hardened steel disks against each other at sliding speed 1.2m s⁻¹ for the range of normal.

Normal load (N)	Wear rate of Ti base TiC coatings pin (m ³ m ⁻¹) x 10 ⁻¹² at 1.2 m s ⁻¹	Wear rate of hardened steel disk (m ³ m ⁻¹) x 10 ⁻¹² at 1.2 m s ⁻¹
10	0.022	0.219
20	0.307	0.184
30	0.146	0.272
40	0.252	0.445
50	0.285	0.401

Table 51 Wear rate of Ti base TiC coatings pins and hardened steel disks.

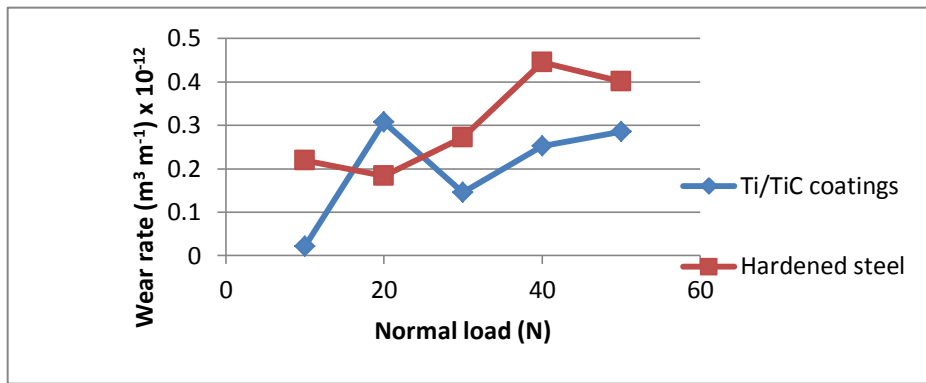


Figure 124 Wear rate of Ti base TiC coatings pins and hardened steel disks.

7.2.5. Wear at 1.5 m s⁻¹ sliding speed for the range of normal loads

Table 52 and Fig. 125 show the wear rate of Ti base TiC composite coatings pins and hardened steel disks against each other at sliding speed 1.5m s⁻¹ for the range of normal loads.

Normal load (N)	Wear rate of Ti base TiC coatings pin (m³ m⁻¹) x 10 ⁻¹² at 1.5 m s ⁻¹	Wear rate of hardened steel disk (m³ m⁻¹) x 10 ⁻¹² at 1.5 m s ⁻¹
10	0.048	0.120
20	0.095	0.182
30	0.475	0.108
40	0.786	0.157
50	0.753	0.302

Table 52 Wear rate of Ti base TiC coatings pins and hardened steel disks.

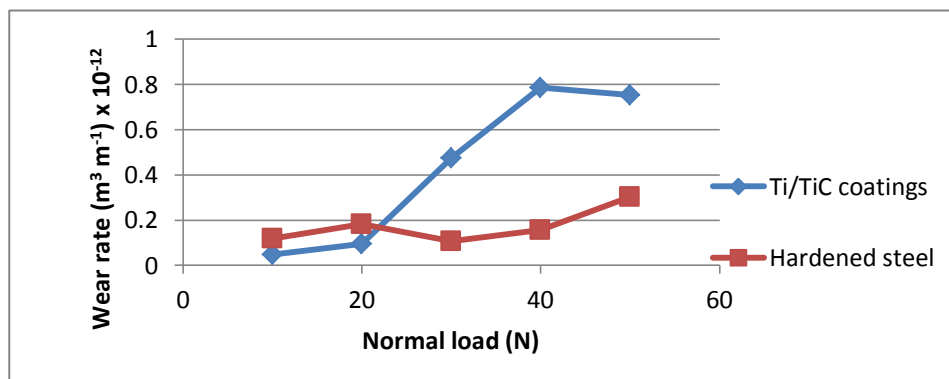


Figure 125 Wear rate of Ti base TiC coatings pins and hardened steel disks.

Tables 48-52 and Figs. 121-125 show the wear rate comparison of Ti base TiC composite coatings pins and hardened steel disks at different constant sliding speeds for the range of normal loads. At sliding speeds 0.38 m s⁻¹ more wear rate of hardened steel was found as compare to Ti base TiC coatings Fig. 121. For the rest of sliding speeds fluctuation in wear rates of both materials were found Figs. 122-125. The fluctuation in wear rate of the tribo

couple occurred due to the formation of mechanical mixes layer, high oxidation rate and mechanical damages of the contact surfaces during dry sliding against each other. Moreover low wear rate of Ti base TiC coatings observed up to normal loads 20 N against it counterface for the range of sliding speeds, which was due to high oxidation rate and material transfer from hardened steel.

7.2.6. Wear rate of Ti base TiC coatings against hardened steel at constant sliding speeds and various normal loads

Table 53 Fig. 126 show the wear rate of Ti base TiC composite coatings pins against hardened steel disks at different constant sliding speeds and various normal loads.

Normal load (N)	Wear rate $(m^3 m^{-1}) \times 10^{-12}$ at 0.38 m s ⁻¹	Wear rate $(m^3 m^{-1}) \times 10^{-12}$ at 0.5 m s ⁻¹	Wear rate $(m^3 m^{-1}) \times 10^{-12}$ at 0.86 m s ⁻¹	Wear rate $(m^3 m^{-1}) \times 10^{-12}$ at 1.2 m s ⁻¹	Wear rate $(m^3 m^{-1}) \times 10^{-12}$ at 1.5 m s ⁻¹
10	0.004	0.011	0.091	0.022	0.048
20	0.098	0.040	0.161	0.307	0.095
30	0.018	0.102	0.954	0.146	0.475
40	0.095	0.885	0.113	0.252	0.786
50	0.084	1.641	0.994	0.285	0.753

Table 53 Wear rate of Ti base TiC coatings pins against hardened steel disks.

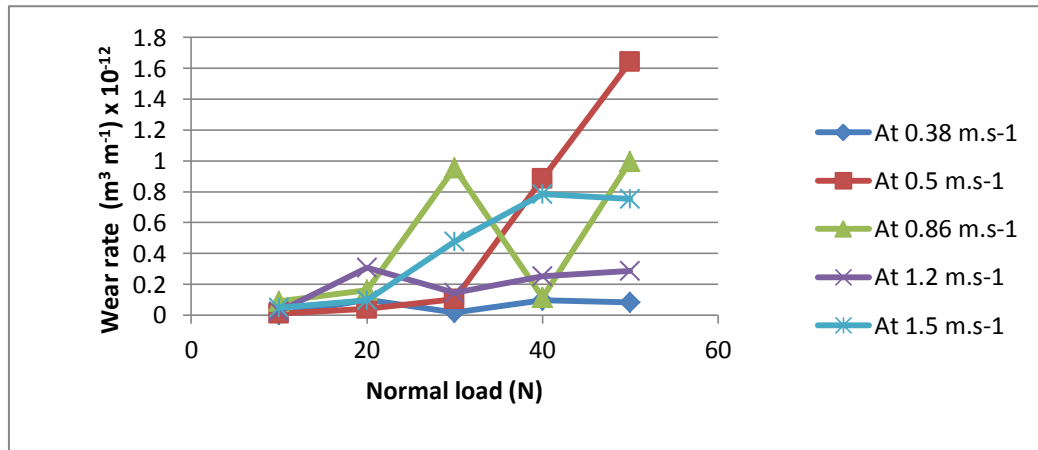


Figure 126 Wear rate of Ti base TiC coatings pins against hardened steel disks.

7.2.7. Wear rate of Ti base TiC coatings against hardened steel at constant normal loads and various sliding speeds

Table 54 Fig. 127 show the wear rate of Ti base TiC coatings pins against hardened steel disks at different constant normal loads and various sliding speeds.

Sliding speed (m s ⁻¹)	Wear rate (m ³ m ⁻¹) x 10 ⁻¹² at 10N	Wear rate (m ³ m ⁻¹) x 10 ⁻¹² at 20N	Wear rate (m ³ m ⁻¹) x 10 ⁻¹² at 30N	Wear rate (m ³ m ⁻¹) x 10 ⁻¹² at 40N	Wear rate (m ³ m ⁻¹) x 10 ⁻¹² at 50N
0.38	0.004	0.098	0.018	0.095	0.084
0.5	0.011	0.040	0.102	0.885	1.641
0.86	0.091	0.161	0.954	0.113	0.994
1.2	0.022	0.307	0.146	0.252	0.285
1.5	0.048	0.095	0.475	0.786	0.753

Table 54 Wear rate of Ti base TiC coatings pins against hardened steel disks.

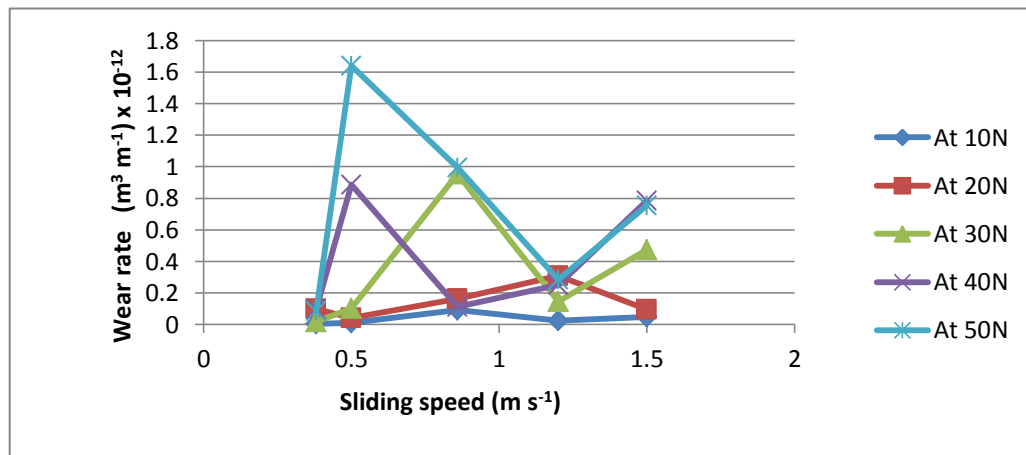


Figure 127 Wear rate of Ti base TiC coatings pins against hardened steel disks.

Tables 53-54 and Figs. 126-127 show the wear rate of Ti base TiC composite coatings pins against hardened steel disks at constant sliding speeds and constant normal loads respectively. It is clear from Fig. 126 that there was very mild and mild wear for all the combinations of sliding speeds and normal loads except sliding speed 0.5 m s⁻¹ and normal load 50 N. Steady wear rate was found for sliding speed 0.38 & 1.2 m s⁻¹ mean no wear mode transition occurred at these sliding speeds for the range of normal loads. At 0.5 m s⁻¹ wear mode regime transitions occurred from very mild wear to mild wear then to medium wear with the increase in normal load. At 0.5, 0.86 & 1.5 m s⁻¹, fluctuation in wear rates were found for the range of normal loads Fig. 127. Overall very mild wear was dominated for Ti base TiC coatings against hardened steel.

7.2.8. Wear rate of hardened steel against Ti base TiC coatings at constant sliding speeds and various normal loads

Table 55 Fig. 128 show the wear rate of hardened steel disks against Ti base TiC coatings pins at different constant sliding speeds and various normal loads.

Normal load (N)	Wear rate ($\text{m}^3 \text{m}^{-1}) \times 10^{-12}$ at 0.38 m s^{-1}	Wear rate ($\text{m}^3 \text{m}^{-1}) \times 10^{-12}$ at 0.5 m s^{-1}	Wear rate ($\text{m}^3 \text{m}^{-1}) \times 10^{-12}$ at 0.86 m s^{-1}	Wear rate ($\text{m}^3 \text{m}^{-1}) \times 10^{-12}$ at 1.2 m s^{-1}	Wear rate ($\text{m}^3 \text{m}^{-1}) \times 10^{-12}$ at 1.5 m s^{-1}
10	0.062	0.131	0.148	0.219	0.120
20	0.235	0.302	0.323	0.184	0.182
30	0.244	0.400	0.115	0.272	0.108
40	0.692	0.404	0.579	0.445	0.157
50	0.960	0.120	0.221	0.401	0.302

Table 55 Wear rate of hardened steel disks against Ti base TiC coating pins.

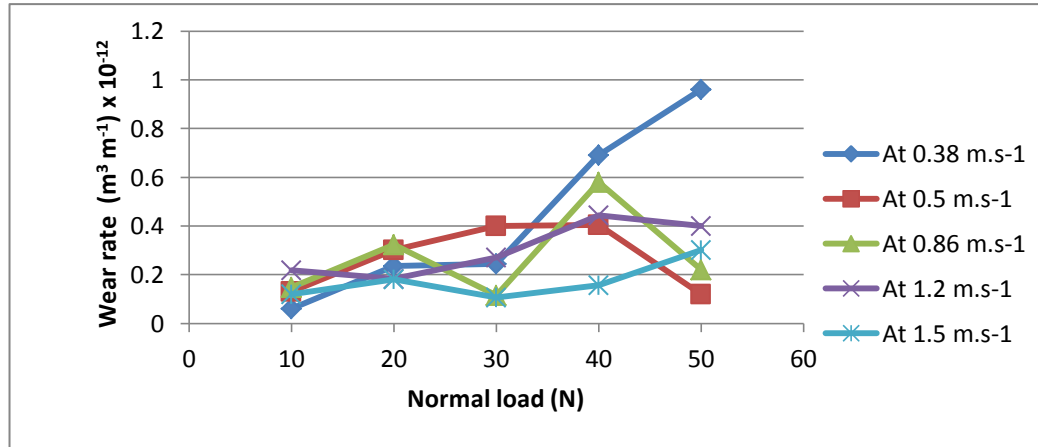


Figure 128 Wear rate of hardened steel disks against Ti base TiC coatings pins.

7.2.9. Wear rate of hardened steel against Ti base TiC coatings at constant normal loads and various sliding speeds

Table 56 Fig. 129 show the wear rate of hardened steel disks against Ti base TiC coatings pins at different constant normal loads and various sliding speeds.

Sliding speed (m s^{-1})	Wear rate ($\text{m}^3 \text{m}^{-1}) \times 10^{-12}$ at 10N	Wear rate ($\text{m}^3 \text{m}^{-1}) \times 10^{-12}$ at 20N	Wear rate ($\text{m}^3 \text{m}^{-1}) \times 10^{-12}$ at 30N	Wear rate ($\text{m}^3 \text{m}^{-1}) \times 10^{-12}$ at 40N	Wear rate ($\text{m}^3 \text{m}^{-1}) \times 10^{-12}$ at 50N
0.38	0.062	0.235	0.244	0.692	0.960
0.5	0.131	0.302	0.400	0.404	0.120
0.86	0.148	0.323	0.115	0.579	0.221
1.2	0.219	0.184	0.272	0.445	0.401
1.5	0.120	0.182	0.108	0.157	0.302

Table 56 Wear rate of hardened steel disks against Ti base TiC coating pins.

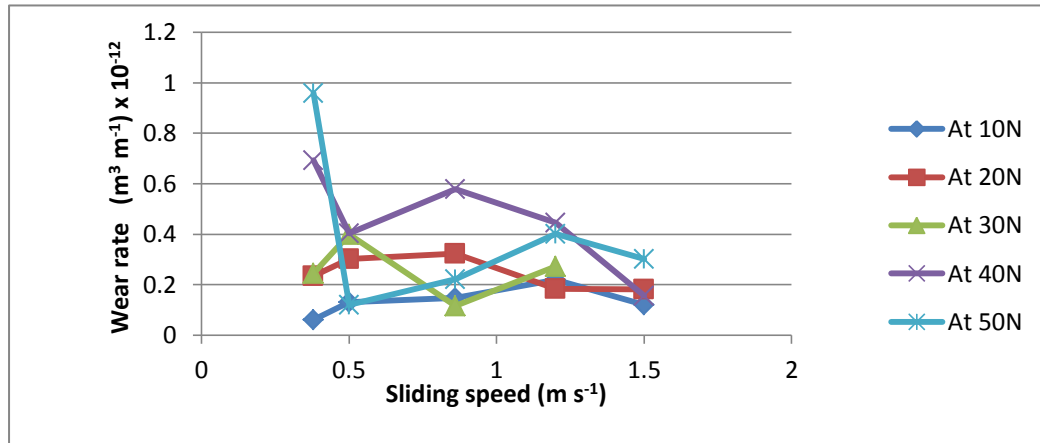


Figure 129 Wear rate of hardened steel disks against Ti base TiC coatings.

Tables 55-56 and Figs. 128-129 show the wear rate of hardened steel disks against Ti base TiC composite coatings pins at constant sliding speeds and constant normal loads respectively. It is clear from Fig. 128 that there was mild wear occurred for all the combinations of sliding speeds and normal loads. At sliding speed 0.38 m s^{-1} wear rate increased with the increase in normal load. Fig. 129 shows the fluctuation in wear rate and wear rate of hardened steel was decreasing with increase in sliding speed for the range of normal loads.

7.2.10. Total mass loss comparison of Ti base TiC coatings pins and hardened steel disks

Table 57 and Fig. 130 show the total mass loss of the Ti base TiC composite coatings pins and hardened steel disks at different constant sliding speeds for the range of normal loads i.e. at variable loads from 10 to 50 N, and increasing in 10 N increments for the total sliding distance 27,800 m. At sliding speeds 0.38 & 1.2 m s^{-1} the total mass loss of the Ti base TiC coatings was lower than that of hardened steel and for the rest of the sliding speeds mass loss of the hardened steel was lower. Moreover, the mass loss of the hardened steel was decreasing with the increase in sliding speed. The fluctuation in the total mass loss of Ti base TiC coating against hardened steel may be attributed to formation of mechanical mixes layer, higher oxidation rate and mechanical damages of the contact surfaces during dry sliding.

Sliding speed (m s^{-1})	Total mass loss of hardened steel disk ($\text{g} \times 10^{-2}$)	Total mass loss of Ti base TiC coatings pin ($\text{g} \times 10^{-2}$)
0.38	9.51	0.80
0.5	6.72	7.33
0.86	6.00	6.33
1.2	6.60	2.77
1.5	3.77	5.90

Table 57 The Total mass loss of Ti base TiC composite coatings pins and hardened steel disks.

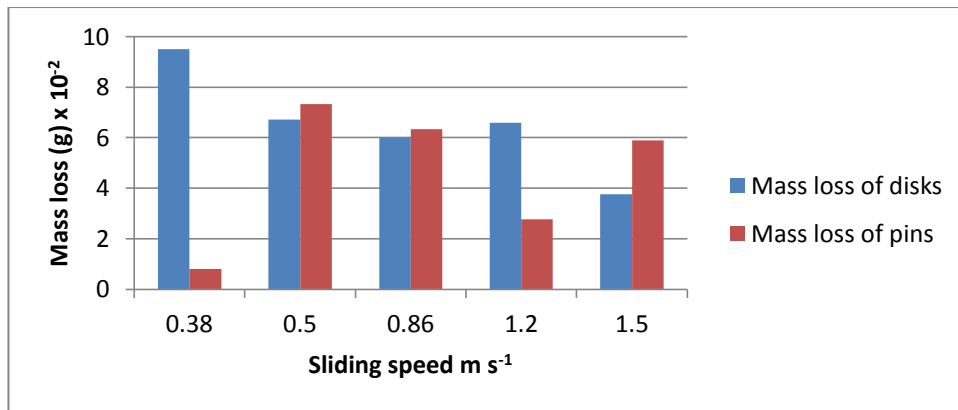


Figure 130 The total mass loss comparison of hardened steel disks and Ti base TiC coatings pins.

7.2.11. Coefficient of friction of Ti base TiC coatings pins against hardened steel disks

Table 58 and Fig. 131 show the trend of friction of the Ti base TiC pins and hardened steel disks sliding against each other at different constant sliding speeds and various normal loads.

Normal load (N)	Coefficient of friction at 0.38 m s^{-1}	Coefficient of friction at 0.5 m s^{-1}	Coefficient of friction at 0.86 m s^{-1}	Coefficient of friction at 1.2 m s^{-1}	Coefficient of friction at 1.5 m s^{-1}
10	0.61	0.50	0.33	0.50	0.27
20	0.28	0.35	0.26	0.27	0.34
30	0.35	0.34	0.25	0.28	0.29
40	0.27	0.31	0.34	0.33	0.29
50	0.44	0.24	0.25	0.31	0.24

Table 58 Coefficient of friction of Ti base TiC coatings pins against hardened steel disks.

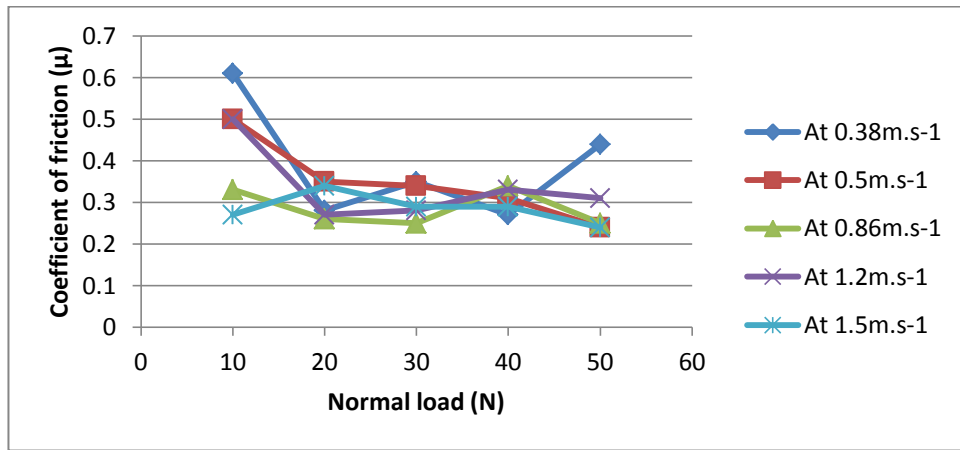


Figure 131 Coefficient of friction of Ti base TiC coatings pins against hardened steel disks.

Table 59 and Fig. 132 show the trend of friction Ti base TiC pins and hardened steel disks sliding against each other at different constant normal loads and various sliding speeds.

Sliding speed $m s^{-1}$	Coefficient of friction at 10 N	Coefficient of friction at 20 N	Coefficient of friction at 30 N	Coefficient of friction at 40 N	Coefficient of friction at 50 N
0.38	0.61	0.28	0.35	0.27	0.44
0.5	0.50	0.35	0.34	0.31	0.24
0.86	0.33	0.26	0.25	0.34	0.25
1.2	0.50	0.27	0.28	0.33	0.31
1.5	0.27	0.34	0.29	0.29	0.24

Table 59 Coefficient of friction of Ti base TiC coatings pins against hardened steel disks.

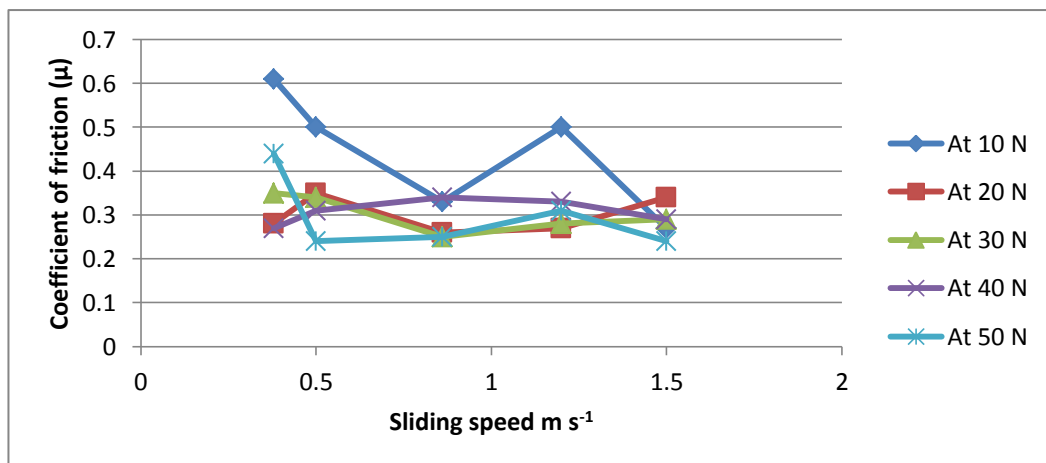


Figure 132 Coefficient of friction of Ti base TiC coatings pins against hardened steel disks.

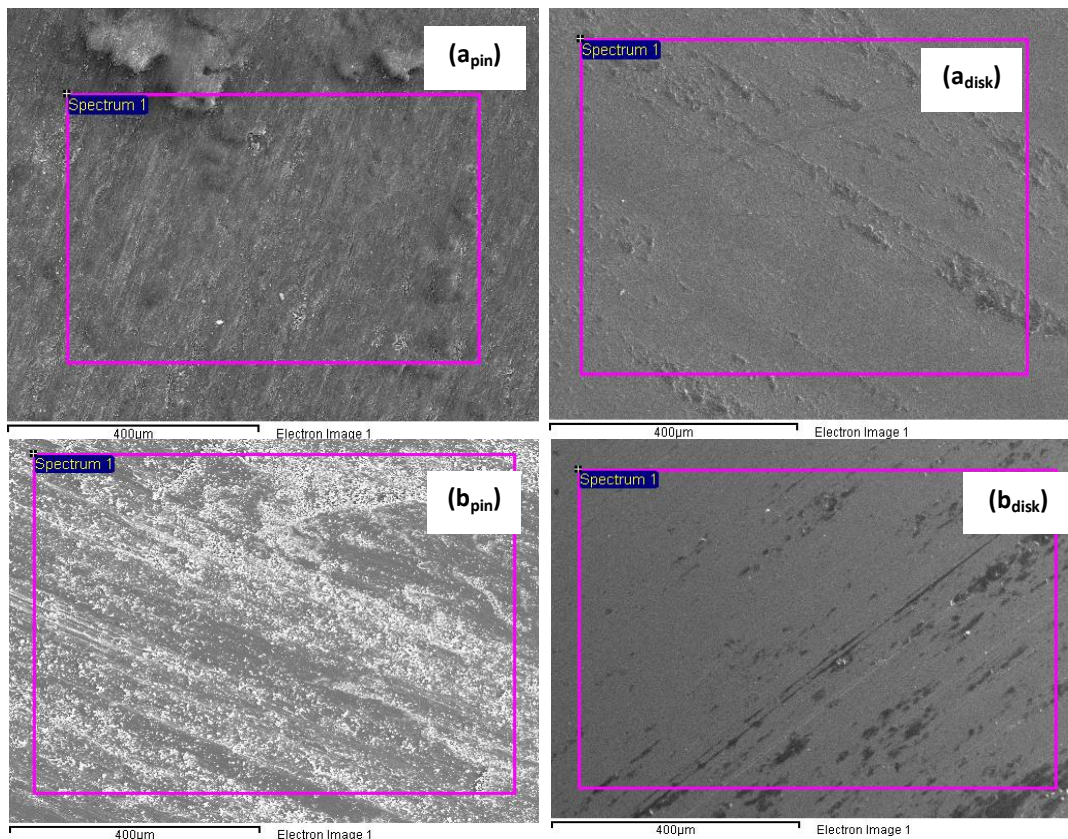
7.2.12. SEM micrographs of Ti base TiC coatings pins and hardened steel disks worn surfaces

Figs. 133-134 show the SEM micrographs and EDX analysis of the worn surfaces of the Ti base TiC composite coatings pins and wear tracks on the hardened steel disks respectively.

Tribo-corrosion maps for steels, titanium and titanium carbide materials

At a sliding speed of 0.38 m s^{-1} and normal loads of 10, 30 & 50 N; 0.5 m s^{-1} and 10 & 20 N; 0.86 m s^{-1} and 10, 20 & 30 N and at 1.2 m s^{-1} and 10 to 40 N high oxidation of the hardened steel occurred. Iron oxide was transferred to the pins' mating surfaces. The worn surfaces of the pins are not completely visible as they are masked by the transferred iron oxides Figs. 133(a_{pin}, c_{pin}) - 134(a_{pin}, c_{pin}). At 0.38 m s^{-1} and 20 & 40 N; 0.5 m s^{-1} and 30, to 50 N; 0.86 m s^{-1} and 30 N and at 1.5 m s^{-1} and 10 & 30 N higher oxidation rate of the pins occurred and comparatively less iron oxide transferred to the worn surfaces of the pins. The worn surfaces of the pins are showing adhesive and plastic deformation marks as well Figs. 133(b_{pin}, e_{pin}) - 134(b_{pin}, e_{pin}). At 0.86 m s^{-1} and 50 N; 1.2 m s^{-1} and 50 N and at 1.5 m s^{-1} and 20 & 40 N worn surfaces of the pins are showing marks of adhesive wear, plastic deformation and abrasive wear Figs. 133(d_{pin}) - 134(d_{pin}).

On the other hand for hardened steel disks at 0.38 m s^{-1} and 10 to 30 N; 0.86 m s^{-1} and 10, 20 & 40 N and at 1.2 m s^{-1} and 10 & 20 N adhesive wear and mild abrasive wear were found Figs. 133(a_{disk}, c_{disk}) - 134(a_{disk}, c_{disk}). At 0.38 m s^{-1} and 40 & 50 N normal load abrasive-oxidative wear occurred. At 0.5 m s^{-1} and 40 & 50 N; 0.86 m s^{-1} and 30 & 50 N; 1.2 m s^{-1} and 30 to 50 N and at 1.5 m s^{-1} and 20 to 50 N adhesive, plastic deformation, delamination and oxidative wear and little Ti transferred to wear tracks Figs. 133(b_{disk}, d_{disk}, e_{disk}) - 134(b_{disk}, d_{disk}, e_{disk}). While at 1.5 m s^{-1} sliding speed and 10 N normal load abrasive wear occurred.



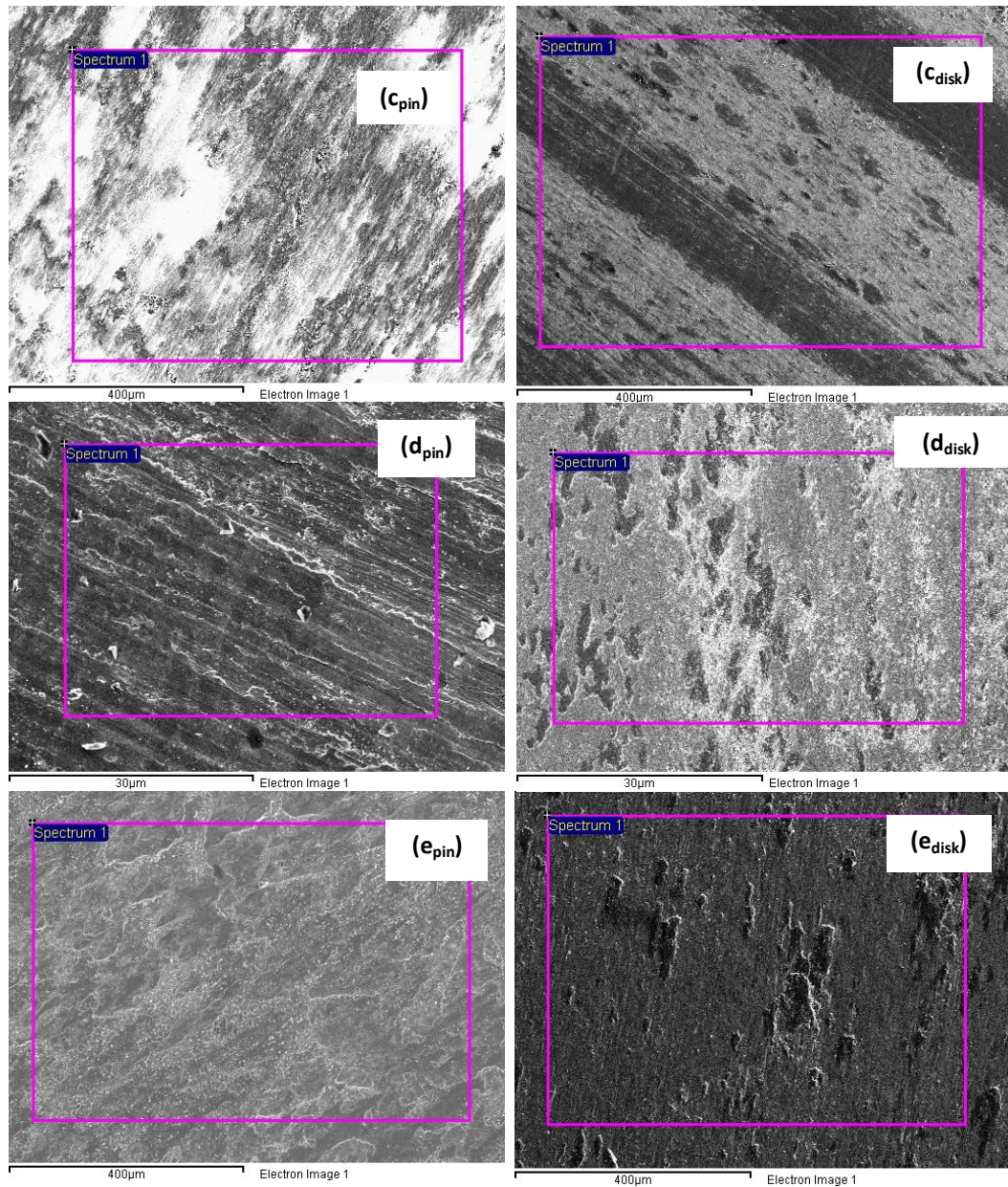
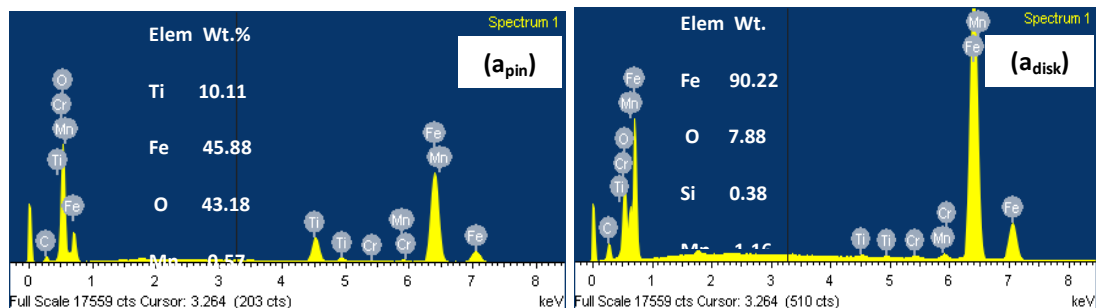


Figure 133 SEM micrographs of the worn surfaces of the TiC coatings pins and wear track of the hardened steel disks, (a) at normal load 30 N and sliding speed 0.38 m s^{-1} , (b) at 50 N and 0.5 m s^{-1} , (c) at 40 N and 0.86 m s^{-1} , (d) at 50 N and 0.86 m s^{-1} and (e) at 50 N and 1.5 m s^{-1} .

7.2.13. EDX analysis of Ti base TiC coatings pins and hardened steel disks worn surfaces

Fig. 134 shows the EDX analysis of the worn surfaces of the Ti base TiC composite coatings pins and wear tracks on the hardened steel disks.



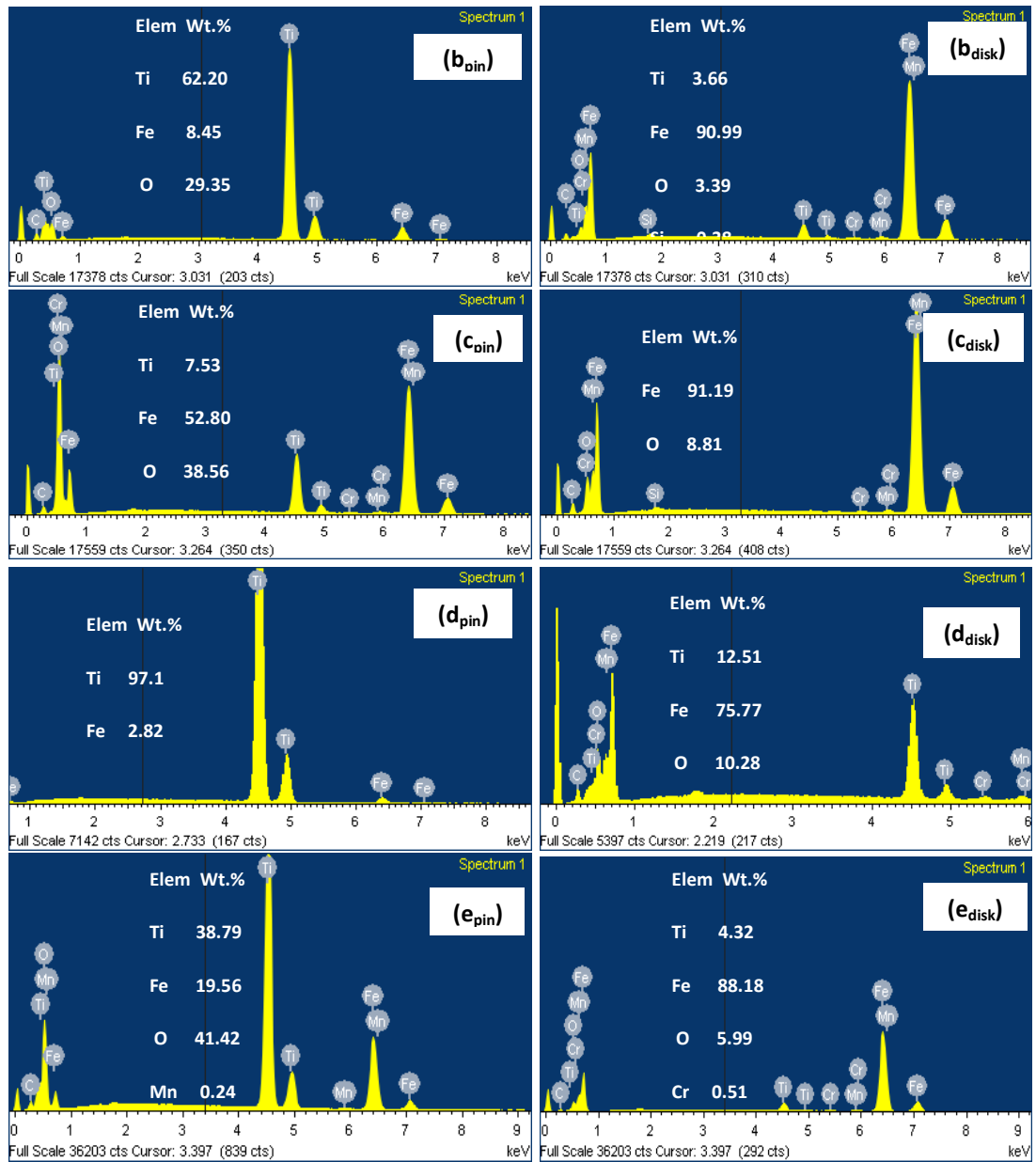


Figure 134 EDX analysis of the wear surfaces of the TiC coatings pins and wear track of the hardened steel disks, (a) at normal load 30 N and sliding speed 0.38 m s^{-1} , (b) at 50 N and 0.5 m s^{-1} , (c) at 40 N and 0.86 m s^{-1} , (d) at 50 N and 0.86 m s^{-1} and (e) at 50 N and 1.5 m s^{-1} .

7.2.14. SEM micrographs of wear debris of Ti base TiC coatings pins against hardened steel disks

Fig.135 shows the SEM micrographs of the wear debris of the Ti base TiC composite coatings pins and the hardened steel disks sliding against each other.

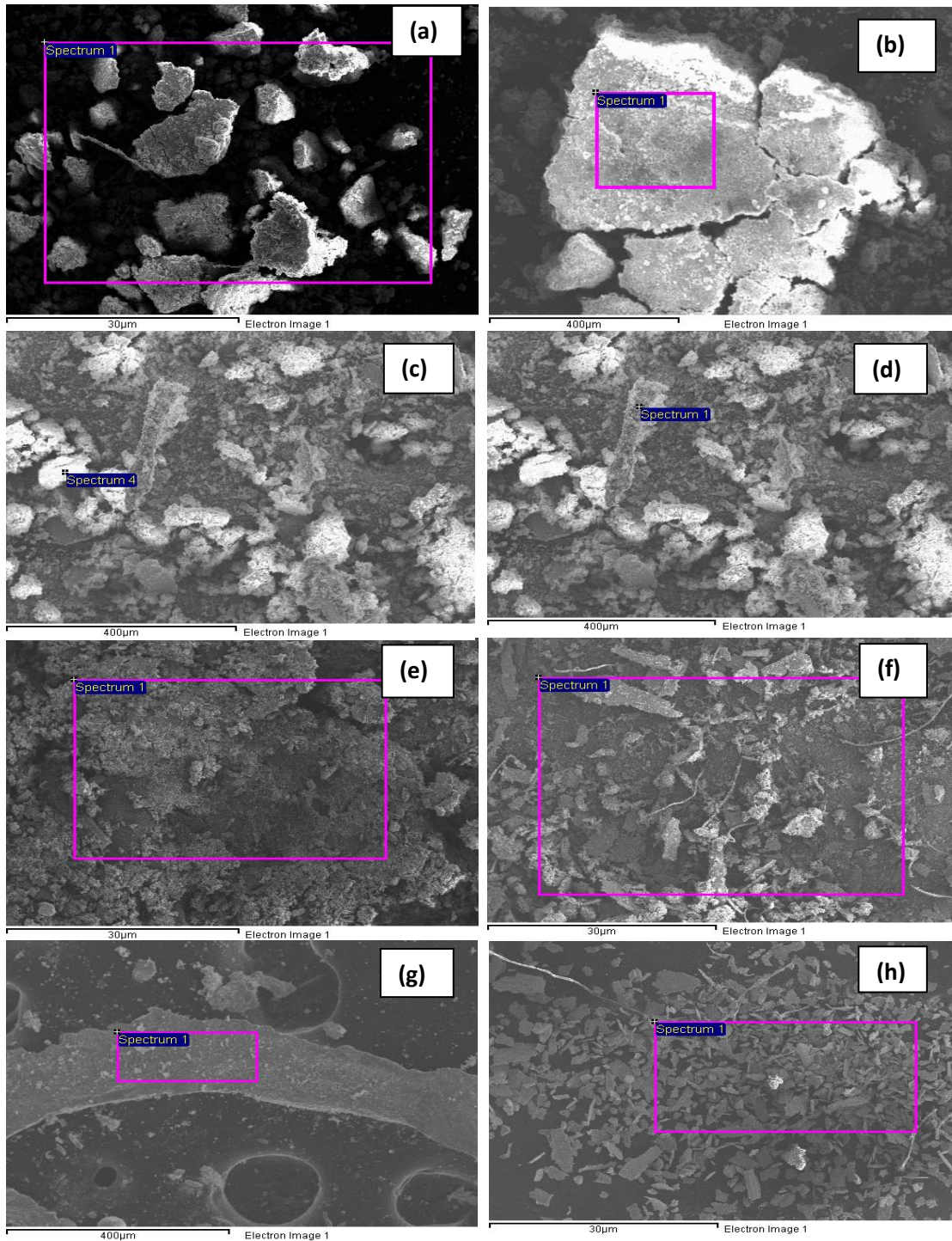


Figure 135 SEM micrographs of wear debris of Ti base TiC coatings against hardened steel, (a) at sliding speed 0.38 m s^{-1} and normal load 30 N, (b) at 0.38 m s^{-1} and 30 N at high magnification, (c) at 0.5 m s^{-1} and 40 N point analysis, (d) at 0.5 m s^{-1} and 40 N point analysis, (e) at 0.5 m s^{-1} and 50 N, (f) at 0.86 m s^{-1} and 50 N, (g) at 1.2 m s^{-1} and 20 N high magnification, and (h) at 1.5 m s^{-1} and 50 N.

7.2.15. EDX analysis of wear debris of Ti base TiC coatings pins against hardened steel disks

Fig. 136 shows the EDX analysis of the wear debris of the Ti base TiC composite coatings pins and hardened steel disks sliding against each other.

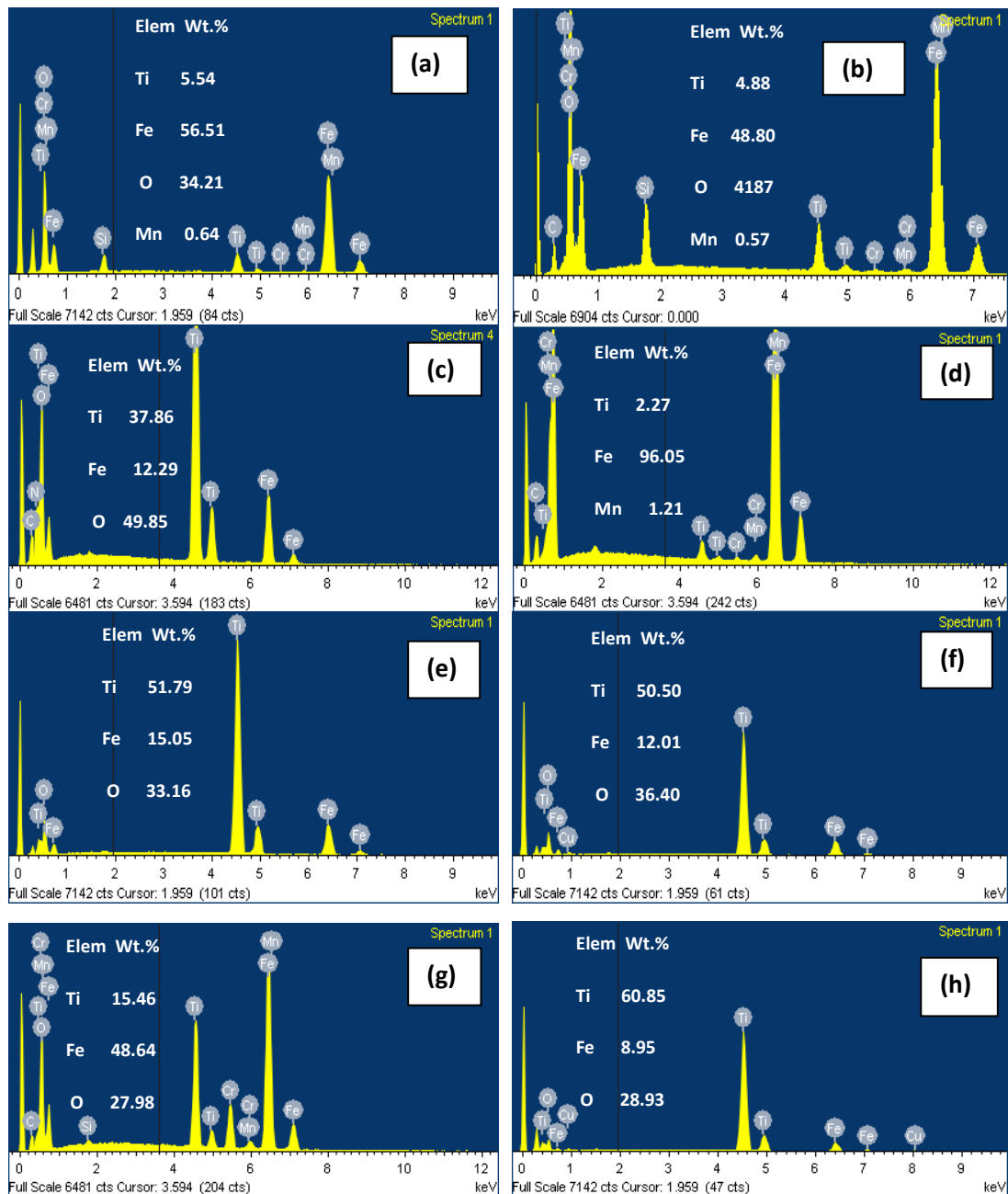


Figure 136 EDX analysis of wear debris of Ti base TiC coatings against hardened steel, (a) at sliding speed $0.38 m s^{-1}$ and normal load 30 N, (b) at $0.38 m s^{-1}$ and 30 N at high magnification, (c) at $0.5 m s^{-1}$ and 40 N point analysis, (d) at $0.5 m s^{-1}$ and 40 N point analysis, (e) at $0.5 m s^{-1}$ and 50 N, (f) at $0.86 m s^{-1}$ and 50 N, (g) at $1.2 m s^{-1}$ and 20 N high magnification, and (h) at $1.5 m s^{-1}$ and 50 N.

Figs. 135-136 show the SEM micrographs and EDX analysis of the wear debris respectively. The composition of wear debris mainly consisted of Ti, O and Fe with high percentage of disks material at lower sliding speeds and higher percentage of coated pins material at higher sliding speeds Fig. 136. This confirms that debris particles came from the both specimens and counterparts materials. The shapes of the wear debris were different for

lower sliding speeds and for the higher sliding speeds irrespective of normal loads. The wear mechanisms change with the change in sliding speeds and wear modes are dependent on sliding speeds and normal loads.

From the SEM micrographs of the wear debris, the physical nature and shapes of the wear debris are different for the range of sliding speeds Figs. 135(a-h). The shape of the wear debris is changed with the increase in sliding speed. The compact brown powdery wear debris came from counterface at lower sliding speeds for the range of normal loads Figs. 135(a-b) - 136(a-b) and at lower normal loads for the range of sliding speeds Figs. 135(, g) - 136(g). The grey oxide powdery products came from Ti base TiC composite coatings pins at higher normal loads at sliding speeds 0.5, 0.86 and 1.5 m s⁻¹ Figs. 135(c, e-f, h) - 136(c, e-f, h). The micro flake-like shape particles in wear products came from hardened steel disks Figs. 135(d, g) - 136(d, g). The species of Ti, O and Fe in EDX analysis Fig. 136(a-h) are evident that the oxides of both Ti and iron were present in the wear debris. The brown powdery brittle wear products came from the iron oxide at lower normal loads and the grey powdery wear products came from Ti oxide at higher normal loads for the range of sliding speeds. As clear from the nature of the wear debris, the wear mechanisms for this tribo couple were the combinations of micro abrasion, oxidative wear, iron oxide transfer, plastic deformation, micro delamination, micro adhesive, micro abrasive and oxidative wear for the range of sliding speeds and normal loads.

7.2.16. Optical micrographs of coatings layers on Ti pins

Fig. 137 shows optical micrographs of the cross sections of the Ti base TiC coatings pins' coated surfaces thickness. Fig. 137(a) shows the thickness of the finish surface of the coating prior to testing. Figs. 137(b-c) show the thickness of coatings left after the tests carried out.

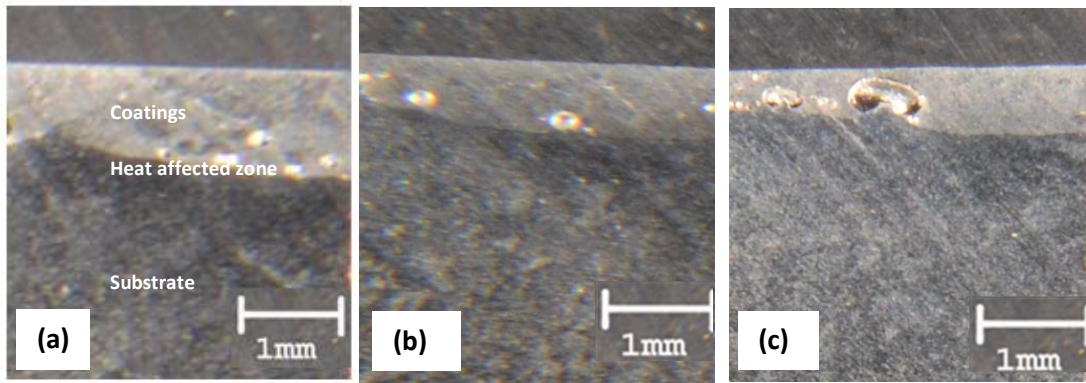


Figure 137 Optical micrographs of Ti base TiC coatings pins, (a) thickness of the coatings layer after grinding the surface of the coatings, (b) thickness of the coatings layer after test at sliding speed 1.2 m s^{-1} and normal load 50 N and (c) thickness of the coatings layer after test at sliding speed 1.5 m s^{-1} and normal load 40 N.

7.2.17 Experimental error

Table 60 and Fig. 138 show the mass losses at repeat tests and experimental error of this tribo system respectively. The experimental error (repeatability) for Ti base TiC composite coatings pins against hardened steel disks, calculated on the basis of repeat tests carried out at sliding speed 0.5 m s^{-1} and normal load 50 N (number of tests carried out = $n=3$). The experimental error 8% was found for this tribo-couple on the basis accepted average value of mass loss of the TiC pins for these tests [193, 194].

Number of experiment =n	Sliding speed (m s^{-1})	Normal load (N)	Mass loss of Ti base TiC coatings pin (g)	Experimental error %
1	0.5	50	0.0514	+ 5.33
2	0.5	50	0.0501	+ 2.66
3	0.5	50	0.0449	- 7.99
Average			0.0488	- 8 to + 8

Table 60 Mass loss of Ti base TiC composite coatings pins against hardened steel disks for repeat tests at and experimental error.

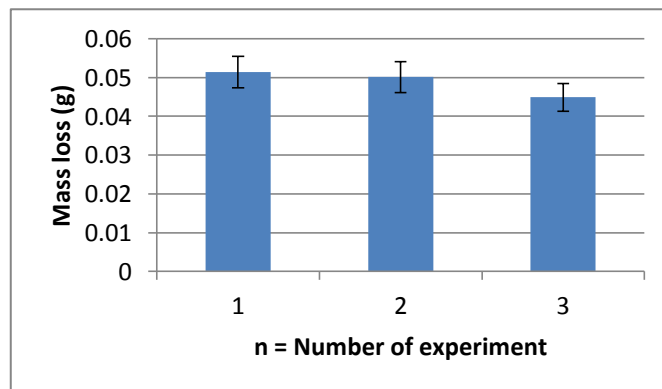


Figure 138 Experimental errors (8%) for the Ti base TiC coatings pins against steel disks.

7.3. Discussion

7.3.1. Wear mechanisms and regimes

The dry sliding wear tests of TiC composite coatings on Ti substrate against hardened steel were carried out. TiC composite coatings showed higher wear resistance against its counterpart Figs. 121-125. The higher wear resistance of TiC composite coatings, which resulted in very mild and mild wear against its counterpart Fig. 139(a), is attributed to its high hardness, thickness of the coatings layer on the substrate, good internal (compressive) stress level, load bearing capacity i.e. the ability of a coating-substrate system to withstand load on the coated surface without spalling or cohesion failure and due to favourable coefficient of thermal expansion of substrate and coatings materials [55]. The counterpart also showed mild wear against Ti base TiC composite coatings due to its high hardness Fig. 139(b). When this hard metal rubbed against TiC composite coatings there was very low chance of micro-welding taking place between mating surfaces which reduced the tendency of adhesion between pins and disks contacts during sliding [122], which resulted in mild wear of both materials Fig. 139.

The fluctuation in wear rates of Ti base TiC coating and hardened steel, against each other, within the mild wear regimes for the range of sliding speeds and normal loads, Figs. 126-127 & Figs. 128-129 respectively; because of the formation of mechanical mixed layer and variation in temperature between contact areas. The increase in flash temperature and frictional heating results in thermal softening effects and oxidation of the mating surfaces during sliding for different combinations of sliding speeds and normal loads. Both materials behaved differently under the ambient conditions when temperature changes occurred between sliding contacts. The wear rate of Ti base TiC coatings increased with the increase in normal loads for the range of sliding speeds Figs. 126-127. The same trend of wear was found in the study of 303SS base TiC coatings dealt with in Chapter 5, by Tyler L et al. in the study of sliding wear of TiC and Ti(C, N) cermet prepared with a stoichiometric Ni Al binder [190] and in the work of the others researchers found in literature for the composite coatings, where coatings were carried out by the different methods [55, 143, 171]. These observations are in consistence with the previous studies that demonstrate the total mass loss during sliding depends upon both the sliding time and applied load [29, 191].

The frictional behaviour of metals, when sliding in the air against one another, depends on the composition and microstructure of the materials and on the tests conditions [62]. The

coefficient of friction (μ) data and plots are on the basis of average values that were observed for each combination of sliding speed and normal load during sliding. Figs. 131-132 show the coefficient of friction is higher at 10N for the range of sliding speeds. Higher coefficient of friction at this normal load might have been due to more actual areas of contact and lower frictional heat but for the rest of normal loads the values of μ was found between 0.25-0.35 for the range of sliding speeds. The lower values of μ at those combinations of sliding speeds and normal loads might have been because of higher frictional heat that resulted in oxidation and surface softening effects. Generally the lower coefficient friction for this tribo-system might have been because of poor adhesion between the incompatible pins and disks material [55]. The fluctuation in friction force was observed, either might have resulted from the wear particles that trapped between the mating surfaces during sliding and changed the contact conditions or from oxidation, plastic flow and adhesion effects for various combinations of the sliding speeds and normal loads [161, 181].

From Fig. 140(a) for the wear mechanisms, “micro-abrasion”, TiC coatings was not prone to tribo-oxidation degradation due to the humidity in the environment for these combinations of sliding speeds and normal loads. It may be possible that increased asperity contact heating, arising from contact loads and sliding speeds, eliminates absorbed moisture on the TiC surfaces and inhibits tribo-oxidation wear effects. The reduced tribo-chemical oxidation of TiC in this regime suggested that wear in this regime was largely controlled by micro-abrasion (mechanically) of TiC coatings by hard carbides in the hardened steel or by brittle iron oxide particles, SEM micrographs of the worn surfaces Figs. 133(a_{pin}, c_{pin}) and EDX analysis of the worn surfaces 134(a_{pin}, c_{pin}). The transferred Fe oxide formed tribo-layers on the pins’ mating surfaces [190, 192], then the wear of that layers occurred. The wear debris generated in this wear mechanisms regime was powder of iron oxide had reddish brown appearance, brittle in nature and micro-flake-like shape iron particles Fig. 135(a, b, g). EDX analysis of the wear debris showed dominance of Fe and O Fig. 136(a, b, g) that changed the order of wear magnitude in hardened steel for these combinations of sliding speed and normal loads due to abrasive and oxidative wear, Fig. 140(b), against the TiC composite coatings surface asperities which were less prone to tribo-oxidation polishing effects. Same observations were found by S. Wilson, A. T. Alpas for TiN coating against HSS [74]. Thus less wear rate of Ti base TiC composite coatings as

Tribo-corrosion maps for steels, titanium and titanium carbide materials

compare to wear rate of hardened steel was found for these combinations of sliding speeds and normal loads Tables 48-52, 57 and Figs. 121-125, 130, 139(a).

For the wear mechanisms, “adhesive-oxidative wear”, Fig. 140(a) higher wear rate of TiC coatings than that of hardened steel was found in this wear mechanisms regime Figs. 122-124, 130. Higher oxidation of the pins occurred and comparatively less iron oxide transferred to the worn surfaces of the pins, EDX analysis of the worn surfaces Figs. 134(b_{pin}, e_{pin}). The worn surfaces of the pins show adhesive and plastic deformation marks as well, SEM micrographs of the worn surfaces Figs. 133(b_{pin}, e_{pin}). Analysis of the wear products for these tests, suggest that the cause of wear of TiC coatings were mechanical as well as by tribo-chemical (tribo-oxidation) degradations mechanisms, EDX analysis of the wear debris Figs. 136(c-e). The micro (very small) flaky, metallic debris in wear products, Figs. 135(c-e), indicates that adhesive, delamination wear occurred along with oxidation for TiC coatings [137]. Rabinowicz E. [177] suggests that the size of the flaky wear debris is linked with the severity of adhesive wear. The presence of micro size compact wear products implies that coating undergone mild wear. The second type of wear mechanism in this regime was thought to be tribo-oxidational wear. The presence of dark grey powdery particles and compact scales in wear debris Fig. 135(e) and Fig. 136(e) are the evidence of this wear mechanism. For the counterface Fig. 140(b), the presence of the micro flaky iron debris Fig. 135(c-d) and composition of Ti, Fe and O in the wear debris Fig. 136(c) confirm that wear occurred by adhesive, mild delamination and oxidative wear along with Ti transfer in this wear regime.

For the wear mechanisms, “oxidative-adhesive wear”, Fig. 140(a), the increase in sliding speeds and normal loads, resulted increase in mechanical effects and in bulk temperature led to wear of Ti base TiC coatings pins by adhesive, plastic deformation and delamination wear along with oxidation of pins mating surfaces in this wear regime. SEM micrograph of the worn surface of the pin Fig. 133(d_{pin}) shows marks of adhesive wear and plastic deformation wear. EDX analysis Fig. 134(d_{pin}) shows the absence of O on the worn surface of the pin. The coatings surfaces damage was increased by adhesion, mild delamination along with ductile deformation of the TiC coatings due to frictional heating effects. The same observations are found in literature for the pin-on-disk experiment of TiN versus HSS [171]. The increased frictional heating effects appear to introduce rapid ductile wear of the coatings that result in transition in wear mechanisms [6]. The wear debris is consisted of

comparatively bigger micro flakes and oxide powder from TiC coatings and counterpart, SEM micrograph of the wear debris Fig. 135(f). EDX analysis of the wear debris Fig. 136(f) shows the presence of Ti, Fe and O species with larger percentage of Ti and O; which indicates that oxidation of the pins' mating surface occurred as well at higher sliding speeds and normal loads but the rate of removal of oxide was greater than that of the rate of oxidation. The further transitions in wear mechanisms regime seemed to be occurring with increase in sliding speed Fig 125 as the sizes of the micro flake in wear debris are smaller than that of the former combination of sliding speed and normal load Fig. 135(h) and Fig 136(h).

On the other hand, for the hardened steel Fig. 140(b), the wear rate was lower than that of the TiC coatings for these combinations of sliding speed and normal loads Table 57 and Fig. 130. The lower wear rate of counterface is attributed to the thermal softening effects on the specimens mating surfaces that led to transfer of pins material to counterface Fig. 133(d-e) and Fig. 134(d-e). The transitions in wear modes and wear mechanisms of the metals in sliding contact have been attributed to their increased sensitivity to the onset of intense shear location phenomena, surface sliding temperatures and shear deformation rates, in the wear contact zone [178].

7.3.2 Wear mode regimes and maps

The development of wear maps is a useful tool to study and predict the wear behaviour of metals sliding against each other at different sliding speeds and normal loads. The wear mode regimes, namely (a) very mild wear (b) mild wear (c) medium wear and (d) severe wear are defined in consistent with the research work found in literature [34, 72], experimental work carried out (dealt with in Chapters 4, 5 and 6), tests results, mass loss data, wear rate (volume loss rate), physical observations of the worn surfaces, SEM and EDX of the worn surfaces and the wear debris. The mild wear results in dark smooth worn surfaces, lower wear rate and oxide powdery wear debris at the end of test due to oxidation during sliding of mating surfaces. On the other hand, bright, rougher worn surfaces and larger metallic wear debris at the end of sliding tests and higher wear rates results in medium and severe wear [33]. The Wear modes regimes limits are as follows:

- a) Very mild wear $\leq [0.1 \times 10^{-12} \text{ (m}^3 \text{ m}^{-1})]$
- b) $[0.1 \times 10^{-12} \text{ (m}^3 \text{ m}^{-1})] < \text{mild wear} \leq [1.12 \times 10^{-12} \text{ (m}^3 \text{ m}^{-1})]$
- c) $[1.12 \times 10^{-12} \text{ (m}^3 \text{ m}^{-1})] < \text{medium wear} \leq [3.35 \times 10^{-12} \text{ (m}^3 \text{ m}^{-1})]$
- d) Severe wear $> [3.35 \times 10^{-12} \text{ (m}^3 \text{ m}^{-1})]$

Fig. 139, the various wear mode regimes are identified for pins and disks during dry sliding contact as a function of sliding speeds, showing distinctive differences in the wear mode transitions. It can be clearly seen that very mild wear is more prevalent with respect to normal load for TiC coatings pins Fig. 139(a) whereas, mild wear is prevalent for the hardened steel Fig. 139(b). It can be clearly seen that the medium wear occurred only for one combination of sliding speed and normal load for TiC coatings and severe wear did not occur for both specimen and counterpart. Moreover, in Fig. 139(a-b), the combination of the very mild and mild wear zone can be regarded as the safe operation zone for the Ti base TiC composite coatings and hardened steel against each other for this range of sliding speeds and normal loads.

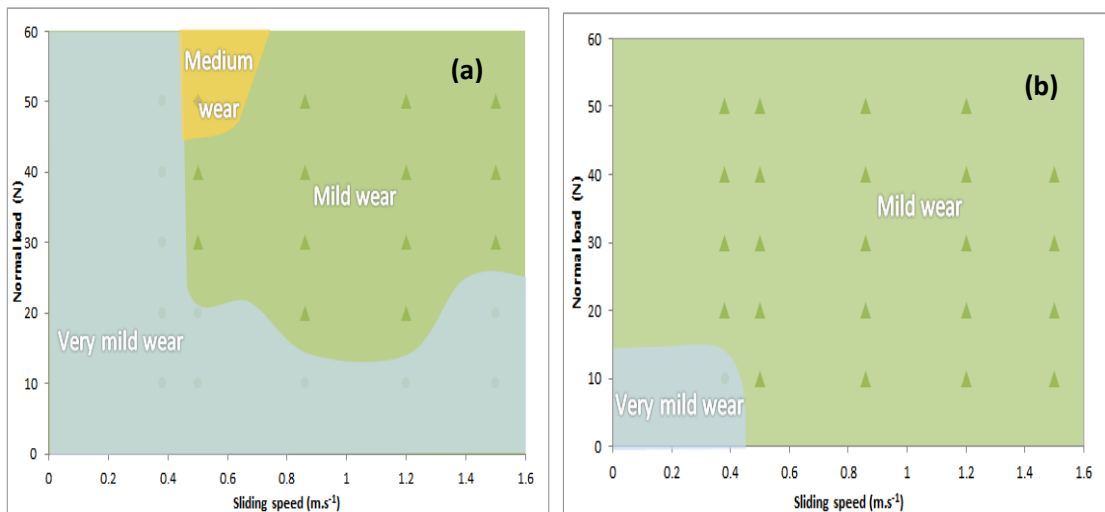


Figure 139 Wear modes maps, (a) Ti base TiC coatings pins against hardened steel disks and (b) hardened steel disks against Ti base TiC coatings pins.

7.3.3 Wear mechanism regimes and maps

Wear mechanism maps are useful tools for analysing the change in wear regime over a multi-parameter space. Wear rates of Ti base TiC coatings pins and hardened steels disks are represented in wear mechanisms maps form on the normal load versus sliding speeds

axis Fig. 140. The wear mechanism regimes below are based on the experimental observations and tests results as discussed above. These can be summarized as:

- Oxidative – adhesive wear
- Adhesive - oxidative wear
- Oxidative – abrasive wear
- Abrasive - oxidative wear
- Micro-abrasion
- Abrasive wear

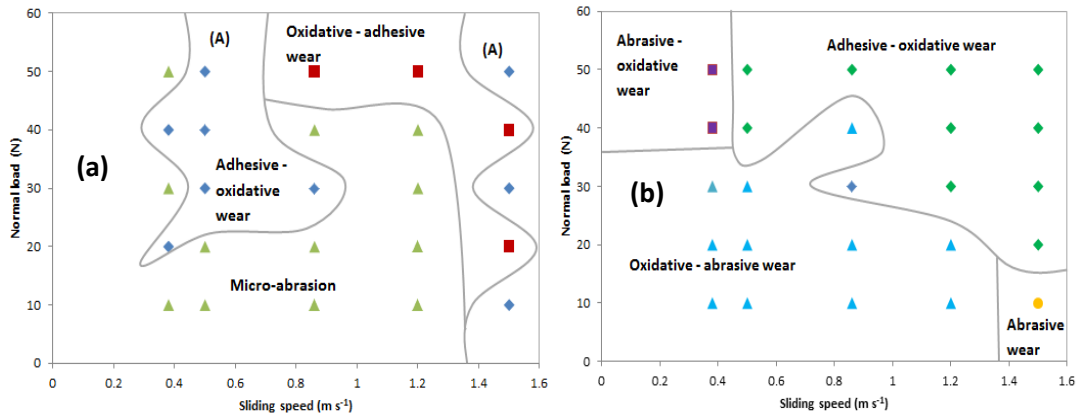


Figure 140 Wear mechanisms maps, (a) Ti base TiC coatings pins against hardened steel disks and (b) hardened steel disks against Ti base TiC coatings pins.

A tribo-system approach has been adopted rather than having to investigate Ti base TiC coatings and hardened steel wear behaviour individually. Fig. 140 shows the wear mechanisms maps of specimen and counterface; the boundaries on the diagrams are only approximate. As clear from the Fig. 140(a) for the TiC coatings pins against hardened steel disks micro-abrasion wear is predominated along with adhesive and oxidative wear. For hardened steel disk against TiC coatings pins adhesive – abrasive - oxidative wear is predominated, Fig. 140(b).

7.4. Wear modes comparison between Ti base TiC coatings sliding against hardened steel counterface and 303SS base TiC coatings sliding against alumina counterface [Chapter 5]

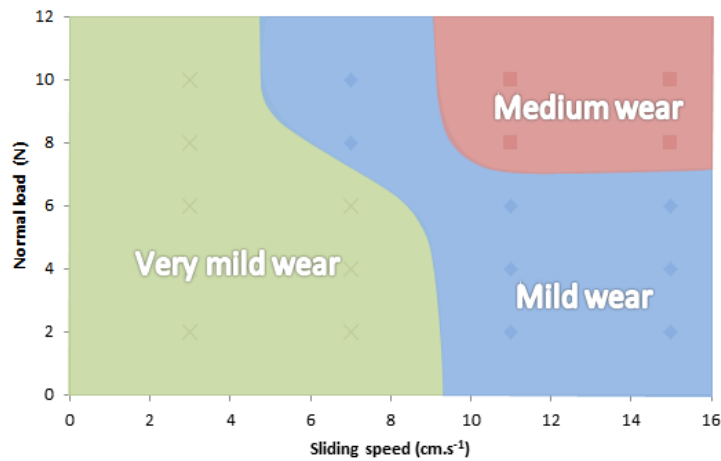


Figure 141 Wear mode map for 303stainless steel base TiC composite coatings disk against alumina ball (taken from Chapter 5).

Fig. 141 shows the range of sliding speeds and normal loads dealt with in chapter 5 for 303SS base TiC composite coatings, involved in the present study, for comparison between different substrate coated with the similar composite coatings by the similar coating method i.e. TIG welding torch melting method. It is clear from these figures that the wear rate of the 303SS base TiC composite coatings is higher than that of the Ti base TiC composite coatings Fig. 139(a) for the range of sliding speeds and normal loads of the previous work. The higher wear resistance of the Ti base TiC composite coatings is attributed to the dense structure with low porosity of the coatings Fig. 137(a), [158] and the absence of cracking as the substrate and coating system have closer/ favourable coefficient of thermal expansion [55].

7.4. Conclusions

1. TiC composite coatings made by TIG process were found to be stable and sliding wear resistant on Ti substrate. Hence TIG welding torch melting coating method is comparable with the other coating process.
2. The sliding wear of TiC hard coatings can change significantly with variation of parameters such as normal load and sliding speed.

Tribo-corrosion maps for steels, titanium and titanium carbide materials

3. Significant levels of iron oxide were transferred to TiC coatings pins at lower sliding speed while some transfer of pins material to disks occurred at higher sliding speeds and normal loads due to increases in frictional heat.

4. The wear mechanisms involved in the wear of TiC coatings were included one or more of the following: TiC micro-abrasion, Fe oxide transfer, adhesive, delamination and oxidative wear.

Chapter 8

Tribo-corrosion maps for titanium uncoated and coated with titanium carbide composite coatings

8.1. Introduction

The use of titanium is limited in a number of industries with regards to sliding applications because of its poor tribological properties and inability to form protective oxide layer. By development and using the different methods and techniques of surface engineering the potential applications of the treated titanium can be increased by improving its tribological properties. In this chapter the wear behaviour of Ti uncoated and coated with TiC composite coatings has been discussed in contents of improvement in tribological properties due to surface treatment by using tribo-corrosion maps techniques.

8.2. Wear tests results

Dry sliding wear tests were carried out in a pin-on-disk sliding wear testing rig, Fig. 34, of Ti (uncoated and coated with TiC coatings) pins against hardened steel disks as counterface; 25 combinations of sliding speeds and normal loads for each material; as per experimental conditions mentioned in Section 3.5. The sliding distance 5,560 m and number of revolutions 30,000 were kept constant for all tests. The pin surface coatings was carried out by TIG welding torch melting method, as mentioned in Section 3.6, Chapter 3. The effects of change in sliding speeds and normal loads on wear behaviour of Ti (uncoated and coated with TiC coatings) pins against hardened steel (A.I.S.I. 0-1-Ground Flat Stock) disks, have been compared to check the improvement in the wear resistance of the substrate after TiC coatings. Tribo-corrosion maps have been constructed for both uncoated and coated materials on the basis of wear rate, total mass loss, frictional behaviour, worn surfaces analysis, wear debris analysis, wear mode and wear mechanisms against hardened steel. Experimental data taken from chapter 6 and 7 is as below:

8.2.1 Wear at 0.38 m s^{-1} sliding speed for the range of normal loads

Table 61 and Fig. 142 show the wear rate of Ti (uncoated and coated with TiC coatings) pins against hardened steel disks at sliding speed 0.38 m s^{-1} for the range of normal loads.

Normal load (N)	Wear rate of Ti/TiC coatings pin ($\text{m}^3 \text{m}^{-1}$) $\times 10^{-12}$ at 0.38 m s^{-1}	Wear rate of Ti pin ($\text{m}^3 \text{m}^{-1}$) $\times 10^{-12}$ at 0.38 m s^{-1}
10	0.004	2.23
20	0.098	1.63
30	0.018	3.6
40	0.095	6.16
50	0.084	9.88

Table 61 Wear rate of Ti and Ti base TiC coatings pins.

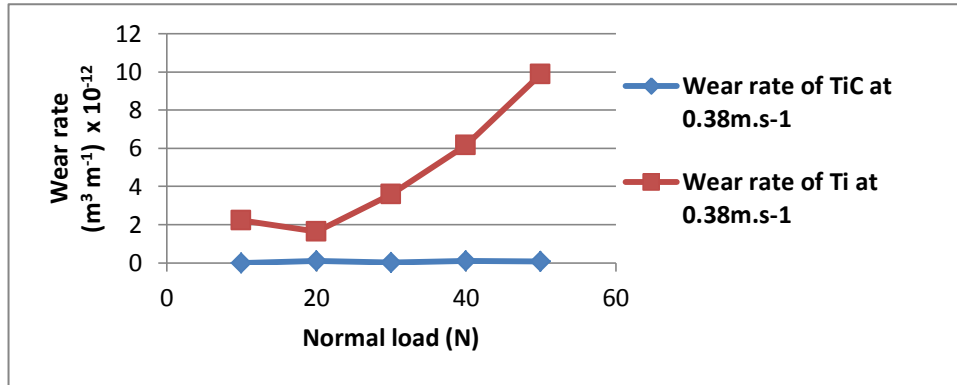


Figure 142 Wear rate of Ti and Ti base TiC coatings pins.

8.2.2. Wear at 0.5 m s^{-1} sliding speed for the range of normal loads

Table 62 and Fig. 143 show the wear rate of Ti (uncoated and coated with TiC coatings) pins against hardened steel disks at sliding speed 0.5 m s^{-1} for the range of normal loads.

Normal load (N)	Wear rate of Ti/TiC coatings pin ($\text{m}^3 \text{m}^{-1}$) $\times 10^{-12}$ at 0.5 m s^{-1}	Wear rate of Ti pin ($\text{m}^3 \text{m}^{-1}$) $\times 10^{-12}$ at 0.5 m s^{-1}
10	0.011	1.13
20	0.040	1.28
30	0.102	2.60
40	0.885	2.87
50	1.641	4.42

Table 62 Wear rate of Ti and Ti base TiC coatings pins.

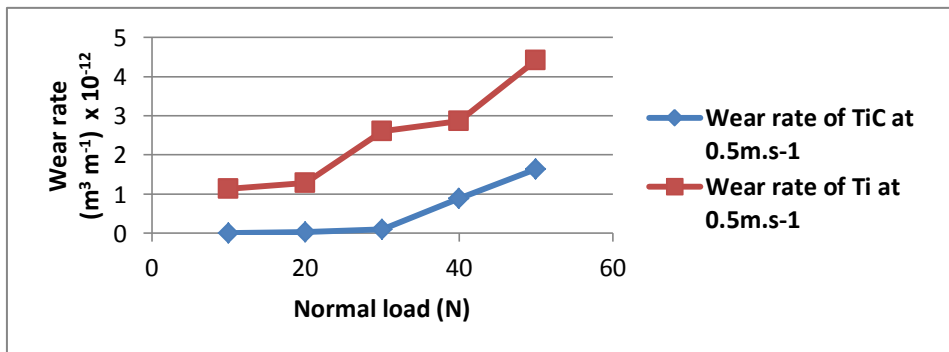


Figure 143 Wear rate of Ti and Ti base TiC coatings pins.

8.2.3. Wear at 0.86 m s⁻¹ sliding speed for the range of normal loads

Table 63 and Fig. 144 show the wear rate of Ti (uncoated and coated with TiC coatings) pins against hardened steel disks at sliding speed 0.86 m s⁻¹ for the range of normal loads.

Normal load (N)	Wear rate of Ti/TiC coatings pin (m ³ m ⁻¹) x 10 ⁻¹² at 0.86 m s ⁻¹	Wear rate of Ti pin (m ³ m ⁻¹) x 10 ⁻¹² at 0.86 m s ⁻¹
10	0.091	0.75
20	0.161	1.25
30	0.954	3.05
40	0.113	4.98
50	0.994	11.92

Table 63 Wear rate of Ti and Ti base TiC coatings pins.

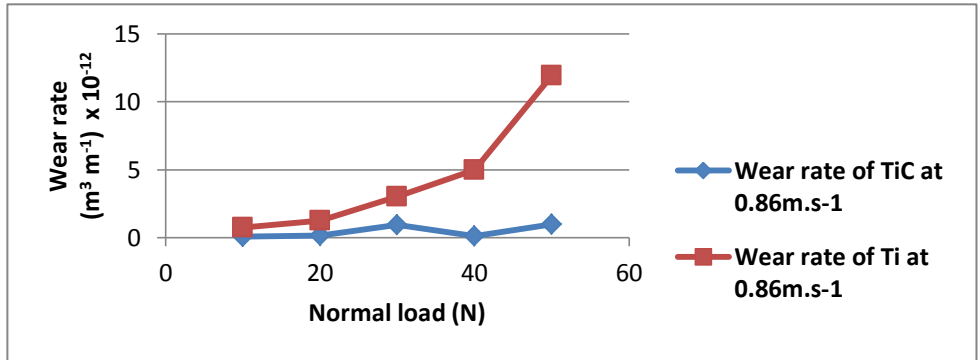


Figure 144 Wear rate of Ti and Ti base TiC coatings pins.

8.2.4. Wear at 1.2 m s⁻¹ sliding speed for the range of normal loads

Table 64 and Fig. 145 show the wear rate of Ti (uncoated and coated with TiC coatings) pins against hardened steel disks at sliding speed 1.2 m s⁻¹ for the range of normal loads.

Normal load (N)	Wear rate of Ti/TiC coatings pin (m ³ m ⁻¹) x 10 ⁻¹² at 1.2 m s ⁻¹	Wear rate of Ti pin (m ³ m ⁻¹) x 10 ⁻¹² at 1.2 m s ⁻¹
10	0.048	0.54
20	0.095	0.88
30	0.475	6.38
40	0.786	8.08
50	0.753	22.36

Table 64 Wear rate of Ti and Ti base TiC coatings pins.

Tribo-corrosion maps for steels, titanium and titanium carbide materials

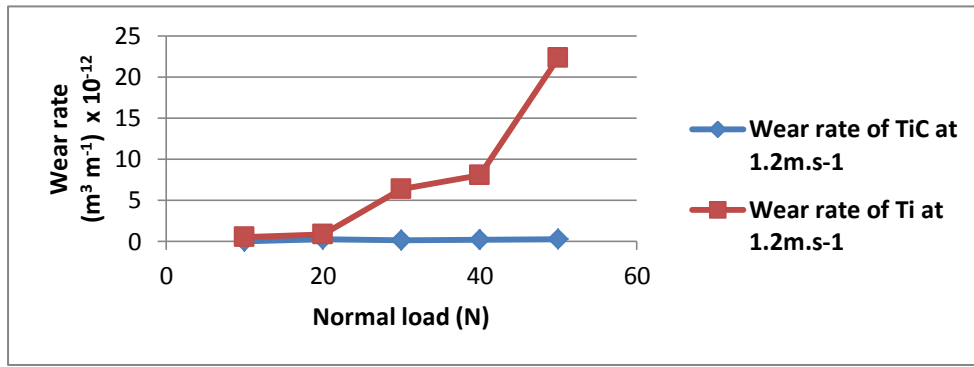


Figure 145 Wear rate of Ti and Ti base TiC coatings pins.

8.2.5. Wear at 1.5 m s⁻¹ sliding speed for the range of normal loads

Table 65 and Fig. 146 show the wear rate of Ti (uncoated and coated with TiC coatings) pins against hardened steel disks at sliding speed 1.5 m s⁻¹ for the range of normal loads.

Normal load (N)	Wear rate of Ti/TiC coatings pin ($\text{m}^3 \text{m}^{-1} \times 10^{-12}$ at 1.5 m s ⁻¹)	Wear rate of Ti pin ($\text{m}^3 \text{m}^{-1} \times 10^{-12}$ at 1.5 m s ⁻¹)
10	0.048	0.76
20	0.095	0.63
30	0.475	6.46
40	0.786	9.25
50	0.753	36.71

Table 65 Wear rate of Ti and Ti base TiC coatings pins.

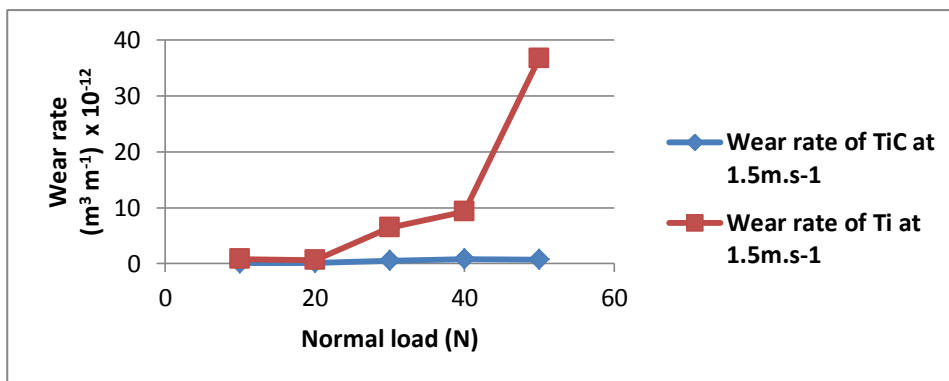


Figure 146 Wear rate of Ti and Ti base TiC coatings pins.

Tables 61-65 and Figs. 142-146 show the wear rate comparison of Ti and Ti base TiC composite coatings pins against hardened steel disks at different constant sliding speeds for the range of normal loads. It is clear from these figures that the wear rate of the substrate was higher than that of the coatings for all combinations of sliding speeds and normal loads. Moreover, the wear rate difference is prominent over the normal load 20 N for the range of sliding speeds.

8.2.6. Wear rate of Ti against hardened steel at constant sliding speeds and various normal loads

Table 66 Fig. 147 show the wear rate of Ti pins against hardened steel disks during dry sliding wear at different constant sliding speed and various normal loads.

Normal load (N)	Wear rate ($\text{m}^3 \text{m}^{-1}$) $\times 10^{-12}$ at 0.38 m s ⁻¹	Wear rate ($\text{m}^3 \text{m}^{-1}$) $\times 10^{-12}$ at 0.5 m s ⁻¹	Wear rate ($\text{m}^3 \text{m}^{-1}$) $\times 10^{-12}$ at 0.86 m s ⁻¹	Wear rate ($\text{m}^3 \text{m}^{-1}$) $\times 10^{-12}$ at 1.2 m s ⁻¹	Wear rate ($\text{m}^3 \text{m}^{-1}$) $\times 10^{-12}$ at 1.5 m s ⁻¹
10	2.23	1.13	0.75	0.54	0.76
20	1.63	1.28	1.25	0.88	0.63
30	3.6	2.60	3.05	6.38	6.46
40	6.16	2.87	4.98	8.08	9.25
50	9.88	4.42	11.92	22.36	36.71

Table 66 Wear rate of Ti pins against hardened steel disks.

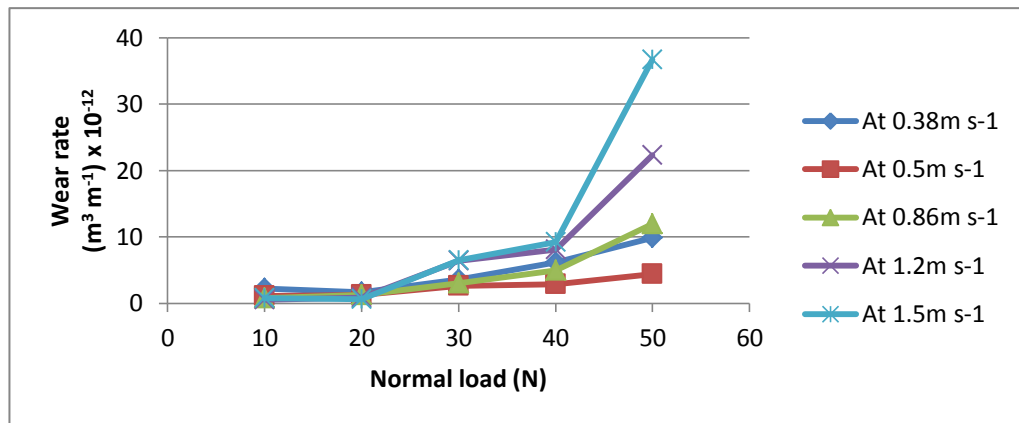


Figure 147 Wear rate of Ti pins against hardened steel disks

8.2.7. Wear rate of Ti against hardened steel at constant normal loads and various sliding speeds

Table 67 and Fig. 148 show the wear rate of Ti pins against hardened steel disks during dry sliding at different constant normal loads and various sliding speeds.

Sliding speed (m s ⁻¹)	Wear rate ($\text{m}^3 \text{m}^{-1}$) $\times 10^{-12}$ at 10 N	Wear rate ($\text{m}^3 \text{m}^{-1}$) $\times 10^{-12}$ at 20 N	Wear rate ($\text{m}^3 \text{m}^{-1}$) $\times 10^{-12}$ at 30 N	Wear rate ($\text{m}^3 \text{m}^{-1}$) $\times 10^{-12}$ at 40 N	Wear rate ($\text{m}^3 \text{m}^{-1}$) $\times 10^{-12}$ at 50 N
0.38	2.23	1.63	3.6	6.16	9.88
0.5	1.13	1.28	2.60	2.87	4.42
0.86	0.75	1.25	3.05	4.98	11.92
1.2	0.54	0.88	6.38	8.08	22.38
1.5	0.76	0.63	6.46	9.25	36.71

Table 67 Wear rate of Ti pins against hardened steel disks.

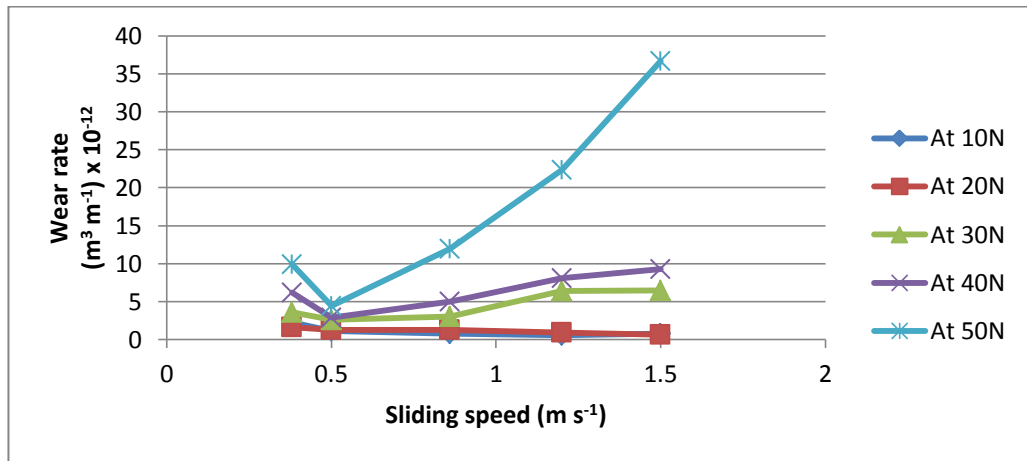


Figure 148 Wear rate of Ti pins against hardened steel disks.

8.2.8. Wear rate of Ti base TiC coatings against hardened steel at constant sliding speeds and various normal loads

Table 68 Fig. 149 show the wear rate of Ti base TiC composite coatings pins against hardened steel disks during sliding at different constant sliding speeds and various normal loads.

Normal load (N)	Wear rate (m³ m⁻¹)x10⁻¹² at 0.38 m s⁻¹	Wear rate (m³ m⁻¹)x10⁻¹² at 0.5 m s⁻¹	Wear rate (m³ m⁻¹)x10⁻¹² at 0.86 m s⁻¹	Wear rate (m³ m⁻¹)x10⁻¹² at 1.2 m s⁻¹	Wear rate (m³ m⁻¹)x10⁻¹² at 1.5 m s⁻¹
10	0.004	0.011	0.091	0.022	0.048
20	0.098	0.040	0.161	0.307	0.095
30	0.018	0.102	0.954	0.146	0.475
40	0.095	0.885	0.113	0.252	0.786
50	0.084	1.641	0.994	0.285	0.753

Table 68 Wear rate of Ti base TiC coatings pins against hardened steel disks.

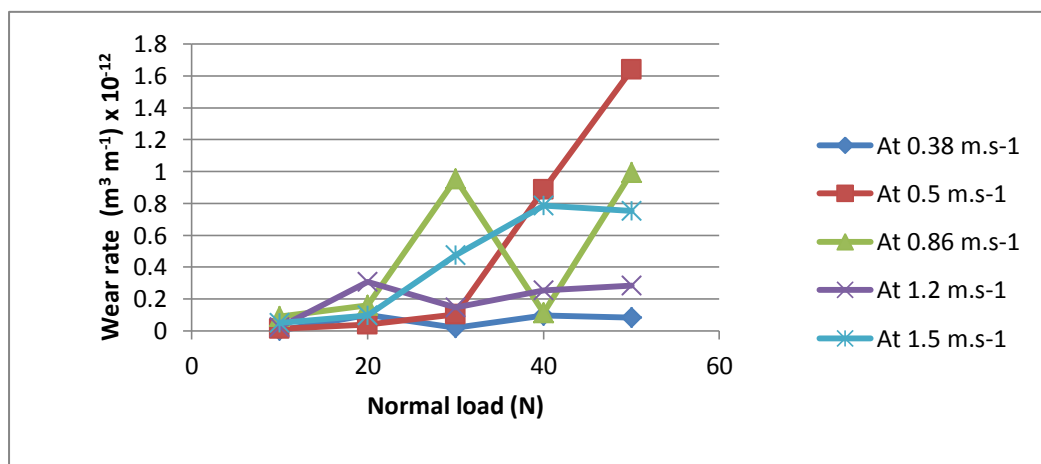


Figure 149 Wear rate of Ti base TiC coatings pins against hardened steel disks.

8.2.9. Wear rate of Ti base TiC coatings against hardened steel at constant normal loads and various sliding speeds

Table 69 Fig. 150 show the wear rate of Ti base TiC coatings pins against hardened steel disks due to dry sliding wear at different constant normal loads and various sliding speeds.

Sliding speed (m s ⁻¹)	Wear rate (m ³ m ⁻¹) x10 ⁻¹² at 10 N	Wear rate (m ³ m ⁻¹)x10 ⁻¹² at 20 N	Wear rate (m ³ m ⁻¹)x10 ⁻¹² at 30 N	Wear rate (m ³ m ⁻¹)x10 ⁻¹² at 40 N	Wear rate (m ³ m ⁻¹)x10 ⁻¹² at 50 N
0.38	0.004	0.098	0.018	0.095	0.084
0.5	0.011	0.040	0.102	0.885	1.641
0.86	0.091	0.161	0.954	0.113	0.994
1.2	0.022	0.307	0.146	0.252	0.285
1.5	0.048	0.095	0.475	0.786	0.753

Table 69 Wear rate of Ti base TiC coatings pins against hardened steel disks.

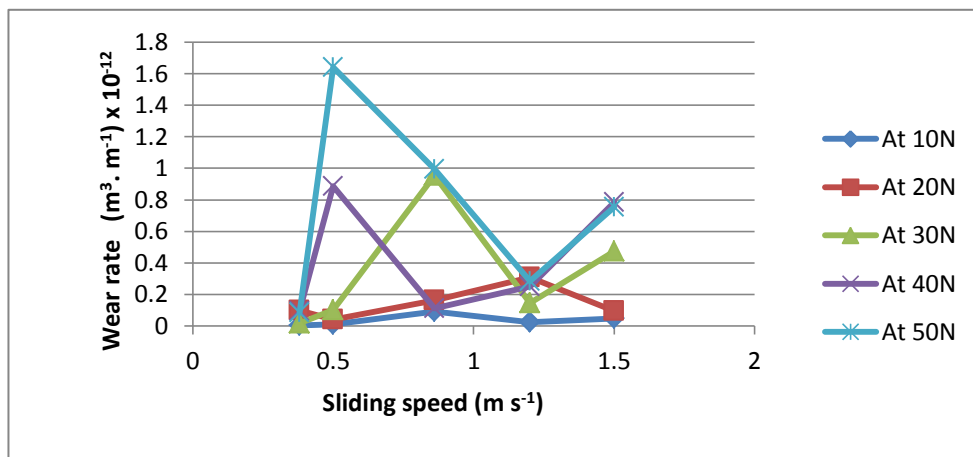


Figure 150 Wear rate of Ti base TiC coatings pins against hardened steel disks.

Fig. 147 shows that wear rate of substrate against hardened steel is increased sharply with the increase in applied normal load after 20 N. Fig. 148 shows that there is lower wear rate up to 20 N normal loads and then it begins to increase with the increase in sliding speeds. Moreover, for each normal load there is a minimum wear rate at an intermediate sliding speed i.e. 0.5 m s⁻¹ in this case and with increase in normal load the minimum became more prominent at this sliding speed. It is also observed that the wear rate of Ti is increasing with the increase in normal loads and sliding speeds. Abrupt increase in wear rate is found at the higher normal load Figs. 147-148. Overall, severe wear is found for the substrate against hardened steel. While, Fig. 149 shows that there was very mild and mild wear rate of the coated material against hardened steel for all the combinations of sliding speeds and normal loads except 0.5 m s⁻¹ and 50 N. Steady wear rate is found for sliding speed 0.38 & 1.2 m s⁻¹, which meant that no wear mode transition occurred at these sliding speeds for

the range of normal loads. At sliding speed 0.5 m s^{-1} wear mode regime transitions occurred from very mild wear to mild wear then to medium wear with the increase in normal load due to greater removal rate of the oxide than that of the rate of oxidation. At sliding speeds $0.5, 0.86 \text{ \& } 1.5 \text{ m s}^{-1}$, fluctuation in wear rate was found for the range of normal loads Fig. 150. Overall very mild wear is predominated for Ti base TiC coatings against hardened steel.

8.2.10. Total mass loss comparison

Table 70 and Fig. 151 show the total mass loss of the Ti and Ti base TiC composite coatings pins against hardened steel disks at different constant sliding speeds for the range of normal loads i.e. at variable loads from 10 to 50 N and increasing in 10 N increments for the total sliding distance 27,800 m. Wear resistance of the titanium substrate is increased by over 17 times because of surface composite coatings. The fluctuation in the total mass loss of Ti and Ti base TiC coating against hardened steel may be attributed to the formation of mechanical mixed layer or thermal softening effects and oxidation of the mating surfaces during dry sliding contact.

Sliding speed (m s^{-1})	Total mass loss of Ti ($\text{g}) \times 10^{-2}$	Total mass loss of Ti base TiC coatings pin ($\text{g}) \times 10^{-2}$
0.38	58.91	0.8
0.5	30.83	7.3
0.86	55.03	6.3
1.2	95.9	2.8
1.5	134.95	5.9

Table 70 The total mass loss of Ti and Ti base TiC composite coatings against hardened steel.

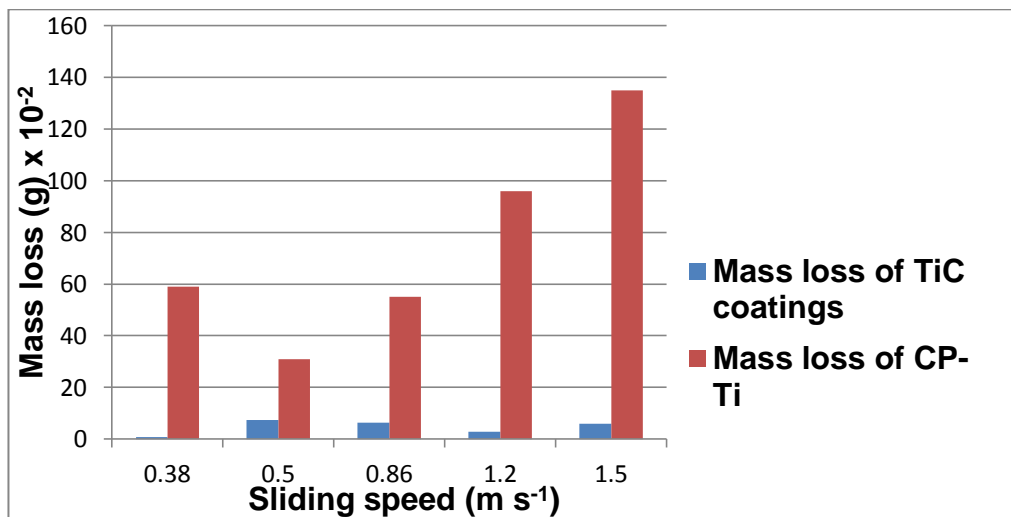


Figure 151 The total mass loss comparison of Ti and Ti base TiC coatings against hardened steel.

8.2.11. Coefficient of friction during sliding of Ti pins against hardened steel disks

Table 71 and Fig. 152 show the trend of friction of Ti pins against hardened steel disks at different constant sliding speeds and various normal loads.

Normal load (N)	Coefficient of friction at 0.38 m s ⁻¹	Coefficient of friction at 0.5 m s ⁻¹	Coefficient of friction at 0.86 m s ⁻¹	Coefficient of friction at 1.2 m s ⁻¹	Coefficient of friction at 1.5 m s ⁻¹
10	0.36	0.26	0.33	0.36	0.41
20	0.22	0.24	0.18	0.25	0.29
30	0.23	0.16	0.28	0.32	0.32
40	0.21	0.30	0.30	0.31	0.30
50	0.24	0.27	0.33	0.26	0.28

Table 71 Coefficient of friction of Ti against hardened steel.

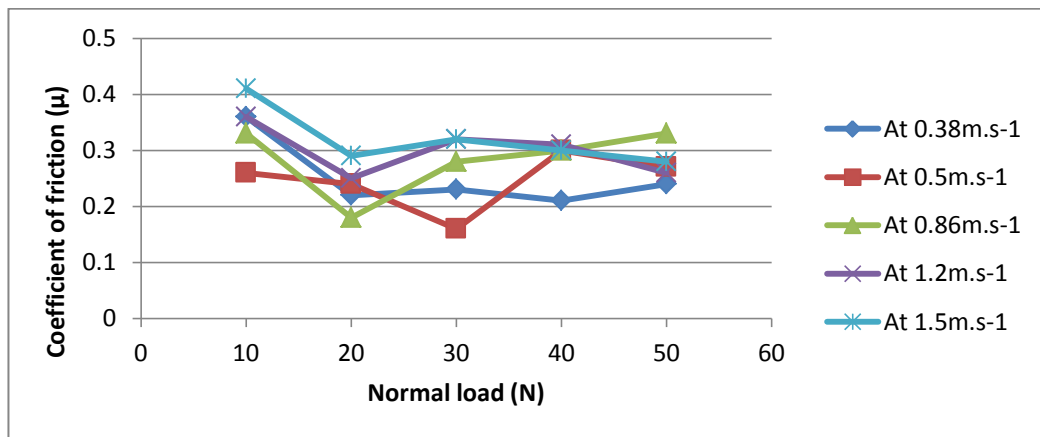


Figure 152 Coefficient of friction of Ti pins against hardened steel disks.

Table 72 and Fig. 153 show the trend of friction of Ti pins against hardened steel disks at different constant normal loads and various sliding speeds.

Sliding speed m s ⁻¹	Coefficient of friction at 10 N	Coefficient of friction at 20 N	Coefficient of friction at 30 N	Coefficient of friction at 40 N	Coefficient of friction at 50 N
0.38	0.36	0.22	0.23	0.21	0.24
0.5	0.26	0.24	0.16	0.30	0.27
0.86	0.33	0.18	0.28	0.30	0.33
1.2	0.36	0.25	0.32	0.31	0.26
1.5	0.41	0.29	0.32	0.30	0.28

Table 72 Coefficient of friction of Ti against hardened steel.

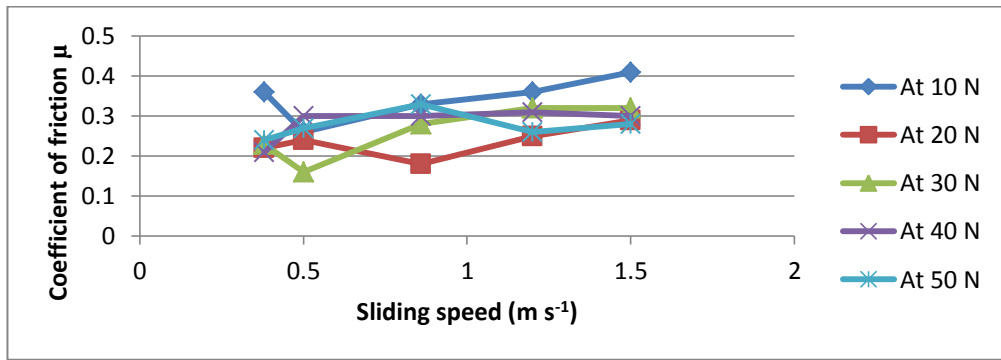


Figure 153 Coefficient of friction of Ti pins against hardened steel disks.

8.2.12. Coefficient of friction of Ti base TiC coatings pins against hardened steel disks

Table 73 and Fig. 154 show the trend of friction Ti base TiC pins against hardened steel disks at different constant sliding speeds and various normal loads.

Normal load (N)	Coefficient of friction at 0.38 m s ⁻¹	Coefficient of friction at 0.5 m s ⁻¹	Coefficient of friction at 0.86 m s ⁻¹	Coefficient of friction at 1.2 m s ⁻¹	Coefficient of friction at 1.5 m s ⁻¹
10	0.61	0.50	0.33	0.50	0.27
20	0.28	0.35	0.26	0.27	0.34
30	0.35	0.34	0.25	0.28	0.29
40	0.27	0.31	0.34	0.33	0.29
50	0.44	0.24	0.25	0.31	0.24

Table 73 Coefficient of friction of Ti base TiC coatings pins against hardened steel disks.

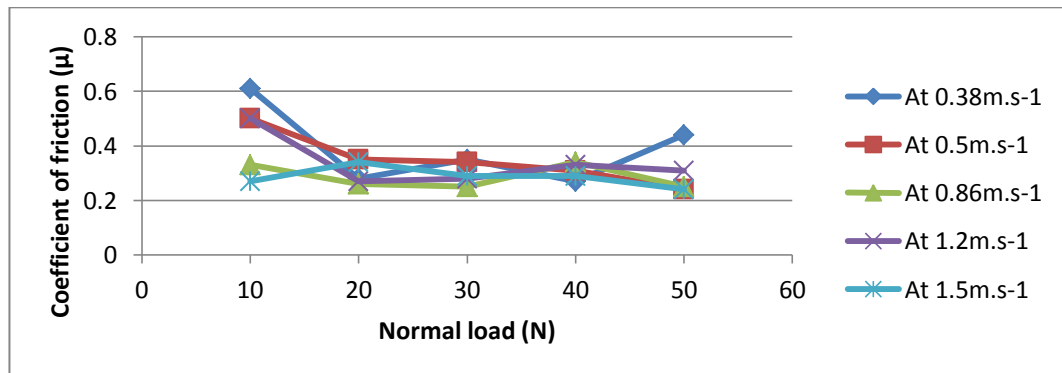


Figure 154 Coefficient of friction of Ti base TiC coatings pins against hardened steel disks.

Table 74 and Fig. 155 show the trend of friction of Ti base TiC pins and hardened steel disks sliding against each other at different constant normal loads and various sliding speeds.

Sliding speed m s^{-1}	Coefficient of friction at 10 N	Coefficient of friction at 20 N	Coefficient of friction at 30 N	Coefficient of friction at 40 N	Coefficient of friction at 50 N
0.38	0.61	0.28	0.35	0.27	0.44
0.5	0.50	0.35	0.34	0.31	0.24
0.86	0.33	0.26	0.25	0.34	0.25
1.2	0.50	0.27	0.28	0.33	0.31
1.5	0.27	0.34	0.29	0.29	0.24

Table 74 Coefficient of friction of Ti base TiC coatings pins against hardened steel disks

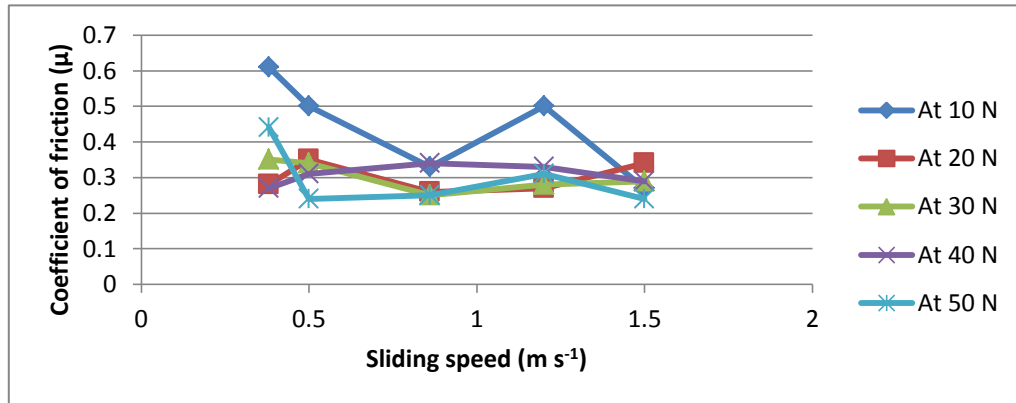
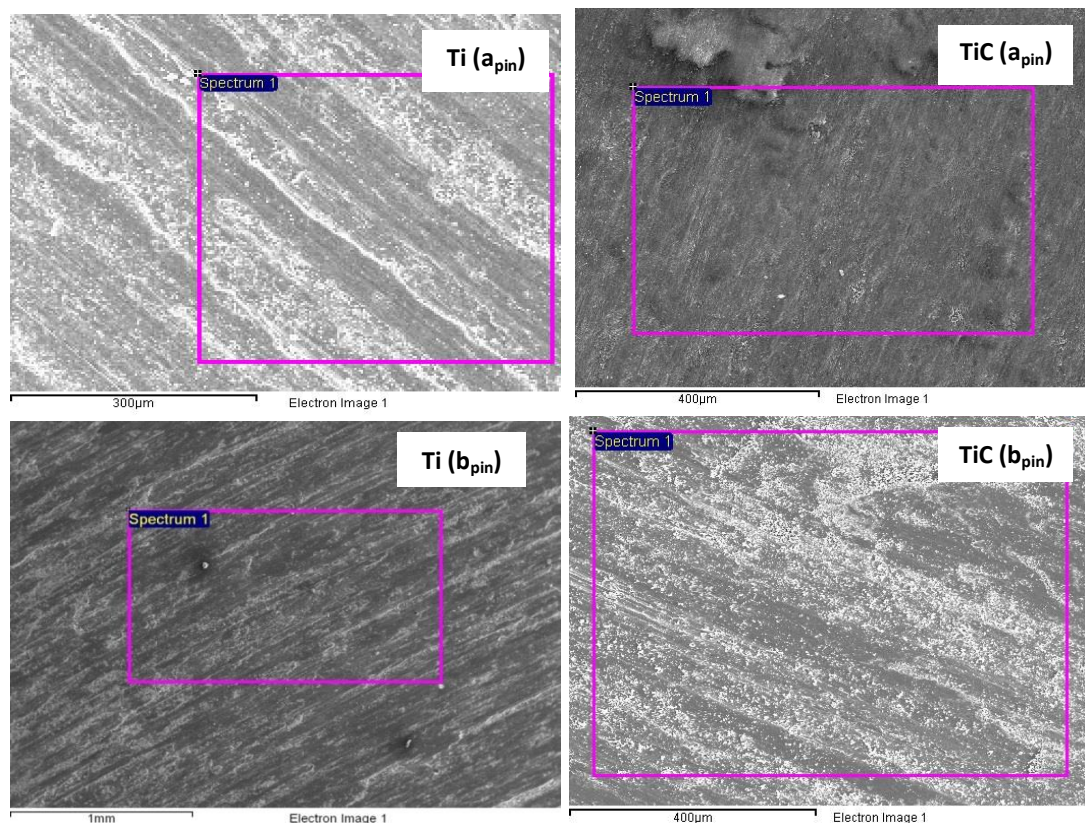


Figure 155 Coefficient of friction of Ti base TiC coatings pins against hardened steel disks.

8.2.13 SEM micrographs of the worn surfaces of Ti and Ti base TiC coatings pins against hardened steel disks

Fig. 156 shows the SEM micrographs of the worn surfaces of Ti and Ti base TiC coatings pins against hardened steel disks.



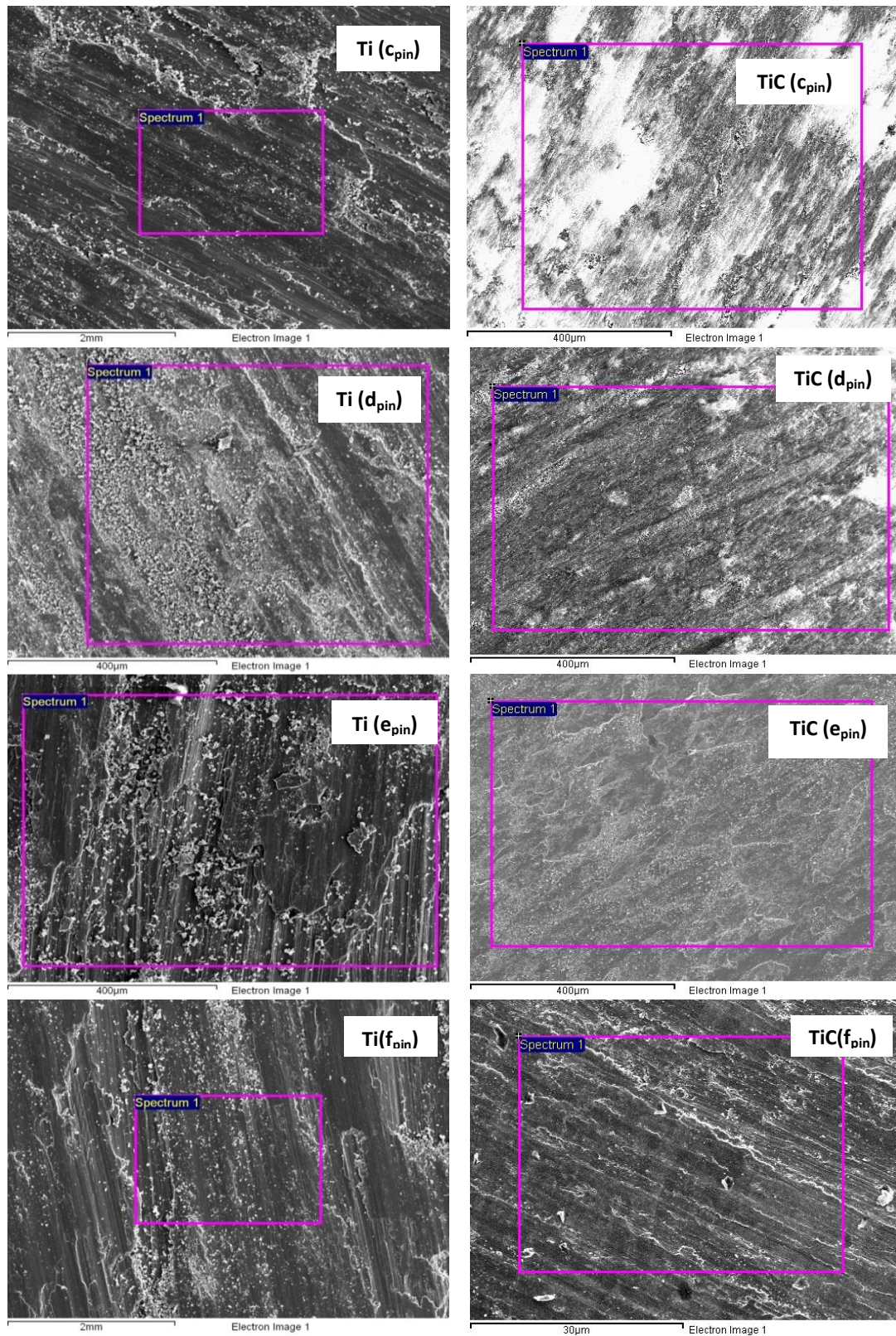
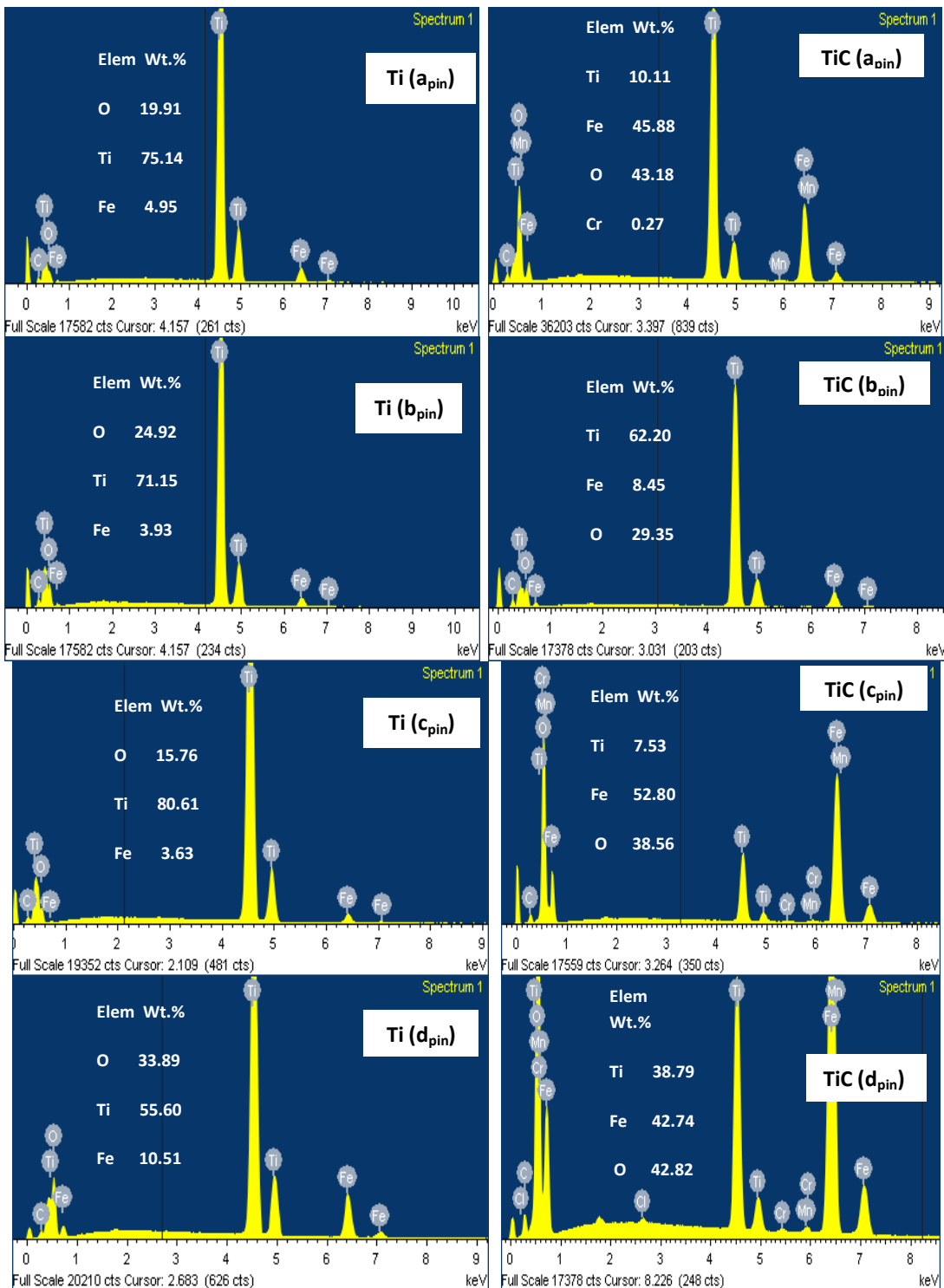


Figure 156 SEM micrographs of the worn surfaces of the Ti and Ti base TiC composite coatings pins against hardened steel disk, (a) at normal load 30 N and sliding speed 0.38 m s^{-1} , (b) at 50 N and 0.5 m s^{-1} , (c) at 40 N and 0.86 m s^{-1} , (d) at 20 N and 1.2 m s^{-1} , (e) at 50 N and 1.5 m s^{-1} and (f) at 50 N and 0.86 m s^{-1} .

8.2.14 EDX analysis of the worn surfaces of Ti and Ti base TiC coatings pins against hardened steel disks

Fig 157 shows the EDX analysis of the worn surfaces of Ti and Ti base TiC coatings pins against hardened steel disks



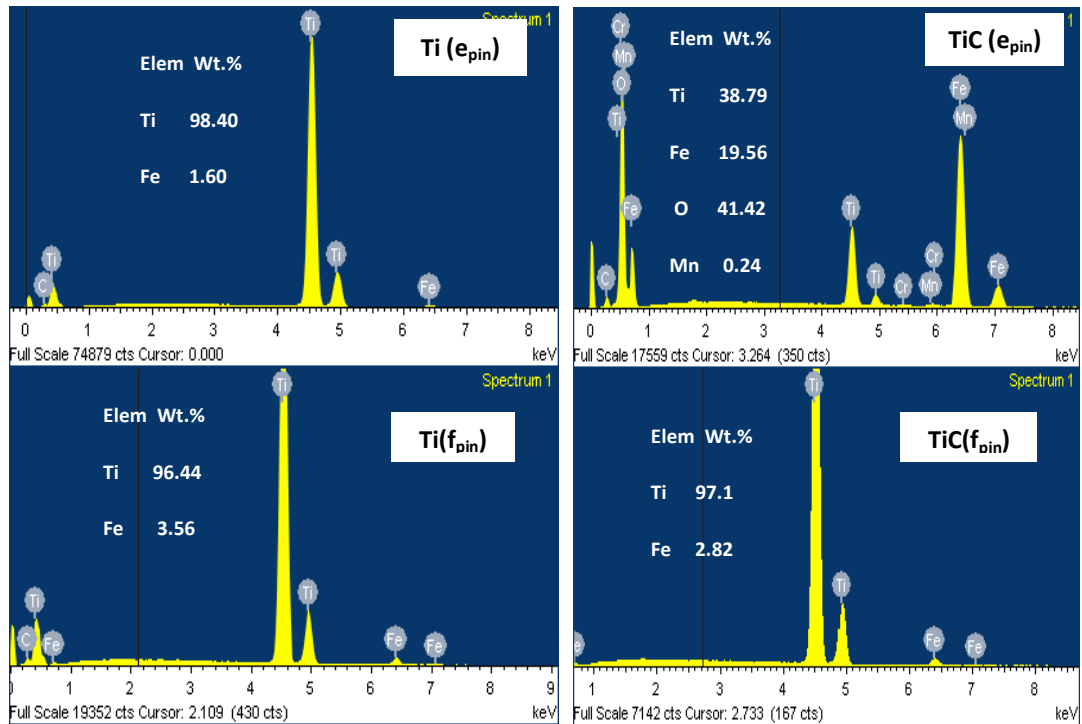


Figure 157 EDX analysis of the worn surfaces of Ti and Ti base TiC composite coatings pins against hardened steel disk, (a) at normal load 30 N and sliding speed 0.38 m s^{-1} , (b) at 50 N and 0.5 m s^{-1} , (c) at 40 N and 0.86 m s^{-1} , (d) at 20 N and 1.2 m s^{-1} , (e) at 50 N and 1.5 m s^{-1} and (f) at 50 N and 0.86 m s^{-1} .

It is clear from the SEM micrographs of the worn surfaces of Ti pins, Figs 156 Ti($a_{pin} - f_{pin}$) that the wear of the substrate occurred by different wear mechanisms i.e. adhesive wear, mild-oxidational wear, plastic deformation and delamination wear mechanisms for the range of sliding speeds and normal loads. The presence of the counterface material on the worn surfaces of the Ti pins is evident that during continuous sliding, the initial transferred fragments were deformed, fractured and blended, leading to formation of mechanically mixed material on the wear track Figs 157 Ti($a_{pin} - f_{pin}$). At lower normal loads for the range of sliding speeds wear of Ti pins occurred by oxidative wear mechanisms with transfer of disk material to the worn surfaces of the pins due to adhesion Figs. 156 Ti(d_{pin}) - 157 Ti(d_{pin}). At higher normal loads for the range of sliding speeds, severe wear occurred due to adhesive wear, oxidative wear, plastic deformation and delamination wear mechanisms Figs. 156 Ti($a_{pin} - c_{pin}, e_{pin}, f_{pin}$) - 157 Ti($a_{pin} - c_{pin}, e_{pin}, f_{pin}$).

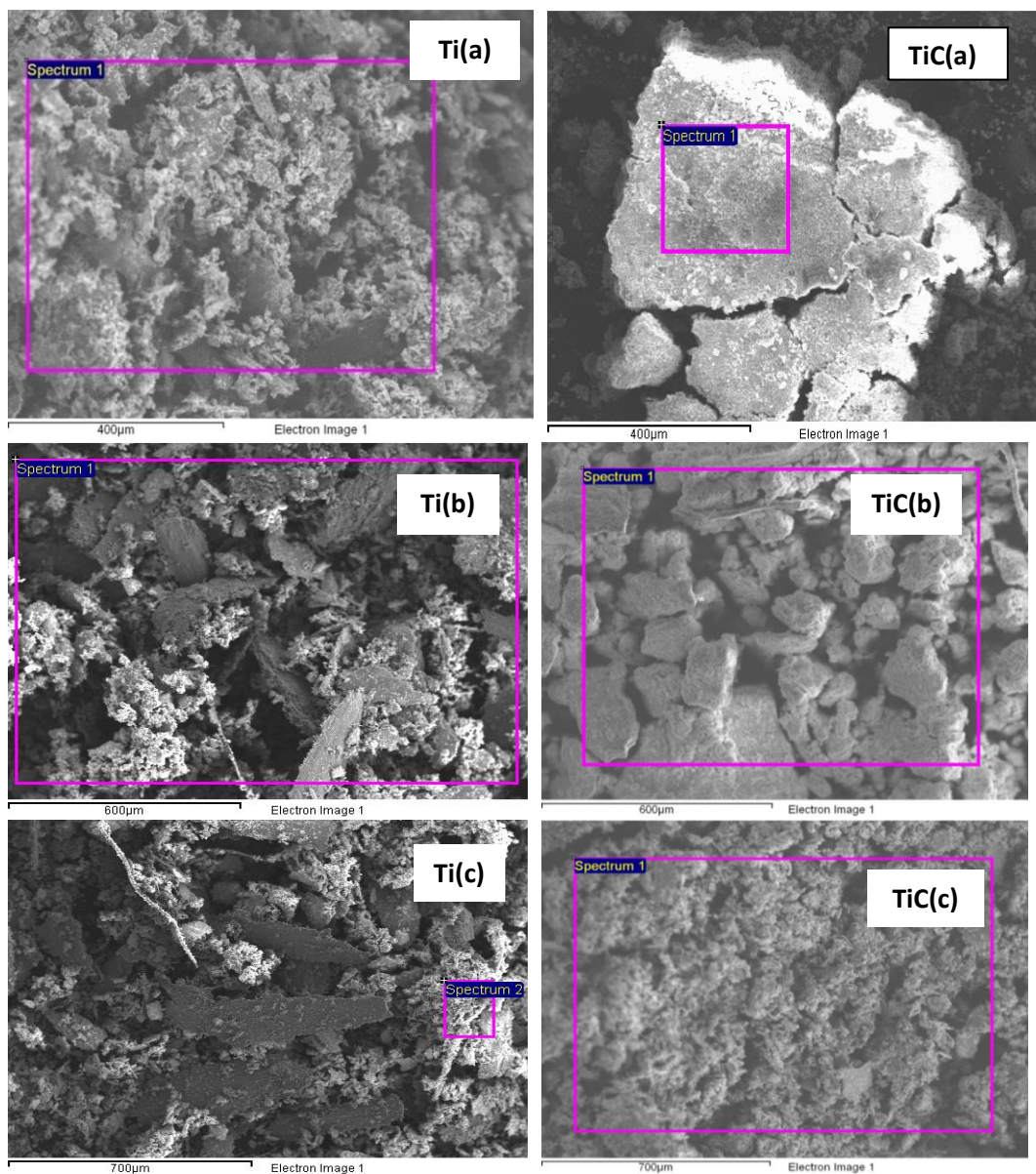
While, for Ti base TiC coatings, at a sliding speed of 0.38 m s^{-1} and normal loads 10, 30 & 50 N; 0.5 m s^{-1} and 10 – 20 N; 0.86 m s^{-1} and 10 – 30 N and at 1.2 m s^{-1} and 10 to 40 N higher oxidation of the counterface occurred. Iron oxide transferred to the pins' mating surfaces. The worn surfaces of the pins were not completely visible as they are masked by the

Tribo-corrosion maps for steels, titanium and titanium carbide materials

transferred iron oxides Figs. 156 TiC(a_{pin}, c_{pin}, d_{pin}) -157 TiC(a_{pin}, c_{pin}, d_{pin}). At 0.38 m s⁻¹ and 20 & 40 N; 0.5 m s⁻¹ and 30 – 50 N; 0.86 m s⁻¹ and 40 N and at 1.5 m s⁻¹ and 10, 30 N and 50 N higher oxidation of the pins occurred and comparatively less iron oxide transferred to the worn surfaces of the pins. The worn surfaces of the pins are showing adhesive and plastic deformation marks as well Figs. 156 TiC(b_{pin}, e_{pin}) - 157 TiC(b_{pin}, e_{pin}). At 0.86 m s⁻¹ and 50 N; 1.2 m s⁻¹ and 50 N and at 1.5 m s⁻¹ and 20 & 40 N worn surfaces of the pins are showing marks of plastic deformation and abrasive wear Figs. 156 TiC(f_{pin}) -157 TiC(f_{pin}).

8.2.15 SEM micrographs of wear debris of Ti and Ti base TiC coatings pins against hardened steel disks

Fig. 158 shows the SEM micrographs of the wear debris from Ti and Ti base TiC composite coatings pins against hardened steel disks.



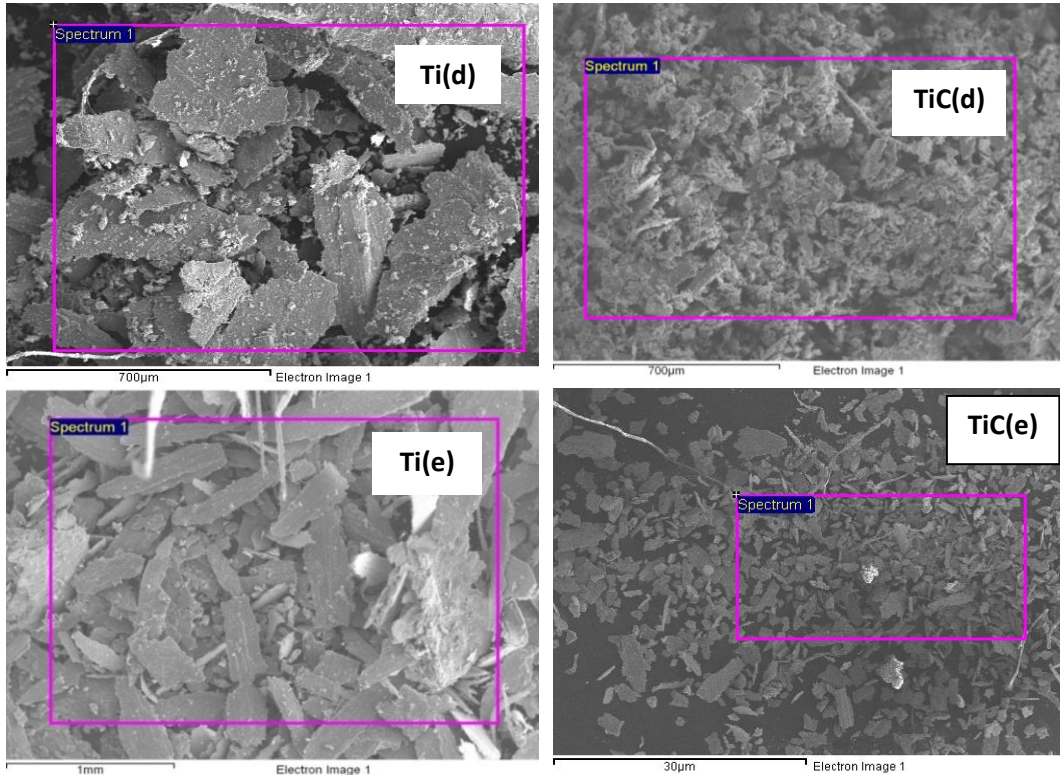
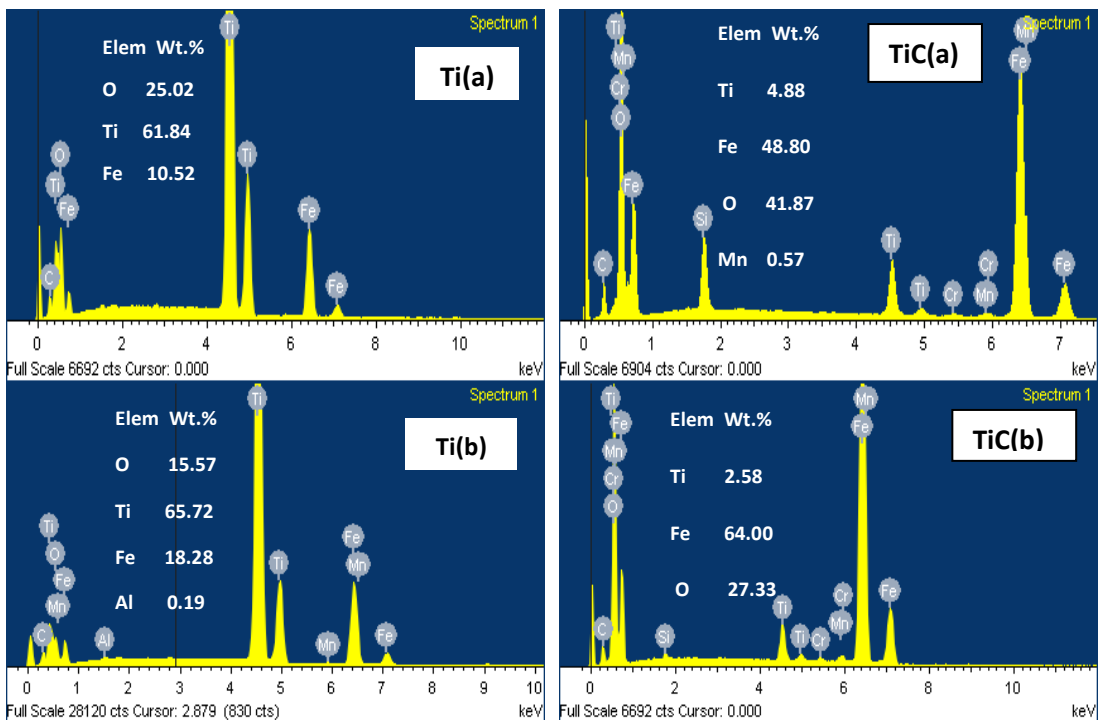


Figure 158 SEM micrograph of the wear debris of Ti and Ti base TiC coatings against hardened steel (a) at sliding speed 0.38 m s^{-1} and normal load 30 N, (b) at 0.38 m s^{-1} and 50 N, (c) at 0.5 m s^{-1} and 50 N, (d) at 0.86 m s^{-1} and 30 N and (e) at 1.5 m s^{-1} and 50 N.

8.2.16 EDX analysis of wear debris of Ti and Ti base TiC coatings pins against hardened steel disks

Fig.159 shows the EDX analysis of the wear debris from Ti and Ti base TiC composite coatings pins and hardened steel disks.



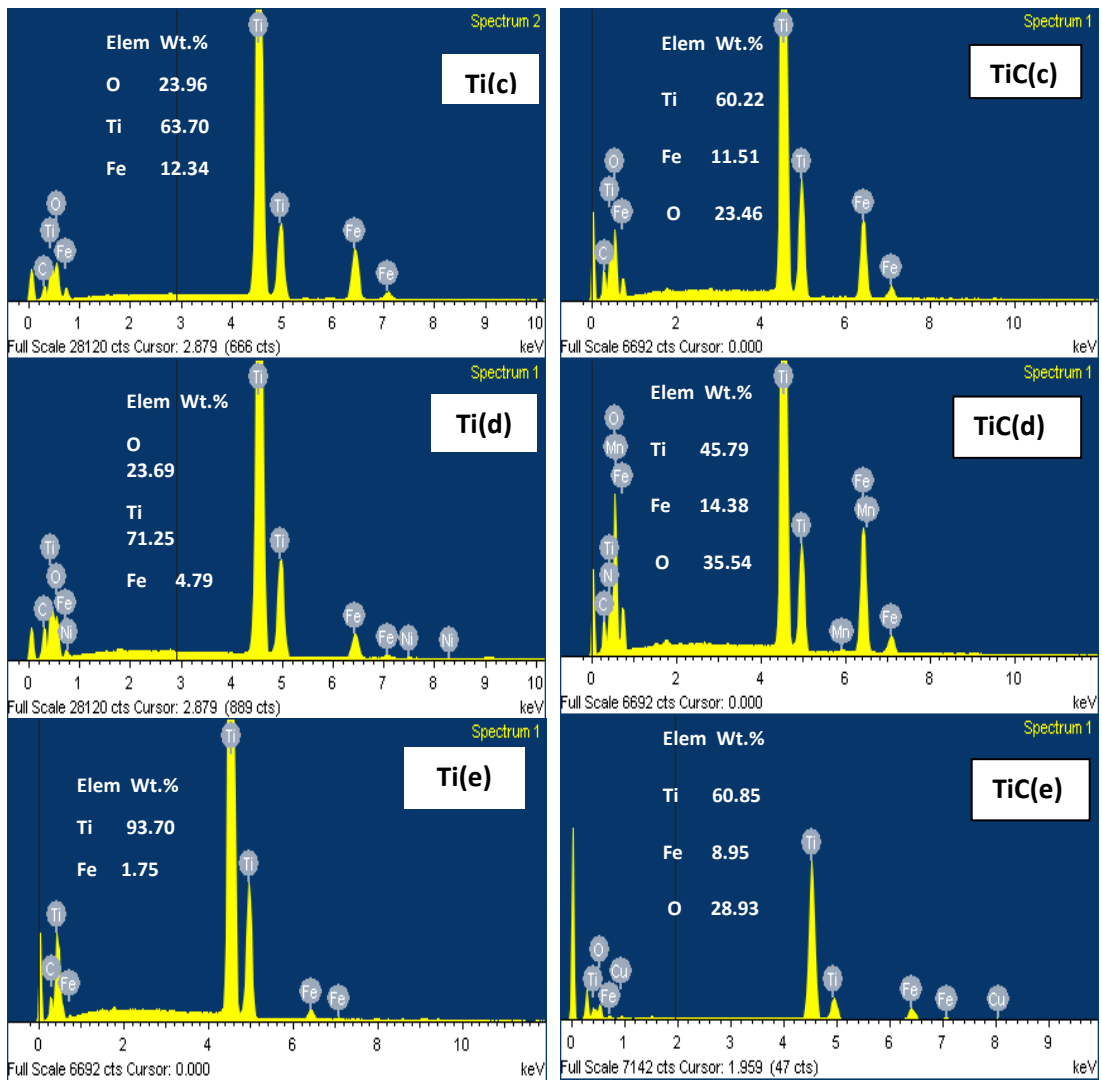


Figure 159 EDX analysis of the wear debris of Ti and Ti base TiC composite coatings against hardened steel, (a) at sliding speed 0.38 m s^{-1} and normal load 30 N, (b) at 0.38 m s^{-1} and 50 N, (c) at 0.5 m s^{-1} and 50 N, (d) at 0.86 m s^{-1} and 30 N, and (e) at 1.5 m s^{-1} and 50 N.

For the Ti pins sliding against hardened steel disks, the shapes of wear debris are different for lower sliding speeds and for the higher sliding speeds irrespective of the normal loads. At lower sliding speeds wear products consisted of fine compact particles, strip shape particles and micro cutting chips along with fine grey powder of titanium oxide, SEM micrographs Figs. 158 Ti(a-c) and EDX analysis Figs. 159 Ti(a-c); while at higher sliding speeds, wear products mainly consisted of flake-like metallic particles of Ti and fine grey powder of titanium oxide, SEM micrographs Figs. 158 Ti(d-e) and EDX analysis Figs. 159 Ti(d-e). It is observed that shapes of the debris are dependent on sliding speed i.e. wear mechanism changes with the change in sliding speeds. The composition of wear debris

Tribo-corrosion maps for steels, titanium and titanium carbide materials

mainly consisted of Ti, O and Fe with higher percentage of debris from pins material in all cases Figs. 159 Ti(a-e). This confirms that debris particles came from the hardened steel counter body as well. The metallic flake types wear debris of Ti, in this tribo couple, resulted from adhesive and delamination wear mechanisms.

On the other hand, generally from the SEM micrographs of the wear debris from Ti base TiC composite coatings pins against steel disks, the physical nature and shapes of the debris are different for the range of sliding speeds Figs. 158 TiC(a-e). The shape of the wear debris changed with the increase in sliding speed. At lower sliding speeds, the compact reddish brown brittle powdery wear debris came from counter face in shape of iron oxide Figs. 158 TiC(a-b) – 159 TiC(a-b). At sliding speed 0.5 m s^{-1} and onward, wear debris came from Ti base TiC composite coatings pins in shape of grey titanium oxide powder along with micro strap-like shape particles of iron from hardened steel disks Figs. 158 TiC(c-e) – 159 TiC(c-e). From EDX analysis Figs. 159 TiC(a-e), the wear products mainly consisted of Ti, O and Fe in all cases, meant that the oxides of both Ti and iron are present in the wear products. At lower sliding speeds, the brown powder came from the iron oxide and at higher sliding speeds the grey powder in wear products came from Ti oxide. As clear from the nature of the wear debris, the wear mechanisms for this tribo couple were the combinations of micro polishing, oxidative wear and iron oxide transfer at the lower normal loads, while plastic deformation, micro delamination, adhesive and abrasive wear at the higher normal loads for the range of sliding speeds.

8.2.17. Optical micrographs of coatings layers on Ti pins

Fig. 160 shows cross sectional optical micrographs of the of the Ti base TiC coatings pins. Fig. 160(a) shows the thickness of the finish surface of the coating prior to testing. Figs. 160(b-c) show the thickness of coatings left after the sliding wear tests carried out at sliding speeds 1.2 m s^{-1} and normal load 50 N and 1.5 m s^{-1} and 40 N respectively.

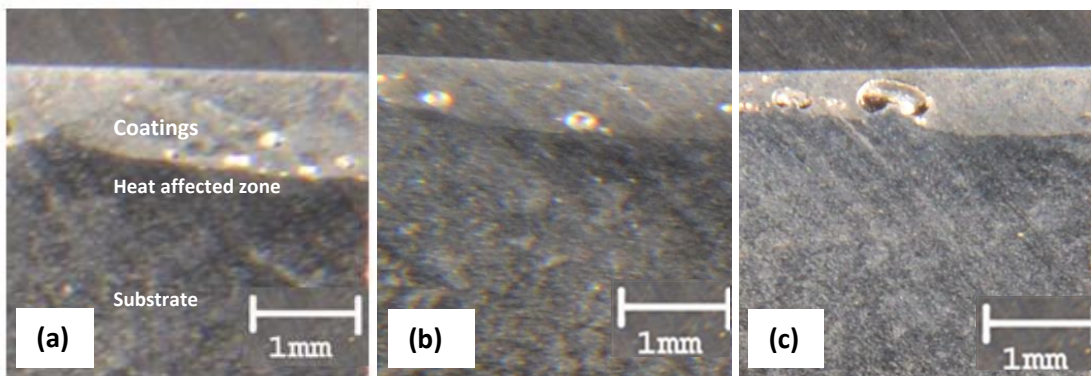


Figure 160 Optical micrographs of Ti base TiC coatings, (a) thickness of the coatings layer prior to test, (b) thickness of the coatings layer after 1.2 m s^{-1} sliding speed and 50 N normal load, (c) thickness of the coatings layer after 1.5 m s^{-1} sliding speed and 40 N.

8.3. Discussion

8.3.1 Wear mechanisms and regimes

The wear rate data of Ti substrate (uncoated and coated with TiC composite coatings) are plotted in Figs. 142-146 for the range of sliding speeds and normal loads. It is clear from these figures that the Ti showed very poor wear resistance than that of coated substrate for all combinations of sliding speeds and normal loads against same counterface. Similar results were found by A. Monfared et al. for these materials against cermet as counterface, where coatings were done by TIG process with cored wire [158] and for the other coating-substrate systems where coatings were carried out by different coatings methods [55]. In the case of uncoated, the pins' mating surfaces were extruded for all the combinations of sliding speeds and normal loads. The lower wear resistance of the substrate is attributed to the lower frictional wear resistance, tendency to seizure and inability to form protective oxide layer during sliding [137, 174, 175] and severe adhesion between the contact surfaces of Ti pins and hardened steel disks [158]. While higher wear resistance of the TiC coatings is attributed to their higher surface hardness, internal stress level, thickness and load bearing capacity [55]. When a coating is cooled from the high temperature of deposition, the internal stress within the coating is generally compressive, which reduces the extent of surface fracture results in increase of wear resistance of the coated surface [59]. The shear stress is also induced between the coating and substrate, which promotes the spalling of coating during sliding [56]. The ability of a coating-substrate system to withstand load on the coated surface without spalling or cohesion failure of the coating is called its load bearing capacity. A higher load bearing capacity increases the sliding wear resistance as well [59-60].

Moreover, in the case of coatings, different sliding wear behaviour was observed. It is assumed that the wear occurs by abrading the matrix and pick and dig up matrix continuously. This process gradually raises the hard TiC particles in the coated surface and then these particles carry the load of the abrasive particles [179]. The matrix and hard particles act differently during sliding process. The metal matrix offer the enough toughness for the hard particles and the hard particles act as a barrier against indentation, grooving, cutting of abrasive materials and reduces the contact area of the mating surfaces. Thus the hardness, fracture toughness, the amount, size and distribution of the hard particles are significant parameters in the resistance of material against sliding wear [180].

Different sliding wear behaviour of uncoated and coated substrate observed against hardened steel Figs. 147-148 and 149-150 respectively. The higher wear rate of Ti against hardened steel is in consistent with A. Monfared et al. observation for this material [158]. The significant pins material was transferred to counterface and a few tests did not complete total sliding distance, the similar situation is evidence when Ti was slid in unlubricated conditions against C45 steel and tool steel [50, 55] and for 303SS against alumina Chapter 5. During continuous sliding, the initial transferred fragments are deformed, fractured and blended, leading to formation of mechanically mixed layer on the wear track. The hardness of this layer is considerably higher than that of the original pins material due to the intense, localised, thermal effects which occurs during rubbing under unlubricated conditions. Typically sliding wear debris particles are come from modified mixed layer [42, 132]. Moreover, there was no fluctuation observed in wear rate of Ti for the range of sliding speeds and normal loads except 0.5 m s^{-1} , which appeared as an intermediate sliding speed in the case of uncoated substrate Fig. 147. Mild wear rate of Ti pins at higher sliding speeds up to normal load 20N, Figs. 147-148, is due to mild oxidative wear and plastic deformation of the mating surfaces as evident from the SEM micrograph of the worn surfaces of the Ti pins Fig. 156 $Ti(d_{pin})$. The presence of Ti, Fe and O species on the worn surface of the Ti pins suggest that the domination of the tribo-oxidation process occurred in the high temperature contact spots at the mating surfaces, EDX analysis of the worn surfaces Fig. 157 $Ti(d_{pin})$. S. Krol et al. observed that oxidative wear with very mild wear rate of the tribo-system occurred, typical for mating of metals of diversified mechanical properties at mild friction conditions [50]. At higher normal loads for the range of sliding speeds, severe wear of Ti occurred due to abrasive, adhesive wear, oxidative wear, plastic deformation and delamination wear mechanisms. Figs. 156 $Ti(a_{pin} - c_{pin}, e_{pin} - f_{pin})$

Tribo-corrosion maps for steels, titanium and titanium carbide materials

show the marks of abrasion, adhesion, plastic deformation and delamination wear. Figs. 157 Ti($a_{pin} - c_{pin}$) show the presence of Ti, Fe and O species on the worn surface of the Ti pins, which is evident that oxidative wear occurred as well with higher oxidation of pin material. The absence of O in EDX analysis, Figs. 157 Ti($e_{pin} - f_{pin}$) show that either no oxidation might have occurred, or the rate of oxidation was lower than that of rate of removal of oxide at higher sliding speed and normal loads. The similar results are found in the literature for Ti and its alloys against hard metals [137, 175, 189]. At higher normal load i.e. 30 to 50N for range of sliding speeds mainly adhesive wear mechanism was predominated. With the increase in sliding speed the surface temperature and a progressive increase in wear is induced because of thermal softening as soon as the yield point of the material starts decreasing significantly. The effects of an increase in sliding speed at higher normal loads results an increased delamination wear [69, 174]. The higher wear rate of Ti with the increase in sliding speed and normal load is attributed to the low resistance to plastic shearing, low work hardening and low protection provided by the surface oxide layers, which can be formed when high flash temperature is induced by frictional heating [181].

While contrary to Ti, for the Ti base TiC composite coatings against hardened steel, significant oxide of the counterface was transferred to coated pins' mating surfaces and formed tribo layer that result in very mild, mild wear rate Figs. 142-146, 156-157. These observations are in consistent with the other studies which are found in the literature [190, 192]. There is a fluctuation in the wear rates within the mild wear regimes Figs. 149-150, for the range of sliding speeds and normal loads. Table 68 and Fig. 149 show that the wear trend of TiC coatings is increasing with the increase in normal load. The increase in wear rate might be due to the increase in contact area, increase in tensile & shear stress, increase in adhesive effect of cold welding, abrasive effect of wear debris, increase in oxidation rate and plastic deformation with an increase in normal load [161]. The Table 69 and Fig. 150 show that the wear trend decreasing with the increase in sliding speeds. This might be due to the increase in plastic flow of coating with decrease in shear strength, oxidation and by local melting at high flash temperatures with an increase in sliding speed. Moreover, it might be due to the fact that at low sliding speeds the wear debris generated were not ejected from the wear track and contributed to wear process as abrasive particles, resulted in higher wear rate at lower sliding speed. At higher sliding speeds, major part of the wear debris generated were ejected out from the wear track, resulted in decrease in wear rate with an increase in sliding speed [161].

The very mild wear of the coatings occurred due to micro-abrasion of the coated surfaces by the hard Fe oxide particles from the counterface, SEM micrographs of the worn surfaces Figs. 156 TiC(a_{pin} , c_{pin} - d_{pin}) and EDX analysis of the worn surfaces 157 TiC(a_{pin} , c_{pin} - d_{pin}), [74]. The wear products from these combinations of sliding speeds and normal loads are consisted of brown brittle powder of Fe oxide and trace of Ti, SEM micrographs of wear debris Figs. 158 TiC(a_{pin} - b_{pin}) and EDX analysis of wear debris Figs. 159 TiC(a_{pin} - b_{pin}). The presence of the larger percentage of Fe and O species in the wear products shows that higher oxidation of the counterface was taken place Figs. 159 TiC(a_{pin} - b_{pin}). The mild wear of coatings occurred due to mild abrasion, adhesion, plastic deformation, oxidative and mild delamination wear. SEM micrographs of the worn surfaces Figs. 156 TiC(b_{pin} , e_{pin} - f_{pin}) and EDX analysis of the worn surfaces Figs. 157 TiC(b_{pin} , e_{pin} - f_{pin}) are evident of these wear mechanisms. SEM micrographs Figs. 158 TiC(c_{pin} - e_{pin}) and EDX analysis Figs. 159 TiC(c_{pin} - e_{pin}) of the wear debris show that wear occurred by plastic deformation, delamination wear and oxidation of both coatings and counterface. The presence of the large percentage of Ti and O species in the wear products shows that higher oxidation of TiC coatings was taken place at higher sliding speeds and normal loads Figs. 159 TiC(c_{pin} - e_{pin}).

The fluctuation in wear rates of Ti base TiC coating against hardened steel is attributed to the variation in temperature between contact areas due to increase in flash temperature and frictional heating result in thermal softening effects and oxidation of the mating surfaces during dry sliding. Material behaved differently under the ambient conditions when temperature changes occurred between sliding contacts. The wear rate of Ti base TiC coatings increased at higher normal loads for the range of sliding speeds Fig. 149. The similar trend of wear was found in the study of 303SS base TiC coatings dealt with in Chapter 5, by Tyler L et al. in the study of sliding wear of TiC and Ti(C, N) cermet prepared with a stoichiometric Ni Al binder [190] and in the work of the others researchers found in literature for the composite coatings, where coatings were carried out by the different methods [55, 143, 161, 171]. These observations are in consistent with the others' studies that demonstrate the total mass loss during sliding depends upon both the sliding time and applied load [29, 191].

The comparative total mass loss of Ti (uncoated and coated with TiC composite coatings) pins is shown in Fig. 151 for a sliding distance of 27,800 m at various constant sliding speeds for the range of normal loads. At each sliding speed the total mass loss of Ti is larger than

that of the coatings, which is evident of improvement in surface hardness of the substrate due to composite coatings as well. Similar findings are available in the literature for the wear of TiC-coated carbide tools in dry turning for flank and crater [65], observation of the others authors for untreated and surface treated materials where surfaces were treated other than TIG process [55, 181] and in our previous work Chapter 5.

The frictional behaviour of metals, when slide in air against one another, depends on the composition and microstructure of the materials and on the tests conditions [62]. Figs. 152-153 and 154-155 show the coefficient of frictions for Ti (uncoated and coated with TiC composite coatings) pins against harden steel disks respectively. The friction curves are on the basis of average values that were observed for each combination of sliding speed and normal load during sliding. For the substrate, Figs. 152-153 show the coefficient of friction was higher at 10N for the range of sliding. Higher coefficient of friction at that normal load might be due to more actual contact areas and wear occurred due to adhesive wear mechanism Fig. 162(a). For the rest of the normal loads, the values of μ were found between 0.2-0.3 for the range of sliding speeds. The lower values of μ at those combinations of sliding speeds and normal loads might have been because of more frictional heat due to increase in normal loads result in surface softening effects; lower actual contact area due to rougher contact surfaces [188] and metallic debris trapped in mating surfaces due to severe wear conditions. Moreover, lower coefficient of friction of the substrate might have attributed to the poor frictional wear properties of the Ti. For the coatings, Figs. 154-155 the same trend was observed at 10N; but for the rest of normal loads, the values of μ was found between 0.25-0.35 for the range of sliding speeds and normal loads. A little higher values of μ might have been due to more actual contact areas and mild wear conditions. Overall both materials showed similar frictional behaviour in this case because of poor adhesion between the incompatible pins and disks material [55]. The fluctuation in friction force was observed, either might have resulted from the wear particles that trapped between the mating surfaces during sliding and changing the contact conditions or from oxidation, plastic flow and adhesion effects for various combinations of the sliding speeds and normal loads [161, 181].

8.3.2 Wear mode regimes and maps

The development of wear maps is a useful tool to investigate and predict the wear behaviour of metals in tribology contact. The generalized classification of wear rate into

three distinct wear mode regimes, mild, medium and severe wear are found in literature [11, 31, 32, 34, 165]. In this study, the wear mode regimes, namely (a) very mild wear, (b) mild wear, (c) medium wear and (d) severe wear are defined in consistent with the research work found in literature [34, 72], experimental work carried out (dealt with in Chapters 4, 5, 6 and 7), tests results, mass loss data, wear rate (volume loss rate), physical observations of the worn surfaces, SEM and EDX of the worn surfaces and the wear debris.

The Wear modes regimes limits are as follows:

- a) Very mild wear $\leq [0.1 \times 10^{-12} \text{ (m}^3 \text{ m}^{-1}\text{)]}$
- b) $[0.1 \times 10^{-12} \text{ (m}^3 \text{ m}^{-1}\text{)]} < \text{mild wear} \leq [1.12 \times 10^{-12} \text{ (m}^3 \text{ m}^{-1}\text{)]}$
- c) $[1.12 \times 10^{-12} \text{ (m}^3 \text{ m}^{-1}\text{)]} < \text{medium wear} \leq [3.35 \times 10^{-12} \text{ (m}^3 \text{ m}^{-1}\text{)]}$
- d) Severe wear $> [3.35 \times 10^{-12} \text{ (m}^3 \text{ m}^{-1}\text{)]}$

Fig. 161 shows the various wear mode regimes that were identified for Ti (uncoated and coated with TiC composite coatings) pins against hardened steel disks during dry sliding for the all combinations of sliding speeds and normal loads. It can be clearly seen that severe wear mode is prevalent for Ti pins Fig. 161(a), whereas very mild wear is prevalent with for TiC coatings pins Fig. 161(b) against hardened steel disks. Moreover, in the case of coatings, medium wear occurred only for one combination of sliding speed and normal load and no severe wear occurred against its counterpart for the range of sliding speeds and normal loads. Due to the coatings, mild wear regimes expanded to higher range of sliding speeds and normal loads for substrate with a new wear mode regime i.e. very mild wear and elimination of severe wear mode regime. In the Fig. 161 the combination of the very mild and mild wear zone can be regarded as the safe operation zone for Ti and Ti base TiC composite coatings and hardened steel for this range of sliding speeds and normal loads. As mentioned above and revealed from the wear mode map Fig. 161(a) that due to poor tribological properties, the use of uncoated Ti in the wear-resistant situation is unwarranted.

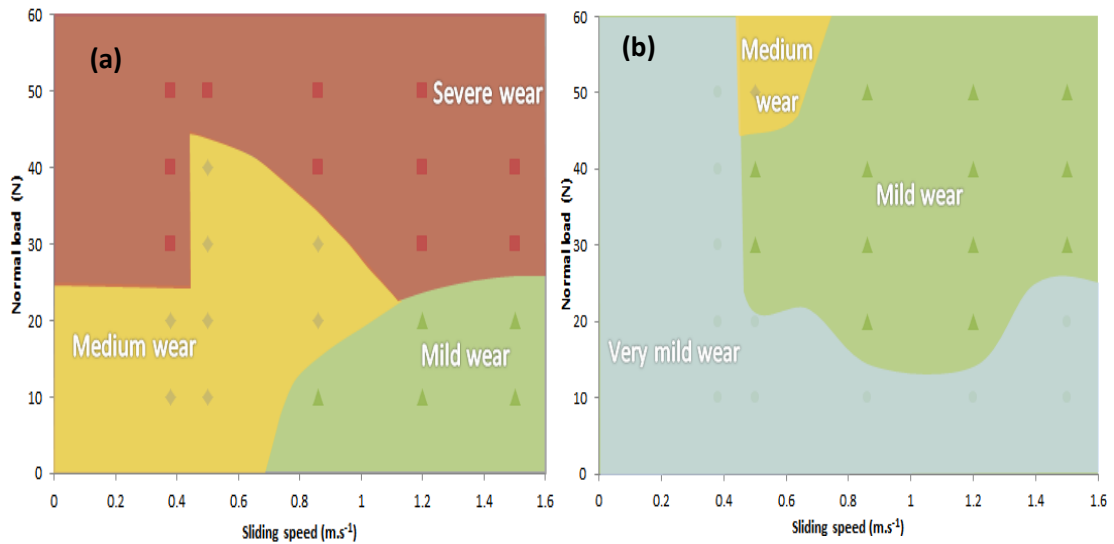


Figure 161 Wear modes maps, (a) Ti pins against hardened steel disks and (b) Ti base TiC coatings pins against hardened steel.

8.3.3 Wear mechanism regimes and maps

Wear mechanism maps are useful tools for analysing the change in regime over a multi-parameter spaces. Wear rates of Ti and Ti base TiC coatings pins against hardened steels disks are represented in wear mechanisms maps form on the normal load versus sliding speeds axis Fig. 162. The wear mechanism regimes are based on the experimental observations and tests results, which can be summarized as follows:

- Oxidative – adhesive wear
- Adhesive - oxidative wear
- Oxidative – abrasive wear
- Abrasive - oxidative wear
- Micro-abrasion
- Abrasive wear

Tribo-corrosion maps for steels, titanium and titanium carbide materials

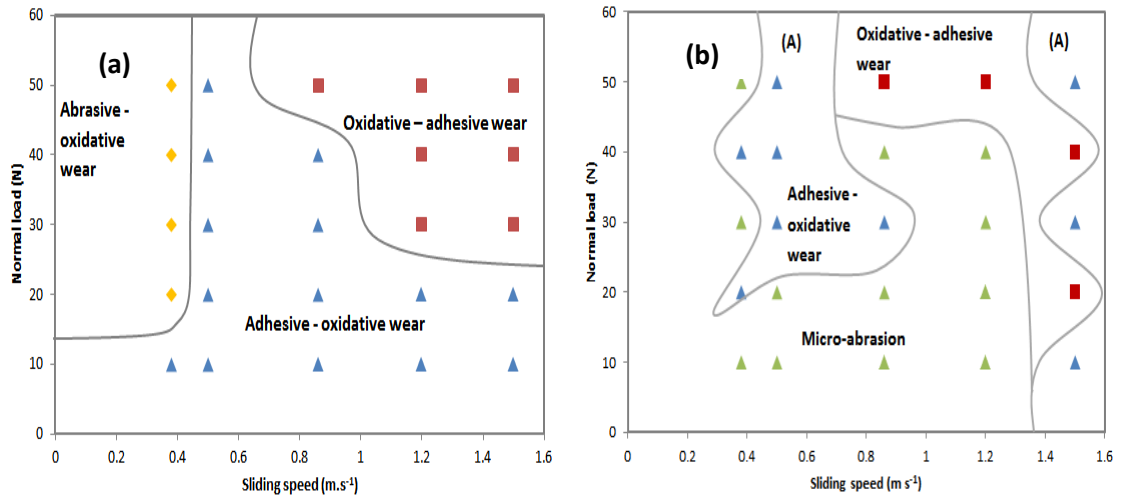


Figure 162 Wear mechanism maps, (a) Ti pins against hardened steel disks and (b) Ti base TiC coatings pins against hardened steel.

The wear mechanisms maps for uncoated and coated Ti exhibit significant transitions with similar regimes at the higher load – sliding speed window but adhesive-oxidative wear dominating the map for Ti material Fig. 162. The wear mechanisms regimes boundaries on the diagrams are only approximate. Fig. 162(a) shows that overall the mechanical wear mechanisms are predominated during dry sliding of Ti pins along with oxidative wear against hardened steel disks, in this tribo-system, which result in severe wear conditions of the uncoated substrate. While, for the TiC coatings, micro-abrasion by hard particles of iron oxide from the counterface is the predominated wear mechanisms Fig. 162(b).

The TiC composite coatings proved to be very effective to increase the wear resistance of the base materials. The increase in wear resistance occurred by several order of the magnitude compared with that of Ti substrate Figs. 142-146, 151, 161. No spalling and/or pulling of hard particles of TiC occurred during dry sliding against hardened steel Figs. 156 TiC($a_{pin} - f_{pin}$), 160(b-c), which result in good protection of the substrate from wear. The higher hardness of TiC particles and low adhesion of the coated surfaces to the counterface are attributed to the high wear resistance of the coatings. The properties of the Ti, especially the coefficient of thermal expansion, affected the Ti/TiC composite coating system and resulted in no cracking of the coated surfaces Figs. 156 TiC($a_{pin} - f_{pin}$), 160(a). This is evident by, as in the case of 303SS base TiC composite coatings (Chapter 5), though TiC coatings showed higher wear resistance as compare to that of uncoated 303SS against alumina but the spalling of coatings surface and pulling out of TiC particles are observed in that case Fig. 91(a). The range of sliding speeds and normal loads were much lower in that

case as compared to that of in Ti/TiC composite coatings system (Chapter 7) but higher wear was observed in that case Table 35 & Fig. 97 and Table 57 & Fig. 130 respectively. The total mass loss 0.023 g occurred for the 303SS base TiC coatings against alumina at sliding speed 0.15 m s^{-1} for the range of normal loads that were up to 10 N for the sliding distance 2,500 m; while in the case of Ti/TiC coating system, total mass loss 0.008 g occurred at much higher sliding speed 0.38 m s^{-1} for the range of normal loads which were up to 50 N for the sliding distance 27,800 m. Wear resistance of the titanium substrate is increased by over 17 times as compare to 7 times of 303SS substrate because of TiC composite coatings. Further it is evident from the wear mode maps Fig. 99(b) (Chapter 5) and Fig. 139(a) (Chapter 7) where very mild wear was found for Ti/TiC coatings as compare to that of 303SS/TiC coatings for the range of sliding speed and normal load. Moreover, it is cleared from the Fig. 100(b), (Chapter 5) and Fig. 140(a), (Chapter 7) that for 303SS/TiC coatings, adhesive, abrasive and oxidative wear were dominated, while for Ti/TiC coatings against hardened steel micro-abrasion was wear mechanism for this range of sliding speed and normal load.

8.4. Conclusion

1. For titanium sliding against steel, oxidative wear predominates at lower normal loads for the range of sliding speeds and is associated with relatively high wear rates indicating the non-protective nature of the oxide formed.
2. The titanium/steel sliding couple results in severe sliding conditions with adhesive wear, delamination, plastic deformation, material transfer and abrasive wear of the pins material.
3. A mechanically mixed metal layer develops under various combinations of sliding speed and normal load on the wear tracks. However, the protective role of this layer depends on the oxide morphology and the contact conditions.
4. Due to poor tribological properties, the use of uncoated Ti in the wear-resistant situation is unwarranted.
5. Ti substrate coated with TiC composite coatings by TIG welding torch melting method and tested for dry sliding wear against hardened steel to investigate the change in wear modes and wear mechanisms at various sliding speeds and normal loads.

6. TiC composite coatings were found to be stable on Ti substrate and did not wear through to the substrate for any combination of sliding speed and normal load. The coatings protected the base material from wear.

7. The wear of TiC hard coatings can change significantly with variation of parameters such as normal load and sliding speed.

8. Significant levels of iron oxide were transferred to TiC coatings pins at lower sliding speed while some transfer of pins material to disks occurred at higher sliding speeds and normal loads due to adhesion resulted from increases in contact temperatures.

9. The wear mechanisms involved in the wear of TiC coatings were one or more of the following: TiC micro-abrasion, Fe oxide transfer, adhesive and oxidation of the contact surfaces.

10. TiC composite coatings Increase the wear resistance of the substrate by over 17 times. Mild wear regime expanded to higher range of sliding speed and normal load with a new wear regime i.e. very mild wear and elimination of severe wear regime.

Chapter 9

Conclusions and future work

9.1 Conclusions

In general, the following conclusions can be extracted from this experimental study:

For 303SS against 8620 low alloy steel in dry sliding contact, fluctuation in the wear of both materials with increases in normal load and sliding speed is attributed to strain hardening, thermal softening and oxidation effects of the mating surfaces due to frictional heating. For highly alloyed material, 303SS, severe wear is more prevalent in the relatively high load and speed regimes, whereas for the 8620 low alloy steel, medium wear is predominant than mild wear for the range of speeds and normal loads. Such observations are interpreted in the role of wear-oxidation mechanisms, material transfer, and the development of a mechanically mixed layer in modifying the wear process in the tribological contact. The differences of the tribo-oxidation area of the map for the stainless steel compared with the low alloy steel are attributed to the role of Cr in reducing the oxidative wear process for the latter material.

Uncoated 303SS exhibited poor wear resistance against alumina which was increased by applying a TiC composite coating. The coating was applied with a TIG welding torch melting process and it substantially increased the wear resistance of the substrate for the tested range of sliding speeds and normal loads. Significant differences in wear regimes were identified for both materials, with more evidence of oxidation for the coated material in these conditions. Adhesive wear was predominated wear mechanisms for the steel, in particular at higher normal loads and sliding speeds. Oxidation wear influenced the wear mechanisms at intermediate normal loads and sliding speeds in each case. Wear maps are indicating many possible wear regimes and significant differences in material degradation mechanisms for the substrate and TiC coatings

Dry sliding wear tests were conducted for Ti pins against hardened steel disks. Wear maps have been constructed for these materials based on the tests results. Significant differences were observed for maps generated for the pin and disk materials. Oxidative wear was predominated at lower load for the range of sliding speeds. Ti/hardened steel pair suggested severe sliding conditions with adhesive wear, delamination wear, plastic

deformation, material transfer and abrasive wear of the pins material. Adhesive and delamination is suggested as the sole wear mechanism. A mechanical mixed metal layer existed on wear tracks under various combination of sliding speed and normal load. However, the protective role of this layer depended on intensity and the nature of the oxide present in the layer. More oxides in tribo-layer may increase its protectiveness property. Ti showed very poor wear resistance in this dry sliding system due to its inability to form protective oxide layer during sliding. Thus the use of Ti under dry sliding condition is unwarranted.

Ti base TiC composite coatings were tested for dry sliding wear against hardened steel to investigate the change in wear modes and wear mechanisms at various sliding speeds and normal loads. Wear maps have been constructed for these materials based on the test results. Significant differences have been observed for maps generated for the pins and disks materials. TiC composite coatings found stable on the Ti substrate and did not wear through substrate for any combination of sliding speed and normal load. The coatings protected the base material well because no spalling of the coatings occurred during sliding. The wear of TiC hard coatings can change dramatically with adjustments of parameters such as normal load, sliding speed, contact geometry and humidity. Very mild wear was predominated for the TiC composite coatings while mild wear was predominated for the hardened steel counterpart against each other and no severe wear was found for both materials under these experimental conditions. Significant iron oxide transferred to TiC coatings pins at lower sliding speed for the range of normal load while some transfer of pins material to hardened steel disks occurred at higher sliding speeds and normal loads. The wear mechanisms involved in the wear of TiC coatings were one or more of the following: TiC micro-polishing, Fe oxide transfer, adhesive and oxidative wear. The coating integrity was maintained for the range of sliding speeds and normal loads. The significant increase in wear resistance of the substrates (303SS and Ti) by TiC composite coatings produced by TIG welding torch melt method suggests that this coating process is a promising method to replace the other expensive coating methods.

9.2 Future work

The Tungsten Inert Gas (TIG) welding torch melting method, which was used for coating substrates (303SS and Ti), has advantages over other coatings processes due to its simple apparatus, ease of operation and low net cost. In the present work, the integrity and

Tribo-corrosion maps for steels, titanium and titanium carbide materials

improvement in sliding wear resistance due to coatings have been found comparable to that of the composite coatings carried out by different processes, found in the literature. Tribo-corrosion maps have constructed on the basis of test results on sliding speeds versus normal loads. A lot of research work is still required to check the integrity and tribo-corrosion behaviour of the coatings produced by this method to replace the other coating processes on commercial basis, a few of which are as follows:

(i) To investigate the wear mechanisms of coatings of varying such as volume fraction and particle size to provide a basis for coating optimization in various conditions.

(ii) To tests above TiC coatings in different environments such as in vacuum, at high temperature, in lubrication and corrosive conditions for the above range sliding speeds and normal loads as well as for the higher range and construction of tribo-corrosion maps.

(iii) To test the coatings produced by TIG process for other than sliding application such as wear by micro-abrasion-corrosion and erosion-corrosion.

(iv) To test the coatings produced by TIG process to study the synergy effects with respect to different applications such as sliding, abrasive and erosive in corrosive environments.

References

- [1] D. Landolt, Electrochemical and materials aspects of tribo-corrosion systems, *J. Physics D: Appl. Phys.* 39, 1-7 (2006).
- [2] S. W. Watson, F. J. Friedersdorf, B. W. Madsen, S. D. Cramer, Methods of measuring wear-corrosion synergism, *Wear* 181-183, (1995), Pages 476-484.
- [3] K. Sasaki, G.T. Burstein, *Philosophical Magazine Letters*, 80 (2000) 489-493.
- [4] M. M. Stack, "Bridging the gap between tribology and corrosion: from wear maps to Pourbaix diagrams," *International Materials Reviews*, vol. 50, no. 1, pp. 1-17, 2005
- [5] H. A. Abdel-Aal, On the interdependence between kinetics of friction-released thermal energy and transition in wear mechanisms during sliding of metallic pairs, *Wear* 254 (2003), Pages 884-900.
- [6] N. Chelliah, S. V. Kailas, Synergy between tribo-oxidation and strain rate response on governing the dry sliding wear behaviour of titanium, *Wear* 266 (2009), Pages 704-712.
- [7] M. A. Chowdhury, M. K. Khalil, D. M. Nuruzzaman, M. L. Rahaman, The effect of slid speed and normal load on friction and wear property of aluminium, *International Journal of Mechanical Mechatronics Engineering IJMME-IJENS* Vol. 11 No: 01, Pages 53-57.
- [8] M. M. Stack, J. Jiang, F.H. Stott, A generic model for dry sliding wear of metals at elevated temperatures, *Wear*, Vol. 256, Issues 9-10, May 2004, Pages 973-985.
- [9] M. M. Stack, J. Jiang, F.H. Stott, Some frictional features associated with sliding wear of the nickle-base alloy N80A at temperature to 250 °C, *Wear* 176 (1994), Pages 185-194.
- [10] J. Jiang, F. H. Stott and M. M. Stack, The role of triboparticulates in dry sliding wear, *Tribology International* 31, (1998), Pages 245-256.
- [11] J. F. Archard and W. Hirst, The wear of metals under unlubricated conditions, *Proc. R. Soc., Lond. A* 236, (1956), Pages 397-410.
- [12] J. K. Lancaster, The formation of surface films at the transition between mild and severe metallic wear, *Proc. R. Soc., Lond. A*, 273 (1963), Pages 466-483.
- [13] N. C. Welsh, The dry wear of steels II. Interpretation and special features, *Phil. Trans. R. Soc., Lond. A*, 257 (1965), Pages 51-70.
- [14] T.S. Eyre, D. Maynard, Surface aspects of unlubricated metal-metal wear, *Wear*, 18 (1971), Pages 301-310.
- [15] F. H. Stott, J. Glascott and G. C. Wood, The sliding wear of commercial Fe-12SgoCr alloys at high temperature, *Wear*, 101 (1985), Pages 311-324.
- [16] P. T. Newman, J. Skinner, The high temperature sliding wear of stainless steel in a CO₂ atmosphere – the effect of adding low concentrations of O₂, *Wear*, 112 (1986), Pages 291-325.

- [17] F. H. Stott, D. S. Lin, G. C. Wood, G. W. Stevenson, The tribological behaviour of nickel and nickel-chromium alloys at temperatures from 20° to 800°C, *Wear*, 36 (1976), Pages 147-174.
- [18] A.F. Smith, The unlubricated reciprocating sliding wear of 316 stainless steel in CO₂ at 20-600°C, *Tribology International*, 19 (1986), Pages 65-71.
- [19] F. H. Stott, J. Glascott and G. C. Wood, Model for the generation of oxides during sliding wear, *Proc. R. Soc., Lond. A*, 402 (1985), Pages 167-186.
- [20] Y. Tsuyu, Microstructure of wear, friction and solid lubrication, *Tech. rep. of Mech. Eng. Lab., Japan*, vol.3, no. 81, 1975.
- [21] Biswas, S. K., and Kailas, S. V., "Strain Rate Response and Wear of Metals," *Tribol. Int.* 30 (1997), Pages 369–375.
- [22] W. Hirst and J. K. Lancaster *J. Appl. Phys.* 1956, 27, 1057.
- [23] N. C. Welsh, The dry wear of steels, *Trans. Roy. Soc. London*. 1965, Vol. 257.A. 1077.
- [24] A. Somi Reddy, B.N. Pramila Bai., K.S.S. Murty and S.K. Biswas, Wear and seizure of binary Al-Si alloys, *Wear*, 1994, 171, Pages 115-127.
- [25] J K Lancaster, Material-specific wear mechanisms: relevance to wear modelling, *Wear*, 141, Issue 1, December 1990, Pages 159-183.
- [26] M. M. Khruschov, *proc. Conf. on Lubrication and Wear*, Inst. of Mech. Eng., London, 1957. Page 655.
- [27] D. A. Rigney, Comments on the sliding wear of metals, *Tribology International*, 30 (1997), Pages 361-367.
- [28] M. M. Khruschev, Cited in Kragelskii I.V. *Friction and wear*, transl. by L. Ronson and J. K Lancaster, Butterworths, London, 1965.
- [29] J. F. Archard, Contact and rubbing of flat surfaces, *J. Appl. Phys.* 1953, 24, Pages 981-988.
- [30] D. A. Rigney, Some thoughts on sliding wear, *Wear* 1992, 152, Pages 187-192.
- [31] J.F. Archard, W. Hirst, An examination of a mild wear process, *Proc. Roy. Soc. London, A* 238 (1957), Pages 515-528.
- [32] C.C. Viafara, A. Sinatora, Influence of hardness of the harder body on wear regime transition in a sliding Pair of steels, *Wear* 267 (2009), Pages 425-432.
- [33] I. A. Inman, S.R. Rose, P.K. Datta, Development of a simple 'temperature versus sliding speed' wear map for the sliding wear behaviour of dissimilar metallic interfaces, *wear*, 260(2006), Pages 919-932.
- [34] A.F. Smith, The sliding wear of 316 stainless steel in air in the temperature range 20-500°C, *Tribology International*, 18 (1985), Pages 35-43.
- [35] T.F.J. Quinn, Oxidational wear, *Wear*, 18 (1971), Pages 413-419.
- [36] T.F.J. Quinn, D.M. Rowson, J.L. Sullivan, Application of oxidational theory of mild wear to the sliding wear of low alloy steel, *Wear*, 65 (1980), Pages 1-20.

- [37] T.F.J. Quinn, Review of oxidational wear, Part 1. The origins of oxidational wear, *Tribology International*, 16 (1983), Pages 257-271.
- [38] H. Hong, W.O. Winer, A fundamental tribological study of Ti/Al₂O₃ contact in sliding wear, *ASME: Journal of Tribology*, 111 (1989) 504-509.
- [39] H. Hong, R.F. Hochman, T.J.F. Quinn, A new approach to the oxidational theory of mild wear, *STLE Transanction*, 31 (1988), Pages 71-75.
- [40] I.I. Garbar, Gradation of oxidational wear of metals, *Triboloy International*, 35 (2002), Pages 749-775.
- [41] L. H. Chen, D.A. Rigney, Adhesion theories of transfer and wear during sliding of metals, *Wear*, 136 (1990), Pages 223-235.
- [42] M. Kerridge, Metal transfer and the wear process, *Proc. R. Soc. London, Sect. B*(2nd edn.), Pages 400-407.
- [43] M. Antler, Processes of metal transfer and wear, *Wear*, 7 (1964), Pages 181-203.
- [44] R. G. Bayer, A. K. Trivedi, Selection and use of wear tests for metals, *ASTM Sp. Tech. Pub.615*, (1975), Pages 91-101.
- [45] M. Kerridge and J. K. Lancaster, The stages in a process of severe metallic wear, *Proc. Roy. Soc. (London)*, A236 (1956), Pages 250-264.
- [46] A. W. J. De Gee and J. H. Zaat, Wear of copper alloys against steel in oxygen and argon, *Wear*, 5 (1962), Pages 257-274.
- [47] R. H. Brown and E. J. A. Armarego, Some observations on the friction and wear of a hardened rider, *Wear*, 6 (1963), Pages 106-117.
- [48] M. Cocks, Interaction of sliding metal surfaces, *J. Appl. Phys.*, 33 (1962), Pages 2152-2161.
- [49] M. Antler, Wear, friction, and electrical noise phenomena in severe sliding systems, *ASLE Trans.*, 5 (1962), Pages 257-274.
- [50] S. Krol, L. Ptacek, M. Hepner, Friction and wear properties of titanium and oxidised titanium in dry sliding against hardened C45 steel, *Journal of Materials Processing Technology*, 157-158 (2004), Pages 364-369.
- [51] A. Devaraju, A. Elaya Perumal, J. Alphonsa, Satish V. Kailas, S. Venugopal, Sliding wear behaviour of plasma nitride Austenitic Stainless Steel Type AISI 316LN in temperature range from 25 to 400 centigrade at 10⁻⁴ bar, *Wear*, 288(2012), Pages 17-26.
- [52] Shiv Kumar, Ashish Bhattacharyya, Dipak Kumar Mondal, Koushik Biswas, Joydeep Maity, Dry sliding wear behaviour of medium carbon steel against alumina disk, *Wear*, 270 (2011), Pages 413-421.
- [53] Y. C. Lin, S. W. Wang, T. M. Chen, A study on the wear behaviour of hardened medium carbon steel, *Journal of Materials Processing Technology*, 120 (2002), Pages 126-132.

Tribo-corrosion maps for steels, titanium and titanium carbide materials

- [54] Y. Guilnard, J. Denape and J. A. Petit, Friction and wear thresholds of alumina- chromium steel Pairs sliding at high speeds under dry and wet conditions, *Tribology International*, 26 (1993), Pages 29-39.
- [55] S. Bahadur, Chien-Nan Yang, Friction and wear behaviour of tungsten and titanium carbide coatings, *Wear*, 196 (1996), Pages 156-163.
- [56] H. E. Hintermaan, Adhesion, friction and wear of thin hard coatings, *Wear*, 100 (1984), Pages 381-397.
- [57] P. Wallen and S. Hogmark, Influence of TiN coating on wear of high steel at elevated temperature, *Wear*, 130 (1989), Pages 123-135.
- [58] J. L. Olivares and L. C. Grigorescu, Friction and wear behaviour of thermally sprayed nichrome-WC coatings, *Surface and Coating Technology*, 33 (1987), Pages 183-190.
- [59] S. J. Bull, D. S. Rickertson and A. Hendry, The abrasive wear resistance of sputter ion plated Titanium nitride coatings, *Surface and Coatings Technology*, 36 (1988), Pages 743-754.
- [60] D. S. Rickerby and P. J. Burnett, The wear and erosion resistance of hard PVD coatings, *Surface And coatings Technology*, 33 (1987), Pages 191-211.
- [61] H. Kitsunai, N. Tsumaki and K. Kato, Transitions of microwear mechanism for Cr₂O₃ ceramic Coatings during repeated sliding observed in an SEM. Tribo system, in K. C. Ludema and R. G. Bayer (eds.), *Wear of materials*, ASME, New York, 1991, Pages 249-255.
- [62] I. M. Hutchings, *Tribology, Friction and Wear of Engineering Materials*, ISBN 034056184X.
- [63] S. C. Lim, Recent developments in wear mechanism maps, *Tribology International* 31 (1998), Pages 87-97.
- [64] D. Tabor, Status and direction of tribology as a science in the 80's., *Proc. Int. Conf. Tribology in the 80's*, NASA Lewis Research Centre, Cleveland, Ohio, (1983), Pages 1-17.
- [65] C. Y. H. Lim, S. C. Lim, K. S. Lee, Wear of TiC-coated carbide tools in dry turning, *Wear*, 225-229 (1999), Pages 354-367.
- [66] M. M. Stack, W. Huang, G. Wang, C. Hodge, Some views on the construction of Bio-tribo-corrosion maps for Titanium alloys in Hank's solution: Particle concentration and applied loads effects, *Tribology International* 44 (2011), Pages 1827-1837.
- [67] M. M. Stack, Mapping tribo-corrosion processes in dry and in aqueous conditions: some new Directions for the new millennium, *Tribology International*, 35 (2002), Pages 681-689.
- [68] N. C. Welsh, Tribo-metallographic behaviour of high carbon steel, *Philos. Trans. R. Soc., Ser. A* 257 (1965) Pages 31-50.
- [69] S. C. Lim, M.F. Ashby, Overview no. 55 wear-mechanism maps, *Acta Metallurgica*, 35(1987), Pages 1-24.
- [70] H. Kato, T. S. Eyre and B. Ralph, Wear mechanism map of nitride steel, *Acta Metall. Mater.* 4 (1994), Pages 1703-1713.

- [71] P. Gautier and K. Kato, Wear mechanism of silicon nitride, partially stabilized zirconia and alumina in unlubricated sliding against steel, *Wear*, 162-164 (1993), Pages 305-313.
- [72] J. Zhang and A. T. Alpas, Transition between mild and severe wear in aluminium alloys, *Acta Mater.*, 45 (1997), Pages 513-528.
- [73] S. Wilson , A. T. Alpas, Wear mechanism maps for metal matrix composites, *Wear*, 212 (1997), Pages 41-49.
- [74] S. Wilson , A. T. Alpas, Wear mechanism maps for TiN-coated high speed steel, *Surface and Coatings Technology*, 120-121 (1999), Pages 519-527.
- [75] W. Grzesik , Z. Zalisz, S. Krol, P. Nieslony, Invetgation of friction and wear mechanisms of the PVD-TiAlN coated carbide in dry sliding against steels and cast iron, *Wear*, 261 (2006), Pages 1191-1200.
- [76] T. F. J. Quinn, *Physical Analysis for Tribology*, Cambridge University Press, Cambridge, 1991.
- [77] D. Landolt, *Corrosion and Surface Chemistry of Metals*, EPFL Press, Lausanne, Switzerland, (2007) Pages 227-274.
- [78] S. Tagella, A.K. Skder, A. Kumar, Tribological Issues and Modeling of Removal Rate of Low-*k* Films in CMP, *J. Electrochem. Soc.* 151 (2004) G205.
- [79] Dowson, D. (1998), *History of Tribology*, Second edition, Instn Mech. Engrs, London, UK.
- [80] Davidson, C.S.C. (1957), "Bearings since the Stone Age," *Engineering* 183, 2-5.
- [81] Amontons, G. (1699), "De la Resistance Causee dans les Machines," *Memoires de l' Academie Royale*, A, 257-282.
- [82] Coulomb, C.A. (1785), "Theorie des Machines Simples, en ayant regard au Frottement de leurs Parties, et. a. la Roideur des Cordages," *Mem. Math. Phys.*, X, Paris, Pages 161-342.
- [83] Parish, W. F. (1935), "Three thousand years of Progress in the Development of Machinery and Lubricants for the hand Crafts," *Mill and Factory* 16 and 17.
- [84] Dowson, D. (1998), *History of Tribology*, Second edition, Instn Mech. Engrs, London, UK.
- [85] Holm, R. (1946), *Electrical Contacts*, Springer-Verlag, New York.
- [86] Bowden. F. P., and Tabor, D. (1950), *The Friction and Lubrication of Solids, Part I*, Clarendon Press, Oxford, UK.
- [87] Bowden. F. P., and Tabor, D. (1964), *The Friction and Lubrication of Solids, Part II*, Clarendon Press, Oxford, UK.
- [88] Bhushan, B. (2001a), *Modern Tribology Handbook*, Vols. 1 and 2, CRC Press, Boca Raton, Florida.
- [89] Bharat Bhushan, *Introduction to Tribology*, ISBN 0-471-15893-3, Page 331.
- [90] Kayaba, T. and Kato, K. (1981), "Adhesive Transfer of the Slip-Tongue and the Wedge," *ASLE Trans.* 24, Pages 164-174.

- [91] Rabinowicz, E. (1953), "A Quantitative Study of the Wear Process," Proc. Phys. Soc. Lond. B66, Pages 929-936.
- [92] Kerridge, M. and Lancaster, J. K. (1956), "The Stages in a Process of Severe Metallic Wear," Proc. R. Soc. Lond. A236, Pages 250-264.
- [93] Bhushan, B., Nelson, G. W., and Wacks, M. E., (1986), "Head-Wear Measurements by Autoradiography of the Worn Magnetic Tapes," ASME J. Trib. 108, Pages 241-255.
- [94] Cook, N. H. and Bhushan, B., (1973), "Sliding Surface Interface Temperatures," ASME J. Lub. Tech. 95, Pages 31-36.
- [95] Bhushan, B., Davis, R. E., and Kolar, H. R., (1985b), "Metallurgical Re-examination of wear Modes II: adhesive and abrasive," Thin Solid Films 123, Pages 113-126.
- [96] Rabinowicz, E. (1995). Friction and Wear of Materials. New York, John Wiley and Sons.
- [97] Suh, N. P. (1986), Tribophysics, Prentice-Hall, Englewood, New Jersey.
- [98] Bhushan, B. (1999), Principles and Applications of Tribology, Wiley, New York.
- [99] Aleinikov, F. K. (1957), "The influence of Abrasive Powder Micro-hardness on the Values of the coefficient of Volume Removal," Soviet Physics-Technical Physics, 2, Pages 505-511.
- [100] Richardson, R. C. D. (1968), "The wear of metals by Relatively Soft Abrasive," Wear, 11, Pages 245-275.
- [101] Rabinowicz, E. (1977), "Abrasive Wear Resistance as a Materials Test," Lub. Eng. 33, Pages 378-381.
- [102] Rabinowicz, E. (1983), "The Wear of Hard Surface by Soft Abrasives," Proc. Of Wear of Materials (K.C. Ludema, ed.). Pages 12-18, ASME, New York.
- [103] Khuschov, M. M. (1974), "Principles of Abrasive Wear," Wear 28, Pages 69-88.
- [104] Mulhearn, T. O. and Samuels, L. E. (1962), "In Abrasion of Metals: A Model of the Process," Wear 5, Pages 478-498.
- [105] Goddard, J. and Wilman, M. (1962), "A theory of Friction and Wear during the Abrasion of Metals," Wear 5, Pages 114-135.
- [106] Misra, A. and Finnie, I. (1981), "Some Observations on Two-body Abrasive Wear," Wear 68, Pages 41-56.
- [107] Khuschov, M. M. and Babichev, M. A. (1958), "Resistance to Abrasive Wear of Structurally Inhomogeneous Materials," Friction and Wear in Machinery, 12, Pages 5-23, ASME, New York.
- [108] Xie, Y. and Bhushan, B. (1996a), "Effect of Particle Size, Polishing pad and Contact Pressure in Free Abrasive Polishing," Wear 200, Pages 281-295.
- [109] Bhushan, B., and Khatavkar, D. V. (1996), " Role of Water Vapor on the Wear of Mn-Zn Ferrite Heads Sliding Against Magnetic Tape," Wear 202, Pages 30-34.
- [110] Bitter, J. G. A., (1963), "A Study of Erosion Phenomena," Wear 6, Part I, Pages 5-21, Part II, Pages 169-190.

Tribo-corrosion maps for steels, titanium and titanium carbide materials

- [111] Finnie, I., (1960), "Erosion of Surfaces by solid particles," *Wear* 3, Pages 87-103.
- [112] Preece, C. M. (ed) (1979), *Treatise on Materials Science and Technology*, Vol 16: Erosion, Academic Press, San Diego, CA.
- [113] Engel, P. A. (1976), *Impact Wear of Materials*, Elsevier, Amsterdam.
- [114] G. Heinicke, (1984), *Tribochemistry*, Carl Hanser Verlag, Munich.
- [115] T. E. Fisher, *Tribochemistry*, *Ann. Rev. Mater. Sci.* 18, (1988), Pages 303-323.
- [116] A. Fischer and Mischler S 2006 Tribocorrosion: fundamentals, materials and applications—editorial *J. Phys. D: Appl. Phys.* 39 issue 15, doi:10.1088/0022-3727/39/15/E01
- [117] Archard JF, Hirst W., An examination of a mild wear process *Proc. R. Soc, A238*, (1957), Pages 515-528.
- [118] Suh NP., The delamination theory of wear, *Wear* 25, (1973), Pages 111-124.
- [119] S. C. Lim, The relevance of wear-mechanism maps to mild-oxidational wear, *Tribology International* 35 (2002), Pages 717-723.
- [120] Williams K, Giffen E. Friction between unlubricated steel surfaces at sliding speeds up to 750 feet per second, *Proc. I Mech E* (1963-64); 178 (3(N)), Pages 24-36.
- [121] Powell DG, Earles SWE, Wear of unlubricated steel surfaces in sliding contact, *ASLE Trans* 11, (1968), Pages 101-108.
- [122] A. Savan, H. J. Boving, E. Fluehmann and H. E. Hintermann, Increased performance of bearing using TiC- coated balls, *Journal DE PhysicsIV*, 3 (1993), Pages 943-948.
- [123] T. F. J. Quinn, *Fundamental of Tribology*, Proc. Int. Conf, MIT Press, Cambridge, Mass, (1978), Page 477.
- [124] T. F. J. Quinn, *Tribo. Int.* 16, (1983), Page 257.
- [125] D. Tabor, *Trans. ASME., J. Lub. Tech.*, 99, (1977), Page 387.
- [126] K. C. Ludema, Review paper for Interdisciplinary Collaboration in Tribology Project, NASA Lewis Research Centre (1981).
- [127] A. A. Reda, R. Bowen and V. C. Westcott, *Wear* 34, (1975), Page 261.
- [128] F. T. Barwell, E. R. Bowen, J. P. Bowen and V. C. Westcott, *Wear* 44, (1977), Pages 163.
- [129] S. C. Lim, M.F. Ashby and J. H. Brunton, Wear-rate transitions and their relationship to wear mechanism, *Acta. Metaa.* 35, (1987), Pages 1343-187.
- [130] T. F. J. Quinn, Oxidational wear, *Wear* 18, (1971), Page 413-419.
- [131] Earles SWE, Kadhim M. J., Friction and wear of unlubricated steel surfaces at speed up to 655 ft s⁻¹, *Proc. I Mech E* 180(1), (1965-66), Pages 531-547.
- [132] D. A. Rigney, L. H. Chen, M. G. S. Naylor and A. R. Rosedfield, Wear process in sliding systems, *Wear*, 100 (1984), Pages 195-219.
- [133] A.F. Smith, The influence of sliding speed on the unlubricated wear of 316 stainless steel at low load, CEGB Report TPRD/B/0456/N84, 1984.

- [134] T.F.J. Quinn, Review of oxidational wear – Part 1. The origins of oxidational wear, *Tribology International*, 16 (1983), pp.257-271.
- [135] Lim S C, Ashby M F and Brunton J H, Wear mode-mode map for unlubricated sliding of steel on steel in the pin-on-disc configuration, *Acta Metall.* 35, (1987), Pages 1343-1348).
- [136] Y. Liu, R. Asthana, P. K. Rohatgi, *J. Materials Sci.* 26 (1991), Pages 99-102.
- [137] Md. Ohidul Alam, A. S. M. A. Haseeb, Response of Ti-6Al-4V and Ti-24Al-11Nb alloys to dry sliding wear against hardened steel, *Tribology International*, 35 (2002), Pages 357-362.
- [138] K. Kato, *Surface coating Technology* 76-77, (1995), Pages 469-474.
- [139] K. Kato, in: H. M. Hawthorne, T. Troczynski (Eds.) *Advanced Ceramics for Structural and Tribological Applications*, Proc. 34th Conf. CIM, Vancouver, 1995, Pages 23-36.
- [140] M. O. Borel, A. R. Nicoll, H. W. Schlapfer and R. K. Schmid, The wear mechanisms occurring in Abradable seals os gas turbines, *Surf. Coat. Technol.*, 39/40 (1989), Pages 117-126.
- [141] C. Y. H. Lim, *Surface coatings for cutting tools*. PhD. thesis. National University of Singapore 1996.
- [142] M. Okoshi and H. Sakai, Research on the mechanism of abrasion. Report III, mechanism of abrasion of cast iron and steel, *Trans. JSME*, 1941, 7, Pages 29-47.
- [143] M. Mustafa Yildirim, Soner Buytoz, Mustafa Ulutan, Dry sliding wear behaviour of TIG welding clad WC composite coatings, *Applied Surface Science* 252 (2005), Pages 1313-1323.
- [144] T. H. C. Childs, The sliding wear mechanisms of metals, mainly steels, *Tribol. Int.*, 13 (1980), Pages 286-293
- [145] T. S. Eyre, *Wear mechanisms*, *Powder Metall.*, 24 (1981), Pages 57-63
- [146] J. Marciniak and T. Otimianowski, An interpretation of the sliding speed effect on the wear of low carbon steel based on the theory of oxidation, In Proc. Eurotrib 81. 1A, The Polis Tribology Council, Warsaw, (1981), Pages 241-256
- [147] K. Egawa, Effects of the hardness of hardened steel on friction wear (3rd report)-cubic model From region of different forms of wear, *J. JSLE Int. Edn* 3 (1982), pages 27-30.
- [148] R. N. Rao, S. Das, D.P. Modal, G. Dixit, S. L. Tulasi Devi, Dry sliding wear maps for AA7010 (Al-Zn-Mg-Cu) aluminium matrix composite, *Tribo. Int.* 60 (2013), Pages 77-82.
- [149] M.M. Stack, T. M. Abd El Badia, Mapping erosion–corrosion of WC/Co–Cr based composite coatings: particle velocity and applied potential Effects, *Surface& Coatings Technology* 201(3-4) (2006), Pages 1335–1347.
- [150] S. Hochstrasser-Kurz, Y. Mueller, C. Latkoczy, S. Virtanen and P. Schmutz, Analytical characterization of the corrosion mechanisms of WC-Co by electrochemical methods and inductively coupled plasma mass spectroscopy, *Corros. Sci.* 49, (2007), pages 2002-2020.
- [151] J. R. Whitehead, Surface deformation and friction of metals at light loads, *Proc. Roy. Soc. London A*201, (1950), Pages109-124.

- [152] B. Bhushan (1996) Tribology and Mechanics of Magnetic Storage Devices, 2nd edition, Springer-Verlag, New York.
- [153] K. Kato, Wear mechanisms, New direction, Tribol. (1997), Pages 39-56, published at the First World Technology Congress, I Mech E.
- [154] Koji Kato, Wear in relation to friction – a review, Wear 241 (200) 151-157.
- [155] K. H. Zum Gahr, Microstructure and wear of materials, Elsevier, Tribol. Ser. 10 (1987), Pages 174-176
- [156] D.M. Kennedy, M.S.J. Hashmi, Methods of wear testing for advanced surface coatings and bulk materials, Journal of Materials Processing Technology 77 (1998), Pages 246-253.
- [157] S. Mridha, A. N. Md. Idriss, TN Baker, 2012, From: Introduction to physical metallurgy of welding, K.E. Easterling 1992 and Incorporation of TiC particulates on AISI 4340 low alloy steel surface via TIG arc melting.
- [158] A. Monfared, A. H. Kokabi, S. Asgari, Microstructural studies and wear assessments of Ti/TiC surface composite coatings on commercial pure Ti produced by titanium cored wires and TIG process, Materials Chemistry and Physics, 137 (2013), Pages 959-966.
- [159] W. Hirst and J. K. Lancaster, Proc. R. Soc. Lond. A 6 December 1960 vol. 259 no. 1297, Pages 228-241.
- [160] N. Saka, A.M. Eleiche and N. P. Suh, Wear 44, 109 (1977).
- [161] L. C. Betancourt-Dougherty, R. W. Smith, Effects of load and sliding speed on the wear behaviour of plasma sprayed TiC-NiCrBSi coatings, Wear 217 (1998), Pages 147-154.
- [162] J. K. Lancaster: Proc. R. Soc. Lond. 1963, 273A, Pages 466-483.
- [163] D. A. Rigney, The roles of hardness in the sliding behaviour of materials, Wear, 175 (1994), Pages 63-69.
- [164] M. M. Stack, F H Stott and G C Wood, The effect of pre-oxidation of chromia and alumina forming alloys on erosion in laboratory simulated fluidized-bed conditions, Corrosion Science 1992, 33, Vol. 6. Pages 965-983.
- [165] J.T. Burwell, C.D. Strang, on the empirical law of adhesive wear, J. Appl. Phys., 23 (1952) Pages 18-28.
- [166] K. H. ZUM GAHR, Sliding wear of ceramic- ceramic, ceramic-steel and steel-steel pairs in lubricated and unlubricated contact Wear, 133 (1989), Pages 1-22.
- [167] J. Q. Jiang, R.-S. Tan, Dry sliding wear of an alumina short fibre reinforced Al-Si alloy Against Steel, Wear, 195 (1996), Pages 106-111.
- [168] K. H. Habig, Wear behaviour of surface coatings on steels, Tribol. Int., 22 (1989), Pages 65-73.
- [169] C.C. Viafara, M.I. Castro, J.M. Velez, A. Toro, Unlubricated sliding wear of pearlitic and bainitic steels Wear, 259 (2005), Pages 405-411.

Tribo-corrosion maps for steels, titanium and titanium carbide materials

- [170] R. Lalitha, Katipelli, Arvind Agarwal, Narendra, B. Dahotre, Laser Surface engineered TiC coating on 6061 Al alloy: microstructure and wear, applied, Surface Science, 153 (2000), Pages 65-78.
- [171] S. Wilson , A. T. Alpas, TiN coating wear mechanisms in dry sliding contact against high speed steel, Surface Coatings Technology, 108-109 (1998), Pages 369-376.
- [172] C. Yang and S. Bahadur, Friction and wear behaviour of alumina-based ceramics in dry and Lubricated sliding against tool steel, Wear 157 (1992), Pages 263-277.
- [172] S. Kataria, N. Kumar, S. Dash, A. K. Tyagi, Tribological and deformation behaviour of titanium Coating under different sliding contact conditions, Wear 269 (2010), Pages 797-803.
- [173] K. G. Budinski, Tribological properties of titanium alloys, Wear, 151 (1991), Pages 203-217.
- [174] A. Molinari, G. Straffelini, B. Tesi, T. Bacci, Dry sliding wear mechanisms of Ti6Al4V alloy, Wear, 208 (1997), Pages 105-117.
- [175] Y. S. Mao, L. Wang, K. M. Chen, S. Q. Wang and X. H. Cui, Tribo-layer and its role in dry sliding wear of Ti-6Al-4V alloy, Wear, 297, Issue 1-2 (2013), Pages 1032-1039.
- [176] C. Hodge and M.M. Stack, M.M. Tribo-corrosion mechanisms of stainless steel in soft drinks. WEAR, 270 (2010), Pages 104-114.
- [177] Rabinowicz E., The least wear, wear 100 (1984), Pages 533-541.
- [178] S. Wilson, A. T. Alpas, Thermal effects on mild wear transitions in dry sliding of an aluminium alloy, Wear. 225-227 (1999), Pages 440-449.
- [179] S. Chatterjee, T. K. Pal, Wear behaviour of hard facing deposits on cast iron, Wear 225 (2003), Pages 417-425.
- [180] C. Fan, M. C. Chen, C. M. Chang, W. Wu, Microstructure Change Caused by (Cr,Fe)₂₃C₆ Carbides in High Chromium Fe-Cr-C Hardfacing Alloys Surf. Coat. Technol. 201 (2006), Pages 908-912.
- [181] S. Krol , W. Grzesik, Z. Zalisz , M. Hepner, Frictional behaviour of oxygen diffusion hardened titanium in dry sliding against Co–28Cr–5W–4Fe–3Ni–1Si cobalt alloy, Tribology International 37 (2004) 633–643
- [182] C. Richard, C. Kowandy, J. Landoulsi, M. Geetha, H. Ramasawmy, Corrosion and wear behaviour of thermally sprayed nano ceramic coatings on commercially pure Titanium and Ti-13Nb-13Zr substrate, International journal of refractory metals & hard materials, 28 (2010), Pages 115-123.
- [183] J. Oh, S. Lee, Correlation of microstructure with hardness and fracture properties of (TiC,SiC)/Ti-6Al 4V surface composites fabricated by high-energy electron-beam irradiation, Surf. Coat. Technol., 179 (2004), Pages 340-348.
- [184] F. Wang, J. Mei. X. Wu, Direct laser fabrication of Ti6Al4V/TiB, J. Mater.Proc. Tech., 195 (2008), Pages 321-326.

- [185] E. Bemporad, M. Sebastiani, F. Casadei, F. Carassiti, Surf., Modelling production and characterisation of duplex coatings (HVOF and (PVD) on Ti–6Al–4V substrate for specific mechanical applications, Surf. Coat. Technol., 201 (2007), Pages 7652-7662.
- [186] S. Mridha, H. S. Ong, L. S. Poh, P. Cheang, Intermetallic coatings produced by TIG surface melting, J. Mater. Proc. Technol. 113 (2001), Pages 516-520.
- [187] S. Mridha, Titanium nitride layer formation by TIG surface melting in a reactive environment, J. Mater. Proc. Technol. 168 (2005), Pages 471-477.
- [188] Yan Pei, Deng Jianxin, Wu Ze, Li Shipeng, Xing Youqiang, Zhao Jun, Friction and wear behaviour of the PVD (Zr, Ti) N coated cemented carbide against 40Cr hardened steel, Int. Journal of Refractory and Hard Materials 35 (2012), Pages 213-220.
- [189] R. Sahoo, B. B. Jha, T. K. Sahoo, Dry Sliding Wear Behaviour of Ti–6Al–4V Alloy Consisting of Bimodal Microstructure, Trans. Indian. Inst Met. 67(2) (2014), pages 239-245.
- [190] Tyler L. Stewart, Kevin P. Plucknett, The sliding wear of TiC and Ti(C,N) cermets prepared with A stoichiometric Ni Al binder, Wear 318 (2014), Pages 153-167.
- [191] J. K. Lancaster, The influence of substrate hardness on the formation and endurance of Molybdenum disulphide films, Wear 10 (1967), Pages 103-117.
- [192] C. C. Onuoha, Z. N. Farhat, G. J. Kipouros, K. P. Plucknett, The reciprocating wear behaviour of TiC-304L stainless steel composites prepared by melt infiltration, Wear 303 (2013), Pages 321-333.
- [193] John R. Taylor, An Introduction to Error Analysis: The Study of Uncertainties in Physical Measurements 2d Edition, University Science Books, 1997.
- [194] Philip R. Bevington and D. Keith Robinson, Data Reduction and Error Analysis for the Physical Sciences, 2d Edition, WCB/McGraw-Hill, 1992.
- [195] K. H. Zum Gahr, Wear by hard particles, Tribol. Int. 31 (1998), Pages 587-596.
- [196] D. Regonini, V. Adamaki, C.R. Bowen, S.R. Pennock, J. Taylor, A.C.E. Dent., AC electrical properties of TiO₂ and Magnéli phases, TiO₂n–1, Solid State Ionics 229 (2012), Pages 38–44.

Annexure

Publications:

1 - G. Rasool and M.M. Stack, Mapping the role of Cr content in dry sliding of steels: comparison between maps for material and counterface, Tribology International, Volume 80, December 2014, pages 49-57 (Published), **based on chapter 4.**

2 - G. Rasool and M.M. Stack, Wear maps for TiC composite based coatings deposited on 303stainless steel, Tribology International, Volume 74, June 2014, Pages 93-102 (Published), **based on chapter 5.**

3 - G. Rasool and M.M. Stack, Tribo-Oxidation maps for Ti against steel, in press in the Journal of Tribology International, **based on chapter 6.**

4 - G. Rasool, S. Mridha and M.M. Stack, Mapping wear mechanisms for TiC/Ti composite coatings, Wear, 328-329 (2015), Pages 498-508, **based on chapter 7.**